Cenozoic Antarctic climate evolution based on molecular and isotopic biomarker reconstructions from geological archives in the Ross Sea region

by

Bella Jane Duncan

A thesis

submitted to the Victoria University of Wellington

in fulfilment of the requirements for the degree of

Doctor of Philosophy

In Geology

Victoria University of Wellington

2017

Geology! the helicopter rises,
the scientists crowd around,
and Emily's drill goes down

through a thousand years of ice:
ghost of a dog, ghost of a pony
Oates going deeper and deeper

Below the surface
*
still perfectly himself
still gone for some time,
lost in whatever Emily might find

of sediments and algae,
the movement and retreat
of seasons, time passing
in samples and traces
-beech and conifer-
stuff from the core

to take home and question
and even then perhaps
not quite be sure…
*
May the years of her life
look after her
Emily's gone to Antarctica

From Hoosh *by Bill Manhire*

Abstract

During the Cenozoic Era (the last 65 Ma), Antarctica's climate has evolved from ice free conditions of the 'Greenhouse world', which at its peak (~ 55 Ma) supported near-tropical forests, to the 'Icehouse' climate of today with permanent ice sheets, and a very sparse macroflora. This long-term cooling trend is punctuated by a number of major, abrupt, and in some cases, irreversible climate transitions. Reconstructing past changes in vegetation, sea surface temperature, hydroclimate and the carbon cycle require robust geological proxies that in turn can provide insights into climatic thresholds and feedbacks that drove major transitions in the evolution of Antarctica's ice sheets. Biomarkers allow climate and environmental proxy reconstructions for this region, where other more traditional paleoclimate methods are less suitable. This study has two aims. Firstly to assess the suitability and applicability of biomarkers in Antarctic sediments across a range of depositional settings and ages, and secondly to apply biomarker-based climate proxies to reconstruct environmental and climate conditions during key periods in the development of the Antarctic Ice Sheets.

The distribution and abundances of n-alkanes are assessed in Oligocene and Miocene sediments from a terrestrial outcrop locality in the Transantarctic Mountains, and two glaciomarine sediment cores and an ice-distal deep marine core from the western Ross Sea. Comparisons are made with n-alkane distributions in Eocene glacial erratics and sedimentary rocks of the Mesozoic Beacon Supergroup, both likely sources of reworked material. A shift in dominant chain length from n-C_{29} to n-C_{27} occurs between the Late Eocene and Early Oligocene, considered a response to a significant climate cooling. Samples from glaciofluvial environments onshore, and subglacial and ice-proximal environments offshore display a reworked n-alkane distribution, characterised by low carbon preference index (CPI), high average chain length (ACL) and high n-C_{29}/n-C_{27} values. Whereas, samples from lower-energy, more benign lacustrine and ice-distal marine environments predominantly contained contemporary material.

Palynomorphs and biomarker proxies based on n-alkanes and glycerol dialkyl glycerol tetraethers (GDGTs) are applied to a Late Oligocene and Early Miocene glaciomarine succession spanning the large transient excursion of the Mi-1 glaciation (~23 Ma) in DSDP Site 270 drill core from the central Ross Sea. While the Late Oligocene is marked by relatively warm conditions, regional cooling initiated a transition into Mi-1. This was likely driven by a combination of decreasing atmospheric CO_2 and an orbital geometry favouring low seasonality and cool summers, leading to an intensification of proto-Antarctic bottom water production as

the Ross Sea deepened and cooled. Mi-1 manifests as a regionally cool period, with minimum subsurface temperatures of ~4°C and onshore mean summer temperatures of ~8°C. A negative n-alkane $\delta^{13}C$ excursion of up to 4.8‰ is interpreted as a vegetation response to cold, restricted growing seasons, with plants driven to lower altitudes and more stunted growth forms. However, ocean temperatures remained too warm for marine-based ice sheets to advance onto the outer continental shelf and over-ride the drill site. The large increase in ice volume associated with this event, implied by global $\delta^{18}O$ records, was probably held on a higher, terrestrial West Antarctica of greater extent than present day. The relative lack of ice rafted debris during Mi-1, suggests the presence of a marginal marine-terminating ice sheet with fringing ice shelves to the south of DSDP site 270, calving icebergs lacking a basal debris layer, similar to those calving from the Ross Ice Shelf today. This extensive ice cover may explain a large decrease in marine n-alkanes at this time restricting marine productivity on the continental shelf. The biomarker data for the Early Miocene in DSDP 270 indicates a relative warming in both terrestrial and marine temperatures following the transient Mi-1 glacial expansion, but an overall baseline cooling of climate between Late Oligocene and the Early Miocene in the Ross Sea embayment.

Isoprenoid GDGTs are used to reconstruct a Cenozoic subsurface ocean temperature compilation for the Ross Sea, a key source region of ocean deep water. The ocean temperature TEX_{86}^{L} calibration and BAYSPAR in standard subsurface mode were considered, through comparison with independent microfossil and sedimentological data, the most appropriate for use in this region. Ocean temperatures cool prior to the Eocene/Oligocene transition and remain cool for the rest of the Cenozoic, with the exception of short periods of relative warmth in the Late Oligocene and Mid-Miocene Climate Optimum, and long-term trends broadly mirror that of the foraminiferal $\delta^{18}O$ record from the deep Pacific. The Δ Ring Index is used to assess non-thermal influences on GDGT distributions, and displays a long term shift from more positive to more negative deviations. This correlates with %GDGT-0, and also relates to a declining trend in the Methane Index, which reflect the contribution of methanogenic and methanotrophic archaea. These changes suggest that these archaea contributed more to the archaeal community in the early to mid Cenozoic, potentially indicating a more anoxic depositional environment in the Ross Sea. The Branched to Isoprenoid Tetraether index (BIT) steadily declines over the Cenozoic, reflecting increasingly hyper-arid conditions onshore, with less active glaciofluvial systems, limited soil development and less ice-free land.

Acknowledgements

This thesis is dedicated to Arden

Above everything, I am most proud to be your mother

Table of Contents

List of Figures

List of Tables

List of Acronyms

AABW: Antarctic Bottom Water

AASW: Antarctic Surface Water

ACL: Average Chain Length

ANDRILL: Antarctic Geological Drilling

ANTOSTRAT: Antarctic Offshore Stratigraphy project

BAYSPAR: Bayesian Spatially-varying Regression

BIT: Branched and Isoprenoid Tetraether index

BMC: Birmingham Molecular Climatology laboratory

BrGDGT: Branched Glycerol Dialkyl Glycerol Tetraether

CAM: Crassulacean Acid Metabolism

CBT: Cyclization of Branched Tetraethers

CIROS: Cenozoic Investigation in the Western Ross Sea

CPI: Carbon Preference Index

CRP: Cape Roberts Project

DCM: Dichloromethane

DIC: Dissolved Inorganic Carbon

DSDP: Deep Sea Drilling Project

E/O: Eocene/Oligocene boundary

EAIS: East Antarctic Ice Sheet

FID: Flame Ionization Detector

GDGT: Glycerol Dialkyl Glycerol Tetraether

GC: Gas Chromatography

GC-MS: Gas Chromatography-Mass Spectrometry

GC-C-IRMS: Gas Chromatography-Combustion-Isotope Ratio Mass Spectrometry

HMW: High Molecular Weight

IODP: Integrated Ocean Drilling Project

IsoGDGT: Isoprenoid Glycerol Dialkyl Glycerol Tetraether

LC-MS: Liquid Chromatography-Mass Spectrometry

LMW: Low Molecular Weight

MAP: Mean Annual Precipitation

MAT: Mean Annual air Temperature

MCDC: Modified Circumpolar Deepwater

MeOH: Methanol

MBT: Methlyation of Branched Tetraethers

MI: Methane Index

MMCO: Mid-Miocene Climate Optimum

MMCT: Mid-Miocene Climate Transition

MST: Mean Summer air Temperature

NHG: Northern Hemisphere Glaciation

OEP: Odd-over-Even Predominance

O/M: Oligocene/Miocene boundary

RI: Ring Index

RSS: Regional Seismic Stratigraphic sequence

RSU: Regional Seismic Unconformity

SST: Sea Surface Temperature

SubT: Sub sea surface Temperature

SW: Shelf Water

TAM: Transantarctic Mountains

TEX$_{86}$: Tetraether index of tetraethers consisting of 86 carbon atoms

TLE: Total Lipid Extract

TOC: Total Organic Carbon

UCM: Unresolved Complex Mixture

WAIS: West Antarctic Ice Sheet

WARS: West Antarctic Rift System

Introduction

Over the course of the Cenozoic Era, the last 65 myr, global climate underwent a progressive transition from a 'Greenhouse' to an 'Icehouse' world (Figure 0.1) (Zachos et al. 2001a, Zachos et al., 2008). In Antarctica, this transition manifested as a change from an ice-free continent, with near-tropical forests (Pross et al. 2012) to permanent ice sheets with a very sparse macroflora dominated by mosses and lichens (Peat et al. 2007). This is coincident with a shift from a high atmospheric CO_2 world (>1000 ppm) to low CO_2 (~180-280 ppm) (Figure 0.1) (Petit et al., 1999, Beerling and Royer, 2011, Masson-Delmotte et al., 2013). Modern Antarctica is mostly covered by two ice sheets containing 27 million km^3 of ice (Fretwell et al., 2013). Two-thirds of the larger East Antarctic Ice Sheet (EAIS) is land based, while the smaller West Antarctic Ice Sheet (WAIS) is mainly marine-based. Data and models indicate that ice sheets grounded below sea level are susceptible to marine ice sheet instability, where ocean warming interacting with grounded ice on an upstream deepening bed can lead to rapid ice sheet retreat (i.e. Schoof, 2007, Jones et al., 2015, DeConto and Pollard, 2016). In turn, input of glacial meltwater can also can result in dramatic changes to the oceans, including the thermal regime, sea ice extent and the production and export of bottom water (Jacobs et al., 2002). The EAIS and WAIS ice-sheets would raise sea levels by ~53.3 m and 4.3 m, respectively, if they were to melt (Fretwell et al., 2013). If current rates of greenhouse gas emissions continue, the Antarctic Ice Sheets could potentially contribute up to a metre of sea-level rise by 2100 (DeConto and Pollard, 2016).

Models of ice sheets and vegetation attempt to reconcile the various feedbacks operating during the major climate transitions of the Cenozoic (Pollard and DeConto, 2005, DeConto et al. 2008, Pollard and DeConto 2009). Such studies are important as the results have implications for assessing the response of the ice sheets to future climate change. Recent models suggest that the marine-based Antarctic Ice Sheets have been very sensitive to minor changes in global mean temperature and CO_2 during the Cenozoic, implying critical thresholds may exist in both the marine and terrestrial parts of the ice sheets (DeConto et al., 2016, Gasson et al., 2016). Importantly, modelling studies require boundary conditions that can only be derived from geological data (i.e. DeConto and Pollard, 2016). Studies on continental margin drill cores offshore of Antarctica, such as those provided by ANDRILL and the Integrated Ocean Drilling Program (IODP), have advanced our knowledge of the timing and extent of ice sheet and oceanic variability (e.g. Barrett 1989, Naish et al., 2001a, Naish et al., 2009, McKay et al.,

2016). However, better reconstructions of past hydrology, land and sea surface temperature using geological proxies are still required. New reconstructions are needed to improve our understanding of marine-terrestrial climate linkages at the Antarctic margin, to reconcile data-model comparisons and to better understand the various climatic thresholds and feedbacks that drove major transitions in the Antarctic ice sheets and global sea-level.

While previous work has focused on using sedimentological characteristics, and micro- and macrofossils to investigate Antarctic Cenozoic climate, there has been limited work using biomarkers to investigate paleoclimate in Antarctica. For example, Pross et al. (2012) and Bijl et al. (2013) used the biomarker based proxies MBT/CBT and TEX$_{86}$ to investigate temperature and vegetation change in Wilkes Land during the Eocene. Feakins et al. (2012) used hydrogen isotopes in ANDRILL 2A to examine the hydrologic regime and temperatures in the Ross Sea sector during the Mid-Miocene Climate Optimum (MMCO). Two studies have published TEX$_{86}$ sea surface temperatures in Neogene sediments recovered from the ANDRILL 1B (McKay et al., 2012a), and the ANDRILL 2A drilling sites (Levy et al., 2016). Other studies have investigated Holocene changes in sea surface temperatures around Antarctica using TEX$_{86}$ (Shevenell et al., 2011, Kim et al., 2012). These studies are all based on offshore core material, and limited to no biomarker based work has yet been published on onshore outcrops.

Investigation of onshore outcrops is important as it provides information on altitudinal and latitudinal gradients and linkages between continental margins, where much of the paleoclimate work in Antarctica is focused. Evidence from the higher altitudes of the Dry Valleys suggests that hyper-arid polar desert conditions existed from the Late Miocene. This is indicated by minimal slope erosion, stagnant glacial ice that has escaped sublimation since it is inferred to have formed ~8.1 Ma, and exceptionally well preserved fossil plants that have had minimal post depositional degradation since 14 myr BP (Sugden et al., 1995, Marchant et al., 2002, Lewis et al., 2008). Although it appears at high altitudes that Antarctica has been a polar desert since the Late Miocene, evidence from the margins shows discharge of significant volumes of sediment laden meltwater derived from the Transantarctic Mountains into the Ross Sea in the Late Miocene, and deglaciation of the WAIS coupled with warmer temperatures during the Pliocene (McKay et al., 2009, Naish et al., 2009, Pollard and DeConto, 2009). Biomarker based proxy evidence from a range of onshore and offshore sample sites can provide geological boundary conditions to help better reconcile how Antarctic climate translated between the coasts and inland during the Oligocene, Miocene and Pliocene.
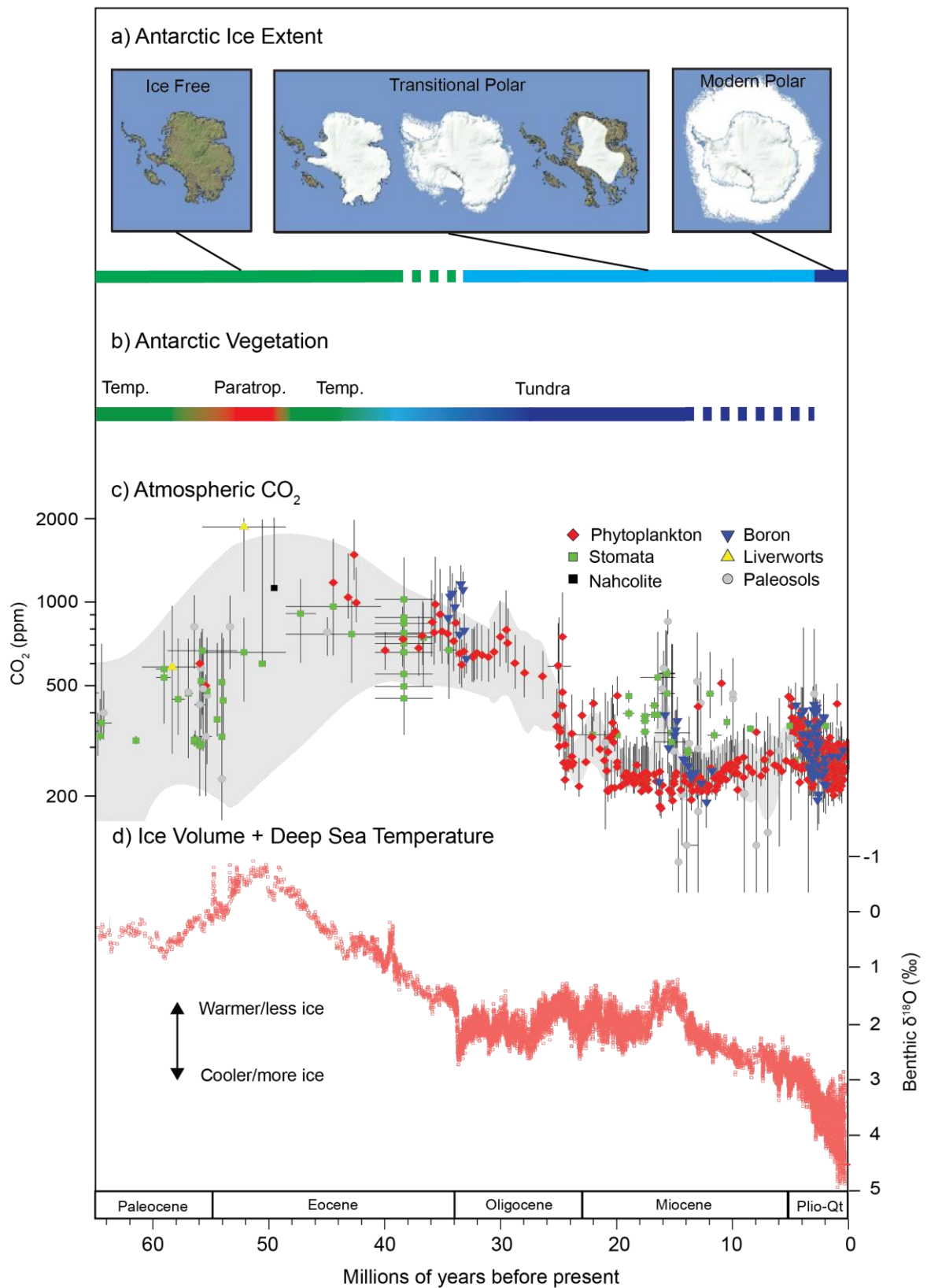
Figure 0.1. Cenozoic transition from Greenhouse to Icehouse conditions; a) Antarctic ice extent (Zachos et al., 2001a, 2008); b) Antarctic vegetation history (Francis et al., 2008,

Anderson et al., 2011, Pross et al., 2012); c) Atmospheric CO_2 (Beerling and Royer, 2011); d) Benthic deep sea foraminifera $\delta^{18}O$ stack (Zachos et al., 2008). Temp=Temperate, Paratrop=Paratropical.

0.1 Research Questions

This thesis focuses on two main research questions;

- *1. How do biomarkers vary across a range of sedimentary facies and ages in Antarctic sediments?* Previous studies of biomarkers in Antarctica have largely focussed on uniform sampling from a stratigraphic section, with less emphasis on rapidly changing depositional settings through time. This study investigates the distribution of biomarkers in various depositional environments, to determine which settings are more or less likely to contain reworked biomarkers, thereby obscuring potential interpretations based on these compounds.

- *2. What can biomarkers tell us about climate conditions during key periods in the development of the Antarctic ice sheets?* Biomarkers can provide a novel way of determining proxy climate data during the Cenozoic, but have been an under-utilised method in the Antarctic. This study uses molecular and isotopic biomarker proxies to gain new insights into the Cenozoic climate of Antarctica.

0.2 Thesis Outline

It is intended that Chapters 3, 4 and 5 will provide the basis for three journal articles, and as such have been written mostly in the format of stand-alone papers. However, through the necessity to maintain stand-alone journal paper format, some repetition between the results chapters and the background and methodology chapters does occur, but has been limited as much as possible.

Chapter 1: Background

This chapter provides an overview of the key literature and research relevant to the rest of the thesis, namely the climate and vegetation history of Antarctica, the geological and tectonic setting of the region, the sample localities and the fundamentals of the biomarker proxies employed. In order to restrict repetition, this chapter aims to briefly summarise these key topics,

with more detailed background information relevant to Chapters 3, 4 and 5 presented upfront within these results chapters.

Chapter 2: Methodology

The methodology chapter describes the key methods and analytical techniques employed in this thesis.

Chapter 3: An assessment of n-alkane distributions across a range of depositional environments in Oligocene and Miocene sediments from the Ross Sea region, Antarctica: Implications for use of biomarker proxies in glacially-influenced settings.

This chapter directly addresses research question 1, by using the distributions and abundances of *n*-alkanes to investigate the variability and potential for reworking of these compounds across a range of depositional settings. *n*-Alkanes are compared between a terrestrial, two glaciomarine, and an ice-distal lower continental rise locality in the Ross Sea region. In particular, this chapter aims to assess the implications for interpreting biomarker proxies in glacially influenced settings.

Chapter 4: The Mi-1 glaciation in the Ross Sea, Antarctica: Climate reconstructions using molecular and isotopic biomarker proxies.

This chapter addresses research question 2 by applying *n*-alkane- and GDGT-based climate proxies to Deep Sea Drilling Project (DSDP) site 270 in the central Ross Sea. This core contains a glaciomarine sediment sequence spanning the Late Oligocene to Early Miocene, a time period characterised by one of the largest transient glaciations of the Cenozoic, the Mi-1 isotopic excursion (i.e. Zachos et al., 2001a, 2001b). This chapter aims to understand the drivers and magnitude of this glacial event in the central Ross Sea.

Chapter 5: A Cenozoic record of ocean temperature from the Ross Sea region, Antarctica: Implications for the use of isoprenoid GDGT-based proxies in ice-proximal, high latitude settings.

This chapter addresses research question 2 by reconstructing a long-term Cenozoic compilation of ocean temperature in the Ross Sea using isoprenoid GDGT-based proxies produced in this thesis and from previous work. This chapter aims to understand the evolution of ocean

temperature in this key region of Antarctica, as well as the implications of applying isoprenoid GDGT-based proxies in a setting which has undergone significant changes to climate, oceanography and tectonics.

Chapter 6: Synthesis and future work.

This chapters summarises and concludes the thesis, and discusses future work that is anticipated to result from this study.

0.4 Contributions to this thesis

This thesis represents original research designed and carried out by myself, with guidance from my supervisors Dr Rob McKay, Dr James Bendle and Prof. Tim Naish. Several collaborators contributed data to this thesis, detailed below.

Chapter 3

Dr Todd Ventura provided bulk pyrolysis data for total organic carbon (TOC) as part of a commercial project through GNS Science funded by this study. Dr Ventura contributed advice and I integrated these results into my thesis.

Chapter 4

Dr Joe Prebble provided palynomorph data and contributed to the interpretation of this data. I then integrated this data into this thesis and expanded the interpretations in the context of this chapter. As above, bulk pyrolysis data was contributed by Dr Todd Ventura as part of a commercial project through GNS Science. Sample extracts were sent to Dr Srinath Krishnan who provided GDGT data which I integrated, compiled for relevant indexes and calibrations, and interpreted. Denise Kulhanek and Richard Levy provided chronostratigraphic data and advice for the DSDP 270 age model. Compound specific isotope data was provided by the Organic Geochemistry Unit at the University of Bristol, as part of a NERC for funded grant (proposal number BRIS/85/1015). The integration of this data into this chapter and all interpretation was conducted by myself.

Chapter 5

Extracts from samples used in this study were sent to Dr Srinath Krishnan who provided GDGT data which I integrated, compiled for relevant indexes and calibrations, and interpreted. GDGT

data from published and unpublished sites contributed to this chapter. Unpublished data from CIROS-1 was provided by Stefan Schouten, Francesca Sangiorgi and Richard Levy. Unpublished data from the McMurdo Erratics was contributed by Francesca Sangiorgi, Veronica Willmott and Richard Levy. Published data from AND-2A was provided by Richard Levy (Levy et al., 2016). Published data from AND-1B was provided by Rob McKay, Francesca Sangiorgi and Courtney Warren (McKay et al., 2012). I compiled this data, calculated the relevant indices and calibrations and interpreted the results. Unpublished age model constraints for CIROS-1 were provided by Dr Joe Prebble.

Chapter 1: Background

This chapter summarises the climate history of Antarctica and describes the geological and tectonic setting of the region. The fundamentals of the biomarker proxies utilised are presented and the sampling localities introduced.

1.1 Cenozoic Climate and Vegetation History of Antarctica

In the Paleocene and Eocene (65-34 Ma), Antarctica was warm and wet, with atmospheric CO_2 estimates >1000 ppm (Masson-Delmotte et al., 2013, Beerling and Royer, 2011, Passchier et al. 2013, Pross et al. 2012, Figure. 0.1). Coastal regions had mild winters (~11°C) and supported highly diverse, near tropical forests in the Early Eocene, with temperate rainforest likely occupying higher elevations and inland areas (Pross et al., 2012). Expansion of temperate rainforest and a decline in near-tropical forests in the mid-Eocene coincided with a prolonged period of global cooling indicated by a ~2‰ increase in deep-sea benthic foraminiferal $\delta^{18}O$, marking the descent into the icehouse world (Zachos et al., 2001a, Pross et al, 2012, Figure 0.1). This cooling was punctuated by several climate excursions, including ~500 kyrs of warmth at the Mid Eocene Climate Optimum (~40 Ma) and a short-lived cooling event potentially associated with ice growth on Antarctica during the Priabonian Oxygen Isotope Maximum at 37.3 Ma (Bohaty and Zachos, 2003, Bohaty et al., 2009, Scher et al., 2014, Pascher et al., 2015). This was followed by aridification, decreasing CO_2 levels (>750 ppm), tectonic isolation of Antarctica, and the development of large-scale Antarctic ice sheets at the Eocene-Oligocene boundary (~34 Ma) (Figure 0.1 and 1.1) (e.g. Pagani et al. 2011, Bijl et al., 2013, Passchier et al., 2013, Scher et al., 2015, Galeotti et al., 2016, Anagnostou et al., 2016). This event occurred as two positive benthic foraminiferal $\delta^{18}O$ excursions between ~34 to 33.2 Ma, with the first isotopic step primarily reflecting a decrease in temperature, and the second interpreted as representing maximum ice extent (Lear et al., 2008). This event is primarily attributed to declining CO_2 and minima in eccentricity and obliquity, resulting in an extended period of low seasonality and cool summers (Galeotti et al., 2016). The Antarctic Ice Sheets appear to have been highly dynamic and strongly sensitive to local insolation forcing until 32.8 Ma, when CO_2 dropped below ~600 ppm, a threshold at which the ice sheets appear less sensitive to insolation forced melt (Galeotti et al., 2016).
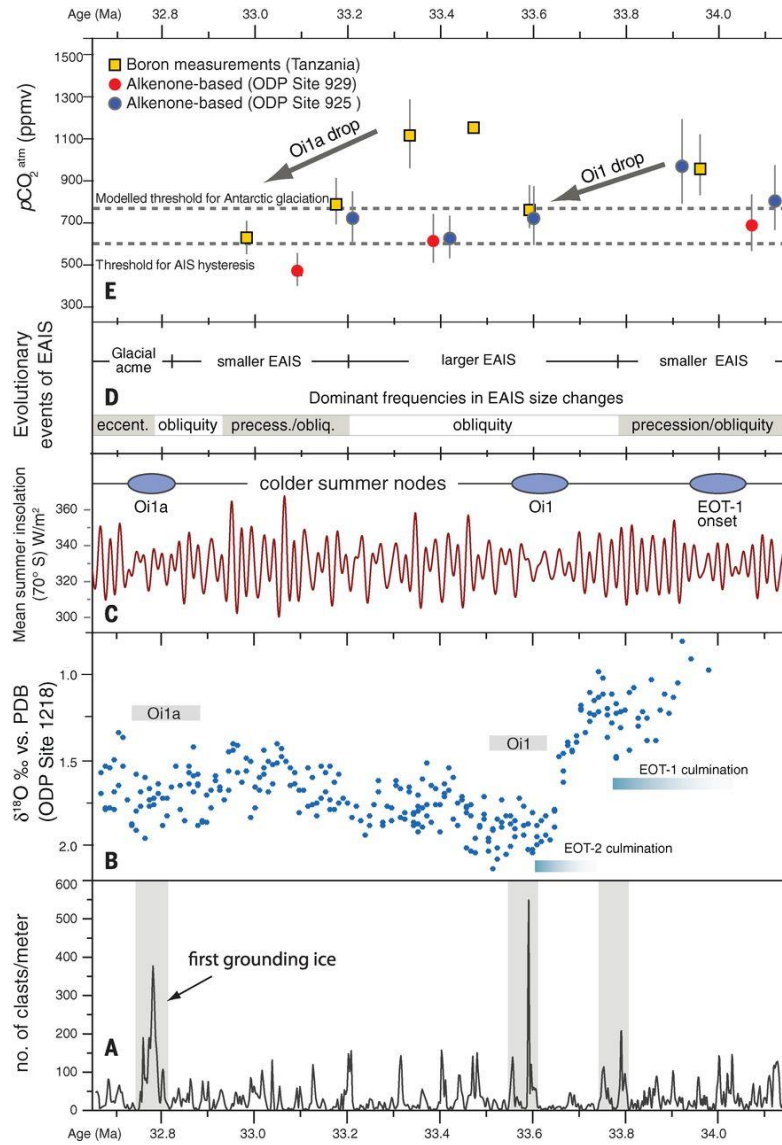
Figure 1.1: Evolution of the EAIS over the Eocene/Oligocene boundary from Galeotti et al. (2016). Clast abundance from Cape Roberts Project 3 in the western Ross Sea (A) is compared to the stepped Eocene/Oligocene transition from benthic $\delta^{18}O$ (B) (Coxall et al., 2005), mean summer insolation at 70°S (C) and atmospheric pCO_2 (E) (Pagani et al., 2005, Pearson et al., 2009), to build a series of evolutionary events of the EAIS (D).

During the Oligocene atmospheric CO_2 concentrations continued to decline (from 600 to 300 ppm), and numerous large-scale, orbitally-paced transient glacial advances occurred, resulting in 30-60m sea level changes (Figure 0.1) (Miller et al., 2005, Pälike et al. 2006b, Pagani et al., 2011). This indicates that although the EAIS persisted through most of this interval, it was likely highly oscillatory in nature (DeConto and Pollard, 2003). Models predict that the EAIS alone cannot account for the amount of global ice suggested by sea level and deep-sea benthic oxygen isotope records in the Oligocene (DeConto et al., 2008). Reconstructions of topography

indicate that much of West Antarctica was actually above sea level prior to the late Oligocene, and was therefore able to grow a land based ice-sheet (Wilson and Luyendyk, 2009, Wilson et al., 2013). Evidence of glacial erosion on volcanic edifaces onshore and in seismic stratigraphy offshore also support a glaciated West Antarctica in the Oligocene (Rocchi et al., 2006, Sorlien et al., 2007). Rifting and erosion in West Antarctica is thought to have resulted in a largely marine setting by Late Oligocene to Early Miocene (De Santis et al., 1995, De Santis et al., 1999), potentially resulting in ice loss if ocean temperatures were too warm to sustain a marine-based ice sheet. Pollen records from the Transantarctic Mountains and the Antarctic Peninsula indicate that the subtropical forests of the Eocene were replaced in the Oligocene by low diversity vegetation, dominated by *Nothofagus* (southern beech) and podocarps, suggesting warm month mean temperatures of ~10°C (Birkenmajer and Zastawniak 1989, Askin and Raine, 2000, Prebble et al. 2006a, Anderson et al., 2011).

The Oligocene/Miocene boundary at ~23 Myr is marked by a 200-300 kyr ~0.6 to 1‰ positive excursion in deep sea benthic foraminiferal $\delta^{18}O$ records, the Mi-1 event, coinciding with the expansion of the EAIS to close to, or exceeding present day volume (Figure 0.1) (Zachos et al., 1997, Naish et al., 2001b, Zachos et al. 2001a, 2001b, Pekar and DeConto, 2006). This event is attributed to declining atmospheric CO_2, coupled with an orbital geometry characterised by a node in obliquity and a minimum in eccentricity, resulting in low seasonality and cool summers (Further detail in Chapter 4) (Naish et al., 2001b, Pagani et al., 2005). The Mi-1 glaciation was not extensive and/or cold enough to extinguish higher plants such as *Nothofagus* from the continent (Askin and Raine, 2000). A cooling trend during the early Miocene was interrupted between 17-15 Ma by the MMCO, during which stratigraphic and proxy data from the western Ross Sea indicate the Antarctic Ice Sheets were periodically reduced in extent and January mean temperatures were ~10°C (Figure 1.2) (Warny et al., 2009, Passchier et al., 2011, Foster et al. 2012, Levy et al., 2016). However, both temperature and CO_2 were only moderately elevated during this time, with boron- and alkenone- based reconstructions of atmospheric CO_2 concentrations ranging between 350-400 ppm (Foster et al. 2012, Zhang et al., 2013). Global temperatures were approximately 3-4°C higher than present, but with sparse proxy-based evidence of significant polar amplification, the magnitude of which is poorly constrained by data and numerical models (You et al. 2009).

The MMCO was followed by the Mid-Miocene Climate Transition (MMCT), one of the largest cooling steps in the Cenozoic, and considered to have culminated in the development of a more stable, cold-based EAIS (Figure 0.1) (Shackleton and Kennett, 1975, Flower and Kennett, 1994, Lewis et al. 2007). Geomorphic studies from the Dry Valleys indicate this time period was associated with meltwater outbursts from a dominantly warm-based ice sheet overriding the Transantarctic Mountains, suggesting significant expansion of the EAIS (Denton and Sugden, 2005). In the Olympus Range, glacial sediments at 1,425 m indicate a permanent change from a warm-based to a cold based glacial regime at approximately 13.94 Ma (Lewis et al., 2007, Lewis et al., 2008). A change to a cold-based glacial regime is also supported by evidence from Marie Byrd Land, where volcanoes younger than 15 Ma show no indication of glacial erosion (Rocchi et al., 2006). Continental shelf sediments from the AND-1B core in McMurdo Sound also show a cold, polar glacial regime during the MMCT, typified by diamictites deposited by grounded ice, sediment starved deposition and limited subglacial meltwater input during interglacials (McKay et al., 2009). This is coincident with a cooling in Southern Ocean surface waters of 6-7°C, and a deep water cooling of ~2°C, inferred to be related to an eccentricity-paced intensification in the Antarctic Circumpolar Current (Shevenell et al., 2004, Shevenell et al., 2008). This intensification is proposed to have been a response to decreasing atmospheric pCO$_2$ coupled with a tectonically-induced reorganisation of the climate system as a result of constriction of the Eastern Tethys Ocean (Shevenell et al., 2004).
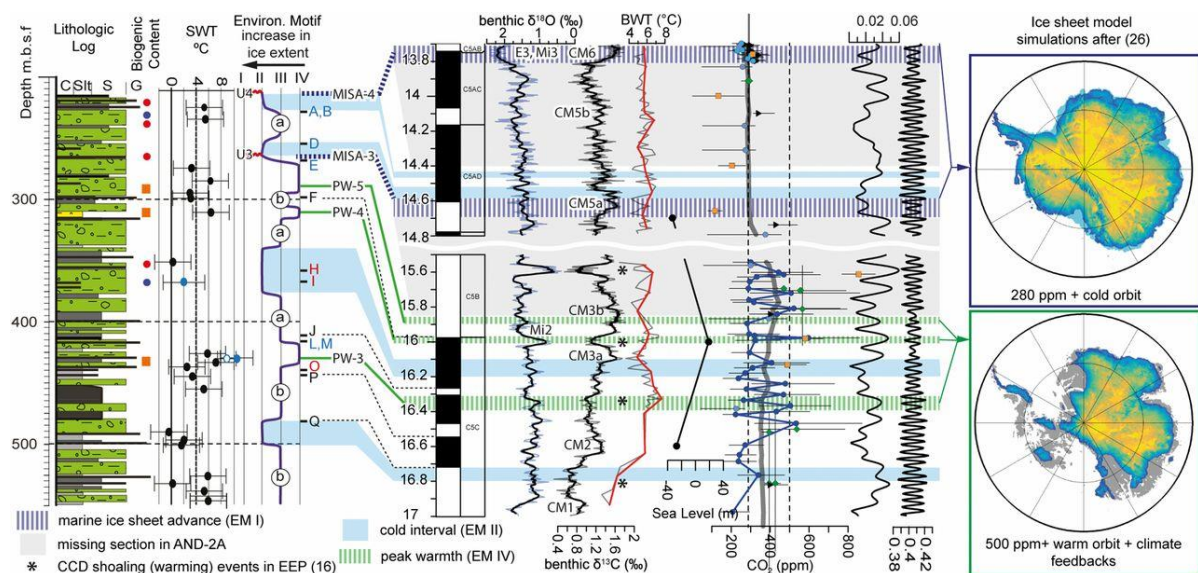
Figure 1.2. The McMurdo Sound AND-2A record of the MMCO and MMCT, from Levy et al. (2016), showing periods of reduced ice extent, coinciding with warmer sea water temperatures, and correlated to records of benthic foraminiferal δ^{18}O and δ^{13}C (Holbourn et al., 2014, 2015),

bottom water temperature (Shevenell et al., 2008), sea level (John et al., 2011), and atmospheric CO₂ (Kürschner et al., 2008, Foster et al., 2012, Badger et al., 2013, Zhang et al., 2013, Greenop et al., 2014). Ice sheet simulations from Gasson et al., 2016.

A decreasing trend in temperatures following on from the MMCT was temporarily interrupted by a period of relative warmth during the Pliocene epoch (5-3 Ma), much of which was characterised by moderately higher-than-present temperatures by ~3°C and CO_2 concentrations of ~330-400 ppm, a greatly reduced WAIS, and higher than present sea levels (Dowsett, 2007, Naish et al. 2009, Seki et al. 2010, Foster and Rohling, 2013). The behaviour of the EAIS during the Pliocene is debated, but marine-based sectors may still have been highly variable during this time, potentially contributing up to 19.2 m sea level equivalent of ice melt (Miller et al., 2012, Fretwell et al., 2013, Pollard et al., 2015). In McMurdo Sound, Late Miocene and Early Pliocene sediments reflect a subpolar glacial regime, characterised by increased subglacial meltwater and terrigenous sedimentation (McKay et al., 2009). Cooling during the Late Pliocene resulted in the expansion of perennial sea ice in the Southern Ocean, a more expansive WAIS, and the development of continental-scale northern hemisphere ice sheets (Figure 1.3) (Maslin et al., 1998, Jansen et al., 2000, McKay et al., 2012a). The glacial regime in McMurdo Sound transitioned to a cold, polar environment by the Late Pleistocene with the Ross Ice Shelf persisting during interglacials (McKay et al., 2012b).

The vegetation history of Antarctica has long been debated with some suggesting that higher plants disappeared from the continent at the MMCT, as geomorphic evidence, and fossil and surface tephra preservation from the high altitude Dry Valleys indicate a cold, hyperarid climate at high elevations since that time (Marchant and Denton, 1996, Marchant et al., 1996, Lewis et al., 2008). However, the presence of Late Miocene sediment laden meltwater deposits in McMurdo Sound indicate that coastal elevations may have been less arid with subglacial ice sheet melt and large glaciofluvial systems, similar to modern Greenland (McKay et al., 2009). Others proposed on the basis of a sparse diatom flora in fossiliferous glacigenic sediment that the extinction of higher plants did not take place until after the Pliocene warmth (Harwood et al. 1983, Webb et al. 1984). The timing of the disappearance of higher plants has implications for both Antarctic climate and ice sheet extent, as well as the age of fossiliferous outcrops such as the Sirius Group (Ashworth and Cantrill, 2004, Francis and Hill, 1996). The Sirius Group contains fossilised prostrate forms of *Nothofagus* in the Beardmore region at 85°S, indicating that summer temperatures at this site would have reached 5°C, with a mean annual temperature

of ~ -12°C, for these shrubs to grow (Francis and Hill, 1996). If this outcrop can be accurately dated, it provides a constraint on near-pole temperatures and climate during a period of the Neogene.
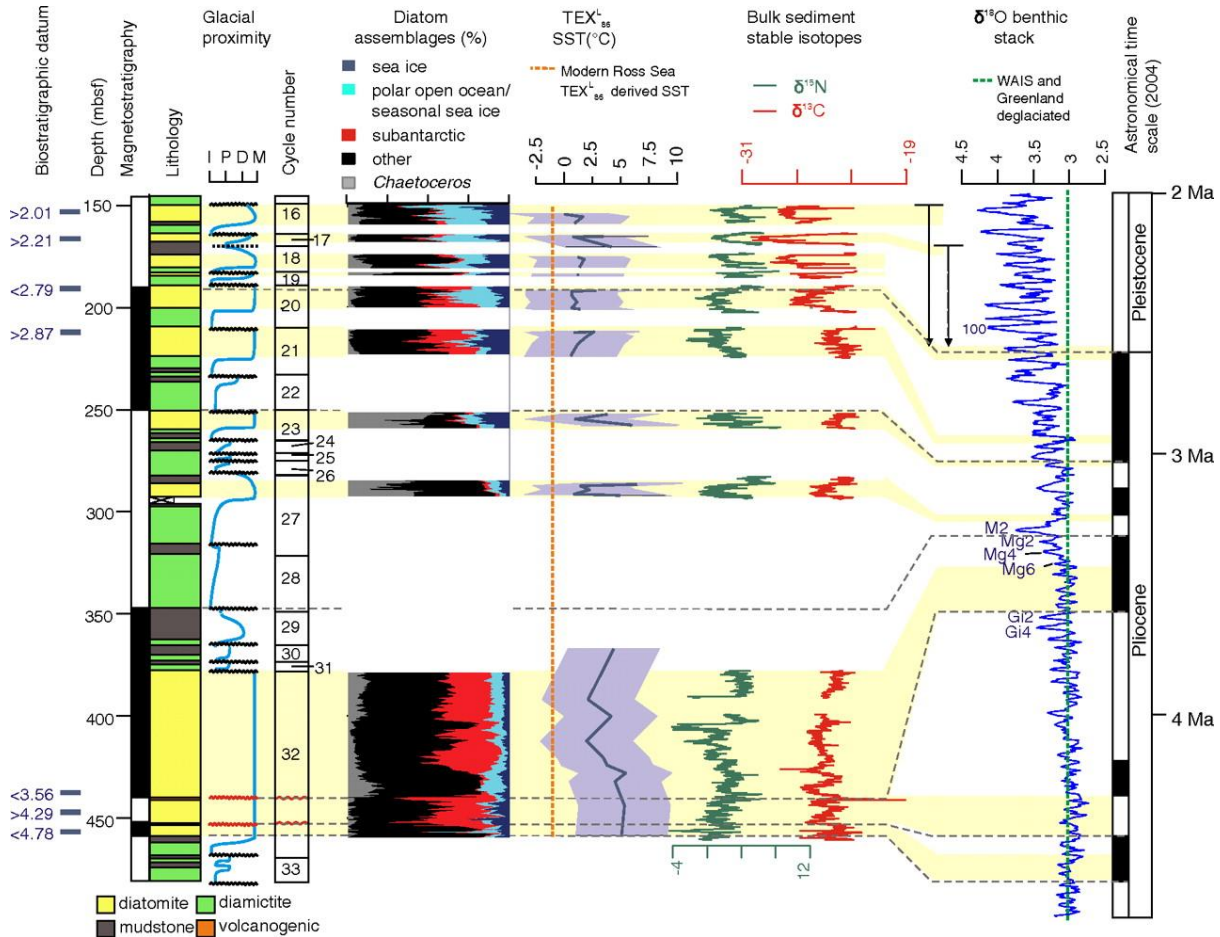
Figure 1.3: The McMurdo Sound AND-1B record of the Pliocene warmth and Late Pliocene/Pleistocene cooling from McKay et al. (2012a), showing a shift to more polar diatom assemblages and cooler sea water temperatures coincident with cooling and increased ice volume displayed by increasingly more positive global benthic foraminifera δ¹⁸O (Lisiecki and Raymo, 2005). An ice proximity curve is also displayed, where I: Ice contact, P: Ice proximal, D: Ice distal, and M: Marine.

1.2 Geology of the Transantarctic Mountains in the Ross Sea region

1.2.1 Pre Cenozoic Geology

The Transantarctic Mountains (TAM) border the Ross Sea embayment. The oldest rocks in this region outcrop occasionally along the western margin of TAM, and consist of the Archean to Early Proterozoic metamorphic crystalline basement of the East Antarctic Shield (Goodge et

al., 2002). Next oldest, and outcropping extensively through the TAM are metasedimentary siliciclastics and carbonates with a minor volcanic component, spanning from the Late Proterozoic to the Cambrian (Goodge et al., 2002). These were intruded and deformed by the Granite Harbour Intrusives, which were emplaced in two main phases, syn-tectonically to the Ross Orogeny from 589-490 Ma, and post-tectonically from 486-455 Ma (Allibone et al., 1993a, Allibone et al., 1993b). A series of volcanics and intrusive granites, primarily the Admiralty Intrusives, were also emplaced in Northern Victoria Land in the mid Paleozoic (Borg et al., 1986).

Overlying the metasediments and intrusives is the Beacon Super Group, consisting of an approximately 2.5 km thick sedimentary sequence spanning the Devonian to the Triassic (Barrett, 1981). The Devonian Taylor Group at the base of the sequence is a quartzose sandstone, with a paleoenvironmental setting varying between shallow marine and alluvial plain. Stratigraphically above this is the late Carboniferous to Triassic Victoria Group. A diamictite at the base of this unit is thought to represent a late Carboniferous glacial, overlain by interbedded sandstones, shales, conglomerates and coals, interpreted as a terrestrial sequence of lakes, braided rivers and alluvial plains (Barrett, 1981). Throughout the Beacon Super Group are common plant macrofossils and palynomorphs, with less common vertebrates and marine invertebrates (Barrett, 1981). In the early Jurassic, as the Gondwana super continent began to separate, the Beacon Super Group was intruded by the Ferrar Dolerite, resulting in extensive low grade thermal metamorphism (Barrett, et al., 1986).

1.2.2 Cenozoic Geology

The Cenozoic geology of the TAM consists of scattered sedimentary outcrops of glacial till, and the McMurdo Volcanic Group. The McMurdo Volcanic group are mainly basaltic volcanics associated with rifting during the mid-late Cenozoic, continuing to the present day (Fielding et al., 2006, Martin et al, 2010). The oldest outcrops onland are found at Mt Morning in the McMurdo Sound region, and are dated back to 18.7 Ma (Kyle and Muncy, 1989, Martin et al., 2010). However, ash layers in the offshore sediment cores from the Cape Roberts project may be from early McMurdo Volcanics, suggesting that volcanism in the region may have initiated as early as ~25 Ma (Smellie et al., 2000, Martin et al, 2010).

The most significant Cenozoic sedimentary unit throughout the TAM is the Sirius Group (Hambrey and Barrett, 1993). These sediments vary between marine, glacio-marine, glacio-lacustrine, lacustrine and periglacial, and extend over 1500 km at high elevations along the TAM (Hambrey and Barrett, 1993, Webb et al., 1996). However, age control and correlation between scattered outcrops is poor (Hambrey and Barrett, 1993). The age of the Sirius Group has long been the subject of debate, since originally being assigned as Pliocene on the basis of diatom assemblages (Harwood, 1983, Webb et al., 1984). The Sirius Group was then interpreted as the result of a large loss of ice from the EAIS interior, with diatoms deposited in an inland sea and then glacially transported and redeposited on less elevated TAM during an EAIS overriding event (Harwood, 1983). This view was challenged by several lines of evidence, including limited slope erosion, well preserved surficial mid-Miocene ash layers and biota in the Dry Valleys signifying a cold, arid climate since deposition (i.e. Sugden et al., 1993, Sugden and Denton, 2004, Lewis et al., 2007, Lewis et al., 2008) and the possibility that the sparse Pliocene diatoms may be aeolian derived contaminants (McKay et al., 2008). A Pliocene age for these deposits also requires rapid uplift rates, which are much larger than those observed from dated marine deposited in the Dry Valleys (Denton et al., 1992). While the age of the Sirius Group is still debated, the weight of evidence lies in favour of the deposits being Mid-Miocene or older (Barrett, 2013).

Other Cenozoic deposits are represented by scattered veneers of glacial tills, colluvium and lacustrine sediments (Marchant and Denton, 1996, Lewis et al., 2007, Lewis et al., 2008). These vary in age from the early Miocene in the case of the Friis Hills (Lewis and Ashworth, 2015) to Holocene (Marchant and Denton, 1996). Deposits younger than the Mid Miocene are largely accumulations formed at the margins of outlet glaciers and from occasional marine incursions into fjordal systems during warmer intervals (Hambrey and Barrett, 1993, Marchant and Denton, 1996, Levy et al., 2012). Sediments older than the Mid-Miocene show evidence for deposition under a warm-based glacial regime and contain a well-preserved biota (Denton and Sugden, 2005, Lewis et al, 2007, Lewis et al, 2008). While not outcropping on land, Cenozoic sediments of Eocene-Pliocene age are also found in the form of glacial erratics in the McMurdo region, and are thought to be eroded from strata beneath the Ross Ice Shelf and transported into morainal deposits during ice sheet expansion (Harwood and Levy, 2000).

1.3 Offshore Stratigraphy

Since the late Cretaceous, the Ross Sea embayment has formed a number of subsiding basins, formed within the West Antarctic Rift System (WARS) and bordered to the west by the Transantarctic Mountains (TAM), and the east by Marie Byrd Land (Behrendt et al., 1991). Extension resulted in several sedimentary basins, the Eastern Basin, Central Trough and Victoria Land basin, separated by the structural highs of the Central High and Coulman High (Figure 1.4) (Cooper et al., 1987, De Santis et al., 1995). Recent models suggest that extension and basin formation took place over three main phases, with late Cretaceous rifting centred in the Eastern Basin, Paleogene rifting centred in the Central Trough, followed by Eocene-Oligocene rifting centred in the Victoria Land Basin (Wilson and Luyendyk, 2009). Sediment infill of these basins therefore potentially began as early as the Late Cretaceous, and may be up to 14 km thick in the Victoria Land Basin (Cooper et al., 1987). However, the oldest known sediments from the WARS infill are glacial erratics from the McMurdo Sound region of ~Mid-Eocene age (Levy and Harwood, 2000). An extensive network of seismic reflection data imply older, potentially high energy fluvial sediments were deposited in the Ross Sea during the initial rift phase of the Cretaceous to Paleogene (Luyendyk et al., 2001, Decesari et al,, 2007, Wilson and Luyendyk, 2009). Very rare reworked Cretaceous dinoflagellates are found in Eocene-aged glacial erratics from McMurdo Sound, indicating a potential Cretaceous marine sediment source in the Western Ross Sea (Askin, 2000). Both surface and Oligocene to Miocene sediments in the Central Ross Sea do not show any reworked Cretaceous microfossils, but a significant component of Late Cretaceous terrestrial palynomorphs is observed in surface sediment from the Eastern Ross Sea (Kemp, 1975, Truswell and Drewry, 1984).

Uplift and erosion of the TAM would have contributed to most of the basin fill in the Western Ross Sea, but rates would have varied along the range front, with uplift in the Central TAM occurring in several phases after initiating at ~115 Ma (Fitzgerald, 1994). Apatite fission track thermochronology and clast provenance studies indicate that the bulk of the exhumation occurred between the Early Eocene and the Early Oligocene, with little uplift since this time (Fitzgerald, 1994, Smellie, 2001). The Central High and Coulman High remained subaerial until at least the Mid Oligocene, and then likely varied between subaerial and submerged during high and low stands of sea level, before permanently submerging as the result of glacial erosion and tectonic subsidence at some stage in the Early-Middle Miocene (De Santis et al., 1995, De Santis et al., 1999, Bart and De Santis, 2012). Continued subsidence resulted in sediment accumulation and shelf progradation throughout the Cenozoic, with several large regional

unconformities representing major erosional surfaces (RSU6 to RSU1) (Figure 1.4) (De Santis et al., 1995, De Santis et al., 1999).
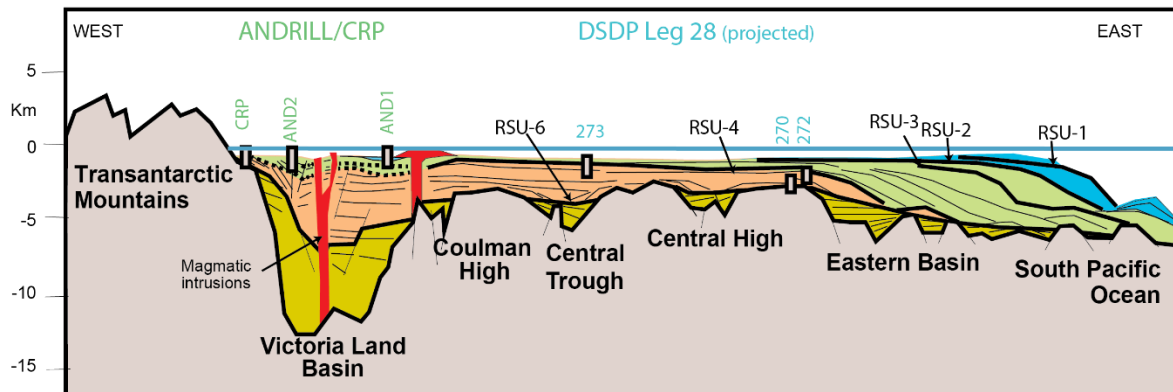
Figure 1.4: Schematic cross-section through the Ross Sea showing sediment infill and age of infill. Approximate location of cross section line shown on Figure 1.5. Previous drill cores from ANDRILL, Cape Roberts Project and DSDP Leg 28 are labelled. Figure adapted from McKay et al. (in press, IODP prospectus Expedition 374).

Eight seismic units are defined by the ANTOSTRAT seismic stratigraphic scheme (RSS-1 to RSS-8), bounded by RSU6 to RSU1 (Table 1.1) (Brancolini et al., 1995). RSS-1 lower and upper represent high energy fluvial to shelf sediments deposited in sedimentary basins between subaerial basement highs, likely between the Late Cretaceous and Early Oligocene (Brancolini et al., 1995, Fielding et al., 2001). Sediments within RSS-2 to RSS-6 (~Late Oligocene to Early Pliocene) indicate seaward-dipping prograding shelf deposition, with periodic grounded ice in the Central Ross Sea apparent from approximately the Mid-Miocene (Table 1.1) (De Santis et al., 1995, 1999). Prior to RSU3, sediments suggest an abundant meltwater regime, with significant glacially sourced sediment transport and discharge to the continental margin (De Santis et al., 1999). Sediments above this unconformity (Late Miocene to recent) are represented by thin beds suggesting progressive sediment starvation as the polar environment intensified (Alonso et al., 1992, De Santis et al., 1999). In the Western Ross Sea however, sediment-laden meltwater suggests a warmer glacial regime until the Early Pliocene (McKay et al., 2009). Above RSU2, seismic facies show an aggrading, landward-deepening shelf deposited by shelf-wide advances of the WAIS (Brancolini et al., 1995, De Santis et al., 1999).

Table 1.1: Ross Sea seismic stratigraphic units and unconformities, based on Brancolini et al. (1995). Table from McKay et al. (in press, IODP prospectus Expedition 374).

Sequence	Sequence seismic character	Age	Bottom unconformity
RSS-8	Aggradational topset beds underlying (locally backstepping grounding zone wedge)	Pleistocene	RSU1 (0.7 Ma?)
RSS-7	Aggradational, topset beds	Pliocene	RSU2 (?4 Ma)
RSS-6	Shelf topset beds and prograding trough mouth fan at the shelf edge	Late Miocene	RSU3 (?12 Ma)
RSS-5	Alternating subsequences made of grounding zone prograding wedges and subhorizontal strata packages	Mid Miocene	RSU4 (14-16 Ma?)
RSS-4	Grounding zone prograding wedges and subhorizontal strata packages	Early Miocene	RSU4a (18.5 Ma?)
RSS-3	Alternating subsequences made of grounding zone prograding wedges and subhorizontal strata packages	Early Miocene	RSU5 (21 Ma?)
RSS-2	Alternating subsequences made of grounding zone prograding wedges and subhorizontal strata packages	Late Oligocene-early Miocene	RSU6 (29 Ma?)
RSS-1-upper	Subhorizontal strata filling basement basins	Late Eocene-early Oligocene	RSU7
RSS-1-lower	Subhorizontal strata filling basement basins	?Late Cretaceous	Basement

1.4 Source Geology for the Central Ross Sea

Deep Sea Drilling Project (DSDP) Leg 28 drilled sites DSDP 270 and DSDP 274 in the Ross Sea in 1973 (Figure 1.5). DSDP 270 is located in the Central Ross Sea and samples sediment deposited on the margin of the Eastern Basin (The Shipboard Scientific Party, 1975a). The basement rocks of the Eastern Basin below DSDP site 270 are calc-silicate gneiss, schist and marble overlain by a breccia containing fragments similar to the basement rocks, along with highly varied granitic and metamorphic rocks (Ford and Barrett, 1975). Clasts throughout the core dominantly reflect a metasedimentary source terrane, are of a range of lithologies including greywacke, argillite, hornfels, granofels, phyllite and schist (Barrett, 1975). There are no clasts of the Beacon Group or Ferrar Large Igneous Province dolerite, suggesting that the Transantarctic Mountains are unlikely to be the source for sediments in DSDP 270 (Ford and Barrett, 1975). The granitic clasts do not show similarities to granites outcropping along coastal Marie Byrd Land, and the core also contains none of the Cenozoic volcanics from this region (Barrett, 1975). The most likely source for clasts is therefore the proximal basement

high, the Central High, and the region between coastal Marie Byrd Land and the TAM, presently covered by the WAIS (Barrett, 1975). Sediments may also be sourced from reworking of older rift infill (Figure 1.4).
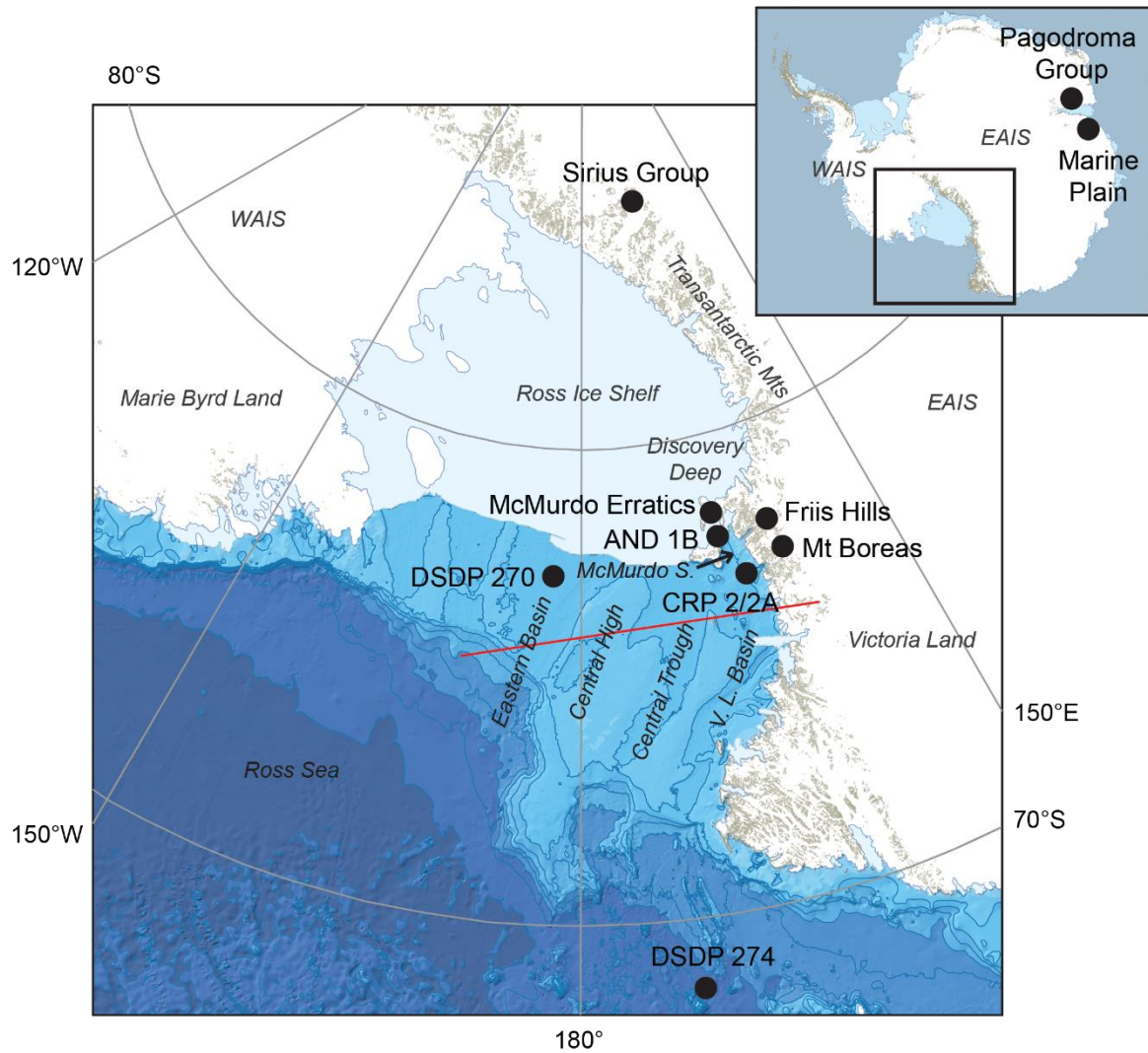
Figure 1.5: Sample locations across Antarctica used in this thesis (Section 1.6). CRP= Cape Roberts Project, DSDP= Deep Sea Drilling Project, AND= ANDRILL project, EAIS= East Antarctic Ice Sheet, WAIS= West Antarctic Ice Sheet. Red line indicates approximate location of cross section shown in figure 1.4. Base map from Quantarctica GIS package, Norwegian Polar Institute.

1.5 Source Geology for DSDP 274

DSDP 274 is located on the lower continental rise in the northwestern Ross Sea and contains clasts of similar lithologies to DSDP 270, indicating the dominant source of ice-rafted sediment

as a metasedimentary terrane likely in the interior of Marie Byrd Land (Barrett et al., 1975). However, DSDP 274 also contains clasts reflecting sources in the TAM, including silicic pebbles thought to be sourced from mid-Paleozoic volcanics in Northern Victoria Land, as well as clasts of the Cenozoic McMurdo Volcanics (Barrett, 1975). This indicates that ice reaching DSDP Site 274 was sourced dominantly from Marie Byrd Land, with a component from the TAM in the western Ross Sea (Barrett, 1975). Fine-grained terrigenous sediment is delivered to the site via density flows sourced from the continental shelf, and subsequently reworked by down and along-slope currents (The Shipboard Scientific Party, 1975b, Frakes, 1975). Pelagic sedimentation also has an influence, with diatom-rich sediment occuring throughout (The Shipboard Scientific Party, 1975b).

1.6 Geology of the Prydz Bay region

Samples were also taken from localities in Prydz Bay. These samples are not included in results Chapters 3-5, but are discussed in Chapter 6.

1.6.1 Pre Cenozoic Geology

The basement rock of the Prince Charles Mountains and Lambert Graben in the Prydz Bay region consists of Precambrian metamorphic rocks, ranging from granulite to amphibolite metamorphics in the northern Prince Charles Mountains, to greenschist facies metamorphics at the southern end of the mountain range (Tingley 1991, Dirks and Wilson, 1995). These have been intruded by Precambrian to Paleozoic granites (Dirks and Wilson 1995). Overlying the basement is the Permian-Triassic Amery sedimentary succession, which outcrops in localised areas but is thought to also occur at the subsurface throughout the Lambert Graben (Fielding and Webb, 1995, McLoughlin and Drinnan, 1997a, McLoughlin and Drinnan, 1997b). This consists of coal measures and sequences of fluvial and alluvial sediments, intruded locally in the Beaver Lake area by Cretaceous mafic dykes and sills (Fielding and Webb, 1995, McLoughlin and Drinnan, 1997a, McLoughlin and Drinnan, 1997b). While no outcrops of Cretaceous sediments are found onland, early Cretaceous coal bearing sediments have been drilled on the continental shelf of Prydz Bay (Turner and Padley, 1991).

1.6.2 Cenozoic Geology

Uplifted remnants of early Oligocene to Pliocene strata occur through the Prince Charles Mountains and are collectively known as the Pagodroma Group (Hambrey and McKelvey,

2000a). These sediments are separated into four formations, the early Oligocene Mt Johnston Formation, the late Miocene Battye Glacier and Fisher Bench Formations, and the Plio-Pleistocene Bardin Bluffs formation (Hambrey and McKelvey, 2000a, Whitehead et al., 2004). They are characterised by glaciomarine interbedded massive diamicts, stratified diamicts and laminated mudstones (Hambrey and McKelvey, 2000a). The Pagodroma Group rests unconformably on glacially cut erosion surfaces, and is interpreted as representing deposition from wet-based tidewater glaciers into a fjordal setting during major recessional stages of the Lambert Glacier, suggesting fluctuations of the Lambert glacier in the Paleogene and Neogene with retreat in excess of 500km occuring (Hambrey and McKelvey, 2000b).

The Larsemann and Vestfold Hills on the eastern margin of Prydz Bay have thin veneers of Pliocene and Quaternary sediments (Whitehead et al., 2006). The Sørsdal Formation on Marine Plain in the Vestfold Hills is a diatomaceous siltstone and sandstone with limestone lenses of early Pliocene age (Quilty et al., 2000). It also contains the Graveyard Sandstone member, a sandy diamictite (Quilty et al. 2000). This formation is interpreted as deposition in a shallow marine environment, with the Graveyard Sandstone representing a time of glacial influence (Quilty et al., 2000). Fossiliferous shallow marine sediments of a similar age also occur in thin outcrops in the Larsemann Hills (Quilty et al., 1990, McMinn and Harwood, 1995).

1.7 Sample locations

This study makes use of a range of existing and new sample sets from drill cores, outcrops and glacial erratics, spanning the Ross Sea and Prydz Bay regions. (Figure 1.5). These sample localities contain sediment spanning much of the Cenozoic, representing semi-continuous records in the case of the offshore drill cores, and 'snapshot' records onshore (Figure 1.6).

1.7.1 Mt Boreas

Glacigenic sediments from the Olympus Range in the Dry Valleys record remarkably well-preserved aquatic fossils, representing the last known vestige of vegetation before hyper-arid, cold-based glacial conditions intiated at high altitudes (1,425 m) during the MMCT (Figure 1.5) (Lewis et al., 2008). Sediments record a small alpine lake which formed in a recessional moraine of a local mountain glacier (Lewis et al., 2008). The lake likely persisted for thousands of years during the last phases of wet-based glaciation, dated to 14.07 ± 0.05 Ma, before being infilled by fluvial sands and debris flows (Lewis et al., 2008). Overlying this are sublimation

tills that represent the first stages of cold-based glaciation at this high altitude, and are dated to 13.85 ± 0.03 Ma (Lewis et al., 2008).
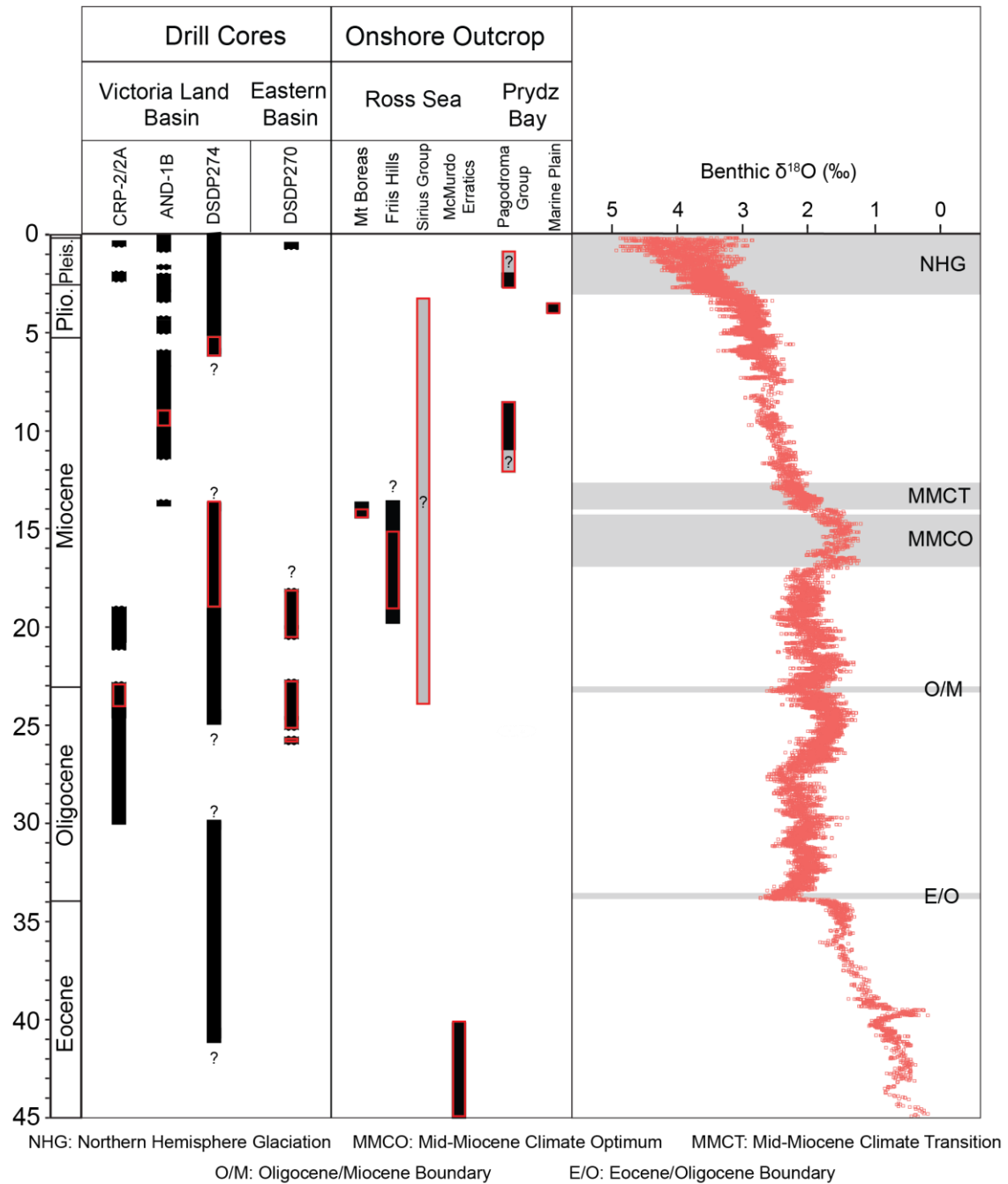
Figure 1.6. Chronostratigraphic summary of samples used in this study, spanning the late Eocene to present. Benthic Oxygen Isotopes from Zachos et al. (2008). While samples were taken throughout the onshore outcrops, red boxes indicate the portions of the drill cores sampled. Plio.= Pliocene, Pleis.= Pleistocene.

1.7.2 Friis Hills

Fossiliferous sediments at the head of the Taylor Valley in the Dry Valleys document the transition from alpine to ice-sheet glaciation over the Early to Mid Miocene (Figure 1.5) (Lewis and Ashworth, 2015). The sediments have been deposited on an inselberg, formed as glacial troughs subsequently cut through the surrounding landscape (Lewis and Ashworth, 2015). Older drift sediments represent deposition from local alpine glaciers, interfingered with fossil-rich fluvial and lacustrine beds which indicate vegetation repeatedly recolonised the area when ice extent was reduced (Lewis and Ashworth, 2015). Younger drift sediments show deposition from outlet glaciers draining the EAIS (Lewis and Ashworth, 2015).

1.7.3 Sirius Group, Beardmore Glacier

Glaciomarine and terrestrial sediments of the Sirius Group in the Beardmore Glacier region were deposited by a fjord and tidewater glacier system extending through the TAM (Webb et al., 1996). Glaciomarine sediments of the Cloudmaker Formation at the base of the succession represent cycles of advance and retreat of a dynamic valley glacier system into a marine environment (Webb et al., 1996). Diamictites, fluvial and laucustrine sediments occur in the overlying terrestrial Meyer Desert Formation (Webb et al., 1996). Well-preserved fossils including wood and leaves demonstrate a tundra vegetation occupied the Beardmore paleofjord region (Francis and Hill, 1996, Webb et al., 1996). The age of these deposits is debated, but the weight of evidence lies in favour of the deposits being Mid-Miocene or older (Section 1.1.2) (Barrett, 2013).

1.7.4 McMurdo Erratics

The McMurdo erratics are located in glacial moraines in the McMurdo Sound region and provide a record of Antarctica in the 'Greenhouse', prior to the development of continental-scale ice sheets in the region (Harwood and Levy, 2000). Fossiliferous Eocene erratics record a fertile coastal setting with a cool temperate climate (Harwood and Levy, 2000). The erratics are thought to have been eroded from Discovery Deep, a basin in the western Ross embayment, and potentially from the margins of outlet glaciers in the TAM (Harwood and Levy, 2000). The erratics would have been transported to the McMurdo Sound region during a periods of ice sheet expansion during the Late Pliocene to Quaternary (Harwood and Levy, 2000). Younger erratics of Oligocene to Miocene age are also present (Harwood and Levy, 2000).

1.7.5 ANDRILL 1B

The ANDRILL AND-IB core was drilled in 2006 as part of the ANDRILL McMurdo Ice Shelf project (Figure 1.5) (77°88.944'S, 167°08.932'E) (Naish et al., 2007). The AND-1B core records orbitally induced oscillations in the WAIS (Naish et al., 2009), with cyclical sequences of subglacial, glaciomarine and marine sediments recording ice sheet advance and retreat over the past 13 Ma (Naish et al., 2007). Marine sediments indicate times when the Ross ice shelf collapsed, resulting in open water conditions with high surface productivity and minimal summer sea ice (Naish et al., 2009).

1.7.6 Cape Roberts 2/2A

The Cape Roberts Project recovered sediment cores off the Victoria Land coast of Antarctica (Figure 1.5) (Cape Roberts Science Team, 1999). The cores collected from this site sample sediment from an EAIS outlet glacier deposited off the coast in a seaward thickening nearshore wedge (Naish et al., 2001a). Sequences of sediment through the core record the expansion and contraction of the EAIS (Naish et al., 2001b). During glacial advance, diamictites, with a sharp lower contact representing a glacial surface of erosion, were deposited at the core site indicating the expansion of outlet glaciers over the continental shelf (Fielding et al., 2000, Powell et al., 2000, Naish et al., 2001a). During periods of glacial retreat, mudstone with ice rafted debris suggests the core sites lay in an open, wave-dominanted coast with floating ice depositing occasional ice rafted debris (Naish et al., 2001a). Samples for this study come from Core CRP 2/2A (77°00.6'S, 163°71.9'E).

1.7.7 DSDP 270

DSDP site 270 was drilled on the continental shelf in the Eastern Basin of the central Ross Sea in 1973 (77°26.48'S, 178°30.19'W), as part of DSDP Leg 28 (Figure 1.5) (The Shipboard Scientific Party, 1975a). DSDP 270 was deposited on the flank of the Central High, a bathymetric high that was subaerial until approximately the Early Miocene (Section 1.3). This core records a deepening sequence of variably ice-distal to ice-proximal sediments in the Central Ross Sea, a region which is a principle drainage area for the WAIS (Allis et al., 1975, Leckie and Webb, 1983, De Santis et al., 1999, Kraus, 2016). This core contains a relatively continous glaciomarine sediment sequence with no clear evidence for glacial overriding, spanning the Late Oligocene to Early Miocene including the Mi-1 glaciation (Kraus, 2016, Kulhanek et al., in prep.).

1.7.8 DSDP 274

DSDP 274 was drilled in the Northwestern Ross Sea (68°59.81'S, 173°25.64'W) as part of DSDP Leg 28 (Figure 1.5) (The Shipboard Scientific Party, 1975b). DSDP 274 is located on the lower continental rise, approximately 250 km north-northeast of Cape Adare (The Shipboard Scientific Party, 1975b). This area is currently in the path of a major outflow for Antarctic Bottom Water, spilling out over the continental shelf of the Ross Sea (Orsi and Wiederwohl, 2009). Sediments in this core range in age from Late Eocene through to Quaternary, with several unconformities separating different lithological units (The Shipboard Scientific Party, 1975b). Samples for this study are taken from Mid-Miocene to Late Miocene sediments (McCollum, 1975, Crampton et al., 2016). An unconformity or condensed section at the MMCT marks an increase in ice-rafted material, ferromanganese nodules and a drop in accumulation rate, interpreted as stronger ocean currents winnowing and reworking the sediment (Frakes, 1975).

1.7.9 Pagodroma Group

The Pagodroma Group occurs as uplifted remnants of strata through the Prince Charles Mountains in Prydz Bay (Figure 1.5) (Hambrey and McKelvey, 2000a). Scattered outcrops of Early Oligocene to Plio-Pleistocene glaciomarine sediments represent deposition from wet-based tidewater glaciers into a fjordal setting during major recessional phases of the Lambert Glacier (Hambrey and McKelvey, 2000a, Whitehead et al., 2004). Glaciomarine facies are characterised by interbedded diamicts and mudstones are separated into four formations, the early Oligocene Mt Johnston Formation, the late Miocene Battye Glacier (10.7-9.0 Ma) and Fisher Bench (12.1 or 10.7-8.5 Ma) Formations, and the Plio-Pleistocene Bardin Bluffs formation (2.6-1.8 or 0.99 Ma) (Hambrey and McKelvey, 2000a, Whitehead et al., 2004).

1.7.10 Marine Plain

The Sørsdal Formation outcrops on Marine Plain in the Vestfold Hills, near Prydz Bay in East Antarctica (Figure 1.5) (Quilty et al., 2000). Early Pliocene (4.5-4.1 Ma) diatomaceous shallow marine sediments and a glacially-influenced sandstone were deposited in a marine embayment with sea surface temperatures 1.6-3°C warmer than present (Harwood et al., 2000, Quilty et al., 2000, Whitehead et al., 2001). The formation contains a diverse marine invertebrate fauna and fossil cetaceans (Quilty et al., 2000).

1.8 Biomarkers

This study employs biomarkers, the fossilised organic molecules of once living organisms. The distribution and occurrence of biomarkers in geological archives can provide insights in to past environmental conditions, such as sea surface and air temperature, soil pH and precipitation (Eglinton and Eglinton, 2008, Castañeda and Schouten, 2011, Sachse et al., 2012, Schouten et al., 2013).

1.8.1 *n*-Alkanes

In sediments, *n*-alkanes are very stable compounds and are among the most abundant biomarkers (Eglinton and Hamilton, 1963, Eglinton and Hamilton, 1967). *n*-Alkanes with different carbon chain lengths originate from different biological sources. Algae and some photosynthetic bacteria typically produce dominantly n-C_{17}, with lesser amounts of n-C_{15} and n-C_{19} (Clark and Blumer, 1967, Han and Calvin, 1969, Cranwell et al., 1987). Other species of bacteria, including non-photosynthetic bacteria often demonstrate an even carbon number preference between n-C_{12} and n-C_{22}, commonly with high n-C_{16} and n-C_{18}, and occasionally n-C_{14} and n-C_{20} (Han and Calvin, 1969, Grimalt and Albaigés, 1987). Non-emergent aquatic plants show enhanced production of n-C_{23} and n-C_{25} (Ficken et al., 2000). For example, in sphagnum mosses n-C_{23} is usually the dominant *n*-alkane, although certain species will also commonly show high, or even dominant n-C_{25}, and occasionally n-C_{21} and n-C_{31} (Baas et al., 2000, Pancost et al., 2002, Nichols et al., 2006, Bingham et al., 2010). Variation in chain lengths produced by different species of sphagnum mosses may be related to habitat, with mosses inhabiting moisture-rich hollow areas of bogs typically displaying a dominance of n-C_{23}, whilst mosses found on drier hummock areas of bogs commonly show a dominance of n-C_{25} and n-C_{31} (Nichols et al., 2006). Long chain *n*-alkanes (n-C_{25} and higher), usually with a high odd-over-even predominance, are most abundant in the epicuticlar waxes on leaves and stems of terrestrial higher plants (Eglinton and Hamilton, 1963).

A homologous series of *n*-alkanes can be described using a carbon preference index (CPI), which indicates whether there is a dominance of *n*-alkanes with an odd number of carbon atoms (Figure 1.7). This is calculated following an equation from Bray and Evans (1961):

$$CPI = \frac{1}{2}\left(\left(\frac{\Sigma_{odd}(n-C_{25-33})}{\Sigma_{even}(n-C_{24-32})}\right) + \left(\frac{\Sigma_{odd}(n-C_{25-33})}{\Sigma_{even}(n-C_{26-34})}\right)\right) \qquad \text{(Eq. 1.1)}$$

A CPI of >1 is indicative of a terrestrial plant source, as most plants produce an odd-over-even predominance of long chained *n*-alkanes in their leaf waxes (Eglinton and Hamilton 1967, Bush and McInerney, 2013). A CPI of ~1 is commonly considered to indicate an *n*-alkane distribution altered by diagenesis (initial post-depositional alteration for example by microbial processes) or catagenesis (post-diagenetic thermal alteration) as odd chain length *n*-alkanes crack into smaller chain lengths with increasing thermal maturity and lose an odd-over-even predominance (Bray and Evans, 1961, Grimalt et al., 1985). Some matured sediments will also display an unresolved complex mixture (UCM) of compounds, which can be especially prominent in biodegraded petroleums as UCMs appear relatively resistant to microbial degradation (Gough and Rowland, 1990, Gough et al., 1992).
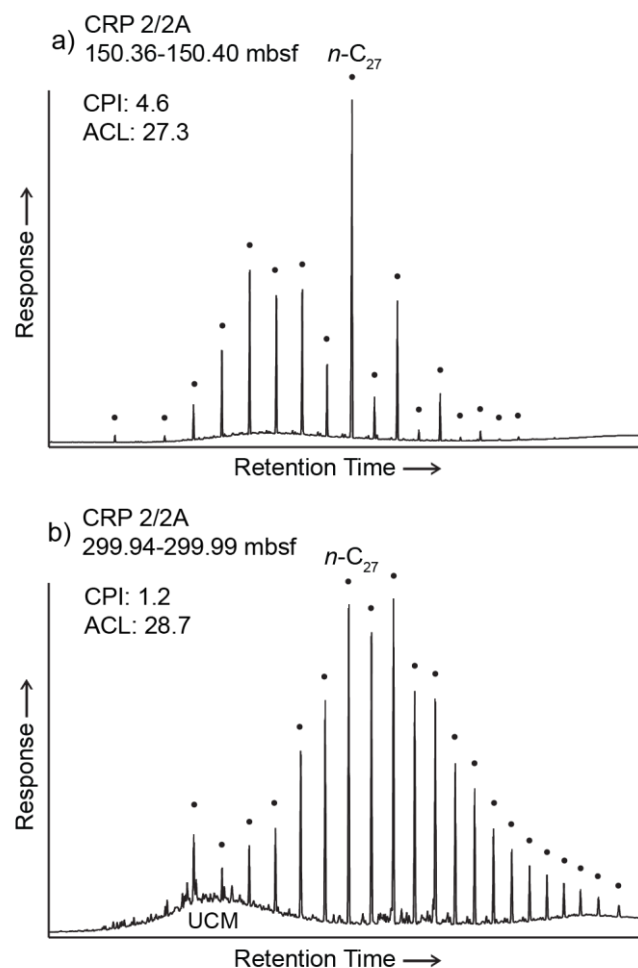
Figure 1.7: Example chromatograms from the Late Oligocene in Cape Roberts 2/2A of a) a high CPI sample and b) a low CPI sample. n-Alkanes are peaks are shown as filled circles,

with n-C27 for reference. CPI: Carbon preference index, ACL: Average chain length, UCM: unresolved complex mixture.

Average chain length (ACL) indicates the dominant *n*-alkane in the sample, calculated by inputting the most dominant *n*-alkanes in a homologous series into the following equation (Figure 1.7) (Poynter et al., 1989, Schefuß et al., 2003):

$$ACL = \frac{\Sigma(C_{odd\ 25-33} \cdot x_{odd\ 25-33})}{(x_{odd\ 25-33})} \qquad \text{(Eq. 1.2)}$$

Where $C_{odd\ 25-33}$ represents the carbon number of the odd chain length *n*-alkanes and $x_{odd\ 25-33}$ represents the concentrations of the odd *n*-alkanes in the sample. Variation in average chain length through time likely reflects the interplay of two key factors; climate-driven plastic response of *n*-alkanes to temperature or aridity within a plant community, or changes to the composition of the plant community in response to climate (Section 3.1.1) (Bush and McInerney, 2013).

1.8.2 Compound specific isotopes of hydrogen and carbon

1.8.2.1 n-Alkane Hydrogen Isotopes

The relative abundance of stable isotopes of deuterium and hydrogen (^{2}H/H) in leaf wax and lipids are related to the ^{2}H/H of the source water, as water is the primary source of hydrogen for photosynthesising plants and aquatic organisms (Sachse et al., 2012). The hydrogen isotopic composition is described either in delta notation, or as an enrichment factor.

$$\delta^2H = \frac{\frac{^2H}{H}_{sample} - \frac{^2H}{H}_{standard}}{\frac{^2H}{H}_{standard}} \qquad \text{(Eq. 1.3)}$$

Where the standard is usually Vienna Standard Mean Ocean Water and δ^2H is described in units of per mil (‰).

$$\varepsilon_{l/w} = \frac{\left(\frac{^2H}{H}\right)_l}{\left(\frac{^2H}{H}\right)_w} - 1 = \frac{\delta^2H_l + 1}{\delta^2H_w + 1} - 1 \qquad \text{(Eq. 1.4)}$$

The enrichment factor describes the hydrogen isotopic fractionation ($\varepsilon_{l/w}$) between the source (δ^2H_w) and the lipid (δ^2H_l), in units of ‰ (Sachse et al., 2012).

Lipid biomarkers record a δ^2H value which is offset from, but highly correlated with, the δ^2H of the water source used by the organism which synthesised the lipids, usually reflecting meteoric water (Sessions et al., 1999, Sauer et al., 2001, Chikaraishi and Naraoka, 2003). The isotopic composition of meteoric water varies spatially and temporally. This is due to Rayleigh fractionation processes as the water moves from one state to another. When seawater evaporates, the vapour is depleted in the heavier ^2H, and when it condensates as rain, the precipitate is enriched in the heavier isotope. The δ^2H of precipitation is affected by the 'continental effect', with rain further inland becoming increasingly depleted in ^2H due to moisture loss. Temperature also has an effect, as fractionation between water and vapour is greater at colder temperatures. The δ^2H is also impacted by the amount of rain falling, with a stronger depletion occurring with higher precipitation rates (For review see Sachse et al. 2012). While the rainfall amount effect imparts a larger control on δ^2H in the tropics, at mid to high latitudes δ^2H is strongly associated with temperature gradients (Bowen, 2008).

Soil water is the main water source for terrestrial higher plants, and predominantly reflects an amount weighted average of precipitation inputs. However, the uppermost horizons can have ^2H enrichment due to evaporation (Sasche et al., 2012). Shallow rooted plants may therefore incorporate a δ^2H affected by evaporation, although in arid environments many plants utilise deep roots to source water from groundwater or deeper in the soil profile (Dawson and Pate, 1996). While there is typically no fractionation between source water and root uptake, leaf composition can have a wide range of variability due to transpiration, a process mainly driven by relative humidity, temperature and the isotopic composition of the water vapour around the leaf (Kahmen et al., 2013a, 2013b). Fractionation also occurs during biosynthesis of lipids in leaf wax, with n-alkyl lipids demonstrating the smallest ^2H depletion relative to the water source (Sessions et al., 1999, Chikaraishi and Naraoka, 2003).

While a strong relationship exists between n-alkane δ^2H (δ^2H_l) and mean annual precipitation δ^2H (δ^2H_w), other climatic and plant physiological factors can affect this relationship, including the life-form of the plant itself (i.e trees, shrubs, forbs) (Sasche et al., 2012). Values of δ^2H_l from terrestrial higher plants therefore reflect changes in meteoric water, with the added influence of aspects such as leaf evapotranspiration. To take account of these variations, δ^2H values can be corrected for $\varepsilon_{l/w}$, representing the apparent fractionation between δ^2H_l and δ^2H_w,

and incorporating potential fractionations from soil water evaporation, leaf-water transpiration and biosynthetic fractionation (Sasche et al., 2012).

While δ^2H_l can show a large variation when measured on individual organisms, analysing soil and sediment results in significantly reduced variability, due to spatial and temporal integration in the catchment (Sasche et al., 2012). In these settings, δ^2H_l has been used to reconstruct aspects of the climate such as hydrological changes, air temperature and paleoaltimetry (e.g. Schefuß et al., 2005, Polissar et al., 2009, Feakins et al., 2012).

The δ^2H of n-C_{23} from submerged wetland plants and peat bogs also correlates well with source water (Xie et al., 2000, Nichols et al., 2010). In these cases, the source water from the lake or bog reflects the catchment integrated meteoric water source, but also can be strongly impacted by evaporation (Xie et al., 2000). Particularly in arid regions, evaporative processes result in the δ^2H of the n-C_{23} alkane reflecting temperature and relative humidity, with warmer periods leading to greater bog and lake evaporation and an enrichment in δ^2H_l (Xie et al., 2000, Xie et al., 2004). In non-arid regions, the n-C_{23} of aquatic plants should faithfully record meteoric water. As the δ^2H of long chained n-alkanes from terrestrial higher plants can be affected by leaf evapotranspiration, the difference between the δ^2H of the mid- and long-chained n-alkanes may effectively remove the meteoric water signal and show changes in terrestrial evapotranspiration (e.g. Sasche et al., 2004, Seki et al., 2009).

1.8.2.2 n-Alkane Carbon Isotopes

The $\delta^{13}C$ composition of n-alkanes are described in delta notation:

$$\delta^{13}C = (R_{sample} / R_{standard} - 1) \times 1000 \qquad (Eq. 1.5)$$

Where the standard is Vienna Pee Dee Belemnite, R is $^{12}C/^{13}C$, and $\delta^{13}C$ is described in units of per mil (‰).

The $\delta^{13}C$ of long chain n-alkanes from leaf waxes reflects the $\delta^{13}C$ of its leaf source. The $\delta^{13}C$ value of a leaf is the result of two factors; the isotopic composition of the carbon source, atmospheric CO_2 ($\delta^{13}C_{atm}$), and carbon isotope discrimination by the plant (Farquhar et al., 1989). Plants are depleted in $\delta^{13}C$ relative to $\delta^{13}C_{atm}$ due to enzymatic and physical processes that discriminate against ^{13}C (Marshall et al., 2007). In C_3 plants, the net discrimination by the leaf (Δ) can be described by the relationship:

$$\Delta = a + (b - a) \times p_i / p_a \qquad \text{(Eq. 1.6)}$$

Where a is a fractionation of 4.4‰ caused by the diffusion of CO_2 from the atmosphere into the stomata, b is the photosynthetic fractionation by Rubisco of 27‰, and p_i/p_a is the ratio between the partial pressure of CO_2 in the leaf (p_i) to the atmosphere (p_a) (Farquhar et al., 1989). The p_i/p_a ratio reflects the balance between stomatal conductance and photosynthetic uptake of CO_2, and is considered to be largely controlled by water availability (Farquhar et al., 1989, Marshall et al., 2007). If the $\delta^{13}C_{atm}$ is known or can be estimated, then the magnitude of carbon isotope discrimination (Δ) can be calculated;

$$\Delta = (\delta^{13}C_{atm} - \delta^{13}C_{TT})/(1 + \delta^{13}C_{TT}/1000)$$

$$\Delta \cong \delta^{13}C_{atm} - \delta^{13}C_{TT} \qquad \text{(Eq. 1.7)}$$

Where $\delta^{13}C_{atm}$ represents the carbon isotopic value of the atmosphere, and $\delta^{13}C_{TT}$ refers to the carbon isotopic value of the total plant tissue (Farquhar et al., 1989). To calculate the carbon isotopic value of the total plant tissue ($\delta^{13}C_{TT}$), an enrichment factor must be applied to account for isotopic fractionation between plant tissue and individual n-alkanes (ε_{lipid}). This enrichment factor varies between n-alkane chain lengths, as well as different plants, and commonly n-alkane specific averages from published data will be applied (e.g. Collister et al., 1994, Chikaraishi and Naraoka, 2003, Vogts et al., 2009, Diefendorf et al., 2011).

Values of p_i/p_a and Δ are considered to be largely controlled by water availability (Farquhar et al., 1989, Marshall et al., 2007). Global datasets of Δ show a strong positive correlation with mean annual precipitation (MAP) (Diefendorf et al., 2010, Kohn 2010). However, Δ also demonstrates correlations to other factors including altitude, nutrient concentrations, irradiance, temperature and tree height (e.g. Marshall et al., 2007, Diefendorf et al., 2010, Kohn, 2010, McDowell et al., 2011). Variability is also caused by differences in Δ across different species and plant functional types. Angiosperms discriminate against ^{13}C more than gymnosperms, with $\delta^{13}C_{alkanes}$ from angiosperms ~3-5‰ more depleted than gymnosperm n-alkanes (Chikaraishi and Naraoka, 2003, Diefenforf et al., 2011). Differences in discrimination are also found between deciduous and evergreen plants. For example, globally evergreen angiosperms discriminated against ^{13}C more than deciduous angiosperms by Δ of 1.5‰ (Diefendorf et al., 2010). In general, p_i/p_a and Δ has not been thought to respond to changes in atmospheric pCO_2 in recent observations, laboratory experiments, and from Cenozoic fossil evidence, although this has been a subject of debate (e.g. Polley et al., 1993, Ehleringer and

Cerling, 1995, Arens et al., 2000, Ward et al., 2005, Kohn 2010, Schubert and Jahren, 2012, 2015, Kohn, 2016).

In sediments younger than the Late Miocene, when C_4 plants expanded globally, the $\delta^{13}C$ of long chain n-alkanes in leaf wax can be used to distinguish between vegetation using the C_3, C_4 or crassulacean acid metabolism (CAM) photosynthetic pathways of carbon fixation (Smith and Epstein, 1971, Cerling et al., 1993, Collister et al., 1994). C_3 plants are depleted in ^{13}C relative to C_4 and CAM plants, with plant leaf tissue $\delta^{13}C$ values of ~-25 to -30‰ for C_3 plants, and ~-10 to -16‰ for C_4 and CAM plants (Collister et al., 1994). The relative abundances of plants utilising the different photosynthetic pathways can be related to environmental indicators such as temperature and aridity (Castañeda et al., 2009). The relative contribution from C_3 and C_4 plants to n-alkanes is determined using a binary mixing model between the end member values for each pathway, although different species with the same photosynthetic pathway can have different $\delta^{13}C$ enrichments (Castañeda et al., 2009).

The n-C_{23} alkane is typical of submerged aquatic plants and mosses, such as species of sphagnum (Baas et al., 2000, Ficken et al., 2000, Pancost et al., 2002, Nichols et al., 2006, Bingham et al., 2010). Submerged aquatic plants living in lakes and rivers incorporate carbon differently to emerged plants due to variety of reasons. The source carbon comes from the water surrounding the plant, but dissolved inorganic carbon (DIC) in aquatic environments is not usually in equilibrium with $\delta^{13}C_{atm}$ (Keeley and Sandquist, 1992). Instead DIC can vary depending on factors such as the substrate, whether the water is flowing or standing, and the impact of respired CO_2 from aquatic flora and fauna (Keeley and Sandquist, 1992). Unlike terrestrial plants, submerged aquatic plants do not necessarily incorporate carbon just from CO_2 and may also use carbon from HCO_3^-, which is typically 7-11‰ less negative (Mook et al., 1974, Maberly and Spence, 1983). In submerged plants, the resistance of water to the diffusion of CO_2 can also counteract the photosynthetic discrimination by Rubisco, a process that varies depending on whether the water is standing or flowing, and how fast that flow is (Keeley and Sandquist, 1992). Some of these factors must be known or assumed in order to interpret $\delta^{13}C$ from aquatic plants (Keeley and Sandquist, 1992).

The n-C_{23} alkane can also be sourced from emergent or semi-emergent bryophytes such as mosses (Baas et al., 2000, Pancost et al., 2002, Nichols et al., 2006, Bingham et al., 2010). As bryophytes are non-vascular, they do not have stomata to regulate their CO_2 or water uptake (Rice and Giles, 1996, Williams and Flanagan, 1996). The incorporation of CO_2 is therefore

dependent on whether the plant surface is wet or dry, due to the much lower diffusivity of CO_2 in water than air (Rice and Giles, 1996, Williams and Flanagan, 1996). When plants are covered by a water film they discriminate less against the heavier ^{13}C resulting in less negative $\delta^{13}C$ values. Whereas when plants are dry and diffusion and photosynthetic rates are optimised, the lighter ^{12}C is favoured and a more negative $\delta^{13}C$ values results (Rice and Giles, 1996, Williams and Flanagan, 1996). On the basis of this, the $\delta^{13}C$ on non-vascular plants has been used as a proxy for growth water, although other factors have also been also been found to have an influence of $\delta^{13}C$ in mosses, including temperature, light levels and species specific variation (Ménot and Burns, 2001, Pancost et al., 2003, Ménot-Combes et al., 2004, Bramley-Alves et al., 2015, Bramley-Alves et al., 2016).

1.8.3 Glycerol Dialkyl Glycerol Tetraethers

Glycerol dialkyl glycerol tetraethers (GDGT's) are membrane lipids formed by archaea and some bacteria, and are ubiquitous in oceans, lakes, soils and marine and lacustrine sediments (Schouten et al., 2002, Schouten et al., 2013). Two main types of GDGT's exist, isoprenoid GDGT's (IsoGDGT's), produced by Thaumarchaeota, ammonia-oxidising archaea found in the ocean and lakes, and branched GDGT's (brGDGT's) thought to be produced by soil bacteria (Peterse et al., 2010, Sinninghe Damsté et al., 2011, Schouten et al., 2013).

1.8.3.1 Isoprenoid GDGTs

Thaumarchaeota have been found to increase the number of cyclopentane moieties in the isoGDGTs they produce with increasing water temperature, which allows for isoGDGT's to be used for reconstructions of past lake and ocean temperature (Figure 1.8) (Schouten et al., 2002, Schouten et al., 2013). TEX$_{86}$, the tetraether index of tetraethers consisting of 86 carbon atoms, is a ratio based on the relative abundance of certain IsoGDGT's (Schouten et al. 2002).

$$TEX_{86} = \frac{(\text{GDGT} - 2) + (\text{GDGT} - 3) + (\text{cren}')}{(\text{GDGT} - 1) + (\text{GDGT} - 2) + (\text{GDGT} - 3) + (\text{cren}')} \qquad (\text{Eq. } 1.8)$$

Where GDGT-1, -2, and -3 indicate GDGTs containing 1,2 and 3 cyclopentane moieties, and cren' is the crenarchaeol regio-isomer (Schouten et al., 2002) (Figure 1.8). The number of cyclopentane moieties increases with increasing temperature, usually considered to be mean annual sea surface temperature (SST) or subsurface temperature, or lake temperature (Figures

1.8 and 1.9) (Schouten et al., 2002, Castañeda and Schouten, 2011). The TEX_{86} index excludes GDGT-0 and crenarcheaol as their large abundance has an overpowering influence on the index (Schouten et al., 2002).
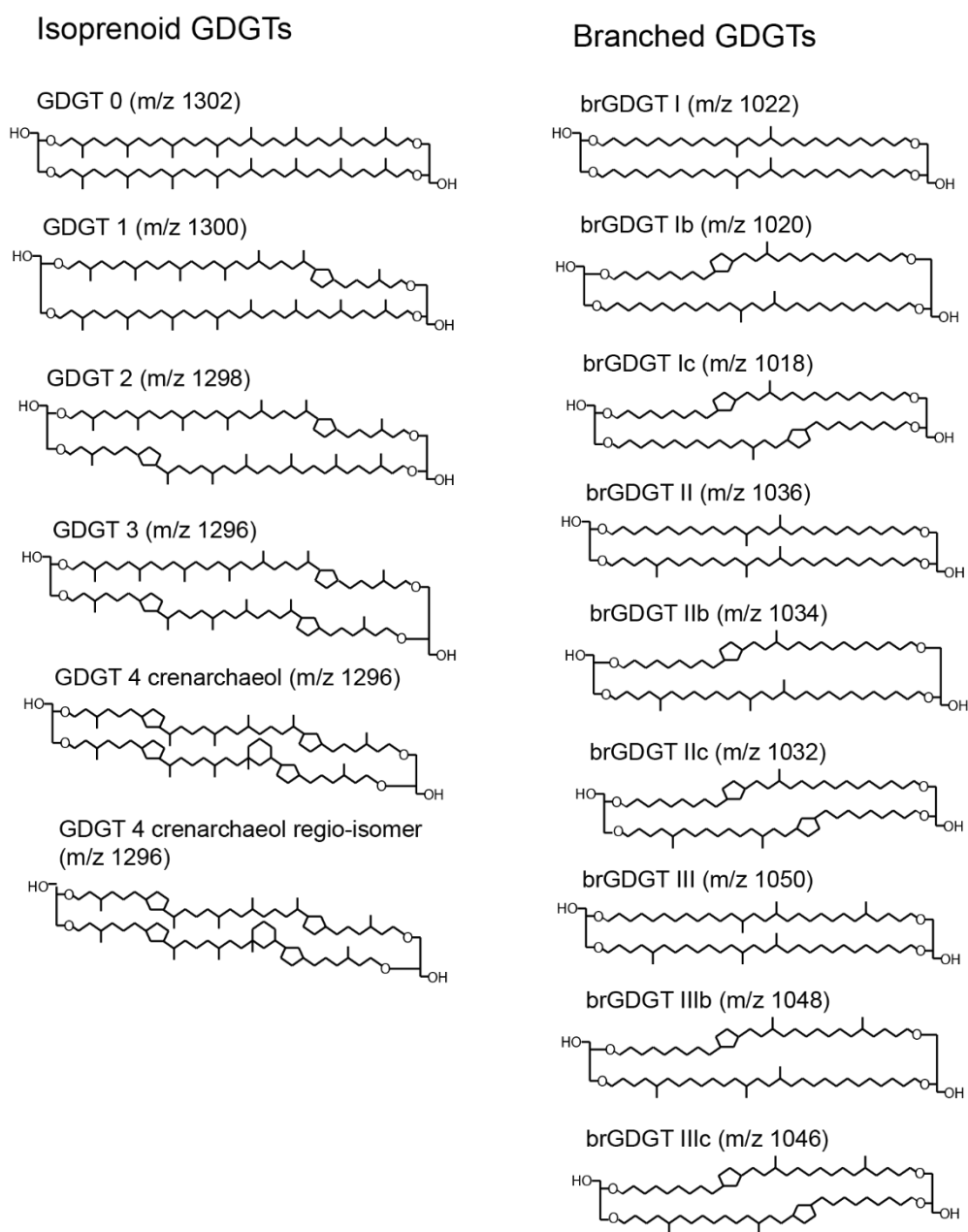
Figure 1.8: Structures of isoprenoid and branched GDGTs.

Early studies found that the relationship between TEX_{86} and SST was linear for temperatures between 5-30°C, but below 5°C (the polar oceans) changes in TEX_{86} were relatively minor

with temperature and the relationship was non-linear (Schouten et al., 2002, Kim et al., 2008). Calibrating TEX_{86} at high latitudes has therefore been challenging. Several different approaches have been taken to address this, including global calibrations which integrate more high latitude data and regional specific calibrations (Kim et al., 2010, Shevenell et al., 2011, Kim et al., 2012, Tierney and Tingley, 2014, 2015). These calibrations are described in detail in Chapter 5.
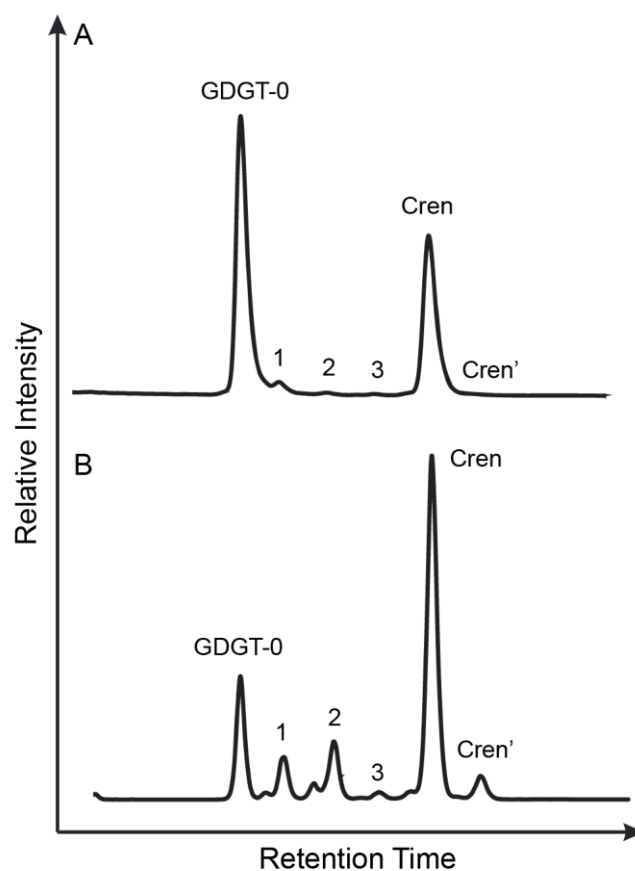
Figure 1.9: Example chromatograms of typical GDGT distributions; A) A cold water site, from the Ross Sea, Antarctica (McKay et al., 2012a), and B) a warm water site, from the Sulu Sea, tropical Pacific Ocean (Zhang et al., 2014). GDGTs are identified by their number and refer to structures in figure 1.8.

Archaeal GDGTs can also be produced in sediments post deposition, as methanotrophic Euryarchaeota, another type of archaea, synthesise GDGTs during anaerobic oxidation of methane (Zhang et al., 2011). This means that methane-rich sediments can exhibit GDGT profiles reflecting a strong contribution from GDGTs produced within the sediment, rather than

those produced in the water column, resulting in a signal that no longer reflects sea surface temperature (Zhang et al., 2011). To take account of this, Zhang et al. (2011) developed the methane index (MI), which quantifies the relative contribution of methanotrophic produced GDGTs to those produced in the water column:

$$MI = \frac{[GDGT-1] + [GDGT-2] + [GDGT-3]}{[GDGT-1] + [GDGT-2] + [GDGT-3] + [Crenarchaeol] + [Cren\ isomer]}$$

(Eq. 1.9)

Where a value of MI ranges from 0-1, with high MI values corresponding to a large production of GDGT's produced within the sediment. As even ocean temperatures of >30°C cannot produce a value >0.3, Zhang et al., (2011) suggests this as a lower limit indicative a significant contribution of GDGT-1, GDGT-2 and GDGT-3 from a source other than normal marine sedimentation.

Several studies have also investigated the impact of methanogenic Euryarchaeota on TEX_{86} in both lacustrine and marine settings, as these archaea can also synthesise GDGT-0, and to a lesser extent GDGT-1, GDGT-2 and GDGT-3 (e.g. Pancost et al., 2001, Blaga et al., 2009, Sinninghe Damsté et al., 2012, Inglis et al., 2015). The impact of these archaea can be described using the ratio of GDGT-0/crenarchaeol (Blaga et al., 2009) or the %GDGT-0 (Sinninghe Damsté et al., 2012):

$$\%GDGT-0 = \left(\frac{[GDGT-0]}{[GDGT-0] + [Crenarchaeol]}\right) \times 100$$

(Eq. 1.10)

When values of GDGT-0/crenarchaeol exceed 2 or %GDGT-0 exceeds 67%, then a sample is considered to contain a substantial input of methanogenic GDGTs (Blaga et al., 2009, Sinninghe Damsté et al., 2012).

When analysing for TEX_{86} in marine environments, one source of error can also be introduced from the addition of GDGT's from terrestrial soils, which when washed out to sea can influence TEX_{86} values (Hopmans et al., 2004). The BIT (branched versus isoprenoid tetraethers) index has been developed as a tracer for terrestrial organic soil carbon, based on the abundance of

branched GDGT's versus the isoprenoid GDGT crenarchaeol which is almost exclusively produced in the marine realm (Hopmans et al., 2004).

$$BIT = \frac{[brGDGT - I] + [brGDGT - II] + [brGDGT - III]}{[brGDGT - I] + [brGDGT - II] + [brGDGT - III] + [Crenarchaeol]} \quad \text{(Eq. 1.11)}$$

This index ranges from 0, representing no branched GDGT input, to 1, representing no Crenarchaeol input (Hopmans et al., 2004).

Qin et al. (2015) found that oxygen content was at least as important as temperature in controlling TEX_{86} values in culture. [GDGT-2] and [GDGT-3] were found to increase relative to [GDGT-1] with increasing O_2 limitation, leading to an elevation in TEX_{86} based temperatures. This indicates that this process could play a significant role in TEX_{86} values at sites underlying oxygen minimum zones, or in records that span low oxygen events. Qin et al. (2015) also found significant variations in TEX_{86} values between different strains of archaea, despite being cultured at the same growth temperatures, suggesting biological variation between strains of archaea. They suggest that a better proxy for temperature could be the Ring Index, originally proposed by Pearson et al. (2004), as they found a linear relationship between Ring Index and temperature for all strains of archaea.

The Ring Index (RI), the weighted average of ring numbers in GDGT compounds, is used in this study as defined by Zhang et al. (2016b):

$$RI = 0 \times [GDGT - 0] + 1 \times [GDGT - 1] + 2 \times [GDGT - 2] + 3 \times [GDGT - 3] + 4 \times [Cren] + 4 \times [Cren']$$

$$\text{(Eq. 1.12)}$$

Where the relative weight of each compound is determined by the number of cyclopentane rings, and each GDGT is represented by its proportion of the total, adding up to 1. While GDGT-0 has a weight of 0 in this equation, it has an impact on the relative abundance of the cyclized GDGTs. Higher values indicate warmer temperatures. The linear relationship between RI and temperature in culture experiments suggests that the RI could potentially be a better proxy for temperature, but no calibrations to absolute temperatures have yet been produced. Analysis by Zhang et al. (2016b) shows that in the modern ocean, TEX_{86} and RI are correlated, and that RI can be calculated from TEX_{86} using a regression.

$$RI_{TEX} = -0.77(\pm0.38) \times TEX_{86} + 3.32(\pm0.34) \times (TEX_{86})^2 + 1.59(\pm0.10) \quad (Eq.\,1.13)$$

If a sample's RI deviates from the calculated RI enough that it does not lie within the 95% confidence interval of the modern regression (±0.3 RI units), then the TEX_{86} values for that sample is considered to be potentially influenced by non-thermal factors and/or deviate from modern analogues. These factors include the impact of GDGTs derived from soil or methanotrophic archaea, or potentially other non-thermal impacts on GDGT biosynthesis such as archaeal growth rates (Zhang et al., 2016b).

Other factors that can bias the TEX_{86} index include seasonality of isoGDGT production and export, and water column biases (e.g. reviews in Schouten et al., 2013, Taylor et al., 2013). For instance, seasonal timing of the production of isoGDGTs varies in different regions, i.e. maximum abundances during winter in the North Sea, to maximum abundances during summer in the Arabian Sea (Huguet et al., 2006, Pitcher et al., 2011). IsoGDGTs are also thought to be exported to the sea floor in faecal pellets primarily from depths of maximum zooplankton grazing. Thaumarchaeota live throughout the water column, but sedimentary isoGDGTs usually reflect a signal from the top 100-200 m of the ocean, likely as this is the predominant depth range grazed by zooplankton (Wuchter et al., 2005). However, the possibility of subsurface isoGDGT export has been highlighted, with a marked difference in TEX_{86} datasets found depending on whether core tops are from shallow or deep (>1000 m) settings (Taylor et al., 2013, Kim et al., 2015). This difference may be attributed to Thaumarcheaota in deeper water producing a different distribution of isoGDGTs, a proportion of which is then incorporated into deep water sites, although this may also vary on a site-by-site basis depending on export dynamics (Taylor et al., 2013, Kim et al., 2015).

A study comparing the latitudinal gradients derived from TEX_{86}^H and alkenone based sea surface temperature proxy $U_{37}^{K'}$ notes that TEX_{86}^H gradients in the early Eocene were unable to be replicated by models, as they consistently produce flat gradients with very warm poles (Ho and Laepple, 2016). It is suggested that this results from TEX_{86}^H overestimating the magnitude of past temperature changes as it reflects the subsurface ocean, but is calibrated to the sea surface, which demonstrates a steeper latitudinal temperature gradient. Ho and Laepple (2016) do not find that separating data by 0-1000 m and >1000 m water depth results in significantly different calibrations in their data set.

1.8.4.2 Branched GDGTs

Branched GDGTs are found in terrestrial soils and have been shown to vary their number of methyl groups and cyclopentane moieties with changes in both soil pH and mean annual air temperature (MAT) (Weijers et al., 2007a). When washed offshore these compounds are also deposited in marine environments. Branched GDGTs differ to archaeal GDGTs as their carbon skeletons are not isoprenoid and are instead branched carbon chains (Weijers et al., 2006a) (Figure 1.8). Branched GDGTs have 4-6 methyl groups, and can contain up to 2 cyclopentane moieties (Weijers et al., 2006a, De Jonge et al., 2013). They are thought to be primarily produced by soil bacteria (Weijers et al., 2006a, Peterse et al., 2010, Sinninghe Damsté et al., 2011).

MBT (Methlyation of Branched Tetraethers) and CBT (Cyclization of Branched Tetraethers) indices were developed to correlate to mean annual temperature and pH, respectively (Weijers et al., 2007a). For the MBT index, temperature dependent membrane changes affect the relative abundance of methyl branches, correlating to MAT and to a lesser degree, soil pH (Weijers et al., 2007a). For CBT, the relative abundance of cyclopentyl moieties is linked to the pH of the soil (Weijers et al., 2007a).

$$MBT = \frac{([I] + [Ib] + [Ic])}{([I] + [Ib] + [Ic]) + ([II] + [IIb] + [IIc]) + [III] + [IIIb] + [IIIc])} \quad \text{(Eq. 1.14)}$$

$$CBT = -\log\left(\frac{([Ib] + [IIb])}{([I] + [II])}\right) \quad \text{(Eq. 1.15)}$$

Where the [I] values refer to the different structures outlined in Figure 1.8.

Wiejers et al., (2007) used a globally distributed soil sample data set to determine relationships between MBT/CBT with MAT and soil pH, with an uncertainty of ~± 1 pH unit and ~5°C.

$$CBT = 3.33 - 0.38 \times pH \quad \text{(Eq. 1.16)}$$

$$MBT = 0.122 + 0.187 \times CBT + 0.020 \times MAT \quad \text{(Eq. 1.17)}$$

Peterse et al., (2012) extended the original calibration dataset and excluded brGDGTs-IIIb and IIIc from the MBT index due to their low abundances, and derived new relationships between MBT/CBT and MAT and soil pH, with a standard error of 0.8 pH units and 5°C.

$$MBT' = \frac{([I] + [Ib] + [Ic])}{([I] + [Ib] + [Ic]) + ([II] + [IIb] + [IIc]) + [III])} \quad \text{(Eq. 1.18)}$$

$$pH = 7.90 - 1.97 \times CBT \quad \text{(Eq. 1.19)}$$

$$MAT = -0.64 + 22.9 \times MBT' \quad \text{(Eq. 1.20)}$$

Local calibrations have also been developed to take account of regional variances. For example, Zink et al. (2016) refined a temperature calibration for the Southwest Pacific, using a modified version of MBT termed MBT_m:

$$MBT_m = \frac{([III] + [IIIb] + [IIIc])}{([I] + [Ib] + [Ic]) + ([II] + [IIb] + [IIc]) + [III] + [IIIb] + [IIIc]} \quad \text{(Eq. 1.21)}$$

$$MAT = -31.664 \times MBT_m + 16.252 \quad \text{(Eq. 1.22)}$$

$$MST = -28.274 \times MBT_m + 19.993 \quad \text{(Eq. 1.23)}$$

Where the root mean standard error is 1.74°C and 1.56°C respectively.

Recently, improved chromatography has allowed better identification and separation of 6-methyl isomers of brGDGTs, which when excluded from calculating MBT' (the MBT'$_{5me}$ index), improves correlation with MAT (De Jonge et al., 2014). 6-methyl brGDGTs correlate strongly with pH, and calculations of pH improve when CBT is calculated using 6-methyl brGDGTs (the CBT' index) (De Jonge et al., 2014). As well as offering a range of new indices and calibrations for MAT and pH, the study of De Jonge et al. (2014) also highlighted that MAT can also still be reconstructed at sites where only the ubiquitous brGDGTs are present, using MAT$_{mrs}$:

$$MAT_{mrs} = 5.58 + 17.91 \times [I] - 18.77 \times [II] \quad \text{(Eq. 1.24)}$$

Where I and II are fractional to the combined abundances of I, II and III. The residual mean standard error using this method is 5°C, and can be applied in settings where the maximum temperature is not expected to exceed 23.5°C.

A study by Peterse et al. (2009) on high latitude MBT/CBT in both soils and fjords found that the influence of *in situ* production of brGDGTs in marine settings vastly overestimated the temperatures produced by MBT/CBT. This can also apply in lakes, where the resulting MBT/CBT reflects a mixture of soil derived and *in situ* branched GDGT (Zink et al., 2010). A further study in a stratified lake setting also found a significant *in situ* brGDGT input, and noted that the production of different brGDGTs varied with dissolved oxygen levels and water depth (Zhang et al., 2016a). Peterse et al. (2009) suggests that MBT/CBT can only be applied in lake and marine environments with significant input from terrestrial sources, such as near river mouths, when using the Weijers et al. (2007a) calibration. However the calibration developed by Zink et al. (2016) is a calibration for a lake environment, and as such, has included a significant input from *in situ* production.

There are other constraints on the application of MBT/CBT indices that still need to be better understood, including the potential for MBT to be biased towards a certain season, the possibility of a contribution from pre-aged material when washed offshore, and the impact of oxic degradation on the proxy (for review see Schouten et al., 2013). When examining ancient sediments the impact of diagenesis and maturation also needs to be taken into account, as brGDGTs containing cyclopentane moieties are thermally less stable, preferentially degrading and leading to biases in reconstructions of MAT and pH (Schouten et al., 2013).

As well as MBT/CBT, other branched GDGT-based temperature calibrations have been developed for mean summer air temperature (MST) using lake sediments. Pearson et al., (2011) developed a global lake calibration for MST, which was found to not be significantly influenced by pH, conductivity or water depth.

$$MST = 20.9 + (98.1 \times GDGT - Ib) - (12.0 \times GDGT - II) - (20.5 \times GDGT - III)$$

(Eq. 1.25)

This calibration has a residual mean standard error of 2.32°C. However, this calibration only contained 6 sites with MST below 5°C and none below 1.5°C, and performed poorly at low temperatures (Pearson et al., 2011). To improve on this, Foster et al., (2016) developed a local calibration for Antarctic and sub-Antarctic lakes, and found a different relationship between brGDGT's and temperature, with a residual mean standard error of 1.45°C.

$$MST = 18.7 + (80.3 \times GDGT - Ib) - (25.3 \times GDGT - II) - (19.4 \times GDGT - III) +$$

$$(369.9 \times GDGT - IIIB)$$

$$(\text{Eq. } 1.26)$$

Chapter 2: Methodology

2.1 Sample collection

Subsamples of sediment from the McMurdo erratics and Mt Boreas were taken from archived samples held by Richard Levy (GNS Science) and Adam Lewis (North Dakota State University), respectively. Samples for CRP 2/2A were obtained from archived samples held at GNS Science while samples from DSDP 270 and 274 were obtained from the IODP core repository at Texas A&M University. Samples from ANDRILL 1B were obtained from the Antarctic Research Facility, Florida State University. Sites sampled for preliminary analysis but not included in Chapters 3 to 5 are discussed in Chapter 6. These include samples from Oliver Bluffs and the Cloudmaker formations supplied by Tim Naish (Victoria University of Wellington), samples from the Friis Hills from Adam Lewis (North Dakota State University) samples of the Pagodroma Group from David Harwood (University of Nebraska-Lincoln) and Marine Plain from Pat Quilty (University of Tasmania). A total of 204 samples were analysed, 38 from terrestrial settings, and 166 from glaciomarine or deep-sea settings.

2.2 Sample preparation for biomarker analysis

Samples for biomarker analysis were prepared, extracted and separated at the Birmingham Molecular Climatology laboratory (BMC), University of Birmingham, United Kingdom (Figure 2.1).

Sample

↓

Freeze dry and homogenise

↓

Ultrasonic Extraction

↓

Total Lipid Extract

↓

Silica gel column chromatography

N1	N2	N3	N4	
↓	↓	↓	↓	↓
Aliphatic hydrocarbons	Aromatic hydrocarbons	Aldehydes and ketones	Alcohols	GDGTs
↓	↓	↓	↓	↓

———— GC, GC/MS, GC/C/IRMS ————   LC/MS
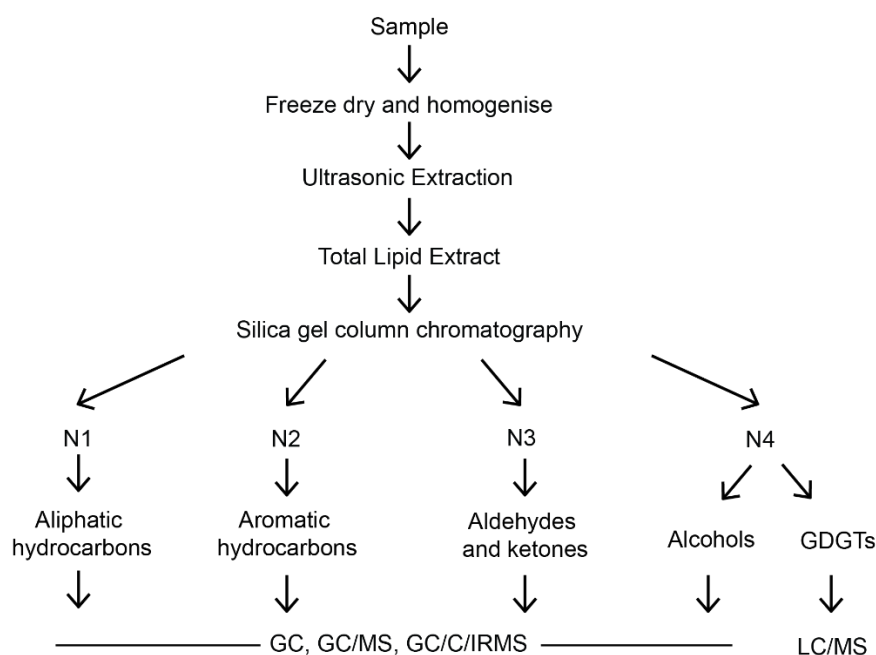
Figure 2.1. Flow chart of the steps involved in sample preparation for biomarker analysis, biomarkers separated by this process and analysis methods.

2.2.1 Homogenisation

Sampling from hyper-arid locations in Antarctica meant that many samples were suitably desiccated. However, any samples that were wet were freeze-dried for 48 hours to remove water from the sediment. Approximately 10 g of sample was then homogenised into a powder using a mixer mill.

2.2.2 Extraction
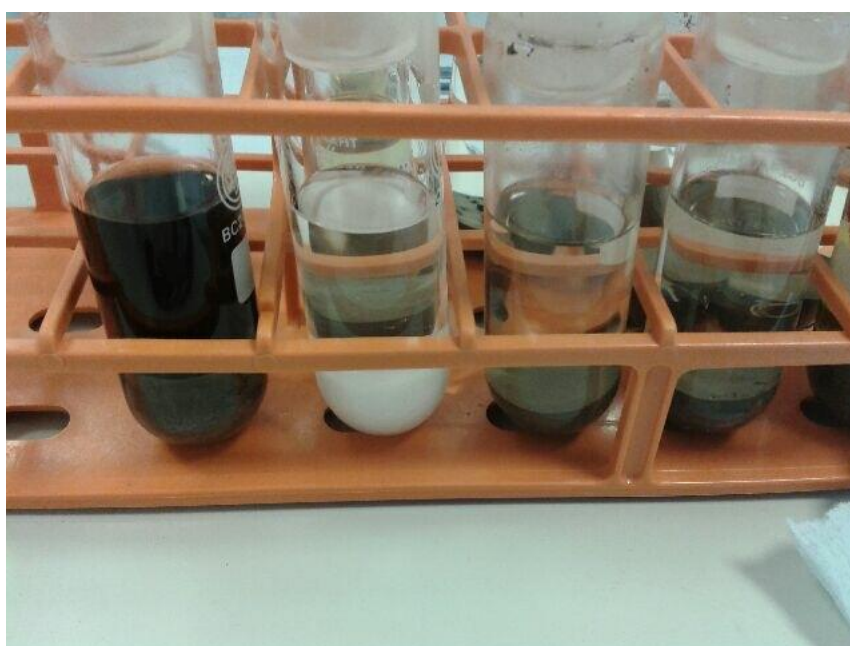
Figure 2.2: Sediment samples during the extraction process. The central white sample is a glass bead 'blank'.

Glassware used in the sample work up was either cleaned by rinsing three times with *n*-hexane followed by three rinses with dichloromethane (DCM), or was washed with detergent, dried and placed in a furnace at 450°C for 8 hours. Organics were extracted from the sediment using ultrasonic extraction. Approximately 10 g of homogenised sediment was placed in a pre-weighed 50ml glass test tube. 20 ml of dichloromethane (DCM):methanol (MeOH) (3:1) was added to the sample, mixed thoroughly using a vortex agitator and then ultrasonicated for 20 minutes (Figure 2.2). The samples were placed in a water bath at 40ºC for an hour, and then centrifuged for 3 minutes at 3000 rpm. The liquid was pipetted using glass pipiettes into separate 500 ml glass test tubes (Figure 2.3) and a further 10 ml DCM:MeOH 3:1 was added

to the sediment. The samples were then agitated and ultrasonicated for 20 minutes before being centrifuged and the liquid decanted off into the same 500 ml test tube. This process was repeated a further 2 times. The resulting total lipid extract (TLE), was then rotor-evaporated, transferred to pre-weighed vials and dried down under a continuous stream of dry nitrogen using a low temperature hotplate. Each batch of samples included a glass bead 'blank' to check for any contamination during the extraction and column chromatography process.

Figure 2.3: Extracted organics before roto-evaporation.

2.2.3 Column chromatography

An aliquot of <20 mg of TLE was eluted through silica gel columns. The silica gel was pre-cleaned by heating in a furnace for 450ºC for 8 hours, and then deactivated with 1 v/v% deionised water. A small amount of glass wool was placed in the bottom of a glass Pasteur pipette. The pipette was filled with 4cm of the prepared silica gel (1.2 g), and then ~4mm of furnaced sea sand. The TLE was redisolved in 500μl of *n*-Hexane:DCM (9:1) and ultrasonicated for 5 minutes. The column was conditioned with 2 ml of *n*-Hexane, then a portion of the TLE equivalent to <20 mg was added to the column. The TLE was eluted through the columns using solvents with increasing polarity: 4 ml of *n*-Hexane, 2 ml of *n*-Hexane:DCM (2:1), 4 ml of DCM, and 5 ml of MeOH (Figure 2.4). This yielded 4 different fractions which were collected in 7ml vials beneath the column:

- N1: Containing aliphatic saturated and unsaturated hydrocarbons i.e. *n*-alkanes.

- N2: Containing aromatic hydrocarbons
- N3: Containing aldehydes, esters and ketones i.e. alkenones.
- N4: Containing alcohols, sterols, fatty acids and GDGTs.

Each of these fractions were transferred to 1.5 ml glass vials, dried down under N_2 and stored. Samples were extracted in three sample runs over the course of the PhD with the initial (BMC numbered samples 1-164) and last (BMC numbers 1450-1473) runs following the above method. The middle run (BMC numbers 397-462) focused on just retrieving *n*-alkanes and GDGTs in two separate fractions, an N1 and N2+N3+N4 fraction. For this run the chromatography was adjusted to the addition of 4 ml of *n*-Hexane to elute the N1 fraction, followed by 5 ml of DCM/MeOH 9:1 to elute the N2+N3+N4 fraction. Fractions were then transferred to 1.5 ml glass vials, dried down under N_2 and stored.

Figure 2.4: The N4 fraction moving through a column.

2.3 Gas chromatography and mass spectroscopy

The N1 and N2 fractions were prepared for analysis by dissolving the fraction in 200 μl *n*-Hexane and ultrasonicating for 5 minutes. An aliquot of 100 μl was removed from the sample and placed into a 200 μl capacity insert in a 1.5 ml vial, and then dried down under a continuous stream of N_2. The remaining 100μl was stored as an archive fraction in a fridge. The sample in the insert was diluted in 10μl of *n*-Hexane in preparation for analysis.

The N3 and N4 fractions were dissolved in 200 μl *n*-Hexane and ultrasonicated for 5 minutes. An aliquot of 100 μl of the N3 fraction and 50 μl of the N4 fraction was placed into a 200 μl capacity insert in a 1.5 ml vial, and then dried down under a continuous stream of N_2. The remaining 100 μl and 150 μl was stored as an archive fraction in a fridge. As the N3 and N4 fractions contain hydroxyl- and carboxyl-functional groups, samples were derivatised before analysing by diluting in 30 μl *n*-hexane and 20 μl N,O-Bis-(trimethylsilyl)-trifluoroacetamide (BSTFA), and heating for 1 hour at 70ºC.

All fractions were analysed using an Agilent 7890B series gas chromatograph (GC), equipped with a 7639ALS autosampler, a BP5-MS column (SGE Analytical Science, 60 m x 0.32 mm x 0.25 μm), and a Flame Ionization Detector (FID), using hydrogen as a carrier gas. Compound separation was achieved by using the following temperature program: the oven was held at 70 °C/1 min, then heated to 120 °C at 30 °C/min, and then to 320 °C with 3 °C/min, where it was held for 20 minutes. Samples were run interspersed with an external standard containing known abundances of certain compounds such as *n*-alkanes to check for column contamination and analytical consistency, and to allow for quantification of *n*-alkanes.

GC-Mass spectroscopy (GC-MS) was performed, to confirm n-alkane identifications, using an Agilent 7890B GC, coupled to an Agilent 5977A MSD. The same capillary column and temperature program as used for GC-FID analyses was also used throughout for consistent compound separation. Helium was used as a carrier gas.

2.3.1 Identification and quantification of *n*-alkanes

n-Alkanes were identified in GC-FID traces by comparison to known *n*-alkanes in the external standard and confirmed using GC-MS data from representative samples. Samples were run in 15 different runs across several years. *n*-Alkane peaks were integrated in Aglient OpenLAB Data Analysis Version A.01.01 - Build 1.93.0. Concentrations of *n*-alkanes were calculated by using the average area and known concentration of the *n*-C_{25} alkane in external standards analysed during the sample run. Across the 15 sample runs the percentage standard deviation for *n*-alkane concentrations averaged 7.6%.

2.4 Liquid chromatography for GDGTs

N4 fractions were filtered using hexane:isopropanol (99:1) through a 0.4 µm PTFE filter (Alltech part 2395), before being dried under a continuous stream of N_2. Samples were then sent to Yale University for analysis by Srinath Krishnan. Samples were redissolved in hexane:isopropanol (99:1), and analysed and quantified on an Agilent single quadrupole Liquid Chromatography/Mass Spectrometer (LC-MS) 6100 series using protocols outlined in Schouten et al. (2007). GDGTs were integrated by myself, using MSD Productivity ChemStation Data Analysis G1701EA E.02.02.1431. Due to frequent low abundances of compounds, some samples were re-run at higher concentrations, and integrations derived from these re-runs were favoured. Samples were integrated multiple times and averaged to account for potential integration variation due to low abundances, with an average TEX_{86} standard deviation of 0.007 between integrations.

2.5 *n*-Alkane compound specific isotope analysis for hydrogen and carbon isotopes

The N1 fractions were sent to the Organic Geochemistry Unit, University of Bristol for determination of the $\delta^{13}C$ and δ^2H values of *n*-Alkanes $n\text{-}C_{23} - n\text{-}C_{31}$.

The $\delta^{13}C$ values were measured in two sample runs. Samples from DSDP 270 (BMC 396-429) were determined using an Isoprime 100 instrument interfaced via a GC5 interface to an Agilent 7890A GC with a split/splitless injector operating in splitless mode (splitless time of 2 minutes). Using Helium as a carrier gas, 1µl of sample was injected on to a Restek column (Rtx-1 50 m x 0.32 mm x 0.17 µm) and analysed with the following temperature program. The temperature was held at 40°C for 1 minute, then increased to 300°C at a rate of 10°C/min and then held at 300°C for 10 minutes. Sample 462 from DSDP 270 and samples from all other sites were analysed in a second sample run using a ThermoQuest Delta Plus XL GC-C-IRMS interfaced via a GCCIII interface to a TracePlus gas chromatograph with an injector in splitless mode (splitless time of 1 minute), and the same instrument conditions described above. The precision for $\delta^{13}C$ determinations was ± 0.3‰ for natural abundance isotope determinations. Duplicate analyses of samples were run, with the average of these analyses used as the value for that sample. In some samples with low concentrations, $\delta^{13}C$ values are based on triplicate measurements.

The δ^2H values were determined using a ThermoFisher Scientific Delta V IRMS interfaced via a GC Isolink Combustion and High Temperature Conversion interface to a Trace GC Ultra, operating in splitless injection mode (splitless time of 1.5 minutes). Using helium as a carrier gas, 0.5µl of sample was co-injected with 0.5µl standard (comprising ethyl decanoate and pentadecane), on to a Phenomenx column (ZB-1 30 m x 0.25 mm x 0.25 µm). The temperature program consisted of an initial temperature of 70°C, held for 1 minute, then ramped to 300°C at a rate of 10°C/min, and then held at 300°C for 8 minutes. The H_3^+ Factor was calculated daily prior to sample analyses and was typically in the range of 1.5-1.8 ppm nA^{-1}. δ^2H values were initially calibrated to two H^2 reference pulses introduced directly into the ion source. All results were subsequently normalised using the equation of linear fit of measured against known δ^2H values for a standard suite of 15 *n*-alkanes (n-C_{16} – n-C_{30}, Schimmelmann Mixture B3, University of Indiana), which was analysed daily prior to every two sample runs. The instrument residual mean standard error was typically less than 5‰, calculated using the same n-alkane standard reference. Duplicate analyses of samples were run, with the average of these analyses used as the value for that sample. In some samples with low concentrations, δ^2H values are based on triplicate measurements.

2.6 Palynology

Palynomorph processing and counting for DSDP 270 was done by Dr Joe Prebble at GNS Science. A subset of samples were processed for palynomorphs in the GNS pollen laboratory. Cold 33% hydrochloric acid was added into ca. 10-15g of dried sample to remove carbonate, while silicate was removed by 24 hours immersion in cold 40% HF, followed by a second cold 33% HCl wash and a brief ultrasonic treatment. All other samples except for two were floated with heavy liquid to remove additional silicates. The fines were removed with 6µm filter and samples were mounted on glass coverslips using glycerine jelly. At least one slide was examined per interval, with a mean dinoflagellates cyst count sum of 165. The ratio of protoperidinoid to all other dinoflagellates cysts was counted, and all protoperidinoid cysts noted. Total palynomorph census counts were done to 300 grains, with any further pollen additionally counted for total pollen species abundances.

2.7 Bulk pyrolysis analysis

Pyrolysis measurements were sent to Dr Todd Ventura at GNS Science for analysis using a Source Rock Analyser from Weatherford Laboratories. Approximately 100 mg of powdered

sediment was used for each bulk pyrolysis sample measurement. The pyrolysis program was set with the sample crucible entering the pyrolysis oven where it was held isothermal at 300 °C for 3 min under a continuous stream of He carrier gas using a 100 ml/min flow rate. This was followed by a 25 °C/min ramp to 650 °C. The S1 and S2 signal intensities were recorded with a Flame Ionization Detector (FID) operated under a 65 ml/min stream of H_2 gas and 300 ml/min air. The pyrolysis cycle was then followed by an oxidation cycle performed at 630 °C for 20 min during which time the oven and crucible were flushed with dry air at 250 ml/min. The generated carbon monoxide and carbon dioxide gases were measured by the instrument's IR cells. All sample sequences were run with three IFP 160000 analytical standard replicates (from Vinci Technologies, Institut Français du Pétrole) placed at the beginning, middle and end of each sample sequence.

Chapter 3: An assessment of n-alkane distributions across a range of depositional environments in Oligocene and Miocene sediments from the Ross Sea region, Antarctica: Implications for use of biomarker proxies in glacially influenced settings.

This chapter explores how the distribution and abundance of n-alkanes varies through a range of depositional environments in Antarctica. n-Alkanes are assessed in a terrestrial outcrop, two glaciomarine drill cores and an ice-distal deep marine drill core. This chapter aims to investigate the contribution of contemporary and reworked n-alkanes into Oligocene and Miocene sediments in the Ross Sea region, and to understand the implications of this for the use and interpretation of biomarker proxies in glacially-influenced settings.

3.1 Introduction

Proxies of climate and vegetation based on biomarkers (molecular fossils preserved in the geological record) are increasingly utilised to reconstruct ancient environments. In Antarctic sediments, traditional microfossil-based methods of reconstructing climate, for example those that use palynomorphs or skeletal remains such as foraminifera can be challenging due to sparse distribution, low diversity of species, or poor preservation in sediments. Biomarkers therefore have the potential to provide environmental proxy information when other methods are challenging or unsuitable. To date, only a few studies have employed biomarkers to investigate paleoclimate changes in Antarctica (i.e. Feakins et al., 2012, McKay et al., 2012a, Pross et al., 2012, Bijl et al., 2013, Feakins et al., 2014, Levy et al., 2016). These studies are all based on offshore core material, and as yet, no biomarker based work has been published on onshore outcrops.

The depositional environment of much of the Antarctic Cenozoic record can present some challenges to the application of biomarkers. Onshore outcrops of Cenozoic age are sparse, and are represented by relatively superficial and poorly-dated deposits of glacially-derived tills, lacustrine and fluvial deposits, with occasional marine and glaciomarine sediments (i.e. Hambrey and Barrett, 1993, Marchant and Denton, 1996, Lewis et al., 2007, Lewis et al., 2008, Lewis and Ashworth, 2016). Sediments from drillcores on the continental margin are usually glaciomarine in origin and provide better-dated records of fluctuating ice sheets periodically overriding the drill site, with ice shelf or open water conditions in between (e.g. Barrett 1989, Naish et al., 2001a, Naish et al., 2009). The variability of lithologies in these sediments and the nature of their deposition mean that reworking of older sediments and associated fossil material

is potentially a significant issue, and one that has been highlighted by previous fossil based work (e.g. Kemp and Barrett, 1975, Askin and Raine, 2000, Prebble et al., 2006a).
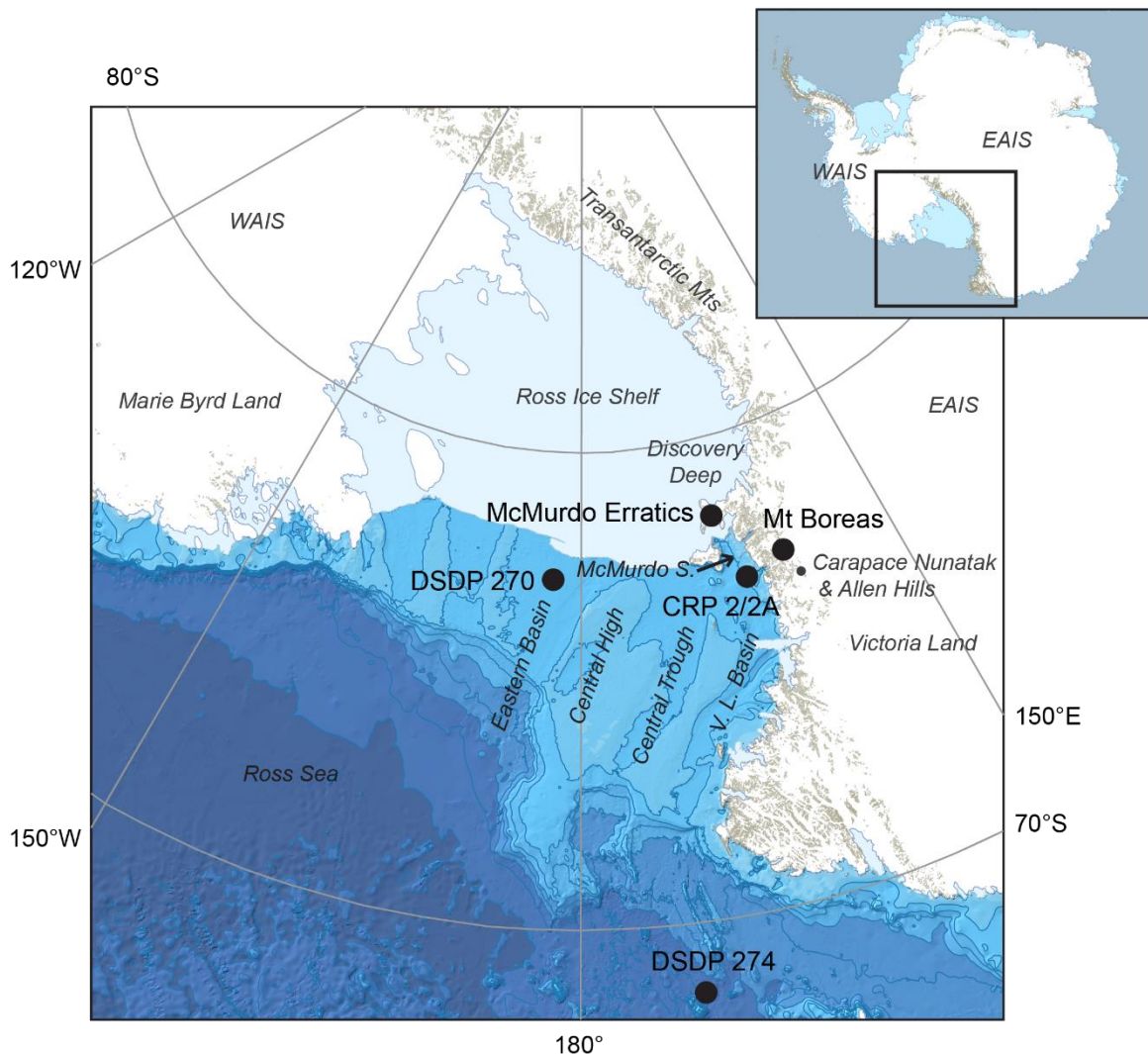
Figure 3.1: Location of sample sites in the Ross Sea region of Antarctica, and features mentioned in this chapter. WAIS: West Antarctic Ice Sheet, EAIS: East Antarctic Ice sheet, DSDP: Deep Sea Drilling Project, CRP: Cape Roberts Project, McMurdo S.: McMurdo Sound, V.L. Basin: Victoria Land Basin. Base map from Quantarctica GIS package, Norwegian Polar Institute.

Here, I used *n*-alkanes to investigate how these compounds vary between different lithologies and depositional environments in Eocene to Late Miocene age Antarctic sediments from the Ross Sea region of Antarctica, and whether *n*-alkane distributions can be used to assess inputs of contemporaneously sourced or reworked biomarkers into a sedimentary deposit. Localities and sediment drill cores have been chosen to sample an array of depositional environments

forming a transit from high elevation terrestrial deposits to the deep sea (Figure 3.1). These include;

i). A Mid-Miocene lacustrine/fluvial sequence from a small mountain glacier catchment at Mt Boreas.

ii). An Oligocene/Miocene glaciomarine sequence in Cape Roberts Project 2/2A drill core sampling a coastal sediment catchment from an EAIS outlet glacier.

iii). An Oligocene/Miocene glaciomarine drill core sequence in DSDP site 270 sampling sediment sourced from now submerged islands and ice caps in the central continental shelf of the Ross Sea, West Antarctica.

iv). An Early Miocene to Late Miocene marine drill core sequence from DSDP 274 from the Western Ross Sea abyssal plain, sampling a wide sediment source catchment from both East and West Antarctica.

3.1.1 *n*-Alkanes

n-Alkanes are ubiquitous across our sample sites. *n*-Alkanes with different carbon chain lengths originate from different biological sources (Section 1.8.1). In sediments, *n*-alkanes represent a mixture of autochthonous inputs from organisms living at the site or in the water column in the case of lacustrine and marine sediments, as well as allochthonous material transported from elsewhere and deposited at the site i.e. by fluvial, aeolian or glacial processes (Grimalt et al., 1985, Madureira and Piccinini, 1999). Once deposited, *n*-alkanes may undergo microbial or geochemical alteration, modifying their distributions (Grimalt et al., 1985). During early diagenesis, odd chained *n*-alkanes in sediments can also be derived from the defunctionalisation of even-numbered fatty acids, alcohols or esters (Tissot and Welte, 1984).

High molecular weight *n*-alkanes can be characterised by their CPI (Eq. 1.1, section 1.8.1). Most plants produce an odd-over-even predominance of long chained *n*-alkanes in their leaf waxes resulting in a CPI of >1 (e.g. Eglinton and Hamilton, 1963). However, CPI varies considerably among modern plants. A survey by Bush and McInerney (2013) of 1722 modern plants found values from 0.1 to 99 across all plant types, with angiosperms demonstrating a higher average CPI than gymnosperms. However, 96% of the samples had a CPI of above 1, thus confirming a CPI of >1 as a reliable threshold value indicative of immature, terrestrial higher-plant material.

A CPI of ~1 is commonly considered to indicate an *n*-alkane distribution altered by diagenesis or catagenesis (Bray and Evans, 1961). This can lead to a range of *n*-alkane distributions depending on the original *n*-alkane distribution of the sediment, as well as the degree of thermal maturity (Tissot and Welte, 1984). However, certain micro-organisims can preferentially produce even *n*-alkanes, also resulting in CPIs of ~1 or >1 (Han and Calvin, 1969, Cranwell et al., 1987). Low CPIs can be the result of *in situ* thermal maturity of sediments, or an input of thermally mature organic matter. Commonly, as smaller chain lengths increase in abundance with increasing catagenesis, *n*-alkanes will show a distribution of decreasing abundance with increasing carbon chain length and a CPI ~1 (Tissot and Welte, 1984). However some crude oils do not display this trend and instead still contain a large amount of long chained *n*-alkanes, sometimes with a CPI >1, potentially due to a largely terrestrial source and extensive microbial reworking (Tissot and Welte, 1984). Some matured sediments will also display a UCM of compounds (Gough and Rowland, 1990, Gough et al., 1992). These can be especially prominent in biodegraded petroleums as UCMs appear relatively resistant to microbial degradation (Gough and Rowland, 1990, Gough et al., 1992). In recent sediments, *n*-alkanes have a lower susceptibility to microbial degradation than most other types of organic matter as they lack functional groups, but studies done on peat bogs and lake sediments suggest that microbial degradation does occur (Meyers and Ishiwatari, 1993, Lehtonen and Ketola, 1993). Shorter chain lengths appear more degradable than longer chain lengths, and microbial degradation can result in a decrease in CPI (Meyers and Ishiwatari, 1993, Lehtonen and Ketola, 1993). The degree of microbial degradation of *n*-alkanes in sediment may also be related to climate, with several studies suggesting that low CPI in peat bogs is coincident with warmer and/or wetter periods when microbial activity increases (e.g. Xie et al., 2004, Zhou et al., 2005, Vogts et al., 2012).

Average chain length (ACL) indicates the dominant *n*-alkane in a given range (Eq. 1.2, section 1.8.1) (Poynter et al., 1989, Schefuß et al., 2003). Variations in ACL are influenced by a number of factors. Studies of plants and aerosols often show a relationship between latitude and ACL. Higher chain length *n*-alkanes are typically more abundant in warmer, tropical regions, whilst lower chain lengths are more common in plants from cooler, temperate regions, suggesting that ACL could in some cases be related to air temperature (Gagosian and Peltzer, 1986, Poynter et al., 1989, Dodd and Afzal-Rafii, 2000, Kawamura et al., 2003, Bendle et al., 2007, Vogts et al., 2009, Bush and McInerney, 2015). Other studies have suggested that aridity

has a strong control on ACL, with the synthesis of longer *n*-alkanes in more arid environments providing plants with a more efficient wax coating to restrict water loss (Dodd et al., 1998, Dodd and Afzal-Rafii, 2000, Schefuß et al., 2003, Calvo et al., 2004, Zhou et al., 2005, Moossen et al., 2015). ACL is also strongly controlled by the contributing vegetation, with large inter- and intra-species variation in *n*-alkane distributions (i.e. Vogts et al., 2009, Bush and McInerney, 2013, Feakins et al., 2016). Variation in average chain length through time therefore likely reflects the interplay of two key factors; climate-driven plastic response of *n*-alkanes to temperature or aridity within a plant community, or changes to the composition of the plant community in response to climate (Bush and McInerney, 2013). When sediments undergo diagenesis or catagenesis, the ACL may change as the distribution of *n*-alkanes responds to varying degrees of microbial or geochemical degradation (Tissot and Welte, 1984).

3.1.2 Geological Setting

The western Ross Sea region of Antarctica is bounded by the TAM, which were uplifted in the early Cenozoic, with the bulk of their exhumation occurring before the early Oligocene (Fitzgerald, 1994, Smellie, 2001). The basement rocks of the TAM are dominated by metasediments and intrusives, formed from the Archean through to the mid-Paleozoic (Section 1.2.1) (Allibone et al., 1993a, Allibone et al., 1993b, Goodge et al., 2002). The Devonian to Triassic Beacon Supergroup overlies this basement (Section 1.2.1) (Barrett, 1981). Lithologies vary through the sequence, with interbedded sandstones, shales, conglomerates and coals interpreted to have been deposited in a paleoenvironmental setting moving from shallow marine to a terrestrial system of lakes, braided rivers and alluvial plains (Barrett, 1981). Throughout the Beacon Supergroup are common plant macrofossils and palynomorphs (Barrett, 1981). In the early Jurassic, as the Gondwana super-continent began to separate, the Beacon Supergroup was intruded by the Ferrar Dolerite, resulting in extensive low grade thermal metamorphism (Barrett, et al., 1986). The Jurassic Ferrar Group also contains extrusive volcanic rocks with fossiliferous sedimentary interbeds containing terrestrial microfossil assemblages (e.g. Ribecai, 2007).

Scattered sedimentary outcrops and the basaltic McMurdo Volcanic Group form the Cenozoic geology of the TAM (section 1.2.2) (Marchant and Denton, 1996, Fielding et al., 2006, Martin et al, 2010). A significant and controversial Cenozoic sedimentary unit distributed throughout the TAM is the Sirius Group, which comprises glacial and non-glacial sediments with well preserved fossil woody vegetation, leaf material and peat beds, deposited in terrestrial and

proximal marine environments (Hambrey and Barrett, 1993, Francis and Hill, 1996, Barrett, 2013). The age of the Sirius Group is debated but is likely diachronous and of Mid-Miocene age or older (Section 1.2.2) (Barrett, 2013). Scattered veneers of glacial tills, colluvium and lacustrine deposits are also dispersed through the TAM, varying from early Miocene to Holocene in age (Section 1.2.2) (Marchant and Denton, 1996, Lewis et al., 2007, Lewis et al., 2008, Lewis and Ashworth, 2015). Glacial erratics of Eocene to Pliocene age are found in the McMurdo region (Sections 1.2.2 and 1.7.4) (Harwood and Levy, 2000).

Much of what is known of Cenozoic climate in Antarctica has been determined by seismic stratigraphy and continental margin drilling (section 1.3). In the Ross Sea region, this has included DSDP Leg 28, CIROS, The Cape Roberts Project and ANDRILL. Continental margin drill cores from the Ross Sea contain successions of subglacial, glaciomarine and marine sediments reflecting the cyclical advance and retreat of the Antarctic Ice Sheets (i.e. Barrett, 1989, Naish et al., 2001, Naish et al., 2009, McKay et al., 2009, Levy et al., 2016). While these records are generally discontinuous in nature, due largely to glacial erosion processes, they do provide more continuous and datable sedimentary successions relative to the on-land records. They have also proven critical to understanding direct Antarctic influences on global climate through the Cenozoic (McKay et al., 2016).

3.1.3 Sample Sites

3.1.3.1 McMurdo erratics

The McMurdo erratics are glacial erratics collected from the Mt Discovery and Minna Bluff region (Figure 3.1, section 1.7.4). The erratics used in this study have been dated on basis of microfossils to be mid-late Eocene in age and contain varying amounts of micro- and macrofossils, from both marine and terrestrial sources (Harwood and Levy, 2000). Their environment of deposition is interpreted as coastal-terrestrial and nearshore marine, under ice-free conditions (Harwood and Levy, 2000).

Pollen records from the McMurdo erratics show a relatively diverse *Nothofagus*-podocarpaceous conifer-proteaceae vegetation onshore during the mid-late Eocene (Askin, 2000). Pollen, together with fossil wood and leaf macrofossils indicate a cool, moist, temperate climate (Askin, 2000, Francis, 2000, Pole et al., 2000). Permian and Triassic spores eroded out of the Beacon Sandstone are also present, and show varying degrees of discolouration as a

result of thermal metamorphism within the Beacon Super Group (Askin, 2000). Extremely rare occurrences of Cretaceous dinoflagellate cysts suggest the possibility for a very minor contribution from an unknown Cretaceous source rock (Askin, 2000).

3.1.3.2 Mt Boreas

Fossil-bearing strata from Mt Boreas in the Olympus Range record the last known vestige of vegetation in the Transantarctic Mountains before the transition from wet-based to cold-based glaciation at high altitudes (1,425 m) in the Dry Valleys (Figure 3.1, section 1.7.1) (Lewis et al., 2008). The basement geology of the Olympus range comprises Beacon Super Group sandstone and Ferrar dolerite (Cox et al., 2012). Overlying this, scattered surficial deposits demonstrate a change from unconsolidated tills, formed by wet-based alpine glaciers, interfingered with lacustrine deposits, to stacked sublimation tills from cold-based alpine glaciers (Lewis et al., 2007). Samples are derived from glacio-lacustrine sediments and fluvial sands and gravels from the wet based glaciation phase, at outcrops near Mt Boreas.

Well-preserved fossils are found in the outcrops, ranging from mosses, a low diversity assemblage of pollen and spores, freshwater diatoms and ostracodes, and rare insect and terrestrial plant remains (Lewis et al., 2008). The dominant moss species is indistinguishable from *Drepanocladus longifolius*, an extant bryophyte from the semiaquatic family Amblystegiaceae (Lewis et al., 2008). The pollen and spore assemblage is low diversity and is dominated by algal cysts. Gymnosperm pollen is absent, but angiosperm pollen is predominantly represented by abundant grains of *Nothofagidites lachlaniae.* The remainder of the palynoflora is comprised of spores of liverwort and mosses (Lewis et al., 2008).

3.1.3.3 CRP 2/2A

Cape Roberts Project core 2/2A was drilled off the Victoria Land coast of Antarctica (77°00.6'S, 163°71.9'E) (Figure 3.1, section 1.7.6) (Cape Roberts Science Team, 1999). This study investigates glaciomarine sequences dating from the late Oligocene/early Miocene section of the core (Naish et al., 2001b, Naish et al., 2008). Provenance studies using sand-grain detrital mode and basement clasts indicate the main basement sources in the sampled section are plutonic rocks from the Granite Harbour Intrusive Complex, quartzose sandstones from the Beacon Supergroup and Ferrar dolerite, with more minor contributions from the

McMurdo Volcanic Group, Kirkpatrick basalts and Proterozoic metamorphic basement (Smellie, 2000, Talarico et al., 2000).

Terrestrial palynomorphs from CRP-2/2A are rare, likely reflecting a sparse periglacial vegetation onshore, and a diluted signal due to rapid sediment accumulation (Askin and Raine, 2000). Contemporaneous assemblages indicate vegetation in the Late Oligocene and Early Miocene was a low diversity herb-moss tundra with low growing scrub dominated by *Nothofagus* and podocarps (Askin and Raine, 2000, Prebble et al., 2006a). While the presence of pollen aggregates and forms restricted to the Oligocene and younger suggests that at least some of the pollen represents coeval vegetation, a reworked component variably contributes to the palynomorph assemblages in this core (Askin and Raine, 2000, Prebble et al., 2006a). Permian-Triassic and rare Jurassic palynomorphs occur throughout the core, with many of these distinguished by their darkened colour, indicating they were derived from thermally altered strata of the Beacon Supergroup. Some Permian palynomorphs were lighter in colour and likely sourced from parts of the Beacon Supergroup distal to the Ferrar intrusives, where thermal alteration was low (Askin and Raine, 2000, Prebble et al., 2006a). Very rare single specimens from Jurassic-lower Cretaceous strata also occur and are likely sourced from palynomorph bearing beds in the Ferrar Group. Sporadic concentrations of Eocene dinoflagellates also highlight reworking of earlier Cenozoic sediment, and pollen associated with higher abundances of Eocene dinoflagellates is considered likely to be predominantly reworked (Prebble et al., 2006a). Contemporaneous and reworked samples show no regular relationship to lithology or facies (Askin and Raine, 2000).

3.3.1.4 DSDP 270

DSDP 270 was drilled on the continental shelf in the Eastern Basin of the central Ross Sea in 1973 and was relogged in 2015 (77°26.48'S, 178°30.19'W) (Figure 3.1, section 1.7.7) (The Shipboard Scientific Party, 1975a, Kraus, 2016). Samples for this study were taken from 20-385 mbsf. The lowermost section, between 385-350 mbsf, is Late Oligocene in age (~25.9 Ma) and consists of graded sandstones interbedded with mudstones, with dispersed clasts varying from rare to common (Chapter 4) (Allis et al., 1975, Kraus, 2016). This unit is interpreted as deposited by turbidites, sourced from the nearby Central High, with a glaciomarine influence (The Shipboard Scientific Party, 1975a, De Santis et al., 1995). Above an unconformity at 350 mbsf is a sequence spanning the Late Oligocene to the earliest Miocene (Chapter 4) (The

Shipboard Scientific Party, 1975a). This section of the core is characterised by a ~100 mbsf interval of glaciomarine mudstone with common clasts, passing up into massive and stratified diamictites, and interstratified sandstones and mudstones between 202-252 mbsf. The interval between 202-124 mbsf consists of massive mudstone with absent to rare clasts, with the section above 124 mbsf dominated by mudstones with dispersed to common clasts (Kraus, 2016). A disconformity is inferred at 112 mbsf, with sediments above this Early Miocene in age (Chapter 4). Clasts throughout the core dominantly reflect a metasedimentary source and are considered to likely be sourced from the proximal basement high, the Central High, and the region between coastal Marie Byrd Land and the Transantarctic Mountains, presently covered by the WAIS (Section 1.4) (Ford and Barrett, 1975, Barrett, 1975).

Pollen in DSDP 270 was originally investigated by Kemp (1975) and Kemp and Barrett (1975). These studies suggest that the lower sampled section (~350-385 mbsf) contains well preserved and abundant spores and pollen, and abundant plant debris, tissue and cuticle fragments in an assemblage considered contemporaneous. Further up the core pollen and spores were found to be less abundant and thought to have a higher likelihood of containing more recycled material. However, samples analysed by Dr Joe Prebble (GNS Science) for this study (Chapter 4) indicate that throughout the core there is almost no indication of early Cenozoic or Permian/Triassic material, supporting the inference by Barrett (1981) that the Beacon Supergroup is largely absent from the basement geology of the Central to Eastern Ross Sea. The assemblages throughout the core are dominated by *Nothofagus*, mainly the *fusca* group, with podocarps and spores of mosses also common. This low diversity assemblage is comparable to contemporaneous Oligocene assemblages in CRP 2/2A (Prebble et al., 2006a) and Oligocene erratics from the McMurdo erratics suite (Askin, 2000).

3.1.3.5 DSDP 274

DSDP 274 was drilled on the lower continental rise in the Northwestern Ross Sea (68°59.81'S, 173°25.64'W) (Figure 3.1, section 1.7.8) (The Shipboard Scientific Party, 1975b). Samples for this study were taken from 90-156 mbsf, spanning lithologic units 2 and 3, and contains an Early Miocene to Late Miocene succession (McCollum, 1975, Crampton et al., 2016). Unit 3 (123-180.5 mbsf) is characterised by diatom-rich silty clay, with beds, lenses and laminae of silt, before grading up into Unit 2 (85.5-123 mbsf), a diatom-rich silty clay with an absence of bedding and a minor component of ferromanganese nodules (The Shipboard Scientific Party,

1975b). An abrupt increase in coarse detritus above an unconformity or condensed section separating Mid-Miocene sediments from Late Miocene sediments at ~113.6 mbsf is considered to indicate an increased ice-rafting component (Frakes, 1975). This coincides with an increase in the biogenic component of the core, a drop in accumulation rate, and an increase in the presence of ferromanganese nodules. These indicate a period of increased winnowing and reworking of the sediment (Frakes, 1975). Ice rafted detritus indicates that ice reaching DSDP Site 274 was sourced dominantly from Marie Byrd Land, with a component from the TAM in the western Ross Sea (Section 1.5) (Barrett, 1975).

Palynological samples suggest that reworked material is an important contributor to assemblages in DSDP 274 (Kemp, 1975). Unit 2 was found to be barren of pollen, possibly due to oxidation, whilst unit 3 demonstrated a sparse assemblage containing dominantly recycled forms of Permian to Paleogene age, although *Nothofagus fusca* and *Nothofagus Brassi* were present (Kemp 1975). However, high abundances of *Nothofagidities lachlaniae* occur in a single concentrated interval in the mid Pliocene section of core not sampled in this study, between 78.19-77.68 mbsf (Fleming and Barron, 1996).

3.2 Methods

n-Alkanes were extracted, separated and analysed following procedures outlined in Chapter 2. Bulk pyrolysis analyses were also undertaken following the protocol described in Chapter 2.

3.3 Results

3.3.1 Facies compilation

In order to compare results between sites, a facies table was developed combining published facies descriptions for each sample site (Table 3.1). The McMurdo erratics have not been included in this table, as the context and relationship between these samples is uncertain. Instead these samples have been labelled by lithofacies, as described by Levy and Harwood (2000). Samples from Mt Boreas have been assigned facies based on descriptions from Lewis et al. (2008). Facies for CRP 2/2A have been developed based on descriptions of Fielding et al. (2000). Facies for DSDP 270 have been assigned using descriptions of Kraus (2016), and based on previous models of glaciomarine facies successions (Fielding et al, 2000, Powell and Cooper, 2002, McKay et al., 2009). For DSDP 274, facies have been determined by using interpretations from The Shipboard Scientific Party (1975b), Frakes (1975) and Whittaker and

Müller (2006). Figure 3.2 provides a schematic representation of the environments of deposition that these facies represent, with each sample site shown in its relative depositional setting.

Integrated Facies Scheme (This Chapter)	Facies codes: Mt Boreas (Lewis et al., 2008)	Facies codes: CRP 2/2A (Fielding et al., 2000)	Facies codes: DSDP 270 (Kraus, 2016)	Facies codes: DSDP 274 (DSDP shipboard party, 1973, Frakes, 1975, Whittaker and Müller 2006)
Facies 1: Siltstone, varying from diatom rich to diatom poor, and from massive to laminated. Contains moss fragments and beds. Lacustrine environment of deposition.	*Lacustrine facies*: Interbeds of massive and laminated diatom-rich to diatom-poor silts containing scattered moss, including a 4 cm bed of moss peat. Basal massive silt interfingers with glacial debris flows. This facies represents two lacustrine phases separated by a period of shallow water when moss colonized the lake basin.			
Facies 2: Fine to coarse sandstone, with planar and trough crossbedding and occasional gravel beds. Fluvial environment of deposition.	*Fluvial facies*: Planar and trough cross-bedded fine to coarse sands with thin gravel beds. Interpreted as fans of sand and gravel derived from streams draining into the lake basin.			
Facies 3: Massive diamictite. Turbid, ice-proximal marine environment of deposition, close to an ice grounding line, but also possibly subglacial.		*Facies 7:* Massive diamictite. Possible environments of deposition are the same as Facies 6, but it is more likely to have been deposited subglacially. Lower contacts are frequently sharp, with loading and deformation, suggesting a glacial surface of erosion.	*Facies 5:* Massive diamictite. This facies is interpreted as being deposited in a highly turbid, ice proximal environment likely close to the ice grounding line.	
Facies 4: Stratified diamictite. Turbid, ice-proximal marine environment of deposition, in the grounding zone,		*Facies 6:* Stratified diamictite. This facies was most likely deposited by debris flows or the rain out of debris from ice in an ice-proximal marine setting. Deposition in a subglacial environment is also possible.	*Facies 6:* Stratified diamictite. This facies was deposited in a turbid, ice proximal environment, likely close to the ice grounding line, but with an influence of oceanic currents.	
Facies 5: Interlaminated sandstone to mudstone. Cyclopels and cyclopsams deposited from turbid plumes in a tidally influenced ice-proximal marine setting.			*Facies 4:* Rhythmically interlaminated sandstone/siltstone with mudstone, with dispersed clasts. Cyclopels and cyclopsams deposited by suspension settling of turbid proglacial sediment plumes in a tidally influenced ice proximal setting.	
Facies 6: Medium- to coarse-grained sandstone varying from massive to stratified. Marine environment of		*Facies 5:* Moderately sorted, clean, stratified or massive medium- to coarse-grained sandstone. Likely		

deposition close to a glaciofluvial/ glaciodeltaic outwash system.		deposited by marine traction currents close to the shoreline of a glaciofluvial/ glaciodeltaic outwash system.		
Facies 7: Muddy, fine- to coarse-grained sandstone. Deposited as turbidite beds in an ice distal marine environment with some sediment contribution from ice rafting.		*Facies 3:* Poorly sorted, muddy, very fine- to coarse-grained sandstone. Deposited from sediment gravity flows in a marine environment, with some sediment contribution from ice rafting.	*Facies 3:* Sandstone interbedded with mudstone with rare to dispersed clasts. Turbidite beds, likely predominantly deposited in an ice distal environment.	
Facies 8: Mudstone. May contain sand and clasts. Varies between massive and weakly to moderately stratified. Ice distal marine environment with some sediment contribution from ice rafting. Stratified intervals may represent more ice-proximal periods.		*Facies 1:* Sandy mudstone and mudstone. Deposited in a low-energy marine environment, with some sediment contribution from ice rafting.	*Facies 1:* Mudstone, predominantly massive with rare clasts. Ice distal marine environment of deposition.	
			Facies 2: Mudstone with weak to moderate stratification and dispersed to common clasts. The environment of deposition is variable but likely reflects a more ice proximal setting than Facies 1. Bedding are very subtle and may be variations in oceanic currents (and thus sediment winnowing) or proximity of an ice sheet grounding line.	
Facies 9: Volcaniclastic lapillistones. Volcanic sediment deposited in a marine environment.		*Facies 12:* Volcaniclastic lapillistones. This facies is the result of a volcanic eruption contemporaneous with sediment accumulation, deposited in a marine environment.		
Facies 10: Diatom-rich mudstone. Deep marine environment of deposition under a weak bottom current regime, including turbidite beds, reduced ice-rafting component.				*Facies 1:* Predominantly diatom-rich clayey-silts and silty-clays. Contains graded turbidite beds and has a higher sedimentation rate than facies 2. Deposited under a regime of relatively weak bottom currents.
Facies 11: Diatom mudstone with clasts and manganese nodules. Deep marine environment of deposition under a strong bottom current regime, with coarse sediment contribution from ice rafting concentrated by winnowing.				*Facies 2:* Diatom detrital silty clay, with common manganese nodules. Lower sedimentation rate than facies 1. Coarse detritus and slow accumulation suggests sediment winnowing as a result of deposition under a strong current regime, with input of coarse sediment from ice rafting.

Table 3.1. Integrated facies scheme used in this chapter developed from previous geological investigations in western Ross Sea and Transantarctic Mountains.
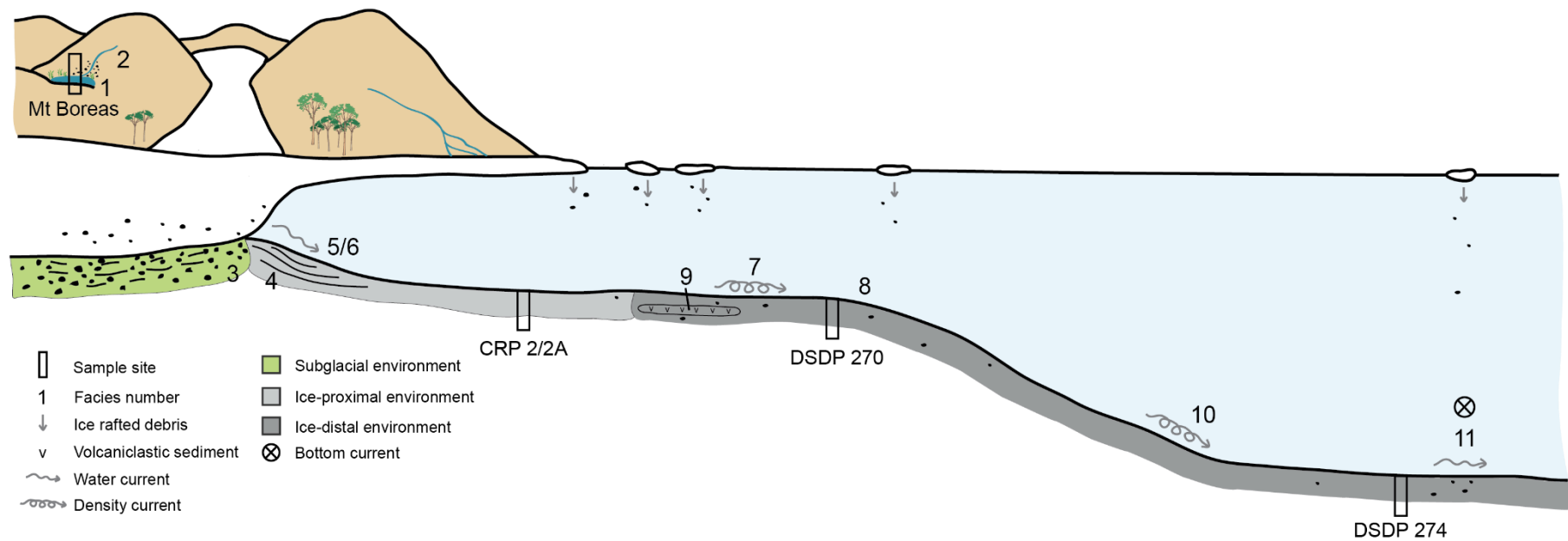
Figure 3.2. Schematic representation of environments of deposition in the Ross Sea Region in the Oligocene and Miocene. Facies descriptions are detailed in table 3.1. Sample sites are placed in their representative depositional setting.

3.3.2 McMurdo Erratics

Six samples of Eocene sediments from the McMurdo erratics suite were analysed for *n*-alkanes. As these samples are from glacial erratics the relationship between samples is uncertain, and the broad age ranges mean that the samples may be both spatially and temporally distinct from one another. The analysed erratics are sourced from a range of lithofacies (Levy and Harwood, 2000) (Table 3.2);

> *Sw*: weakly stratified sandstone, with stratification often indicated by layers of terrestrial organic matter or marine invertebrate fossils. Likely deposited in a nearshore, potentially estuarine or deltaic setting.
>
> *Mmb*: Massive, bioturbated sandy mudstone. Dispersed pebbles or sandy lenses may occur, and terrestrial macroflora or marine invertebrate macrofauna may be present. Likely deposited either within or beyond the offshore transition, and potentially with proximity to a fluvial source.
>
> *Mwb*: Weakly stratified sandy mudstone, with stratification often masked or destroyed by bioturbation. Likely deposited either within or beyond the offshore transition.

Table 3.2: CPI, ACL, n-C_{29}/n-C_{27} and the total abundance of n-alkanes (µg n-alkanes/g TOC) for samples of the McMurdo Erratics. M Eocene: Mid Eocene. M-L Eocene: Mid-late Eocene. LM-M Eocene: late Mid-Late Eocene. Lithofacies codes described in text.

Erratic	Lithofacies	Age	CPI	ACL	*n*-C_{29}/*n*-C_{27}	Total *n*-alkanes (µg/gTOC)
MTD95	sw	M Eocene	2.1	28.5	1.64	738
D1	mwb	M-L Eocene	2.6	28.7	1.58	817
E214	mmb	M-L Eocene	1.8	28.0	1.02	3633
E215	sw	M-L Eocene	1.9	28.0	1.11	390
MB245	mmb	M-L Eocene	3.1	27.9	1.18	930
E219	mmb	LM-M Eocene	5.5	28.0	1.01	1533
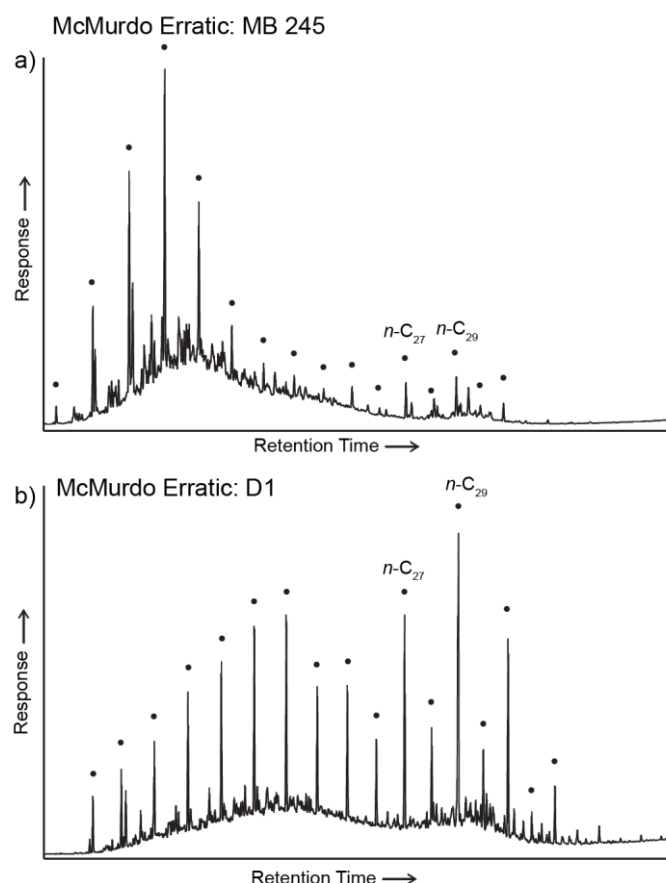
Figure 3.3. Representative GC chromatograms of two samples of the McMurdo erratics. Filled circles above peaks indicate n-alkanes, with the n-C$_{27}$ and n-C$_{29}$ labelled. UCM: unresolved complex mixture.

Three of the samples (E214, MB245 and E215) were dominated by short chained n-alkanes in the n-C$_{17}$ to n-C$_{20}$ range, underlain by a UCM (Figure 3.3). Samples D1, E219 and MTD95 were dominated by mid-long chained n-alkanes, and displayed small UCMs underlying the mid-chain lengths (~n-C$_{20}$ to n-C$_{23}$) and long-chain lengths (centred ~n-C$_{29}$) (Figure 3.3). In all samples, n-C$_{29}$ is the dominant n-alkane, in contrast to younger strata investigated in this study (see below) which are usually dominated by n-C$_{27}$. The ratio between these two chain lengths has been described at all sites to investigate its variance at other, younger, sediment localities. The CPI from the McMurdo Erratics ranges from 1.8 to 5.5, averaging 2.8. ACL varies from 27.9 to 28.7, averaging 28.2, whilst the ratio of the n-C$_{29}$ n-alkane to n-C$_{27}$ ranges from 1.01 to 1.64, with an average of 1.26. The erratics typically contain relatively abundant n-alkanes, with total abundances ranging from 390 µg/gTOC to 3633 µg/gTOC, at an average of 1340 µg/gTOC. Unlike other analysed sites, due to uncertainties in the relationship between samples, the erratics have not been compared by linear regression analysis or lithofacies groupings.

68
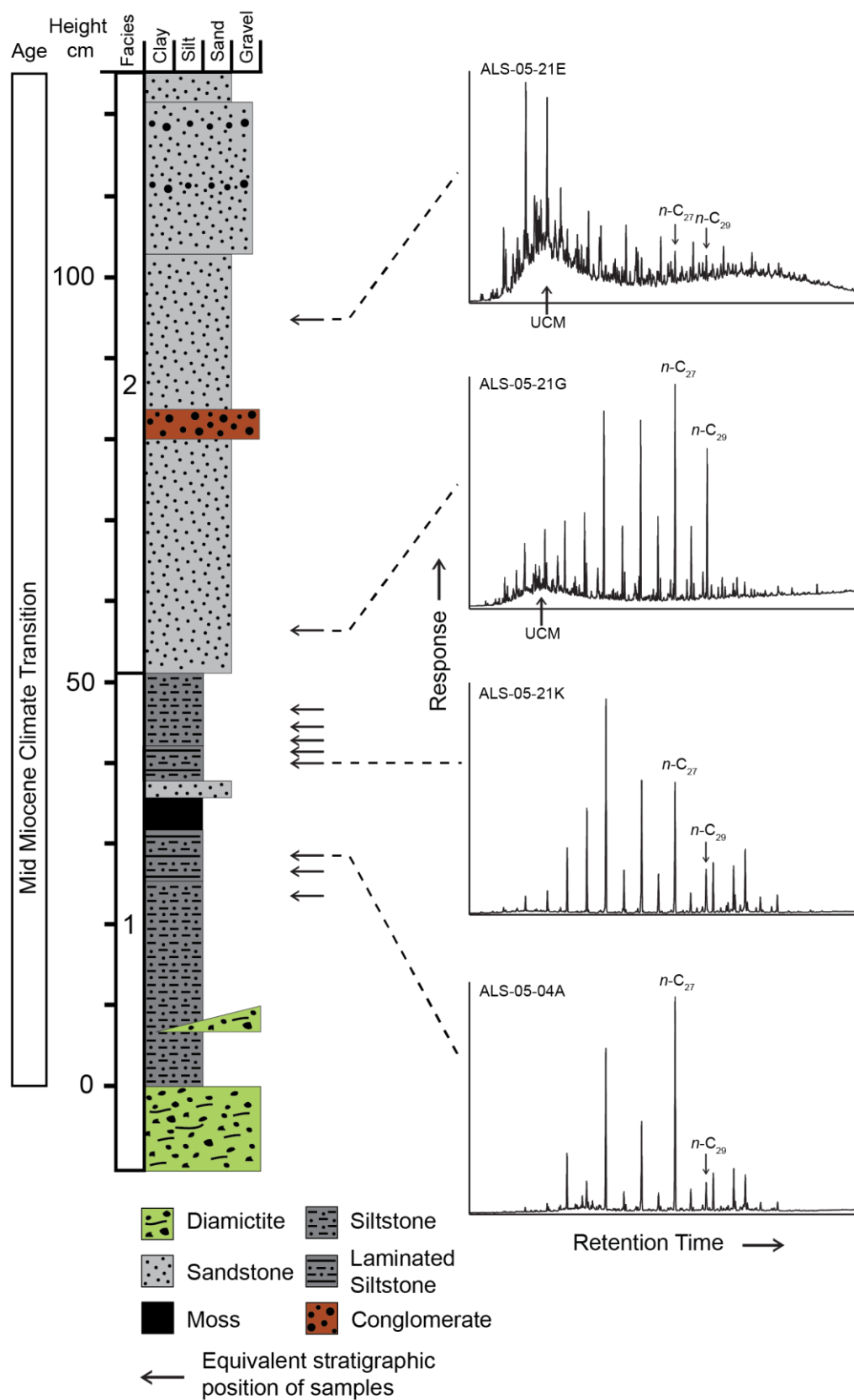
3.3.3 Mt Boreas

Figure 3.4. Stratigraphic column from a site at Mt Boreas (after Lewis et al., 2008) with the equivalent stratigraphic positions of representative GC chromatograms of samples. The n-C_{27} and n-C_{29} are labelled. Facies numbers are described in table 3.1. UCM: unresolved complex mixture.

Samples from Mt Boreas are typically dominated by long chained *n*-alkanes, with *n*-C_{23}, *n*-C_{25} and *n*-C_{27} the dominant *n*-alkanes present (Figure 3.4). Sample ALS-05-21E is the exception, with *n*-C_{19} and *n*-C_{20} demonstrating a greater abundance than the long chained homologs. Some samples display a small UCM underlying ~*n*-C_{19} to *n*-C_{20}, with sample ALS-05-04C showing a small UCM underlying the longer chain lengths centred at ~*n*-C_{31}. Samples were collected from three different sites, but were collected from units that are correlatable to the stratigraphic column shown in Figure 3.4 (Lewis et al., 2008). The total abundance of *n*-alkanes at these sites varies considerably from sample to sample, with a range of 4.5 μg/gTOC to 762 μg/gTOC, at an average of 206.5 μg/gTOC. Two samples taken from the same location west of the main stratigraphic column site contain significantly less *n*-alkanes than the samples from the other two sites (4.5 and 6.6 μg/gTOC). The CPI of the long chained *n*-alkanes ranges from 1.7 to 5.9 and averages 3.4, whilst ACL varies from 26.2 to 27.4, and averages 26.9. The ratio of the *n*-C_{29} *n*-alkane to *n*-C_{27} varies from 0.15-0.97, averaging 0.55, indicating that the *n*-C_{27} dominates the *n*-C_{29} in all samples from these sites.

Linear regression analysis of each *n*-alkane variable compared to other *n*-alkane variables from these sites indicates that only two variables demonstrate a statistically significant correlation to each other; the ratio of *n*-C_{29}/*n*-C_{27} typically decreases with increasing CPI (r =0.711, p =0.0096) (Figure 3.5). There is no statistically significant correlation between the total amount of *n*-alkanes in a sample (μg/gTOC) and CPI, ACL or *n*-C_{29}/*n*-C_{27}.

Samples from fluvial Facies 2 typically display lower CPI, and higher ACL and *n*-C_{29}/*n*-C_{27} values than those from lacustrine Facies 1, although it is noted that Facies 2 is only represented by two samples (Figure 3.6). Both fluvial and lacustrine samples show similar average total abundances of *n*-alkanes, with samples in the lacustrine Facies 1 showing a spread from high to very low values.
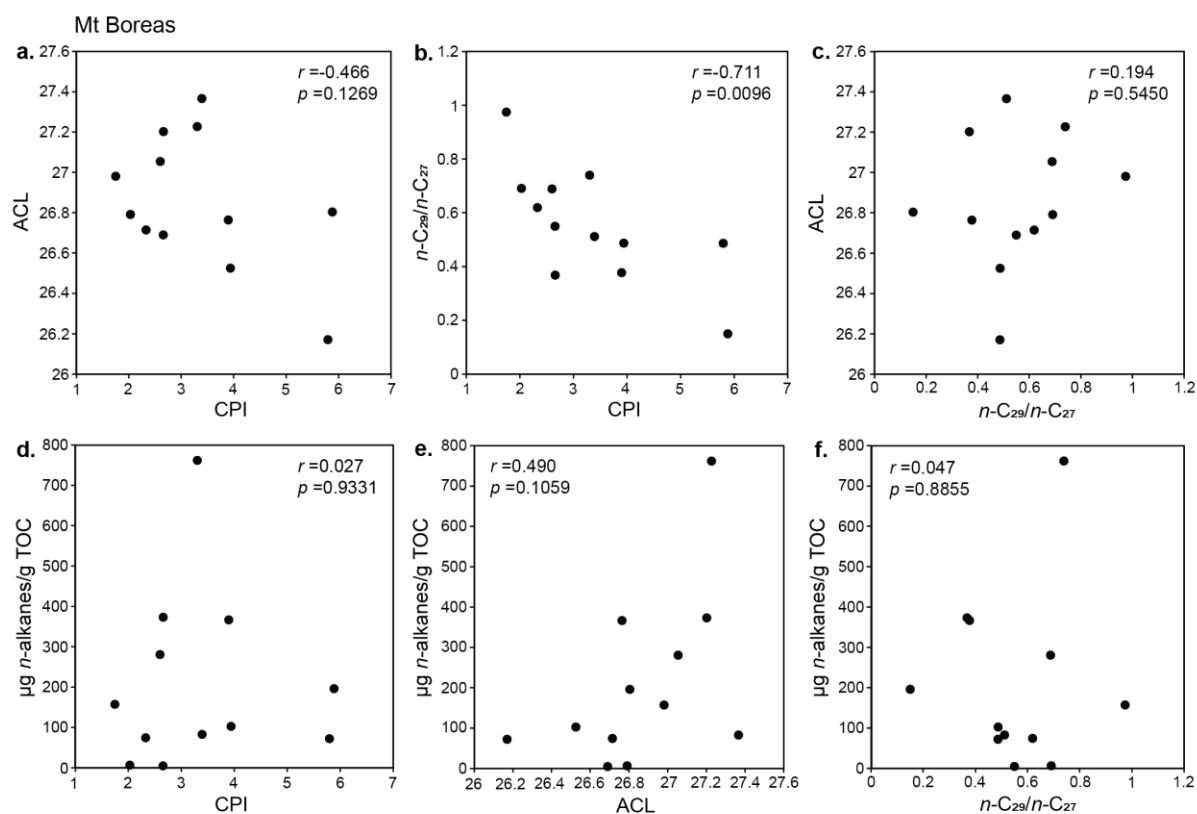
Figure 3.5. Scatter plots from samples from Mt Boreas; a) CPI and ACL; b) CPI and n-C$_{29}$/n-C$_{27}$; c) n-C$_{29}$/n-C$_{27}$ and ACL; d) CPI and the total abundance of n-alkanes (µg n-alkanes/g TOC); e) ACL and the total abundance of n-alkanes (µg n-alkanes/g TOC) and f) n-C$_{29}$/n-C$_{27}$ and the total abundance of n-alkanes (µg n-alkanes/g TOC).
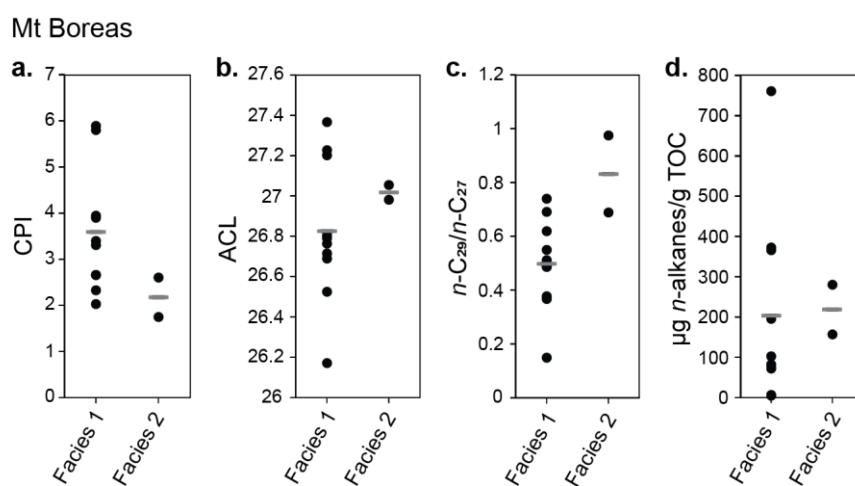
Figure 3.6: Distributions of n-alkane variables across different facies from Mt Boreas; a) CPI, b) ACL, c) n-C$_{29}$/n-C$_{27}$ and d) the total abundance of n-alkanes (µg n-alkanes/g TOC). Grey bars represent average values for each facies. Description of facies in table 1.

3.3.4 Cape Roberts Project 2/2A
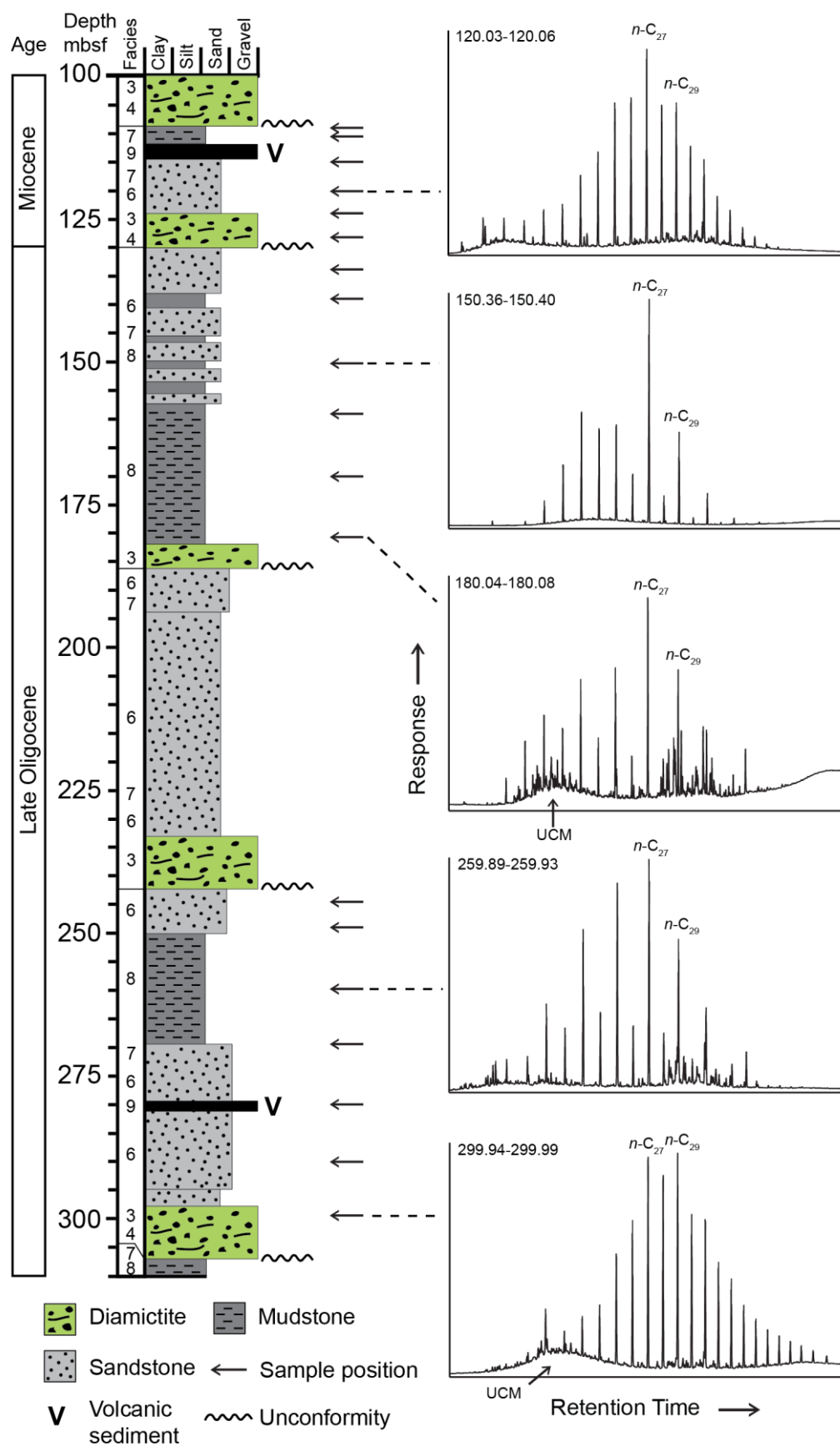
Figure 3.7. Stratigraphic column from CRP 2/2A with the stratigraphic positions of representative GC chromatograms of samples. The n-C_{27} and n-C_{29} are labelled. Simplified facies groupings are labelled, and are described in table 3.1. UCM: unresolved complex mixture.

Long chained n-alkanes typically dominate samples from CRP 2/2A (Figure 3.7). The n-C_{23}, n-C_{25} and n-C_{27} are usually the most abundant homologs, with n-C_{27} often the most prominent of these. In some samples n-alkanes are superimposed on a UCM, which is usually centred between n-C_{19} and n-C_{23}. The total abundance of n-alkanes is highly variable from sample to sample, ranging from 16.5 µg/gTOC to 1893.0 µg/gTOC, averaging 197.2 µg/gTOC. CPI also varies over a wide range, from 1.2-5.5, averaging 2.6, whilst ACL ranges from 26.7-28.7, averaging 27.7. The ratio of the n-C_{29} n-alkane to n-C_{27} varies from 0.25-1.02, and averages 0.67.
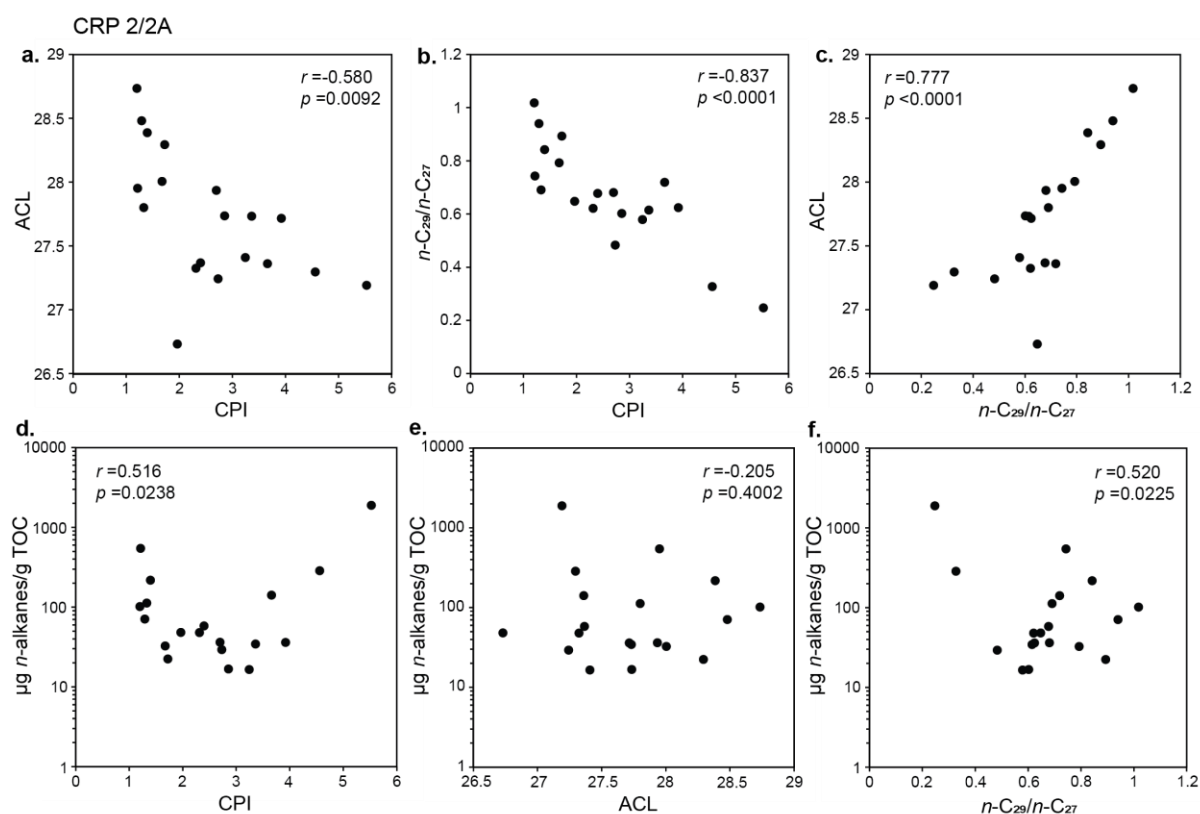
Figure 3.8. Scatter plots from samples from CRP 2/2A; a) CPI and ACL; b) CPI and n-C_{29}/n-C_{27}; c) n-C_{29}/n-C_{27} and ACL; d) CPI and the total abundance of n-alkanes (µg n-alkanes/g TOC); e) ACL and the total abundance of n-alkanes (µg n-alkanes/g TOC) and f) n-C_{29}/n-C_{27} and the total abundance of n-alkanes (µg n-alkanes/g TOC).

Linear regression analysis shows statistically significant correlations between several n-alkane variables. The strongest correlations exist between CPI and n-C_{29}/n-C_{27} ($r =0.837$, $p <0.0001$) and ACL and n-C_{29}/n-C_{27} ($r =0.777$, $p <0.0001$), with a weaker correlation between CPI and ACL ($r =0.580$, $p =0.0091$). Figure 3.8 shows that at both high and low values of CPI and n-C_{29}/n-C_{27}, the total abundance of n-alkanes increases, with weak correlations between these variables ($r =0.516$, $p =0.0238$ and $r =0.520$, $p =0.0225$ respectively). No correlation exists between ACL and the total abundance of n-alkanes in a sample.
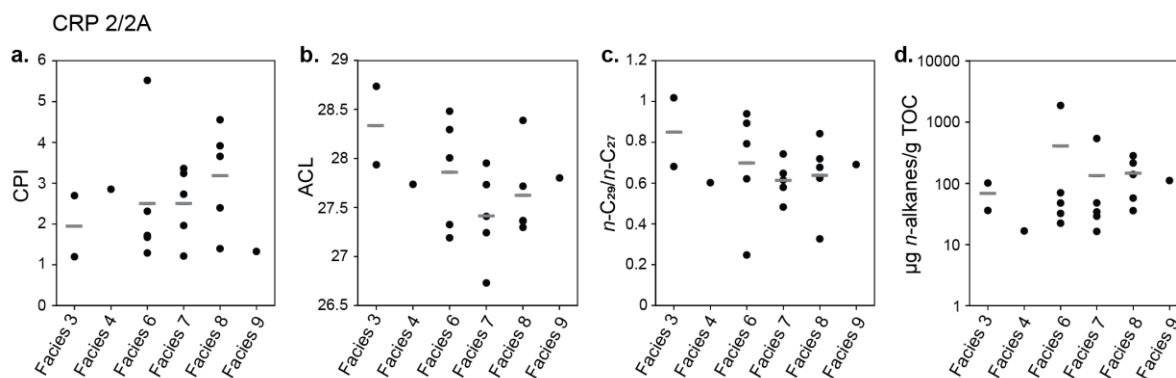
Figure 3.9: Distributions of n-alkane variables across different facies from CRP 2/2A; a) CPI, b) ACL, c) n-C_{29}/n-C_{27} and d) the total abundance of n-alkanes (µg n-alkanes/g TOC). Grey bars represent average values for each facies. Description of facies in table 3.1.

When samples are grouped by facies, there is a considerable amount of intra-facies variability (Figure 3.9). Most facies contain a range of both high and low values of CPI, with the highest average CPI in the low-energy marine mudstones of facies 8. Facies 6, 7 and 8 also have broad ranges of ACL and n-C_{29}/n-C_{27}, with the lowest average ACL and n-C_{29}/n-C_{27} in the poorly sorted sandstones of facies 7, while facies 3, consisting of massive diamictites, has the highest average ACL and n-C_{29}/n-C_{27}. Two samples containing a much higher concentration of n-alkanes than other samples in the facies skew the averages for facies 6 and 7. Without these outliers, facies 8 contains the highest average total abundance of n-alkanes.

3.3.4 DSDP 270
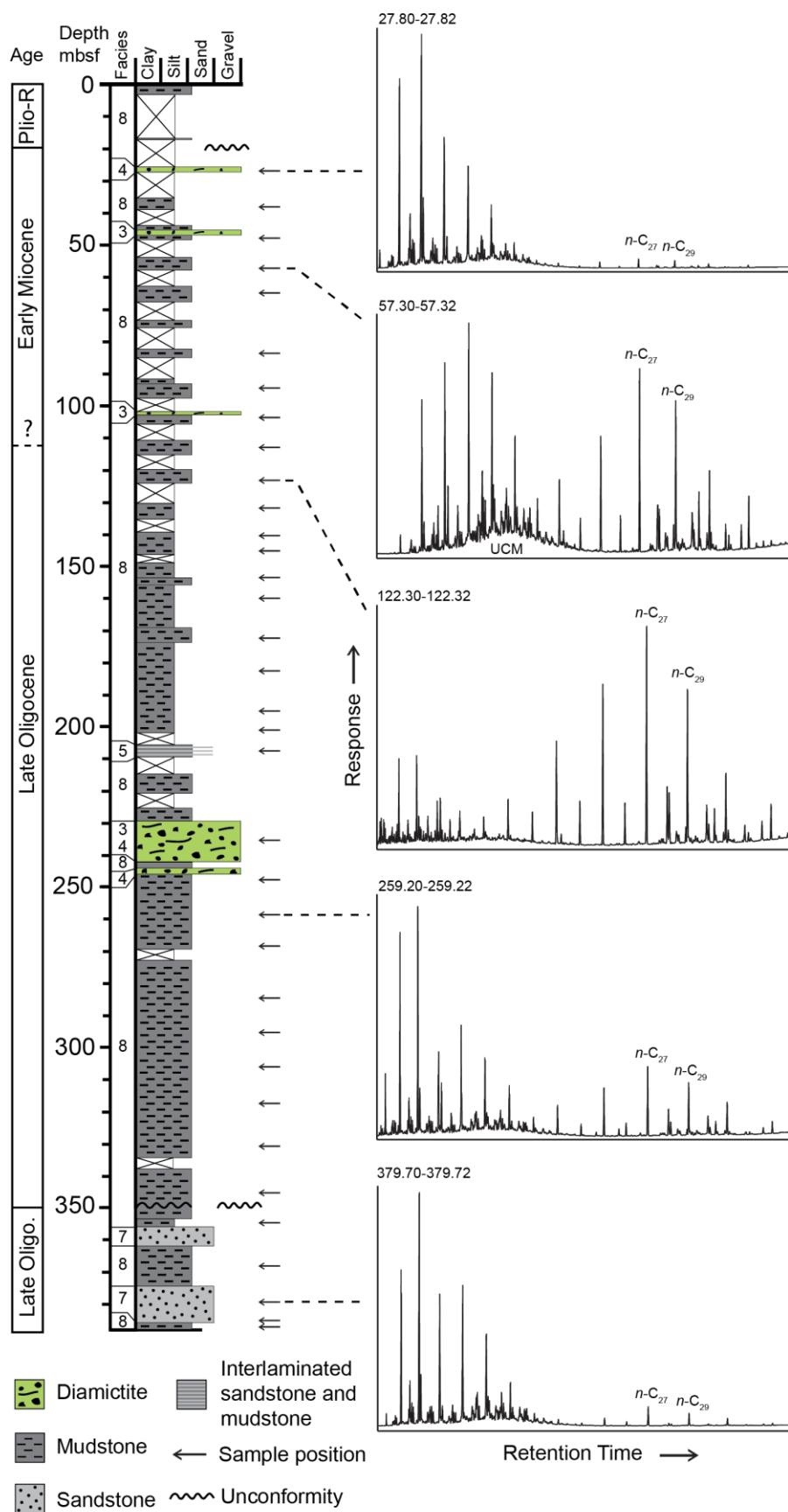
Figure 3.10. Stratigraphic column from DSDP 270 with the stratigraphic positions of representative GC chromatograms of samples. The n-C$_{27}$ and n-C$_{29}$ are labelled. Simplified facies groupings are labelled, and are described in table 3.1. UCM: unresolved complex mixture.

Samples from DSDP 270 typically display bimodal *n*-alkane distributions with a peak at *n*-C$_{17}$ or *n*-C$_{19}$ and another peak *n*-C$_{27}$ (Figure 3.10. The short chained *n*-alkanes are usually more abundant than the long chained homologs, and in four samples from the lowest sampled section of the core, long chained *n*-alkanes were not detected. Some samples display a small UCM underlying ~*n*-C$_{20}$ and *n*-C$_{21}$. CPI of the long chained *n*-alkanes ranges from 2.4-4.8 and averages 3.4. ACL varies from 27.6-28.1, averaging 27.9, whilst the ratio of *n*-C$_{29}$ to *n*-C$_{27}$ ranges from 0.65-0.86, averaging 0.76. The sample with the lowest total abundance of *n*-alkanes (6.9 µg/gTOC) is considerably less than the next lowest (139.4 µg/gTOC), with the rest of the samples ranging in abundance up to 8684.7 µg/gTOC, and averaging 743.4 µg/gTOC.
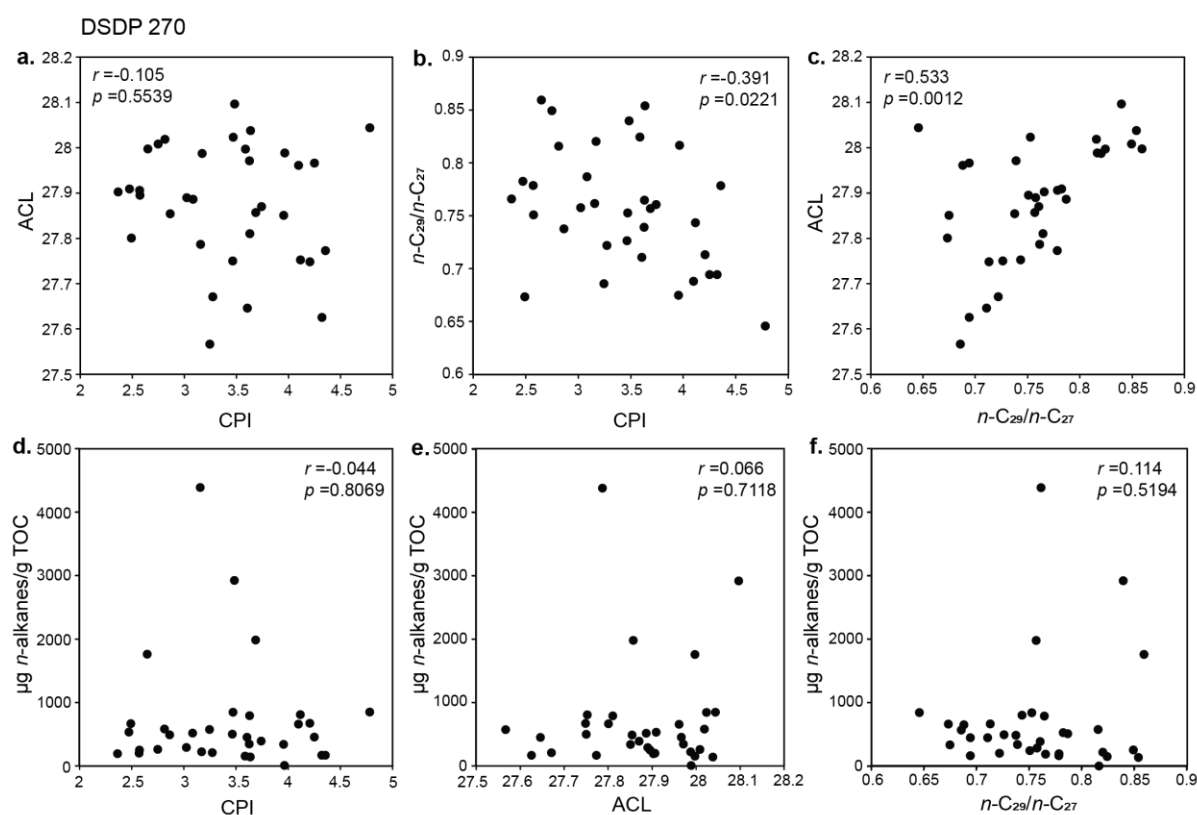
Figure 3.11. Scatter plots from samples from DSDP 270; a) CPI and ACL; b) CPI and n-C$_{29}$/n-C$_{27}$; c) n-C$_{29}$/n-C$_{27}$ and ACL; d) CPI and the total abundance of n-alkanes (µg n-alkanes/g

TOC); e) ACL and the total abundance of n-alkanes (µg n-alkanes/g TOC) and f) n-C$_{29}$/n-C$_{27}$ and the total abundance of n-alkanes (µg n-alkanes/g TOC).

Linear regression analysis of *n*-alkane variables find no particularly strong correlations, with only two correlations considered statistically significant. Increasing *n*-C$_{29}$/*n*-C$_{27}$ with decreasing CPI is very weakly correlated (r =0.391, p =0.0221), with a slightly stronger correlation existing between decreasing *n*-C$_{29}$/*n*-C$_{27}$ with decreasing ACL (r =0.533, p =0.0012) (Figure 3.11). No correlation exists between total abundance of *n*-alkanes and CPI, ACL or *n*-C$_{29}$/*n*-C$_{27}$.
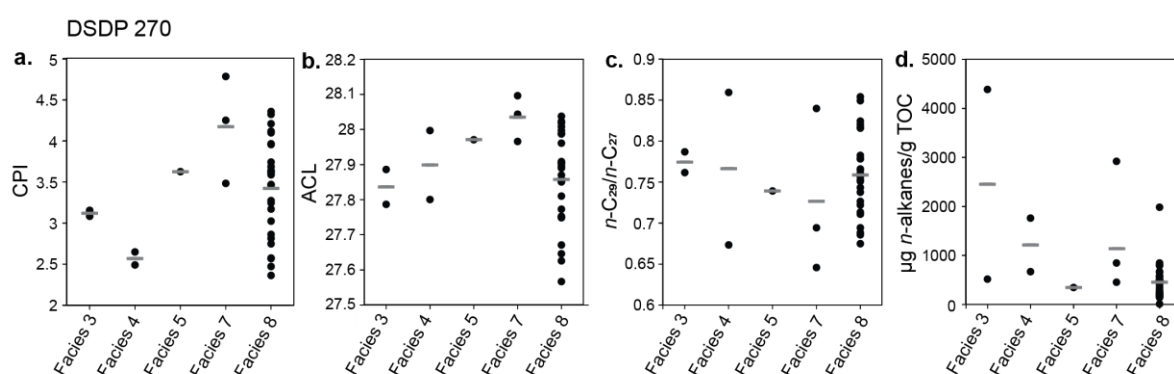
Figure 3.12: Distributions of n-alkane variables across different facies from DSDP 270; a) CPI, b) ACL, c) n-C$_{29}$/n-C$_{27}$ and d) the total abundance of n-alkanes (µg n-alkanes/g TOC). Grey bars represent average values for each facies. Description of facies in table 3.1.

When grouped by facies, facies 7 demonstrates the highest average CPI, and facies 4 contains the lowest average CPI (Figure 3.12). Facies 7 shows the highest average ACL and lowest average *n*-C$_{29}$/*n*-C$_{27}$, but most facies display similar ACL and *n*-C$_{29}$/*n*-C$_{27}$ values. Most facies also contain a similar total abundance of *n*-alkanes, with the highest average abundance in facies 3, although this is skewed by one of the two samples which represent this facies containing a particularly high amount of *n*-alkanes.

3.3.5 DSDP 274
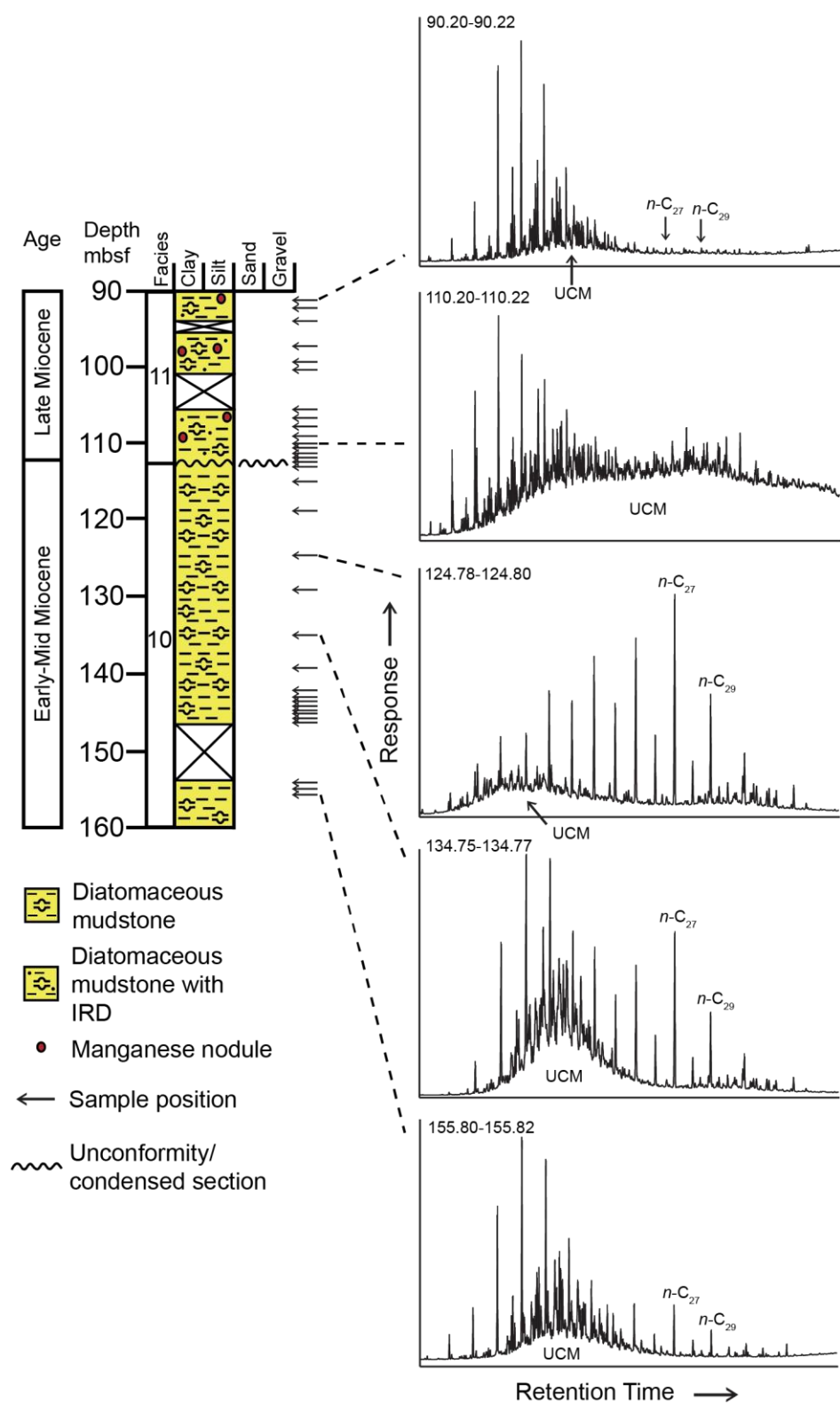
Figure 3.13. Stratigraphic column from DSDP 274 with the stratigraphic positions of representative GC chromatograms of samples. The n-C₂₇ and n-C₂₉ are labelled. Facies are described in table 3.1. UCM: unresolved complex mixture.

Samples taken from above 115m had variable, or even absent, quantities of *n*-alkanes (Figure 3.13). Samples usually contained significant UCMs, which typically dominated the signal, and *n*-alkanes did not display a common dominant *n*-alkane. Some samples displayed an extensive suite of *n*-alkanes, while in other samples *n*-alkanes were restricted to either short or long chain lengths. Samples from the bottom of unit 2, below 115m, and from unit 3 are usually bimodal in distribution, with a peak in short chained *n*-alkanes around n-C_{19}, n-C_{20} or n-C_{21}, underlain by a UCM, and another peak centred around n-C_{27}. CPI ranges from 0.6 to 3.0, averaging 1.6, whilst ACL ranges from 25 to 31.0, with an average of 27.8. The ratio of n-C_{29} to n-C_{27} varies from 0.50 to 1.37, averaging 0.80. The total abundance of *n*-alkanes averages 72.7 μg/gTOC, with a range of 2.7 μg/gTOC to 316.6 μg/gTOC.
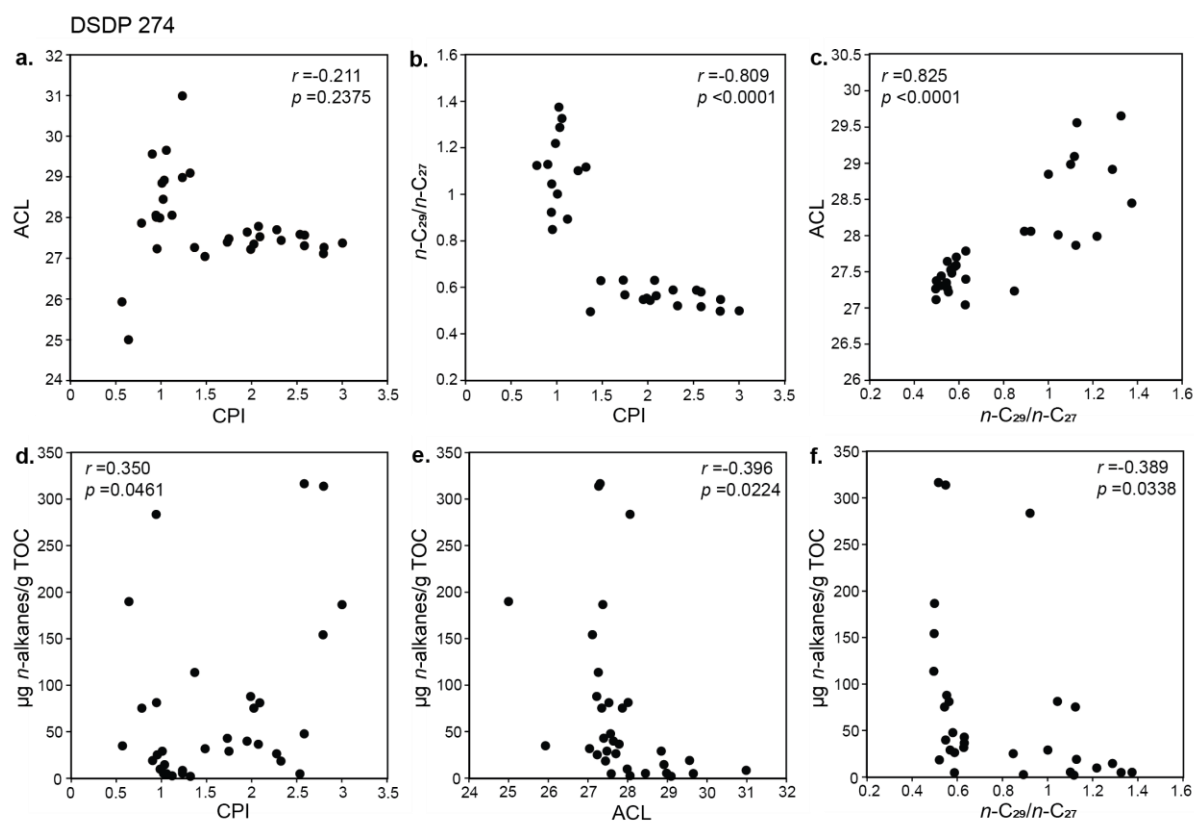
Figure 3.14. Scatter plots from samples from DSDP 274; a) CPI and ACL; b) CPI and n-C₂₉/n-C₂₇; c) n-C₂₉/n-C₂₇ and ACL; d) CPI and the total abundance of n-alkanes (μg n-alkanes/g TOC); e) ACL and the total abundance of n-alkanes (μg n-alkanes/g TOC) and f) n-C₂₉/n-C₂₇ and the total abundance of n-alkanes (μg n-alkanes/g TOC).

Linear regression analysis shows several n-alkane variables are correlated. The strongest correlations exist between CPI and n-C$_{29}$/n-C$_{27}$ (r =0.809, p <0.0000), and ACL and n-C$_{29}$/n-C$_{27}$ (r =0.825, p <0.0000) (Figure 3.14). Weak, but statistically significant, correlations exist between the total abundance of n-alkanes and the other three variables considered; CPI, ACL and n-C$_{29}$/n-C$_{27}$ (r =0.350, p =0.0461; r =0.396, p =0.0224; r =0.389, p =0.0338 respectively). Only one combination, CPI and ACL, does not indicate a statistically significant correlation, as ACL becomes much more variable at low CPIs.
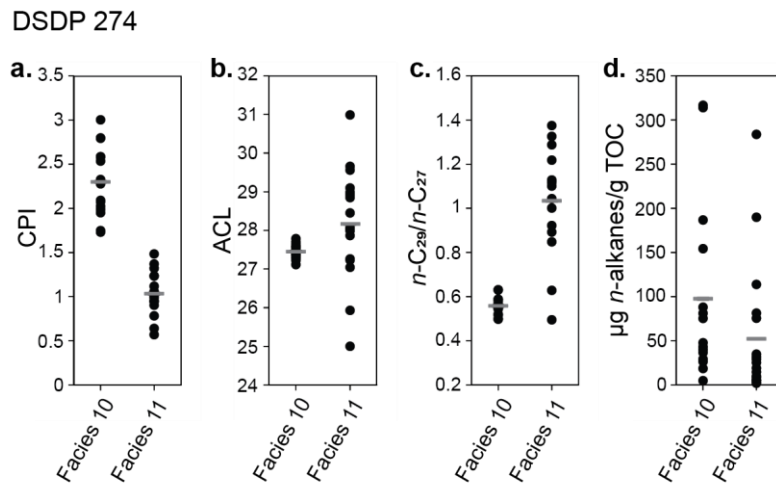
Figure 3.15: Distributions of n-alkane variables across different facies from DSDP 274; a) CPI, b) ACL, c) n-C$_{29}$/n-C$_{27}$ and d) the total abundance of n-alkanes (μg n-alkanes/g TOC). Grey bars represent average values for each facies. Description of facies in table 3.1

Facies 11 has significantly lower CPI and higher n-C$_{29}$/n-C$_{27}$ than facies 10 (averages of 1.0 compared to 2.3 and 1.03 compared to 0.56 respectively) (Figure 3.15). ACL is much more variable in facies 11, and on average higher, while the total abundance of n-alkanes is on average lower than facies 10.

3.4 Discussion

3.4.1 Sources of n-alkanes in Cenozoic sediments

Several sources for n-alkanes in Cenozoic sediments in the Ross Sea Region are proposed:

3.4.1.1 Contemporaneous organic matter

Organic matter from plants and microorganisms living contemporaneously with sediment accumulation would have been a major contributing source for n-alkanes at many, if not all, of

the sites studied. Macro- and micro-fossils from sediment cores, onland outcrops and glacial erratics indicate that the Ross Sea region of Antarctica was vegetated until at least the Mid-Miocene Climate Transition ~14 Ma (e.g. Kemp, 1975, Mildenhall, 1989, Askin, 2000, Askin and Raine, 2000, Pole et al., 2000, Lewis et al., 2008, Warny et al., 2009, Lewis and Ashworth, 2016). While no sediments representing the Paleocene or Early Eocene have been collected from the Ross Sea, sediment cores offshore Wilkes Land indicate a highly diverse, near tropical flora occupied coastal regions, with temperate rain forest inland and at higher elevations (Pross et al., 2012). Following a prolonged period of global cooling, sediments from the Ross Sea region indicate that by the Mid-Late Eocene, vegetation was largely represented by a less diverse, cool, temperate flora dominated by *Nothofagus*-podocarpaceous conifer-proteaceae (Askin, 2000, Francis, 2000, Pole et al., 2000). These sediments, the McMurdo erratics, contain a range of macro- and microfossils of vascular plants indicating contemporary vegetation is a likely primary source for *n*-alkanes in these samples (Askin, 2000, Francis, 2000, Pole et al., 2000). Whilst the *n*-alkane distributions from these erratics are discussed in more detail in section 3.4.2.1, they are distinguished from many of younger samples studied by containing the *n*-C_{29} as the dominant *n*-alkane, as opposed to *n*-C_{27} (Figure 3.3).

The development of large-scale Antarctic ice sheets at the Eocene/Oliocene boundary (~34 Ma) did not extinguish vegetation from the continent. However, the Oligocene and early Miocene was marked by declining vegetation diversity and the development of a sparse, shrubby tundra, dominated by stunted *Nothofagus* (Kemp, 1975, Kemp and Barrett, 1975, Askin and Raine, 2000, Prebble et al., 2006a). This trend was interrupted by the MMCO (~17-15 Ma), when an increase in the abundance of pollen transported offshore may indicate a proliferation of woody vegetation and a possible return to more tree-like forms (Warny et al., 2009, Feakins et al., 2012). This short lived warming was followed by the MMCT, a major cooling step in the Cenozoic considered to have culminated in the development of a more stable, cold-based EAIS (Shackleton and Kennett, 1975, Flower and Kennett, 1994, Lewis et al. 2007). The vegetation history of Antarctica following the MMCT has been debated, with different schools of thought suggesting that higher plants disappeared from the continent at the MMCT (Sudgen et al., 1993, Marchant et al., 1996, Lewis et al., 2008), while others propose that this extinction did not take place until the Mid-Pliocene (Harwood et al. 1983, Webb et al. 1984, Fielding et al., 2012). Samples from Oligocene and Miocene sediments associated with macro and/or microfossils considered to be sourced from contemporary vegetation contain *n*-

C_{27} as the dominant long chained *n*-alkane. This switch in dominant chain length between the late Eocene and the Oligocene is discussed in more detail in section 3.4.2.1.

3.4.1.2 Reworked n-alkanes from older sediments

n-Alkanes could also be sourced from the erosion and redeposition of older sediments. Two main sources are considered here; reworked Cenozoic *n*-alkanes redeposited in younger sediments, and reworked Permian-Jurassic *n*-alkanes sourced from the Beacon Super Group and Ferrar Group. The presence of Cretaceous dinoflagellate cysts in samples of the McMurdo erratics suggests the possibility for a contribution from rocks of this age now either eroded or buried, but as these occurrences are extremely rare the contribution from an unknown Cretaceous source providing sediment to the Western Ross Sea is considered very minor (Askin, 2000). Surface sediment from the Eastern Ross Sea does contain a significant component of Late Cretaceous palynomorphs, however the Central Ross Sea where DSDP 270 is located does not (Truswell and Drewry, 1984), and pollen counts in Oligocene/Late Miocene sediments in this core display no pollen from this time period (Kemp, 1975, Chapter 4). Cores DSDP 270 and DSDP 274 contain metasediment clasts from a range of metamorphic grades, inferred to be sourced from Central Marie Byrd Land and/or the Central High in the Ross Sea (Barrett, 1975). Metasediments in these cores could be a potential source of *n*-alkanes, however as the source lithologies for these clasts are uncertain, no further information is known about their organic contribution.

Microfossil work on Oligocene and Miocene sediments in continental margin drillcores like CRP-2/2A, DSDP 270 and DSDP 274 frequently indicate the presence of older Cenozoic microfossils, likely eroded from older rift infill (Section 1.3). In particular, Eocene aged dinoflagellate cysts of the 'Transantarctic flora' are used to assess reworking of Eocene material into younger sediments (e.g. Kemp, 1975, Askin and Raine, 2000, Prebble et al., 2006a). In addition, Cenozoic microfossils are often considered recycled if their preservation is poor (Prebble et al., 2006a). While the colour of microfossils like palynomorphs can distinguish pollen reworked from thermally altered areas of the Beacon Super Group (see below), limited burial of Cenozoic sediments means that Paleogene forms reworked into younger sediments are still light in colour and display similar autofluorescence (e.g. Askin and Raine, 2000, Prebble et al., 2006a). The presence of pollen aggregates and occasional macrofossils such as leaves suggest that at least some of the microfossil assemblages reflect

contemporary vegetation (Hill, 1989, Mildenhall, 1989, Raine and Askin, 2001, Prebble et al., 2006a). Assessing the relative proportions of reworked and contemporaneous material is also made more challenging by often low abundances of microfossils such as palynomorphs, likely reflecting the sparseness of the onshore vegetation and rapid sedimentation rates (e.g Raine, 1998, Askin and Raine, 2000). Microfossil evidence for reworking from Paleogene sediments suggests that this is also a possible source for *n*-alkanes in Oligocene and Miocene sediments. Prior to this study, limited work had been done on assessing *n*-alkane distributions in early Cenozoic sediments from the Ross Sea. One sample from the Eocene of CIROS-1 was extracted for hydrocarbons due to a potential oil show, and displays a homologous series of *n*-alkanes up to n-C_{35}, but with no odd-over-even predominance (Cook and Woolhouse, 1989). Here, *n*-alkanes extracted from the fossiliferous McMurdo erratics serve as an indication of typical Mid-Late Eocene distributions of these compounds.

The Beacon Supergroup extends throughout the TAM and is a key source of sediment to the sedimentary basins of the Ross Sea (e.g. Talarico et al., 2000, Smellie, 2001, Sandroni and Talarico, 2004, Sandroni and Talarico, 2011). In particular, in the cores from the western Ross Sea, the Beacon Supergroup and subsequent intrusives of the Ferrar dolerite are the main sediment source up until the late Oligocene to early Miocene, when provenance studies indicate a change in sediment related to the deeper unroofing of older basement rocks, coupled with the initiation of sediment input from the McMurdo Volcanic Group (Smellie, 2001, Sandroni and Talarico, 2004). The Beacon Supergroup comprises a Devonian to Triassic sequence of shallow marine to terrestrial sediment containing common micro- and macrofossils (Barrett, 1981). Many of the fossil assemblages come from widespread Permian and Triassic sediments, and indicate a cool, humid Mid-Late Permian climate with high altitude ice and vegetation dominated by *Glossopteris* and *Gangamopteris* (Cúneo et al., 1993, Francis et al., 1994, Collinson, 1997). By the Mid-Triassic, a more diverse flora dominated by *Dicroidium* existed indicating a shift to warmer 'greenhouse' conditions (Collinson, 1997, Cúneo et al., 2003). Microfossils such as palynomorphs from the Beacon Supergroup are frequently identified in Cenozoic sediments. As the Beacon Supergroup outcropping throughout the TAM has undergone widespread intrusion and thermal alteration, more altered palynomorphs likely reflect a local source whilst less altered specimens must be have been transported from now buried or eroded, less extensively intruded sediments cratonwards of the TAM (Askin, 1998, Askin and Raine, 2000). Fossiliferous sediments from sedimentary interbeds of the Jurassic Ferrar group are also known to contribute reworked palynomorphs to offshore sediments, albeit

with much rarer occurrences than those sourced from the Beacon Supergroup (Askin and Raine, 2000). Onshore outcrops of these sediments, such as those from Carapace Nunatak show a range of preservation and thermal alteration, with colours of microflora ranging from yellow to light brown (Ribecai, 2007).

n-Alkanes have been analysed from Beacon sediments, silicified wood and coal at the Allan Hills and Ferrar Group sediments from Carapace Nunatak in Southern Victoria Land (Matsumoto et al., 1986). n-Alkanes ranging from n-C_{12} to n-C_{30} were found in concentrations of 0.24 to 25 µg/g dry samples, and displayed a distribution with a CPI varying from 0.91-1.4. Short chain n-alkanes ($< n$-C_{20}) were typically more abundant than long chain lengths (Matsumoto et al., 1986). A sample from Carapace Nunatak was collected from within 3-5 m of a Jurassic basalt flow, at Allan Hills there were no dyke intrusions or basalt flows within 50 m of samples. However, unlike much of the Beacon Supergroup in the Dry Valleys region, these sediments have not been thought to have been heated to high enough temperatures to remagnetise magnetite to the Jurassic geomagnetic field (Funaki, 1984). Variable thermal alteration is also demonstrated by sterane and triterpane distributions which suggest a range of thermal maturities, with occasional samples still also containing small amounts of compounds unaltered from their biological configurations (Matsumoto et al., 1987). A chromatogram from Matsumoto et al. (1986) indicates that UCMs are also present in these samples, centred around n-C_{18} and n-C_{19}. No n-alkane distributions are known from less altered areas of the Beacon Super Group inferred to exist from palynomorph evidence (Askin, 1998, Askin and Raine, 2000).

Distributions of n-alkanes, kerogen and palynomorphs in surface and Quaternary sediments from the Ross Sea suggest the potential for recycling of n-alkanes from both Cenozoic and pre-Cenozoic sources is occurring via modern depositional processes. n-Alkanes appear in low abundances, with Venkatesan (1988) recovering 15-20 ng/g, and Kvenvolden et al. (1987) finding the aliphatic fraction, dominated by n-alkanes, to constitute 0.2-2.7 µg/g of extractable organic matter. In samples from McMurdo Sound, n-C_{21} or n-C_{23} typically predominate with low molecular weight (LMW) n-alkanes undetectable in some samples. CPI of the higher molecular weight range (n-C_{21}-n-C_{31}) was 0.9-2.1. The source of n-alkanes is considered to be weathered rocks such as the Beacon Sandstone, or older recycled kerogen (Venkatesan, 1988). In the wider western Ross Sea, n-C_{19} is usually the dominant LMW n-alkane, while the high molecular weight (HMW) range is dominated by n-C_{25} and n-C_{27}. The odd-even-predominance

(OEP) ratio (Scalan and Smith, 1970) was used instead of CPI, with LMW OEP_{C19} ranging from 1.0-1.2 and averaging 1.1, and HMW OEP_{C27} ranging from 1.5-2.7, averaging 2.3. In samples from the Victoria Land Basin, LMW n-alkanes dominate, while two samples from the Central Trough show larger quantities of HMW n-alkanes. LMW n-alkanes are attributed to a mixture of primary and recycled material derived from marine organisms, while HMW n-alkanes are considered to be higher plant material either from long range aeolian transport, or reworked from pre-Quaternary sediments (Kvenvolden et al., 1987). A recycled source from n-alkanes in core top and Quaternary samples is supported by studies on similar aged sediments in the western Ross Sea which find kerogen and pollen to be extensively reworked from Paleogene or pre Cenozoic sediment (Sackett et al., 1974, Truswell and Drewry, 1984).

Studies of n-alkanes in soils in the Dry Valleys also suggest mixed sources for modern input. While some soils only contained very low abundances of n-alkanes, certain soil samples contained up to 2200 ng/g of dry soil (Matsumoto et al., 1990a, Feng et al., 2010). The distributions of n-alkanes varied across studies and sample sites, ranging from a CPI across the total range of n-alkanes (both short and long chained) of ~1 up to 2.8 (Matsumoto et al., 1990a, Matsumoto et al., 2010, Hart et al., 2011). The most abundant n-alkanes are usually n-C_{23}, n-C_{25}, or n-C_{27}, however no vascular plants currently exist in the Dry Valleys to provide a source for long chained n-alkanes in soils (Matsumoto et al., 1990a, Matsumoto et al., 2010, Hart et al., 2011). n-Alkanes in soils can likely be attributed to a mixed source input, predominantly derived from endolithic microorganisms and from glacially eroded ancient plant and microorganism debris, sourced from earlier Cenozoic sediment and the Beacon Sandstone (Matsumoto et al., 1990a, Matsumoto et al., 2010). An n-alkane contribution in soils from the Beacon Sandstone is supported by the presence of triterpane and sterane distributions which exhibit a range of thermal maturities, reflecting the variable maturation of the Beacon Sandstone sediments which form a significant component of the basement geology in the Dry Valleys region (Matsumoto et al., 1990b). Aeolian transport as a main source for the n-alkanes in these samples is considered unlikely, as aerosol samples near Antarctica record n-alkane distributions with high ACLs and a dominant n-C_{31}, potentially as a result of large scale meridional air mass circulation transporting n-alkanes from the tropics to high latitudes (Bendle et al., 2007).

3.4.1.3 In situ degradation of n-alkanes

Once deposited in sediment, *n*-alkane distributions can be altered by two processes; microbial degradation or *in situ* thermal alteration (e.g. Tissot and Welte, 1984, Grimalt et al., 1985). In Antarctica and the Sub-Antarctic, hydrocarbon contamination experiments indicate that hydrocarbon degrading microbes are present in soils (Aislabie et al., 1998, Bej et al., 2000, Coulon et al., 2005). Longer chain length *n*-alkanes were found to be more resistant to microbial degradation, and rates of degradation increase with increasing temperature (Coulon et al., 2005). This agrees with down core studies from elsewhere which suggest greater degradation, as indicated by a decrease in CPI, during warmer periods (e.g. Xie et al., 2004, Zhou et al., 2005, Vogts et al., 2012). Microbial degradation can also be affected by other factors, including whether the depositional environment is oxic or anoxic, and how rapid the sedimentation rate is, as microbes are concentrated in surface sediments (Didyk et al., 1978, Canuel and Martens, 1996, Berthe-Corti and Fetzner, 2002).

n-Alkanes in sediments can also undergo alteration due to thermal maturation (Brooks and Smith, 1967, Tissot and Welte, 1984). The sediment sampled in this study comes from near surface sediment in the case of Mt Boreas, or drill cores where the deepest samples come from 385 mbsf in DSDP 270. None of the studied cores contained hydrocarbon residues, and heat flow measurements from CRP-2/2A and other cores in the region (CRP 3, ANDRILL 1B, ANDRILL 2A) range from 24-76.7 °C/km (Bücker et al., 2000, Bücker et al., 2001, Morin et al., 2010, Schröder et al., 2011). While sites near DSDP 270 (DSDP 271-273) did contain gas shows, these are considered more likely to be sourced from shallow biogenic gas rather than of thermogenic origin (McIver, 1975, Claypool and Kvenvolden, 1983). *n*-Alkane distributions in the studied samples are therefore not considered the result of *in situ* thermal maturation.

3.4.2 n-Alkane distributions across sample sites

3.4.2.1 McMurdo Erratics

The McMurdo erratics provide examples of mid-late Eocene *n*-alkane distributions, from a period when Antarctic vegetation was more diverse than in the Oligocene and Miocene, and the climate was warmer and wetter (Askin, 2000, Francis, 2000, Pole et al., 2000). The presence of Eocene terrestrial and marine palynomorphs in younger sediments indicates that Eocene aged sediment is a key source for reworked material in the Ross Sea region. All of the samples except for MTD95 contain a terrestrial palynomorph assemblage, with E215 and E219 also

including leaves, and in the case of E219, wood macrofossils (Harwood and Levy, 2000). However, these erratics do also contain a minor component of reworked material themselves, in the form of mainly Permian and occasionally Triassic palynomorphs displaying a range of thermal alteration, sourced from the Beacon Supergroup (Askin, 2000). Despite this, the occurrence of macro-fossils and dominantly Eocene-aged assemblages of palynmorphs suggest that the *n*-alkanes in these samples are principally sourced from contemporary organic matter. This is likely especially true of the samples demonstrating a higher CPI, as this suggests both that the primary source of long chained *n*-alkanes is terrestrial plant material, and that there is little contribution of thermally altered older material and/or limited post depositional degradation.

The key difference in the *n*-alkane distributions of the McMurdo erratics compared to Oligocene and Miocene samples is the prominence of the *n*-C_{29} as opposed to the *n*-C_{27} (Table 3.2, Figure 3.3). Modern studies suggest two key factors can result in a shift in the average chain length or dominant *n*-alkane in a sample; a change in the composition of the plant community, and/or a change in temperature or aridity (Section 3.1.1) (Bush and McInerney, 2013). Fossil plants and palynomorphs show a decrease in diversity of the plant community between the Eocene and the Oligocene, coincident with significant climate cooling, decreasing CO_2 levels, aridification and the development of large scale Antarctic ice sheets (e.g Francis et al., 2008, Pagani et al. 2011, Passchier et al., 2013, Galeotti et al., 2016). We suggest the shift from a dominant *n*-C_{29} to *n*-C_{27} in the Ross Sea region is likely due to a combination of climate cooling and shift in plant community to a flora dominated by a low diversity tundra of *Nothofagus, podocarpidites* and bryophytes (Askin, 2000, Askin and Raine, 2000, Prebble et al., 2006a, Lewis et al., 2008, this study).

Figure 3.16: Comparison of n-alkane parameters grouped by facies across all four studied sites. Grey bars are used to differentiate between sample sites.
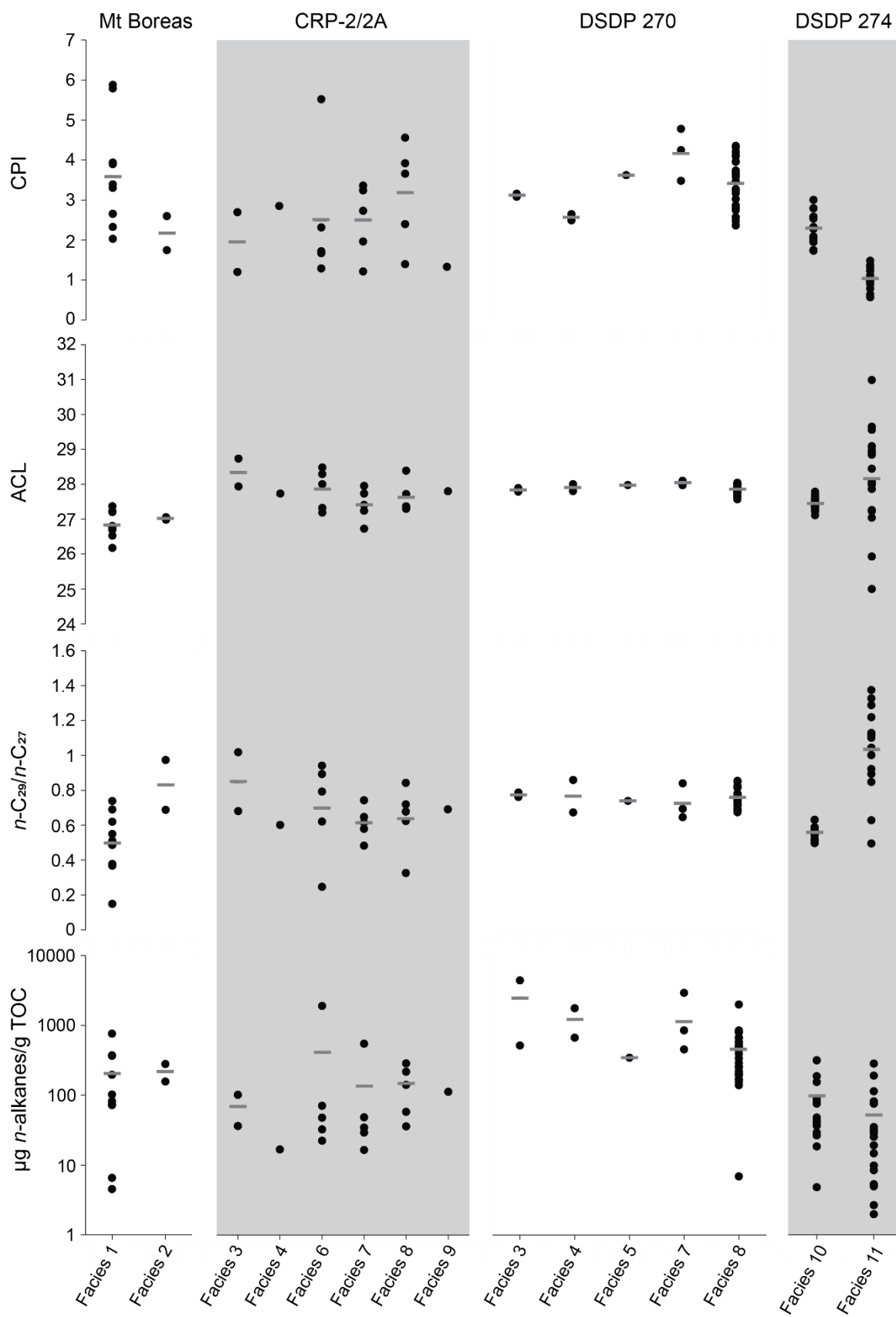
3.4.2.2 Mt Boreas

Samples taken from Mid Miocene sediment at Mt Boreas in the Olympus range represent a terrestrial sequence from a small mountain glacier catchment. Outcrops at this site include well preserved macrofossils of mosses, and a contemporary pollen and spore assemblage (Lewis et al., 2007). The catchment geology for these sediments consists of Devonian sandstones of the Taylor Group, within the Beacon Supergroup (Cox et al., 2012). These sandstones are devoid of body fossils, only containing trace fossils, and have been intruded in the region by the Jurassic Ferrar dolerite (Barrett, 1981, Bradshaw, 2013, Cox et al., 2012). Elsewhere in Southern Victoria Land, usually heavily thermally altered palynomorphs occur in the lowermost and uppermost parts of the Taylor Group (Helby and McElroy, 1969, Kyle, 1977). However, pollen and spores from Mt Boreas sediment are indicative of a low diversity contemporary vegetation living in the catchment (Lewis et al., 2008).

Distributions at this site were marked by high and occasionally prevalent abundances of n-C_{23} and n-C_{25} (Figure 3.4). This prominence of these n-alkanes is in keeping with presence of macro and micro-fossils of bryophytes, dominated by an aquatic moss species indistinguishable from the extant *Drepanocladus longifolius*, as n-C_{23} and n-C_{25} are frequently the major homologs produced by submerged and floating aquatic plants (Ficken et al., 2000). Holocene cores from around Antarctica also commonly contain dominant abundances of these chain lengths, and are interpreted to be sourced from mosses in these sediments (Zhang et al., 2000, Matsumoto et al., 2006). The n-C_{27} homolog is also particularly abundant and is likely sourced from emergent aquatic plants, shrubs and trees such as *Nothofagidites lachlaniae* in the lake catchment (Lewis et al., 2008).

CPI at this site varies considerably but averages 3.4 indicating the primary long chained n-alkane contribution is from terrestrial plants. Samples with a high CPI also suggest that there is little evidence for microbial degradation of the long chain lengths and likely minimal contribution from the heavily thermally altered and microfossil-barren Beacon sediments in the catchment. Only one relatively weak but significant correlation between n-alkane variables exists at this site, between CPI and the ratio of n-C_{29}/n-C_{27} (Figure 3.5). The increase in the amount of n-C_{29} at lower CPI could potentially be the result of either; 1) microbial degradation lowering CPI and preferentially degrading the shorter chain n-C_{27}; or 2) incorporation of recycled material, potentially from both weathered, thermally degraded Beacon Supergroup, and older Cenozoic sediments in the catchment. The chromatogram of the sample with the

lowest CPI and highest $n\text{-}C_{29}/n\text{-}C_{27}$ is shown in Figure 3.4 (ALS-05-21E). The dominance of shorter chain n-alkanes and a UCM underlying the length of the chromatogram suggests that this sample may contain thermally altered n-alkanes from the Beacon Supergroup, and potentially has undergone some microbial degradation too. This is in keeping with the facies interpretation for the sample, i.e. fluvial sands and gravels in this depositional environment would have eroded and transported material from the sediments and bedrock of the surrounding slopes (Figure 3.2, Lewis et al., 2008).

When grouped by facies, samples from lacustrine depositional environments (Facies 1) have higher average CPIs and lower average $n\text{-}C_{29}/n\text{-}C_{27}$ values than fluvial samples (Facies 2) although it is noted that fluvial environments are only represented by two samples (Figures 3.6 and 3.16). Fluvial environments can be erosive settings as coarser sediments require greater water velocity for suspension and movement (Miller et al., 1977). This may explain the above observation, that a fluvial environment is potentially more likely to result in reworked n-alkane distributions, due to the erosion and transport mechanisms invoked by this setting. In the lacustrine setting, high CPI, low ACL and $n\text{-}C_{29}/n\text{-}C_{27}$ in particular occur in the laminated silt beds which occur directly below, and almost directly above the moss peat (Figure 3.4). n-alkane distributions are probably sampling the aquatic plants and mosses deposited during a shallow water phase of the lake. As these plants commonly are dominated by mid chain lengths of $n\text{-}C_{23}$ and $n\text{-}C_{25}$, the resulting ACL is low. Samples from silt beds representing a deeper water phase of the lake (Lewis et al., 2008) are marked by a similar average CPI and $n\text{-}C_{29}/n\text{-}C_{27}$ as the laminated silts, but a higher ACL, perhaps reflecting an increased input of emergent and terrestrial plant matter from the surrounding catchment.

3.4.2.3 CRP 2/2A

The sequence sampled from CRP 2/2A represents Late Oligocene to Early Miocene glaciomarine sediments deposited on a coastal platform adjacent to an EAIS outlet glacier (Cape Roberts Science Team, 1999). Cyclical successions of sediment represent advance and retreat of grounded EAIS sourced ice across the drill site, resulting in a range of facies deposited in distal to ice proximal to subglacial regimes (Figure 3.7) (Fielding et al., 2000). Microfossils show varying abundances of contemporaneous and reworked material, with reworked fossils sourced both from Eocene sediments and the Permian/Triassic Beacon Supergroup, with a much rarer contribution from the Jurassic Ferrar Group (Askin and Raine, 2000, Prebble et al., 2006a). Both dark and light coloured Beacon palynomorphs indicate a

catchment which includes both thermally altered, and less thermally altered sediments (Askin and Raine, 2000, Prebble et al., 2006a).

n-Alkane distributions typically show the n-C_{27} as the dominant homolog, although n-C_{23}, n-C_{25} and occasionally n-C_{29} were also commonly abundant (Figure 3.7). This suggests the source of long chained n-alkanes are trees, shrubs and bryophytes, in line with the palynomorph evidence (Prebble et al., 2006a). However, the variance in CPI through the sample suite also reflects the fluctuating abundances of reworked palynomorphs found in this section of the drill core (Prebble et al., 2006a). Palynomorphs considered reworked (thermally altered, poorly preserved or of a known older range) often also coincide with larger abundances of Transantarctic flora dinoflaggellates (Prebble et al., 2006a), suggesting that reworked samples are sourced from both Permian/Triassic Beacon sediments and earlier Cenozoic sediments, both of which represent periods when Antarctica experienced a warmer climate than during the Oligocene and Miocene. This is potentially an explanation for the correlations between low CPI, and high ACL and n-C_{29}/n-C_{27} (Figure 3.8), reflecting contemporary material mixed with both thermally degraded n-alkane distributions sourced from altered areas of the Beacon Supergroup, and less degraded n-alkanes, but with higher dominant chain lengths, from less altered Beacon and early Cenozoic sediments. In this context, CPI may be a good indicator of mixed and reworked biomarker distributions. While a contribution from more recent recycled material (i.e Early Oligocene n-alkanes) cannot be ruled out, Prebble et al. (2006b) found little evidence for reworking between Early and Late Oligocene sequences. UCMs in these samples typically underlie the lower chain lengths, and may be the result of post-depositional microbial alteration, or could be inherited from the Beacon Supergroup as previous work from these sedimentary rocks demonstrates UCMs at similar chain lengths (Matsumoto et al., 1986).

Very weak but statistically significant correlations also exist between the total abundance of n-alkanes, and CPI and n-C_{29}/n-C_{27} (Figure 3.8). While these correlations may not be meaningful, high abundances of n-alkanes are found in samples with both low and high CPIs. The large variability in n-alkane quantities (from 16.6 to 1893.0 µg/gTOC) also suggests an organic input that varies throughout the catchment, with both reworked (low CPI) and contemporary (high CPI) sediments able to contribute significant abundances of n-alkanes to the offshore sediment.

Facies groupings reflect depositional environments which are predominantly influenced by the proximity of glaciers near the site. These range from marine environments with some ice rafted contribution (sediment gravity flows in facies 7 and low energy facies 8), a more ice-proximal

setting close to the shoreline of a glaciofluvial/glaciodeltaic outwash system (facies 6), and an ice-proximal or subglacial setting (facies 3 and 4) (Figure 3.2) (Cape Roberts Science Team, 1999, Fielding et al., 2000). One sample was also taken from volcaniclastic sediment deposited in a marine environment (facies 9) (Cape Roberts Science Team, 1999, Fielding et al., 2000). There is significant intra-facies variability, although several facies are only represented by one or two samples. However, the more ice-distal, marine facies (7 and 8) have on average high CPIs, low ACL and low n-C_{29}/n-C_{27} (Figures 3.9 and 3.16). Samples from ice-proximal or subglacial settings tend to show the opposite trends, suggesting that these environments are more likely to be transporting and depositing reworked biomarkers. Facies trends in CRP-2/2A suggest that low-energy, more ice-distal marine environments are more likely to contain well preserved n-alkane distributions reflecting contemporaneously sourced n-alkanes, whilst more ice-proximal and subglacial environments have a higher likelihood of containing n-alkanes reworked from both early Cenozoic and pre-Cenozoic sediments.

3.4.2.4 DSDP 270

DSDP 270 samples Late Oligocene to Early Miocene glaciomarine sediments sourced from West Antarctica and basement highs in the Ross Sea (Ford and Barrett, 1975, Barrett, 1975, Kraus, 2016, Kulhanek et al., in prep.). Strata represent an environment which ranges from ice-distal to ice-proximal, although there is no clear evidence of subglacial deposition (Kraus, 2016). Pollen through the core suggest a low diversity, contemporary assemblage that contains almost no indication of early Cenozoic or pre-Cenozoic material.

n-Alkane distributions are typically bi-modal with a peak in relative abundance at n-C_{17} or n-C_{19}, and another peak at n-C_{27} (Figure 3.10). This suggests two primary sources for n-alkanes in this drill core; algae and bacteria are the likely source for the shorter chain lengths, whilst terrestrial higher plants are the main contributor to longer chain lengths (Eglinton and Hamilton, 1963, Clark and Blumer, 1967, Han and Calvin, 1969, Cranwell et al., 1987). The presence of a contemporary pollen assemblage with almost no early or pre-Cenozoic reworked contribution, indicates the long chained n-alkanes likely also reflect the contemporary onshore vegetation. This is reflected in the CPI values that vary less than the other sites sampled, and all sit above 2.4 (Figure 3.16). In this context, the presence of an occasional small UCM underlying the lower chain lengths is more likely a result of minor microbial degradation, rather than an inherited signal from older sediments.

When *n*-alkane variables are plotted against each other no strong correlations are found, with only a very weak correlation between increasing n-C_{29}/n-C_{27} with decreasing CPI, and a slightly stronger correlation between decreasing n-C_{29}/n-C_{27} with decreasing ACL (Figure 3.11). Facies representing more ice-proximal settings (facies 3 and 4) do show the lowest average CPIs suggesting that these settings may be more likely to contain more degraded *n*-alkane distributions, whether as the result of post-depositional processes or some sediment recycling due to glacial erosion and redeposition (Figures 3.12 and 3.16). Minor sediment recycling potentially sourced from weathered older sediments with higher abundances of n-C_{29} may explain the weak correlation between increasing n-C_{29}/n-C_{27} with decreasing CPI. However, in general, the contemporary pollen assemblage, large spread of values across facies, and the consistently high CPIs do suggest that *n*-alkane distributions at this site primarily represent contemporaneous biomarker input. Variations in *n*-alkane distributions, and the correlation between decreasing n-C_{29}/n-C_{27} with decreasing ACL, therefore reflect shifts in composition of the onshore plant community and/or shifts in climate. These factors coupled with the consistently high abundance of *n*-alkanes, especially compared to the other studied sites (Figure 3.16), indicate that DSDP 270 would be a suitable core for deriving a paleoclimate record reflective of conditions at the time of deposition.

3.4.2.5 DSDP 274

Samples taken from DSDP 274 in the northern Ross Sea spans an Early Miocene to Latest Miocene marine sequence (The Shipboard Scientific Party, 1975b, Crampton et al., 2016). Palynological analysis indicates that much of the assemblage in the non-barren samples is reworked, with Permian to Paleogene forms dominating (The Shipboard Scientific Party, 1975b, Kemp 1975). However, some species found are also known from the Miocene of Antarctica and so may represent some contemporary input, i.e *Nothofagus fusca*.

n-Alkane distributions in this drill core were strongly separated into two groups; those sampled from above the unconformity or condensed section at 113.6 m, and those below (Figure 3.13 and Figure 3.16). Increasing n-C_{29}/n-C_{27} with decreasing CPI, and decreasing ACL with decreasing n-C_{29}/n-C_{27} show strongly statistically significant relationships across the total dataset (Figure 3.14). Samples taken from below 113.6 m are Early-Mid-Miocene in age and show bi-modal distributions in chromatograms suggesting a mixed contribution from both algae and bacteria, and terrestrial plants. Other than the uppermost 2 samples from this section of the core, all samples are considered to be part of facies 10, which was deposited with a high

terrigenous and biogenic sedimentation rate, under a regime of weak bottom currents (Figure 3.2) (Frakes, 1975, Whittaker and Müller, 2006). Higher sedimentation rates may have reduced the potential for microbial reworking compared to the upper sampled section described below (Canuel and Martens, 1996). CPIs are higher for this section of the core, averaging 2.2, while ACL and n-C$_{29}$/n-C$_{27}$ varies considerably less than in samples above 113.6 m (Figures 3.15 and 3.16). The presence of reworked palynomorphs, a variable CPI and UCMs suggest that some contribution of reworked n-alkanes is likely, but the generally high CPI, dominance of the n-C$_{27}$ and lack of variation in ACL and n-C$_{29}$/n-C$_{27}$ suggests that much of the n-alkanes present reflect comparitvely higher contemporaneous input than the overlying interval, or at least material recycled from the Oligocene or younger.

Samples above 113.6 m demonstrate low CPIs (averaging 0.99), high n-C$_{29}$/n-C$_{27}$, and variable ACL. Several samples from this section of the core were also barren of n-alkanes or contained very low abundances. The unconformity or condensed section at 113.6 m marks a significant difference in age, as well as a shift in the style of sedimentation. Above this, the sedimentation rate slows, and manganese nodules provide evidence for winnowing by a strong bottom current regime. This interval is also associated with an increase in coarse sediment which could result from ice rafting (Frakes, 1975, Whittaker and Müller, 2006) or winnowing of the fine fraction due to intensification of bottom currents. The Late Miocene is a noted period of cooling in the Antarctic and globally (McKay et al., 2009, Herbert et al., 2016), and glacial expansion at this time could explain the increase in ice rafting or bottom water current intensity. Sediments from this part of the core are also Late Miocene in age, and include and post-date the Mid-Miocene Climate Transition when it has been debated that higher plants became extinct on Antarctica (Sudgen et al., 1993, Marchant et al., 1996, Lewis et al., 2008, McKay et al., 2008), suggesting that n-alkanes from this section of the core may predominantly be derived from older sediments. Low CPIs, high n-C$_{29}$/n-C$_{27}$, often large and dominant UCMs and low sedimentation rates suggest that n-alkanes in these samples have also been extensively degraded, likely by microbial activity as sediments are winnowed and reworked in the surface layers of the seabed.

3.4.3 Synthesis

n-Alkane distributions in Eocene to Miocene sediments from the Ross Sea region vary both with age and sample site. Between the Eocene and Oligocene the dominant chain length recorded in sediments changes from n-C$_{29}$ to n-C$_{27}$, likely reflecting a significant climate

cooling and a shift in plant community (section 3.4.2.1). In Oligocene and Miocene sediments, n-C_{27} remains the dominant long chained n-alkane. While climate continued to cool over these time periods, with the exception of brief episodes of warmth, vegetation remained a low diversity tundra dominated by *Nothofagus* (e.g. Kemp. 1975, Askin and Raine, 2000, Prebble et al., 2006a, Lewis et al., 2008, this study). The dominance of the n-C_{27} in sediments sourced from wide catchments incorporating this cool, low diversity vegetation is in contrast to lower latitudes where n-C_{29} and n-C_{31} are often far more abundant (e.g. Poynter et al., 1989, Kawamura et al., 2003, Sasche et al., 2006, Bendle et al., 2007). This pattern could be the result of two factors; either the dominant vegetation type produced large abundances of n-C_{27} compared to other long chained n-alkanes, or the climate of Antarctica during these periods was such that plants preferably produced shorter n-alkanes. A preference to shorter chain lengths at colder temperatures has been suggested by other studies (e.g. Gagosian and Peltzer, 1986, Poynter et al., 1989, Dodd and Afzal-Rafii, 2000, Kawamura et al., 2003, Sasche et al., 2006, Bendle et al., 2007, Vogts et al., 2009). Limited studies have been done of n-alkane distributions in leaves of *Nothofagus*, but at least one modern species of *Nothofagus* (*N. menziesii*) from New Zealand has been shown to produce n-C_{27} as its dominant n-alkane, with n-C_{27} also abundant in two other species (*N. solandri* and *N. fusca*) (Burrington, 2015). Pollen in sediment from Mt Boreas is characterised by abundant grains of *N. lachlaniae* (Lewis et al, 2008). The high abundance of n-C_{27} in samples from Mt Boreas in this study suggest that *N. lachlaniae* was likely producing large proportions of this n-alkane. The prominence of the n-C_{27} across the Oligocene and Miocene sites of this study likely reflect both a climate adaption by plants growing in the Antarctic tundra to cold temperatures, and the abundance of *Nothofagus* in the catchments.

While the contemporary vegetation of Antarctica in the Oligocene and Miocene was a main source of n-alkanes to the sample sites, reworked biomarkers from early and pre-Cenozoic sediments were a varying contributor. Just as palynomorphs at many of these sites reflect a mixed input of contemporary and reworked material, so too do the n-alkane distributions. In particular, variables which often characterised samples considered to contain more reworked material were low CPI values, and higher ACLs and ratios of n-C_{29}/n-C_{27}. Low CPIs indicate n-alkanes sourced from sediments which have been thermally altered such as extensive areas of the Beacon Supergroup, or have been microbially degraded, although it is noted that this is a process which also may have occurred *in situ* at some of these sites, particularly when sedimentation rates are low. Higher ACLs and n-C_{29}/n-C_{27} values suggest material recycled

from older sediment containing plant matter from warmer climates and/or a difference vegetation assemblage, such as the Eocene sediments represented by the McMurdo erratics. The statistically significant relationship between decreasing CPI, and increasing ACL and n-C_{29}/n-C_{27} demonstrated at some of these sites indicates that samples containing more reworked n-alkanes usually reflect a mixed source input. For example, based on the work of Matsumoto et al. (1986), if a sample contained material solely from reworked thermally altered sections of the Beacon Supergroup, a low CPI would be expected, as would a low ACL and low n-C_{29}/n-C_{27}. The association of low CPIs with high ACL and n-C_{29}/n-C_{27} therefore suggests that reworked samples likely contain a mixture of material derived from thermally matured Beacon sediments, mixed with material containing a higher abundance of longer chained n-alkanes such as n-C_{29} and n-C_{31}, sourced from early Cenozoic sediments and, it is inferred, less altered pre-Cenozoic sources. In some instances, this distribution could also have been the result of microbial degradation which could lower CPI, whilst also preferentially scavenging shorter chain lengths.

Distributions of n-alkanes across the studied sites demonstrate that particular environments may be more likely to result in the deposition of reworked biomarkers. In particular, sediments deposited by glacio-fluvial, ice-proximal glaciomarine and subglacial processes are more likely to contain reworked distributions than those from lacustrine or ice-distal marine environments. Prior to the Mid-Miocene climate transition, glaciers through the Transantarctic Mountains, and likely the exposed areas of the Ross Sea, were warm-based (Marchant et al., 1993, Sugden et al., 1995, Lewis et al., 2007). This warm-based glacial regime would have favoured high rates of glacial erosion and an abundance of meltwater, leading to high sedimentation rates particularly in ice-proximal settings (Sugden and Denton, 2004). These processes likely led to the deposition of greater proportions of reworked n-alkanes in ice-proximal environments whereas ice-distal settings with lower sedimentation rates incorporated more contemporary material, transported offshore by a mixture of glacial, fluvial and aeolian processes.

The varying contribution of contemporary and reworked n-alkanes across sediments sourced from different depositional environments, catchments and ages emphasizes that caution must be exercised when applying biomarker-based paleoclimate proxies. In particular, several aspects should be considered when determining if an n-alkane distribution is likely contemporary, including; the values and variation of factors such as CPI and ACL, whether the catchment and depositional setting of a site is more likely to accumulate and preserve a contemporary distribution, and assemblages of other fossil material such as palynomorphs. For

example, in the sites used for this study, samples demonstrating high CPIs (>2) from sediments which contained lower numbers of reworked microfossils are considered less likely to contain reworked material. Often, these samples were also from settings that were ice distal or lacustrine, depositional environments also typified by finer sediments of mud and silt size. These samples should be prioritised when considering changes in *n*-alkane distributions as paleoclimate indicators, and would be the best focus for future analysis such a compound specific isotopes. When constructing timeseries of biomarker assemblages, it is also important to consider other aspects of the depositional environment in the Ross Sea. The coastal setting of the Ross Sea could be influenced by pulses of reworked material given the potential for point source glacial meltwater discharge, and large-scale meltwater discharge events (i.e. Powell and Domack, 2002, Lewis et al., 2006), which may focus erosion to a certain lithological source. Such events have a high potential to rapidly erode and redeposit older biomarkers and pollen offshore in concentrated numbers, and indeed *n*-alkane distributions could be used as a potential tool to identify such reworking events.

These findings also have potential implications for the application of other biomarker proxies. While many compounds are utilised for paleoclimate investigation, implications for two classes of compounds are considered here as they have been applied to paleoclimate studies in this region; fatty acids and glycerol dialkyl glycerol tetraethers (GDGTs). Fatty acids have been analysed in Ross Sea region from both recent and ancient sediments (Matsumoto et al., 1981, Matsumoto et al., 1985, Matsumoto et al., 1986, Matsumoto et al., 2010, Feakins et al., 2012). Similar to *n*-alkanes, long chained fatty acids originate in the waxes of vascular plants, except distributions of fatty acids are typified by a strong even over odd chain length predominance (Eglinton and Hamilton, 1967). Fatty acids lose their functional group during thermal maturation or diagenesis and convert to *n*-alkanes, resulting in a reduction in CPI and eventual absence of fatty acids from sediment (Bray and Evans, 1961, Tissot and Welte, 1984). Fatty acids have been found in the Beacon Supergroup but vary between sites. While long chained fatty acids with an even-over-odd distribution have been found in samples of silicified wood, most sediment samples are either absent of long chain lengths or they are only present in low abundances (Matsumoto et al., 1985, Matsumoto et al., 1986). This indicates that diagenesis and thermal alteration has likely removed long chained fatty acids from the thermally altered parts of the Beacon Supergroup, although distributions from less altered areas are unknown. Fatty acids were found in Miocene sediments of the ANDRILL 2A core and demonstrated a strong even-over-odd predominance (Feakins et al., 2012). The acids in the sampled sections

were well preserved with an unaltered isotopic composition, and coincided with a contemporary pollen assemblage, indicating that these acids also reflected a contemporary onshore vegetation (Feakins et al., 2012). Long chained fatty acids have been found in recent soil and sediment samples, and have been attributed to reworking of vascular plant material from sediment deposited under warmer environments when plants still lived in the region (Matsumoto et al., 2010). The presence of fatty acids in Cenozoic sediments, coupled with evidence of reworking of fatty acids into modern sediments, suggests that, as in the case of *n*-alkanes, reworking of fatty acids into younger sediments is something that must be considered when these compounds are used for paleoclimate studies.

Another commonly used suite of biomarkers are branched and isoprenoidal GDGTs. GDGTs have been found to be relatively thermally unstable, with GDGTs containing cyclopentane moieties preferentially degrading as temperature increases, biasing GDGT based proxies (Schouten et al., 2004, Schouten et al., 2013). Above ~300 °C GDGTs are found to have completely degraded (Schouten et al., 2004). In the Ross Sea region, this would mean that areas of the Beacon Super Group and Ferrar Group which have been matured to temperatures greater than 300 °C would be absent of GDGTs. However, GDGTs have also only been identified in sediments as old as the Early Jurassic (Robinson et al., 2016), so while it is possible they may be found in the immature areas of the Ferrar Group, it is not known if they would be present in immature regions of the Beacon Super Group. While the pre-Cenozoic rocks of the Ross Sea region are unlikely to contribute GDGTs to younger sediments on and offshore, it is assumed that GDGTs could be recycled from early Cenozoic sediments as they have been found to be present in Paleogene and younger sediments from the Ross Sea and wider region (Pross et al., 2012, McKay et al., 2012a, Levy et al., 2016, Chapters 4 and 5).

3.5 Conclusions

- *n*-Alkane distributions have been determined in Eocene to Miocene sediments from a range of depositional environments in the Ross Sea region of Antarctica.
- Between the Late Eocene and the Oligocene, a shift in dominant chain length was observed from *n*-C$_{29}$ to *n*-C$_{27}$. This is inferred to be a result of both a shift in plant community over this time period, as well as a significant climate cooling coincident with the establishment of continental scale ice sheets on Antarctica.
- *n*-Alkane distributions in Oligocene and Miocene samples varyingly display a contribution from both contemporary and reworked sources. Distributions typical of a

reworked sample were a low CPI, and high ACL and n-C_{29}/n-C_{27} values, reflecting a likely mixed contribution from thermally altered and less thermally altered regions of the Beacon Super Group and Ferrar Group, coupled with material sourced from earlier Cenozoic sediments. Samples dominantly containing more contemporary material displayed a higher CPI, and lower ACL and n-C_{29}/n-C_{27} values, were sourced from the sparse, cold tundra which occupied Antarctica during these time periods.

- Particular environments of deposition appear more likely to contain a reworked or contemporary n-alkane distribution. Fluvial environments onshore, and subglacial and ice-proximal environments offshore are more likely to result in the deposition of reworked n-alkanes. Lacustrine environments onshore, and ice-distal environments offshore, are more likely to reflect contemporary n-alkane input.

- Variable reworking across Oligocene and Miocene sediments in the Ross Sea region indicate that caution must be exercised when n-alkanes are used for paleoclimate interpretations, to ensure a contemporary rather than reworked distribution is investigated. This has potential implications for other compounds used to infer paleoclimate in this region, such as fatty acids and GDGTs, and an integrated sedimentological, paleontological and geochemical approach is essential.

Chapter 4: The Mi-1 glaciation in the Ross Sea, Antarctica: Climate reconstructions using molecular and isotopic biomarker proxies

Chapter 3 distinguished drill core DSDP 270 as containing a predominantly contemporaneous succession of n-alkanes, identifying this site as an appropriate paleoclimate archive for biomarker-based proxy reconstructions. In this chapter, n-alkane- and GDGT-based climate proxies are applied to a glaciomarine sedimentary sequence spanning the Late Oligocene to the early Miocene in DSDP 270. This chapter aims to understand the drivers and manifestation of a large transient glacial event during this time period (Mi-1 glaciation), from the perspective of the Ross Sea, Antarctica.

4.1 Introduction

The Oligocene/Miocene boundary at 23.03 Myr is marked by the Mi-1 event, a transient, but extensive glaciation, which interrupted a period of global warmth (Zachos et al., 1997, Naish et al., 2001b, Zachos et al., 2001a, 2001b). The Mi-1 event is represented by a 200-300 kyr ~0.6-1‰ positive excursion in deep sea benthic foraminiferal $\delta^{18}O$ records, considered to coincide with the expansion of the Antarctic Ice Sheets to up to 25% greater than their present day volume and an apparent sea level change of 40-60 m (Figure 4.1) (Zachos et al., 1997, Zachos et al., 2001a, 2001b, Pekar and DeConto, 2006 Mudelsee et al., 2014, Beddow et al., 2016). This glaciation represents a key shift in Cenozoic climate from relative global warmth and low amplitude climate variability in the Late Oligocene to higher amplitude climate variability with large-scale temperature and ice volume fluctuations in the early Miocene (Zachos et al., 2001a, Billups et al., 2004, Pälike et al., 2006a, Pälike et al., 2006b, Shevenell and Kennett, 2007, Liebrand et al., 2011, Beddow et al., 2016).

4.1.1 Climate drivers of Mi-1 glaciation

The drivers of the Mi-1 glaciation have been the focus of widespread debate. While decreasing CO_2 levels have been considered to be a factor, global proxy evidence indicates that CO_2 dropped from ~650 ppm to between ~400-300 ppm prior to Mi-1, at ~25 Ma (Pagani et al., 2005, Beerling and Royer, 2011, Zhang et al., 2013). The low resolution of these proxy records means that transient CO_2 excursions are not well recorded, so it is possible that CO_2 levels decreased further at Mi-1. Evidence from Cape Roberts 2/2A indicates that cycles of advance and retreat of the Antarctic ice sheets in the lead up to Mi-1 (24.1-23.7 Ma) were orbitally controlled, primarily influenced by obliquity (~40 kyr) and eccentricity (~125 kyr) cycles

(Naish et al., 2001b). This indicates that the Antarctic ice sheets are sensitive to changes in orbital parameters, either via their direct influence on high latitude insolation and seasonality, or on atmospheric and ocean circulation in the mid-latitudes. Mi-1 was preceded by an orbital geometry (high 400-kyr eccentricity and a node in 1.2-myr obliquity) which would have resulted in an extended period of low seasonality and cooler summer temperatures (Zachos et al., 2001b, Pälike et al., 2006b, Figure 4.1). Global records of bottom water temperatures also indicate that several cooling steps preceded maximum ice volume in Mi-1, paced by eccentricity cycles (Mawbey and Lear, 2013).
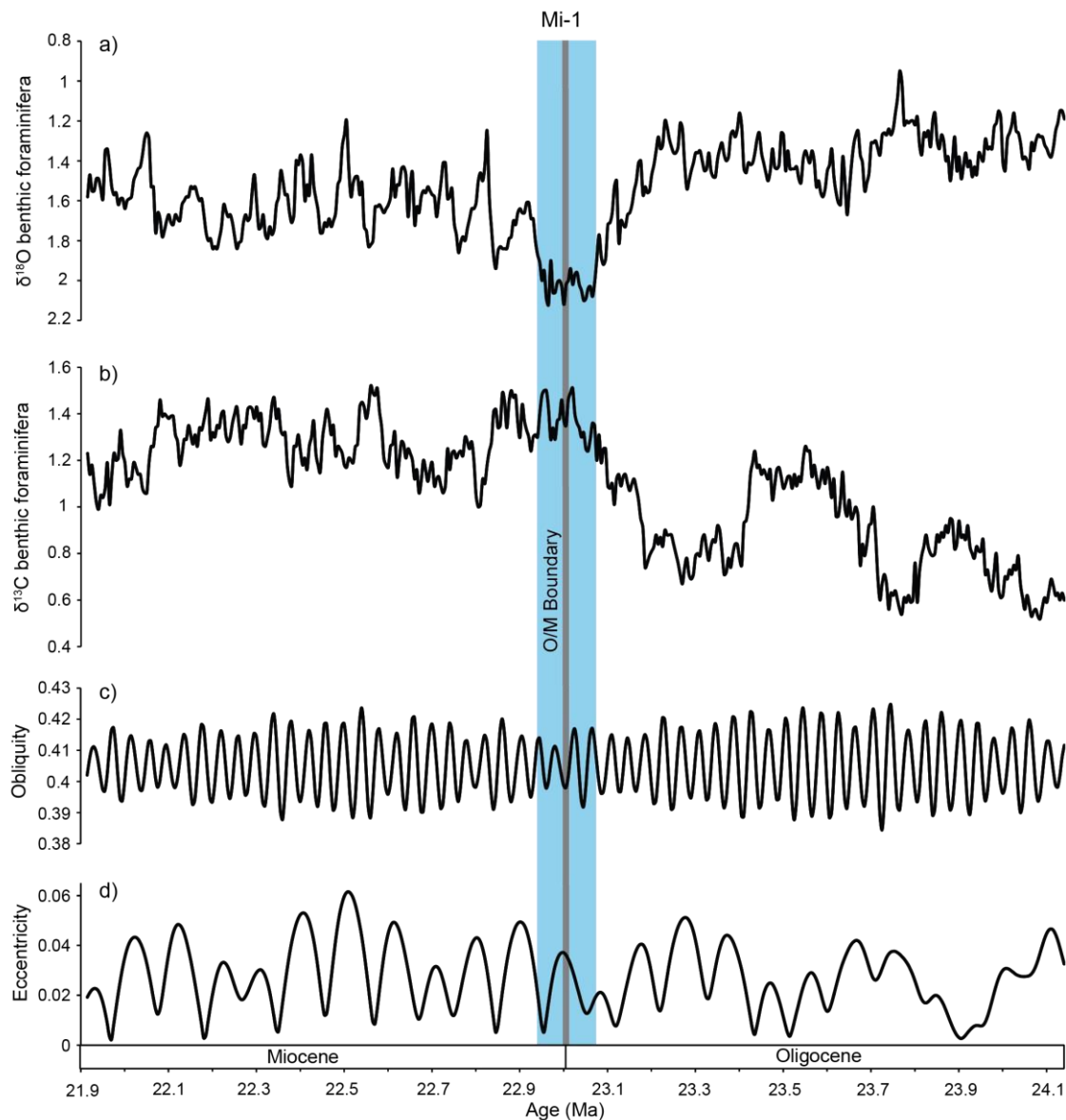
Figure 4.1: Global benthic foraminiferal isotope stack for a) $\delta^{18}O$ and b) $\delta^{13}C$ from Beddow et al. (2016), and orbital parameters of c) obliquity (Laskar et al., 2004) and d) eccentricity (Lasker et al., 2011) over the Oligocene/Miocene boundary.

4.1.2 An Mi-1 Paradox?

Accommodating modelled ice volumes of 125% of the present day requires either some ice in the Northern Hemisphere, or both the East Antarctic Ice Sheet (EAIS) and West Antarctic Ice Sheet (WAIS) to advance to the continental shelf edge, similar to the ice sheet volume at the Last Glacial Maximum (DeConto et al., 2008, Golledge et al., 2012, Golledge et al., 2013). Records of this time are limited around West Antarctica. However, earliest Miocene strata disconformably overlie latest Oligocene strata on King George Island in the South Shetland Islands (Troedson and Riding, 2002). Sediments from this site show a switch from normal marine sedimentation in the latest Oligocene to a glacially-influenced marine shelf in the earliest Miocene, indicating extensive glaciation in the Antarctic Peninsula region and marine-based grounded ice on the continental shelf (Troedson and Riding, 2002). In proximal Antarctic drill cores around the East Antarctic margin, the Mi-1 glaciation occurs as a major regional unconformity, inferred to represent erosion as the result of a significant advance of the EAIS (Hambrey et al., 1991, Naish et al., 2001b, Naish et al., 2008, Wilson et al., 2008, Escutia et al., 2011). However, the Mi-1 glaciation, was not extensive and/or cold enough to extinguish higher plants such as *Nothofagus* from the continent, despite indications of a cooling from pollen and geochemical proxies of several degrees over this time period (Askin and Raine, 2000, Roberts et al., 2003, Passchier and Krissek, 2008).

Large transient glaciations such as the Mi-1 glaciation have been a topic of debate, as models struggle to reconcile the transient excursions indicated by the benthic foraminiferal isotope record with the degree of hysteresis displayed by most Antarctic ice sheet models (Pollard and DeConto 2005). The problem being that much higher concentrations of atmospheric CO_2 are required to remove a continental-scale ice sheet than existed prior to the development of that ice sheet, due to height mass balance and albedo feedbacks (Pollard and DeConto, 2005). Moreover, available proxy evidence suggests CO_2 varied within a relatively narrow range over the Oligocene and Miocene (Pagani et al., 2005, Beerling and Royer, 2011, Zhang et al., 2013). Recent modelling work focusing on transient glaciations in the Early to Mid-Miocene has made significant progress in dealing with this problem by including ice sheet-climate feedbacks within a narrow range of CO_2 variation (Gasson et al., 2016). These include the incorporation of new marine ice sheet and ice cliff instability processes (DeConto et al., 2016), reconstructing appropriate paleogeographies, adjusting basal hydrology, and accounting for changes in the mean $\delta^{18}O$ of the ice sheet (Gasson et al., 2016). These new developments better reconcile ice volume variability implied by deep-sea benthic and far field sea level records and proximal

geological evidence (e.g. Miller et al., 1991, Zachos et al., 2001b, Levy et al., 2016) during these transient events, without invoking large scale CO_2 changes. These new studies imply that the marine-based Antarctic ice sheets are very sensitive to just small changes in global mean temperature and CO_2, and that critical thresholds may exist in both the marine and terrestrial parts of the Antarctic ice sheet.

The bedrock topography of Antarctica, especially West Antarctica, has changed significantly over the Cenozoic, as the result of millions of years of erosion and sedimentation coupled with thermal subsidence and tectonic plate movement (Wilson and Luyendyk, 2009, Wilson et al., 2012). In particular, sediments overlying basement in Deep Sea Drilling Project (DSDP) site 270 in the central Ross Sea indicate that this core site was subaerial in the Early-Mid Oligocene, but now basement sits more than 1000m below sea level (The Shipboard Scientific Party, 1975a). A higher-elevation West Antarctica with more land above sea level is capable of growing a significantly larger ice sheet during the warmer climates of the Cenozoic, when warm ocean temperatures would have restricted the growth of ice shelves and marine grounded ice sheets (i.e. Sorlien et al., 2007, Wilson et al., 2013, Gasson et al., 2016). While a high elevation West Antarctica can help explain ice volume estimates for the Eocene/Oligocene transition, DSDP 270 indicates that subsidence was ongoing through the latest Oligocene to earliest Miocene, suggesting that West Antarctica too had begun to subside by this time (Leckie and Webb, 1983, De Santis et al., 1999, Wilson et al, 2013). The topography of West Antarctica would still likely have been relatively elevated, with the present overdeepened topography not developing until later in the Miocene or Pliocene, when seismic stratigraphy on the continental shelf indicates a shift from progradational glaciomarine foresets, and thus an active sediment supply from West Antarctica, to aggradational till sheets (Brancolini et al., 1995, De Santis et al., 1999).

4.1.3. Site Setting

DSDP 270 was drilled on the continental shelf in the Eastern Basin of the central Ross Sea in 1973 (77°26.48'S, 178°30.19'W), as part of DSDP Leg 28 (Figure 4.2, section 1.7.7) (The Shipboard Scientific Party, 1975a). DSDP site 270 contains a sequence spanning the late Oligocene, through the Mi-1 event to the early Miocene, with minimal or shorter duration hiatuses (<1 Myr) across this important climatic transition relative to other proximal Antarctic records (Kulhanek et al., in prep.). The central Ross Sea is a key area for studying the previous

extent and behaviour of the WAIS. It is a major drainage area of the WAIS with models indicating it is sensitive to changes in climate forcings such as ocean heat flux and sea level, and that it is one of the last sectors of the continent to become glaciated during glacial maxima (De Santis et al., 1999, Pollard and DeConto, 2009, Golledge et al., 2012, Golledge et al., 2013). During the deposition of DSDP 270, seismic studies suggest the Ross Sea embayment was an archipelago of islands, separated by deep basins (De Santis et al., 1995, De Santis et al., 1999). DSDP 270 is located on the western flank of the Eastern Basin, which in the Late Oligocene was bordered to the west by the subaerial Central High, an island that likely hosted valley glaciers and small ice caps (De Santis et al., 1999). During deposition of the Late Oligocene to Early Miocene sequence, foraminifera from DSDP 270 and tectonic models indicate that this region of the Ross Sea subsided, resulting in a gradually deepening environment of deposition and eventual submersion of the Central High (Leckie and Webb, 1983, De Santis et al., 1999).

The interval of the core containing the Late Oligocene to Early Miocene sequence (350-20 mbsf) is characterised by variably ice-distal to ice-proximal sediments, but with no clear evidence of glacial overriding (Section 3.3.1.4) (Kraus, 2016). Clasts throughout the core are considered to be transported to the site by icebergs sourced from glaciers eroding basement lithologies on the proximal adjacent Central High, coastal Marie Byrd Land and the Transantarctic Mountains (Section 1.4) (Ford and Barrett, 1975, Barrett, 1975).

4.1.4 Aims and approach

Traditional microfossil-based methods of reconstructing climate can be challenging to apply in Antarctic glaciomarine sediments. For example, those that use palynomorphs or skeletal remains such as foraminifera, diatoms and nannoflora can be challenging due to sparse distribution, low diversity of species, poor preservation in sediments, and (in deeper time records) a lack of extant fossils to compare to modern analogues of environmental conditions. Biomarkers have the potential to provide environmental proxy information when other methods are challenging or unsuitable. This study assesses the application of a range of proxies in DSDP 270 derived from; 1) *n*-alkanes sourced from algae, bacteria and plants, 2) glycerol dialkyl glycerol tetraethers (GDGTs) sourced from marine archaea and soil bacteria and 3) palynomorphs, to reconstruct terrestrial vegetation, climate and marine conditions in the Ross Sea embayment over the Mi-1 glaciation.
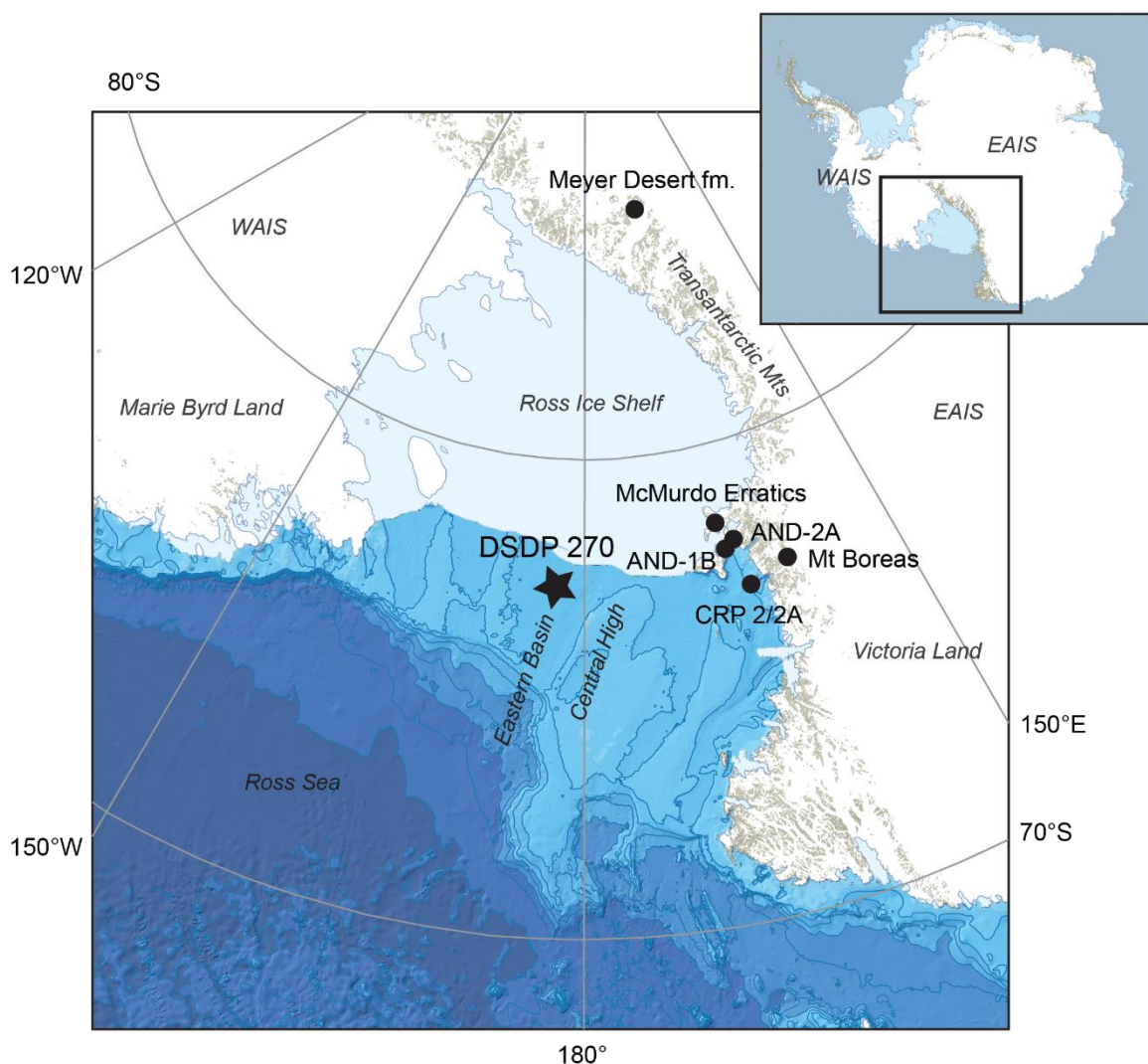
Figure 4.2: Location of DSDP 270 and other sample locations and features mentioned in this chapter. EAIS: East Antarctic Ice Sheet, WAIS: West Antarctic Ice Sheet, Meyer Desert fm.: Meyer Desert Formation, CRP: Cape Roberts Project. AND: ANDRILL project. Base map from Quantarctica GIS package, Norwegian Polar Institute.

4.2 Methods

Samples of DSDP 270 were obtained from the IODP core repository at Texas A&M University and from archive samples held at GNS Science. Samples were taken at approximately 10 m intervals. Subsequently, additional samples were taken to increase the temporal resolution for GDGT-based proxies. Protocols for processing and analysing palynomorph, biomarkers (*n*-alkanes and GDGTs), *n*-alkane compound specific isotopes, and bulk pyrolysis are described in Chapter 2. In DSDP 270, *n*-alkane concentrations have an average percentage standard deviation of 3.9%.

4.3 Proxy results and interpretation

4.3.1 Age model

The age model for DSDP 270 is currently being revised by Kulhanek et al., (in prep.), based on new biostratigraphic and magnetostratigraphic data, strontium isotope ages and K/Ar dating of glauconite. A preliminary age model is inferred in this chapter, based on initial biostratigraphic data, coupled with lithological information and foraminiferal assemblages (The Shipboard Scientific Party, 1975, Leckie and Webb, 1983, Kraus, 2016). An unconformity at ~352 mbsf is inferred from both a significant change in foraminiferal assemblage as well as a lithological shift from interbeds of sandstone and mudstone to a predominantly massive siltstone with ice rafted debris (The Shipboard Scientific Party, 1975, Leckie and Webb, 1983, Kraus, 2016). Below this unconformity, glauconite in the calcareous greensand at the base of the core has been K/Ar dated to 25.9 ± 1.45 Ma, suggesting sediments through this sequence to be Late Oligocene in age (Kulhanek et al., in prep.). The age above the unconformity is constrained to the Late Oligocene by the highest occurence of calcareous nannofossil *Chiasmolithus altus*, dated to ~25.44 Ma (Figure 4.3) (Kulhanek et al., in prep.). The highest occurrence of calcareous nannofossil *Zygrhablithus bijugatus* at 280.25 mbsf indicates sediments above this age are younger than 23.76 Ma (Kulhanek et al., in prep.). The Mi-1 glaciation is broadly constrained by the highest occurrence of calcareous nannofossil *Dictyococcites bisectus* at 150.65 mbsf. This datum occurs in sediments just below the Oligocene/Miocene boundary in the Cape Roberts 2/2A core, and is dated at 23.13 Ma (Naish et al., 2008, Kulhanek et al., in prep.), thus occuring during the initiation of the Mi-1 event, according to global records (Figure 4.1) (Beddow et al., 2016). Therefore, it is inferred in this study that Mi-1 initiates below 150.65 mbsf at DSDP 270, with the peak of the event occurring above this point in the core. At 111.13 mbsf, the lowest occurrence of dinocyst *Batiacasphaera cooperi* suggests an age of 20.71 Ma (Kulhanek et al., in prep), indicating the likely presence of a hiatus somewhere between 150.65 mbsf and 111.13 mbsf. While the presence of ice rafted debris increases from ~125 mbsf, there is no obvious uncomformity from the stratigraphy during this interval, although there are several significant core recovery breaks (Kraus, 2016). Leckie and Webb (1983) noted a shift in foraminiferal assemblages that imply a change to a lower diversity, colder fauna above ~120 mbsf. While the age model continues to be refined, a disconformity is inferred at ~112 mbsf, just below the lowest occurrence of *Batiacasphaera cooperi* (Figure 4.3). The highest occurrence of diatom *Kisseleviella tricoronata* at 105 mbsf,

dated to 20.439 Ma further supports the age suggested by *B. cooperi*. Above ~20 mbsf, sediments are estimated to be Pliocene to recent in age (The Shipboard Scientific Party, 1975).
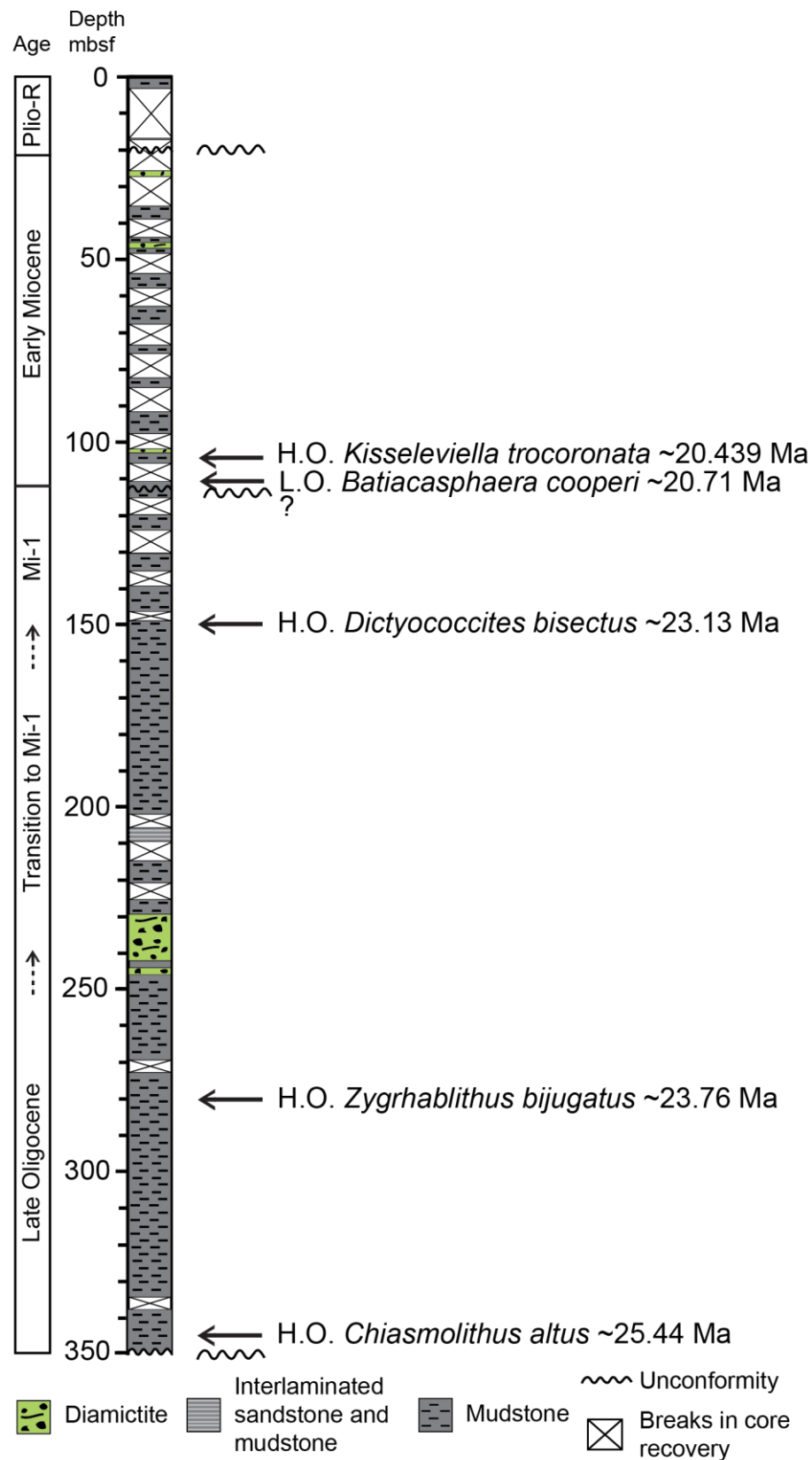
Figure 4.3. Biostratigraphic age diagnostic information for DSDP 270 and stratigraphy.

4.3.2 Palynomorphs

Thirteen samples were selected through DSDP 270 to investigate broad-scale changes in marine and terrestrial palynomorphs. While palynomorph abundances were low in general, with two samples at 209.89 and 294.42 mbsf containing counts of only 28 and 22 respectively, counts increase above 200 mbsf. Thus, while data from these two samples is still displayed in Figures 4.4, 4.5 and 4.6, proportions are unlikely to be representative. Some samples contain a significant number of marine palynomorphs but rare terrestrial palynomorphs. Descriptions of terrestrial palynomorphs and photo plates are detailed in Appendix 2.1.1.

Pollen and spores throughout the sampled section indicate the presence of onshore vegetation prior, during and after Mi-1 (Kemp, 1975, Kemp and Barrett, 1975, this study). The assemblage in the Late Oligocene is dominated by *Nothofagus*, mainly the *Nothofagus lachlanaie*, with *Podocarpidites* spp. also present (Figure 4.4). The most common spores are *Retitrileties* spp.. However, pollen abundances from this stage of the core are commonly very low. Palynomorph abundances increase from 155 mbsf, and above 141 mbsf are typically higher than throughout the Late Oligocene. Through most of Mi-1, *Nothofagus lachlanaie* represents a proportionally smaller component of the assemblage, with spores of *Coptospora* spp. and *Retitrileties* spp. becoming a more dominant component. The modern affinity for *Retitrileties* spp. is thought to be *Lycopodium fastigiatum*, an alpine club moss, whilst *Coptospora* spp. are thought to be a moss, similar to the bryophyte family Bartramiaceae (Raine, 1998, Zamaloa, 2004, Prebble et al., 2006a). *Podocarpidites* spp. remains present through this time, increasing slightly during the early stages of Mi-1. *Retitrileties* spp. declines in abundance through Mi-1, with *Coptospora* spp. replacing it as the dominant spore present. In general, spores increase in abundance relative to pollen during Mi-1 (Figure 4.6). This suggests that either a tundra habitat favouring moss and other bryophytes proportionally expanded in the catchment at the expense of *Nothofagus*, or potentially that the harsh climate during Mi-1 resulted in fewer summers where climate conditions were favourable for flowering, reproduction and seed production of *Nothofagus*, and consequently pollen production (Ashworth and Cantrill, 2004). Assemblages from the Early Miocene are characterised by dominant *Nothofagus lachlanaie* and *Coptospora* spp., with *Podocarpidites* spp., *Nothofagus flemingii*, and *Retitrileties* spp. present to a lesser extent.
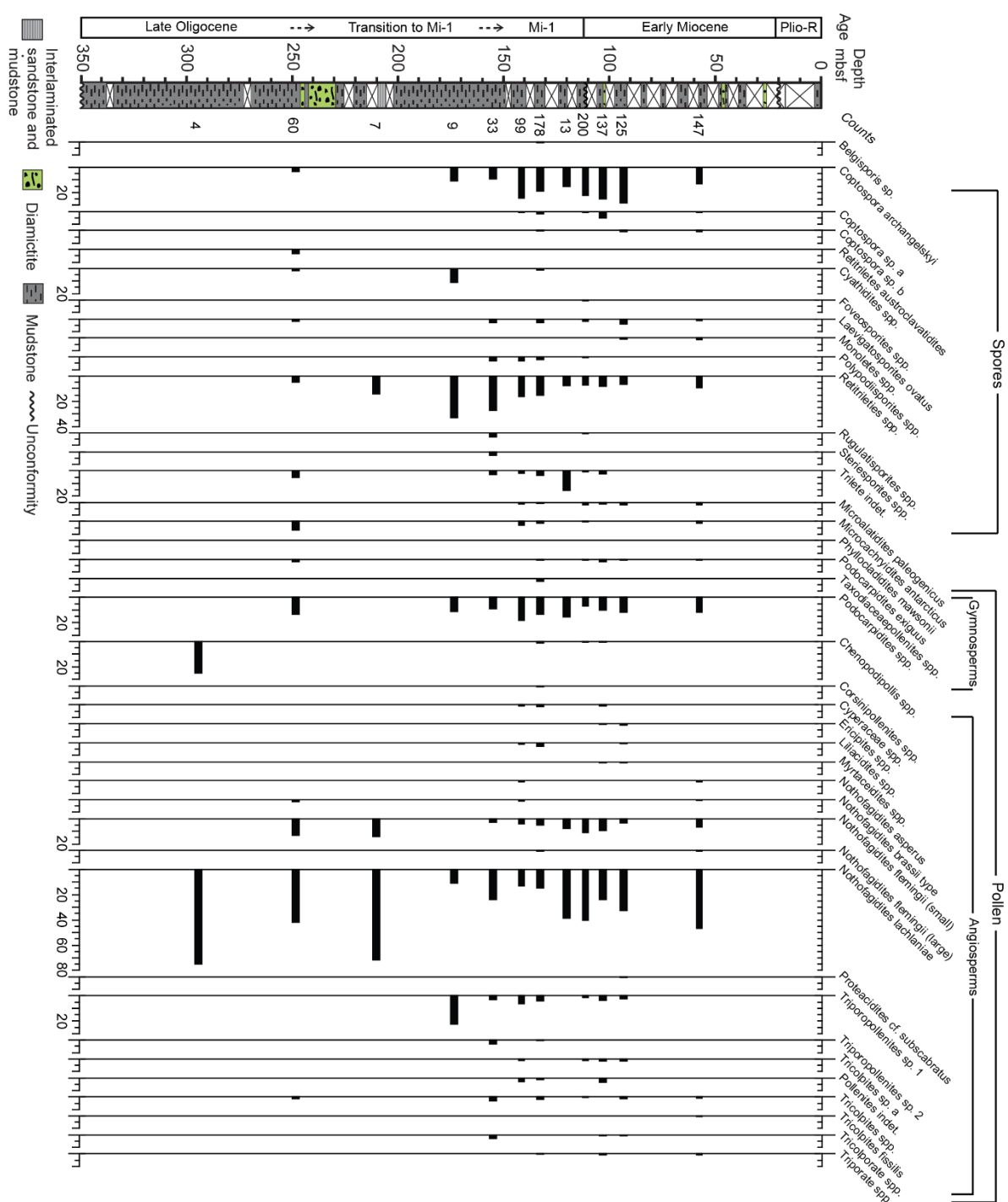
Figure 4.4: Terrestrial palynomorphs from DSDP 270.

The pollen and spore assemblage from DSDP 270 is comparable to assemblages from other late Oligocene and younger locations in the Ross Sea region, comprising a low diversity shrubby tundra usually dominated by *Nothofagus* (Askin and Markgraf, 1986, Raine, 1998, Askin and Raine, 2000, Ashworth and Cantrill 2004, Prebble et al., 2006a, Warny et al., 2009). As initially suggested by Raine (1998), the landscape likely comprised a mosaic of vegetation

with stunted *Nothofagus*-podocarp-Proteaceae scrub on warmer sites, and herb-moss tundra at higher elevations and colder sites. In the Early Miocene, the assemblage closely resembles Miocene assemblages from Cape Roberts 2/2A and the Neogene Meyer Desert Formation from Beardmore Glacier (Askin and Markgraf, 1986, Askin and Raine, 2000, Ashworth and Cantrill 2004). Initial pollen and spore descriptions by Kemp (1975) and Kemp and Barrett (1975) suggested that much of the assemblage in DSDP 270 was comparable to what was known from the Eocene assemblages of the McMurdo Erratics at the time (McIntyre and Wilson, 1966). However, these erratics are now known to contain a more diverse assemblage than that in DSDP 270 (Askin, 2000). Kemp (1975) found dinoflaggellate cysts in a number of samples from ~260-200 mbsf which they suggested may have been recycled from the underlying Eocene strata. However, they are observed in glacial proximal diamictites and rhythmites where some reworking could be anticipated (Figure 4.4). Despite this, the samples processed and investigated in this study contain almost no discernible reworked component from the Eocene or older, although it is noted that due to similarities between assemblages, a contribution from reworked earlier Oligocene palynomorphs is possible.

Marine palynomorphs show a Late Oligocene distribution dominated by *Leiosphaera* spp., an acritarch which primarily lives in freshwater, but is also found in high abundances along the boundary between pack ice and seasonal ice in the Arctic Ocean (Figure 4.5) (Mudie, 1992, Hannah, 2006, Prebble et al., 2006b, Warny et al., 2006). Marine protoperidinoid dinoflagellates are only a minor contributor to the assemblage. This suggests a shallow marine environment dominated by input from freshwater, likely in the form of fluvial systems and/or glacial meltwater from the Central High and other nearby ice masses. At ~210 mbsf and above, this relationship starts to reverse, with protoperidinoid dinoflagellate becoming more dominant, while *Leiosphaera* spp. decreases in abundance (Figure 4.5 and 4.6). This corresponds to a deepening in paleo-water depth (Leckie and Webb, 1983), and the transition to grounding-line distal glaciomarine sedimentary facies. Protoperidinoid dinoflagellates are dominated by *Brigantedinium* spp. and *Selenopemphix* spp. which are common in Antarctic waters at present (Marret and de Vernal, 1997, Harland and Pudsey, 1999). This could relate to either a shift in climate favouring the production of protoperidinoid dinoflagellates over *Leiosphaera* spp., a deepening of the environment, or shift to a more grounding-line distal glaciomarine setting, which would lead to a more marine signal rather than one dominated by freshwater input.
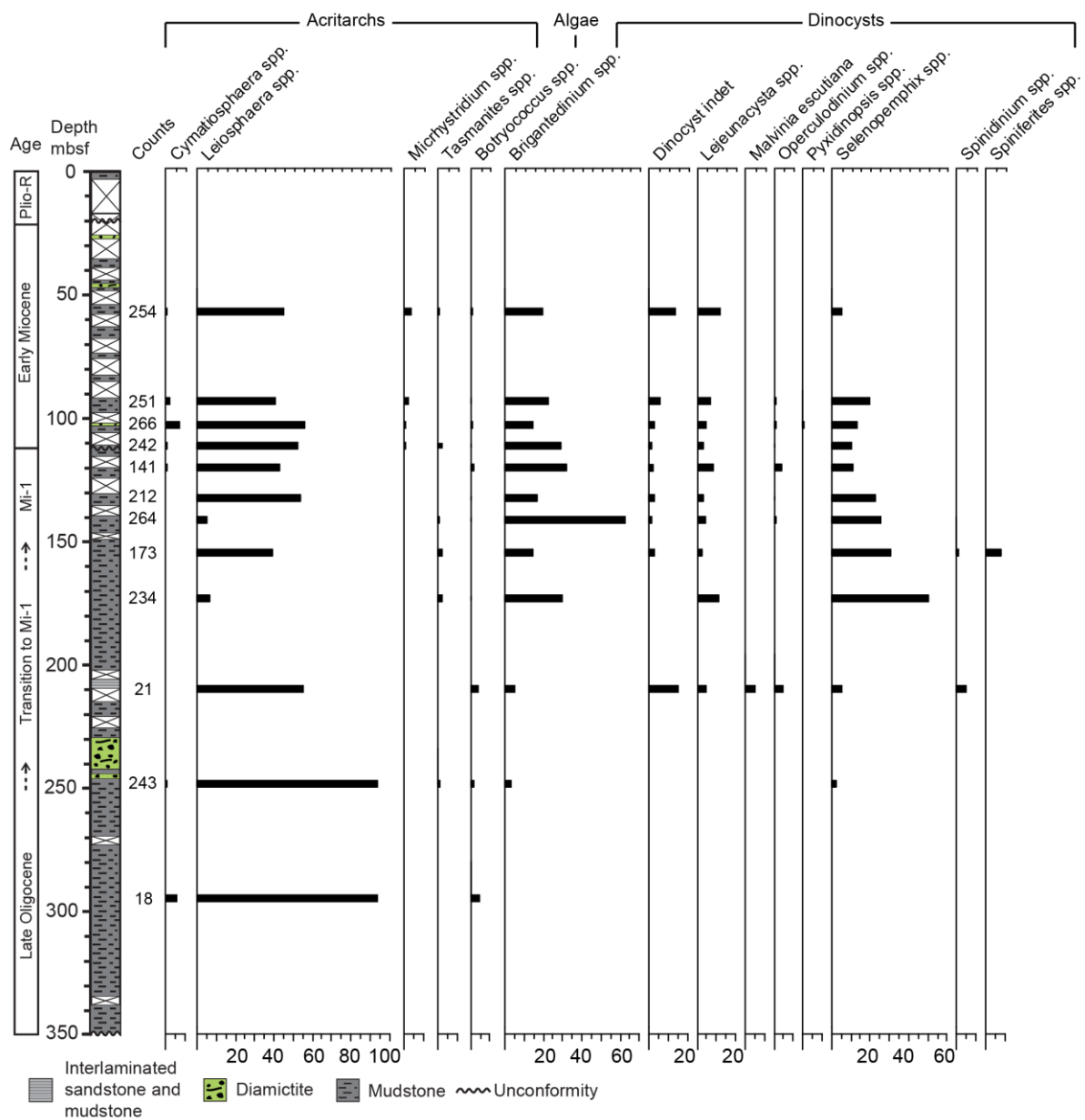
Figure 4.5: Marine palynomorphs from DSDP 270.
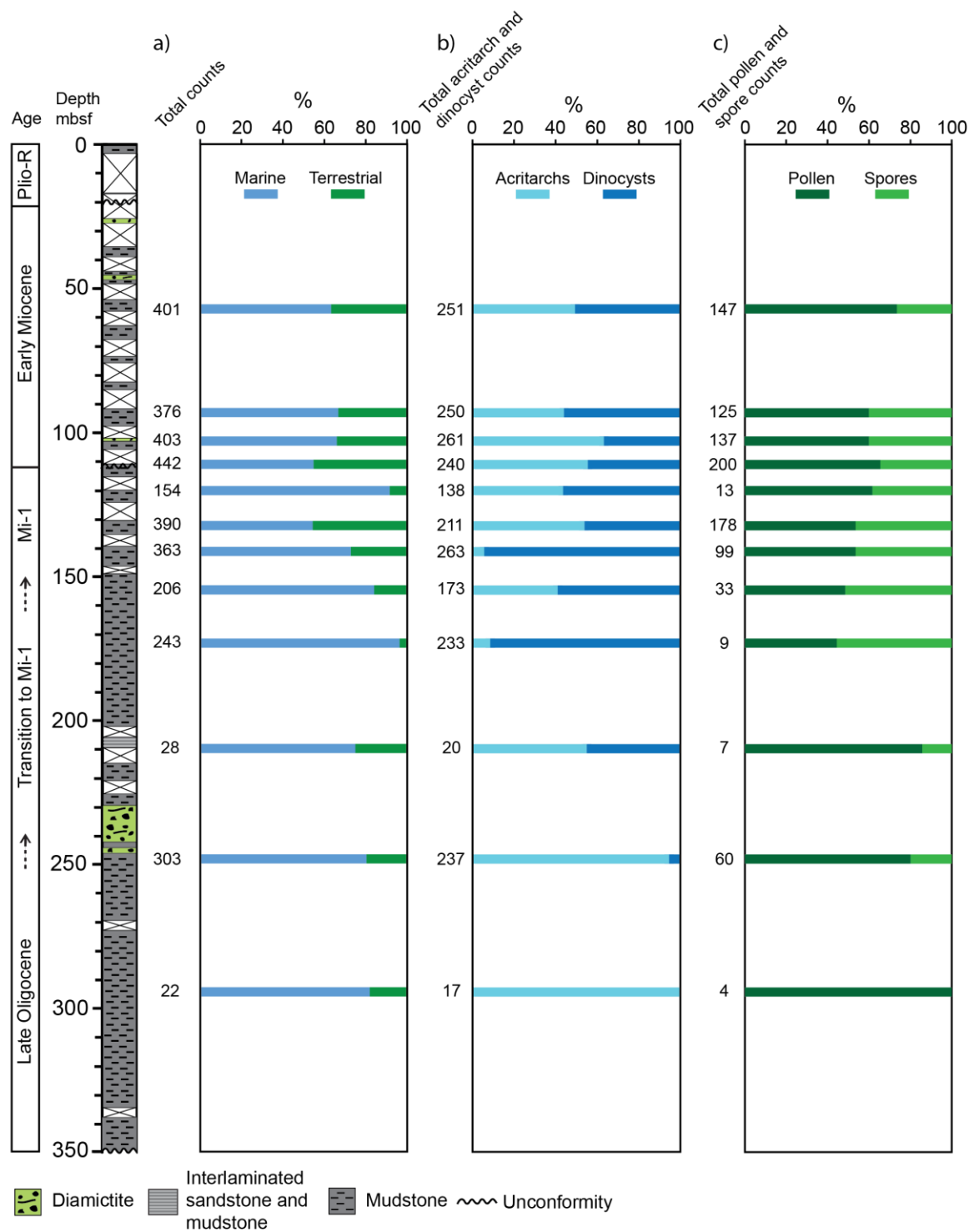
Figure 4.6: Relative proportions of a) marine and terrestrial palynomorphs, b) Acritarchs and dinocysts, and c) Pollen and spores.

4.3.3 GDGTs

Isoprenoid and branched GDGTs have been analysed throughout the core to provide proxies for ocean temperatures (via the TEX_{86} index and Ring Index (RI)), and mean annual air temperatures (via the MAT_{mrs} branched GDGT calibration).
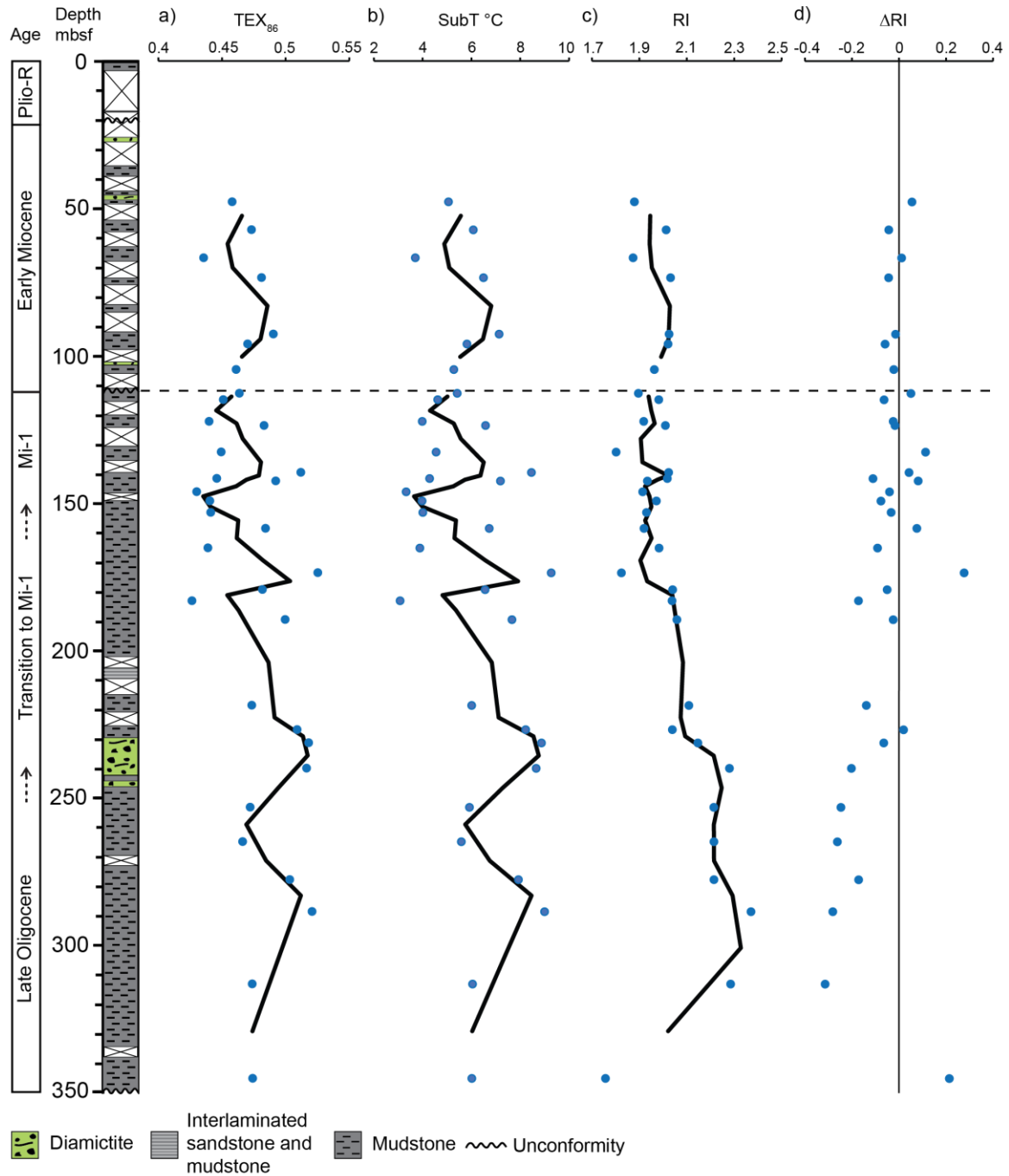
Figure 4.7: Isoprenoid GDGT based proxies in DSDP 270. (a) TEX_{86} index; (b) Sub surface temperatures using TEX_{86} based on BAYSPAR Standard calibration; (c) Ring index; and (d) The difference between sample ring index and calculated ring index. Blue dots represent individual samples, whilst the black lines are two point moving averages.

4.3.3.1 Isoprenoid GDGTs

Isoprenoid GDGTs are membrane lipids formed by marine archaea and have been found to increase the number of cyclopentane moieties they produce with increasing water temperature (Section 1.8.3.1) (Schouten et al., 2002, Schouten et al., 2013). The TEX_{86} index is commonly used to describe the relative abundance of isoprenoid GDGTs (Eq. 1.8) (Schouten et al., 2002). The TEX_{86} index excludes GDGT-0 and crenarcheaol as they often dominate samples and have an overpowering influence on the index (Schouten et al., 2002). At high latitudes and cool temperatures, the GDGTs that are used in the TEX_{86} index are commonly low in abundance, which can make peak integration challenging and results in potential for error. The abundances of these compounds were low in DSDP 270, potentially reflecting either dilution by rapid sedimentation or a sparse archeal community in the water column. This made integrations challenging in some instances, especially of the less abundant isoGDGTs (GDGT-2, GDGT-3 and cren').

The relationship between TEX_{86} and temperature can be influenced by several factors. Methanotrophic archaea can synthesise GDGTs in sediment during anaerobic oxidation of methane (Zhang et al., 2011). Zhang et al., (2011) formulated the Methane Index to investigate if the contribution of GDGTs from methanotrophic archaea may have contributed to a GDGT distribution (Eg. 1.9). Values for the Methane Index from DSDP 270 are all lower than 0.09, well below the value of >0.3 which Zhang et al., (2011) suggests as the lower limit for potential methanotrophic influence (Section 1.8.3.1). GDGTs from methanogenic Euryarchaeota can also bias TEX_{86} (Section 1.8.3.1). This has been assessed via %GDGT-0 with all samples demonstrating values lower than 67%, the suggested lower limit indicating a substantial contribution from methanogenic archaea (Eq. 1.10) (Sinninghe Damsté et al., 2012). The addition of GDGTs from terrestrial soils can also impact the TEX_{86} index in sites close to land. The BIT (branched versus isoprenoid tetraethers) index traces the input of terrestrial GDGTs and can be used to assess the influence of these GDGTs on TEX_{86} values, with 0 representing no terrestrial input, and 1 representing no marine input (Eq. 1.11) (Section 1.8.3.1) (Hopmans et al., 2004). BIT values in DSDP 270 all sit below 0.19, suggesting the terrestrial input is unlikely to have affected the TEX_{86} values.

Calibrating TEX_{86} at high latitudes can be also difficult, as core tops commonly show large scatter and a different relationship with temperature to the rest of the global oceans (Section

1.8.3.1, Chapter 5) (Kim et al., 2008, Kim et al., 2010). BAYSPAR has been used to calibrate to absolute temperatures (Tierney and Tingley, 2014, 2015). BAYSPAR is a Bayesian, spatially varying, regression calibration which takes into account local core top relationships between TEX_{86} and temperature to predict temperatures at high latitude sites (Tierney and Tingley, 2014, 2015). As archaea are predominantly concentrated in the subsurface waters around Antarctica (Chapter 5) (Murray et al., 1998, Church et al., 2003, Kalanetra et al., 2009), BAYSPAR has been applied in subsurface mode (subT), which uses weighted averages for temperatures over 0-200m water depths, weighted towards the shallow subsurface (~50 m) (Figure 4.7) (Tierney and Tingley, 2014, 2015). BAYSPAR is used in its standard subT mode, which assumes oceanographic conditions are similar enough to present that it is reasonable to use a spatially weighted distribution of core tops from the region. While oceanographic conditions were likely different, due to the distinctive nature of high latitude TEX_{86} relationships, it is important to spatially weight the calibration, as opposed to using BAYSPAR in analogue mode which instead finds similar TEX_{86} values from various locations throughout the global data set to form a calibration. Due to the scarcity of core tops in this region, using a spatially-varying calibration in this region results in large 90% uncertainty intervals, averaging ±6.0°C throughout the core.

TEX_{86}-SubTs through the core vary from 3.1°C to 9.3°C and average 6.0°C (Figure 4.7). An overall trend from warmer in the Late Oligocene to cooler in the Early Miocene is apparent. Samples taken from prior to the transition into the Mi-1 glacial, and in the Early Miocene (i.e. below 250 mbsf and above 112 mbsf) average 6.7°C for the Late Oligocene, and 5.6°C for the early Miocene. Samples from Mi-1 and the transitional periods show more scatter but show a general cooling trend, punctuated by several warmer samples during the transition into Mi-1. This is followed by a cool period at ~150 mbsf of ~3.3-4°C, warming up to 8.5°C at ~140 mbsf, before cooling to average ~5.0°C for the rest of the glacial (Figure 4.7). Cooling into Mi-1 of ~5° is of greater magnitude than proximal Antarctic records suggest occurred between the Last Glacial Maximum and present, but is similar to the changes determined in Subantarctic waters (Gersonde et al., 2005, Waelbroeck et al., 2009, Benz et al., 2016). A Mi-1 temperature of ~3.3-4°C is also warmer than modern and LGM temperatures of 0 to -2°C in the Ross Sea (Orsi and Wiederwohl, 2009, Boyer et al., 2013).

Warmer subTs at ~140 mbsf suggest a brief return to warmer SSTs in the Ross Sea during Mi-1. In global deep-sea isotope and temperature records, the transition into Mi-1 and the

glaciation itself display periods of relatively warmer and cooler temperatures (Figure 4.1) (i.e. Mawbey and Lear, 2013, Beddow et al., 2016). Other potential mechanisms for producing warmer SSTs during a cold period were suggested by McKay et al. (2012a), who used TEX_{86} to investigate SSTs in the Ross Sea in the Pliocene, using the ANDRILL-1B drill core. They found sediments which corresponded to times of glacial advance and retreat contained warmer temperatures than during an interglacial, a finding which they put down to enhanced stratification warming the upper water column, either as a result of meltwater input from retreating glaciers or increased duration and/or extent of coastal sea ice. In DSDP 270, marine palynomorphs only show a minor input of *Leiosphaera* spp. at this depth, suggesting there was not a strong fresh water influence. McKay et al. (2012a) also indicated that samples associated with glacial sediments (diamictites) also sometimes showed warmer temperatures, potentially as the result of incorporating some reworked material older, warmer environments. This interpretation was based on the widespread presence of Miocene-aged diatoms incorporated into Last Glacial Maximum tills in the Ross Sea (Sjunneskog and Scherer, 2005).

The low abundance of the GDGTs used in the TEX_{86} index at this site does mean there is larger potential for error. Potentially a better way of assessing temperature change at this high latitude location is the Ring Index (RI), which is the weighted average of ring numbers in GDGT compounds (Zhang et al., 2016b) (Eq. 1.12, section 1.8.3.1), whereby higher values of RI indicate warmer temperatures. In cold samples, GDGT-0 and crenarchaeol dominate the samples, providing much more distinct peaks to integrate. As they have a strong impact on calculating the RI, but are not included in the TEX_{86} index, it is proposed that the relative temperature trends sourced from the RI are potentially more reliable indicators of temperature trends at this site. Culture experiments indicate that the relationship between TEX_{86} and temperature can be variable and non-linear between different strains of archaea, but that the relationship between RI and temperatures was linear across the studied strains (Section 1.8.3.1) (Qin et al., 2015). While RI could potentially be a better proxy for temperature, no calibrations to absolute temperatures have yet been produced. RI in DSDP 270 displays a clear trend from higher values in the Late Oligocene, averaging 2.18 below 250 mbsf, to lower values in the Early Miocene, averaging 1.97 above 112 mbsf (Figure 4.7). Values start to decrease above ~240 mbsf, coincident with glacially proximal sediments in the core. RI remains at a consistently low values from ~170 mbsf and above (Figure 4.7).

Analysis by Zhang et al. (2016b) shows that in the modern ocean, RI can be calculated from TEX_{86} using a regression (Eq. 1.13, Section 1.8.3.1). If an RI value deviates from the calculated RI by more than ± 0.3 RI units, then the TEX_{86} value for that sample is potentially influenced by non-thermal factors. The residual difference between sample RI and calculated RI (ΔRI) range in DSDP 270 between 0.28 and -0.31 (Figure 4.7). The residual tends to be greater during the late Oligocene period of the core. Non-thermal effects that can impact ΔRI include increased terrestrial input and *in situ* production of GDGTs in sediment by archaea associated with anaerobic methane oxidation (Zhang et al., 2016b). However, these factors have been assessed via the BIT and MI indices and were found to have been unlikely to have had an impact on TEX_{86} at this site. An increased ΔRI during the Late Oligocene could be the result of non-thermal influences such as changes in archaeal growth rates, or an archaeal community that does not have a modern analogue (Zhang et al., 2016b). Certainly, archaeal communities at high latitudes in the modern ocean have a different relationship between TEX_{86} and temperature than the rest of the global ocean (Kim et al., 2008, Kim et al., 2010). Potentially, the shallow water setting of DSDP 270 in the Late Oligocene may have contained an archaeal community that, while likely still dominantly controlled by temperature, consisted of an assemblage for which there is not an accurate modern analogue.

4.3.3.2 Branched GDGTs

Branched GDGTs from terrestrial soils vary their number of methyl groups and cyclopentane moieties with changes in both soil pH and mean annual air temperature, and can be washed offshore and deposited in marine environments (Section 1.8.3.1) (Weijers et al., 2007a). Usually, temperatures are calibrated using the MBT or MBT' indices, which use ratios of 9 and 7 different branched GDGTs, respectively (Section 1.8.3.1) (Weijers et al., 2007a, Peterse et al., 2012). At DSDP 270, many of the minor branched GDGTs are either very low in abundance or are below detection limit. Situations like this have been taken into account by De Jonge et al. (2014) who found that MAT could still be reliably estimated using just fractional abundances of the three most dominant branched GDGTs (Ia, IIa, and IIIa) (Eq. 1.24). The residual mean standard error using this method is 5°C. In DSDP 270, there is a relatively large amount of scatter through the Late Oligocene and early stages of the transition into Mi-1, with no consistent trend (Figure 4.8). Low abundance and resultant challenges for integration may account for some of the scatter observed. Temperatures throughout the core average ~10°C. MAT_{mrs} is slightly warmer than average (~11°C) at ~150 mbsf, which is when SSTs indicate

the coolest offshore temperatures. MAT$_{mrs}$ then cools after this point, to a minimum value of 7.6°C at 132 mbsf. Samples in the Early Miocene section (above 112 mbsf) average ~10°C.
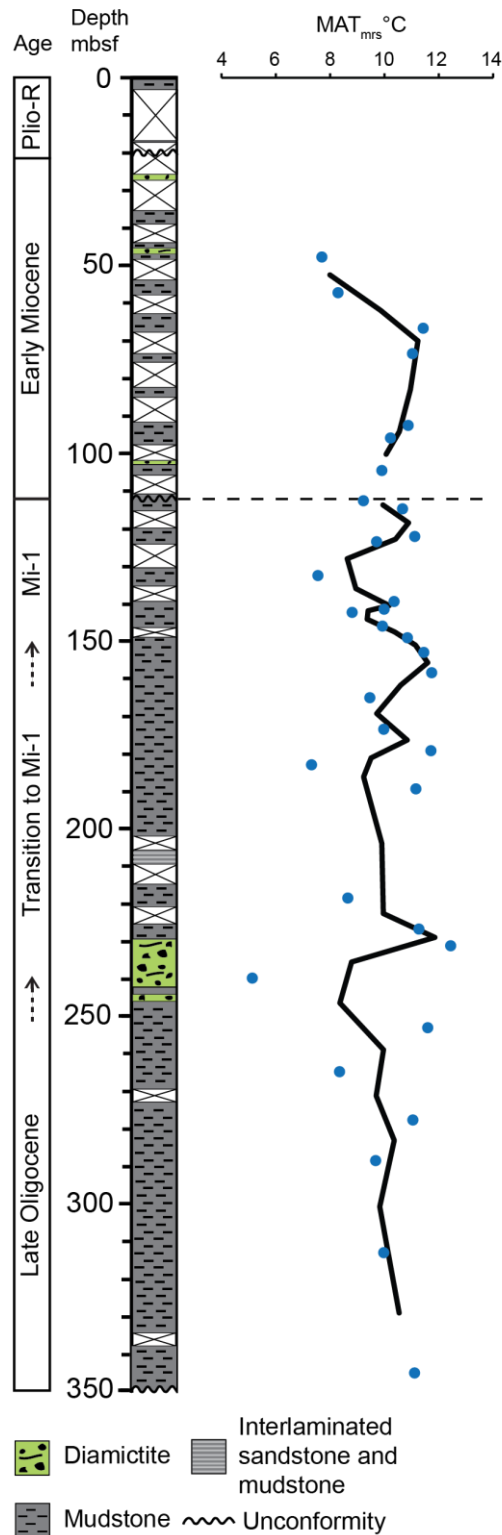
Figure 4.8: Air temperature from DSDP 270, likely reflecting mean summer temperatures, using the MAT$_{mrs}$ index. Blue dots represent individual samples, whilst the black line is a two point moving average.

BrGDGT based proxies can exhibit a seasonal bias, if the soil bacteria producing these compounds have a primary growing season (i.e. Weijers et al., 2007b). It is likely that in Antarctica, the growth season would be over the Austral summer, leading to an MBT_{mrs} bias to summer temperatures. A summer bias was also suggested for MBT-based temperatures offshore Wilkes Land, Antarctica in the Eocene (Pross et al., 2012). A mean summer temperature (MST) of ~10°C aligns well with pollen data during the Oligocene in Cape Roberts 2/2A which suggests an MST in the range of 4-12°C (Prebble et al., 2006a). An estimate for the early Miocene from pollen in Cape Roberts 2/2A suggests cooler MSTs than observed from DSDP 270 of ~7°C (Raine, 1998).

4.3.4 *n*-Alkanes

n-Alkane distributions from DSDP 270 are typically bimodal, with a peak in the lower molecular weight range where $n\text{-}C_{17}$ or $n\text{-}C_{19}$ are the most abundant *n*-alkanes, and a high molecular weight peak where $n\text{-}C_{27}$ is the most abundant, followed by $n\text{-}C_{25}$ and $n\text{-}C_{29}$.

The $n\text{-}C_{15}$, $n\text{-}C_{16,}$ $n\text{-}C_{17}$, $n\text{-}C_{18}$ and $n\text{-}C_{19}$ are grouped together as LMW *n*-alkanes from algal and bacterial sources (Section 1.8.1). In DSDP 270, LMW *n*-alkanes are likely dominated by marine inputs, as samples taken from terrestrial outcrops on land show no, or only very small abundances of LMW *n*-alkanes (Chapter 3).

Compound specific isotope measurements indicate that the $n\text{-}C_{23}$ homologue has a different source from longer chained *n*-alkanes (section 4.3.5), and therefore the down core abundance of $n\text{-}C_{23}$ is displayed separately. The $n\text{-}C_{23}$ is known to be produced by non-emergent aquatic plants and sphagnum mosses (Section 1.8.1). As there are no records of *n*-alkane distributions in the modern analogues of the dominant moss species in DSDP 270 (*Coptospora* spp.), it is assumed that $n\text{-}C_{23}$ dominates these mosses as in the case of sphagnum. Thus, the $n\text{-}C_{23}$ in samples studied from DSDP 270 is likely sourced from mosses and submerged aquatic plants. Critical evidence for this assumption comes from *n*-alkane distributions from Miocene sediments at Mt Boreas in the Transantarctic Mountains (Chapter 3), where high abundances of $n\text{-}C_{23}$ coincide with an assemblage which includes some of the bryophyte species described from DSDP 270, including *Coptospora* spp.
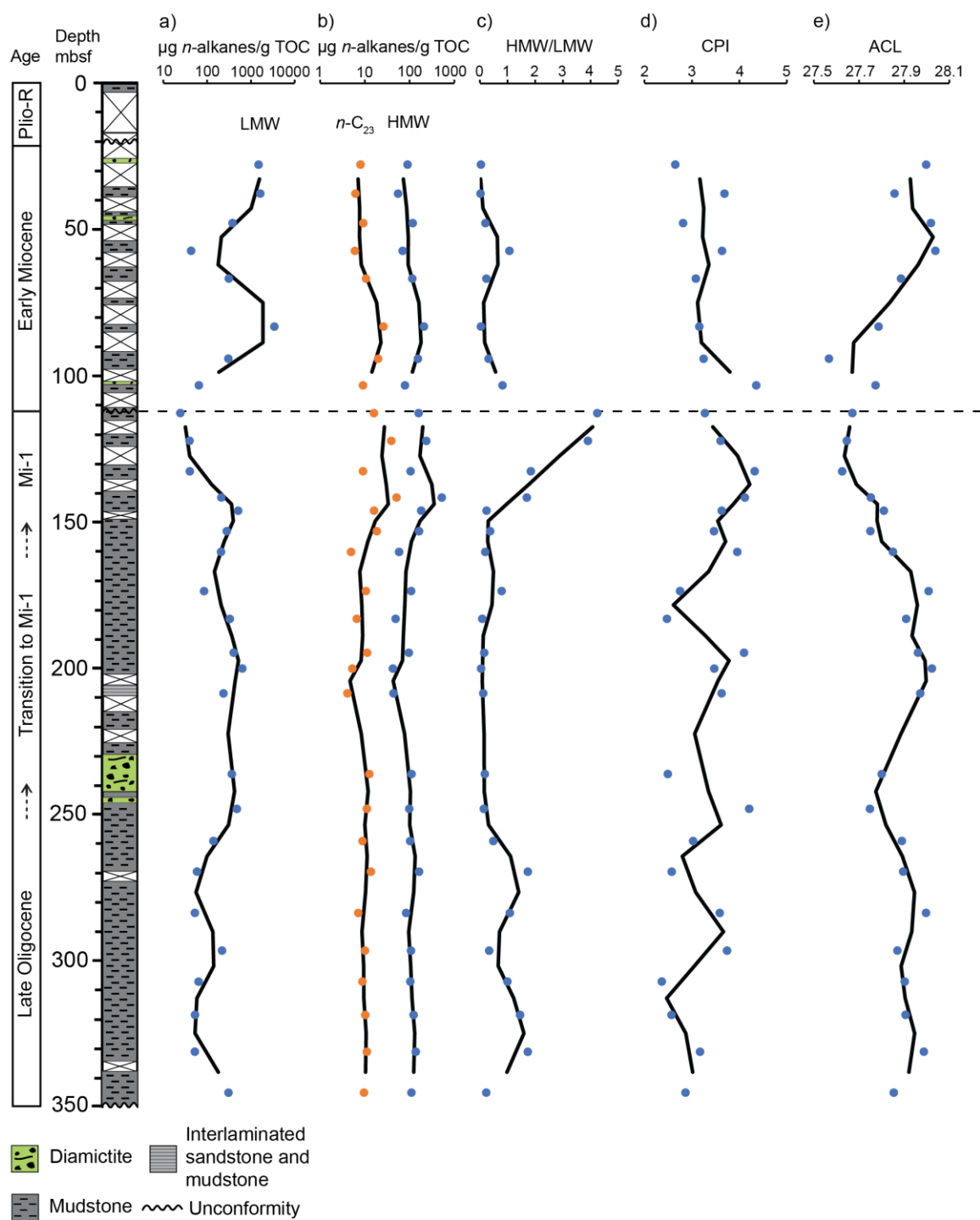
Figure 4.9: n-Alkane abundances and ratios in DSDP 270. (a) Abundance of low molecular weight (LMW) n-alkanes; (b) Abundance of high molecular weight (HMW) n-alkanes and n-C₂₃; (c) ratio of HMW n-alkanes to LMW n-alkanes; (d) carbon preference index (CPI); and (e) average chain length (ACL). Blue dots represent individual samples, whilst black line are two point moving averages.

The n-C$_{25}$, n-C$_{27,}$ n-C$_{29}$ and n-C$_{31}$ are grouped to represent HMW n-alkanes sourced from terrestrial plants (section 1.8.1). Pollen from DSDP 270 shows a dominance of *Nothofagus* spp. (Kemp and Barrett, 1975). A modern study on *Nothofagus* spp. in Southern New Zealand notes that n-C$_{27}$ is the dominant n-alkane in at least one modern species of this tree (Section 3.4.3, Burrington 2015). This study also highlights that n-C$_{25}$ is commonly abundant in *Nothofagus* spp. While there may be some contribution to n-C$_{25}$ from mosses and aquatic plants, the high relative abundances of *Nothofagus* spp. pollen suggest that n-C$_{25}$ is likely to be sourced predominantly from higher plants. This inference is also supported by compound specific isotopes, which show a clear relationship between n-C$_{25}$ and the other long chained n-alkanes, but not between n-C$_{25}$ and n-C$_{23}$ (Section 4.3.5). This indicates that plants producing n-C$_{25}$ are likely the same plants that are producing the longer chain lengths, or at least are growing in similar habitat conditions to these plants. While some studies have shown that certain groups of gymnosperms produce significantly less n-alkanes than angiosperms, Podocarpaceae contains relatively high abundances of n-alkanes (Diefendorf et al., 2011, Bush and McInerney 2013, Diefendorf et al., 2015). As Podocarpaceae are the dominant gymnosperms present in DSDP 270, this indicates that the distribution of n-alkanes at this site reflects a catchment integrated signal of the vegetation assemblage present, without a strong bias towards angiosperms.

Abundances of n-alkanes down core are normalised to TOC (Figure 4.9). LMW n-alkanes dominate the record for most of the core, but do display lower abundances than the HMW n-alkanes over the majority of the Mi-1 event. LMW n-alkanes decrease through Mi-1 to 24 μg/gTOC, their lowest abundance in the core. In the marine palynomorph record, acritarchs (mainly *Leiosphaera* spp.) also decrease in abundance over Mi-1, while dinoflagellates increase. As noted previously, this may be due to a shift in the depth of the depositional environment rather than necessarily a response to climatic changes (section 4.3.2). The increase in protoperidinoid dinoflagellates coinciding with a decrease in LMW n-alkanes suggests that these may not be a dominant source of LMW n-alkanes in sediment. Instead, acritarchs or other marine algae and bacteria may be the primary source of LMW n-alkanes at this site. A decrease in LMW accumulation indicates oceanic conditions may not have been as favourable for LMW n-alkane producers over the Mi-1 glaciation, inferred to have resulted from either a change in oceanographic setting (i.e. increase in water depth) or changing climate parameters (i.e. cooler SSTs, increase in sea ice, changes in nutrient supply).

HMW n-alkanes and n-C$_{23}$ derive from different terrestrial vegetation sources, but their down core abundances follow the same trends. The lowest abundances of HMW n-alkanes are in the Late Oligocene just prior to Mi-1, with values down to 43 μg/gTOC. HMW n-alkanes increase early in Mi-1 to 527 μg/gTOC, and remain moderately high for the rest of the glacial event. There are several possible reasons for this trend. Firstly, as the age model for the core is not yet precisely known, n-alkane abundances are not able to be described in terms of the actual flux to the site through time. It is possible that the increase in HMW n-alkanes and n-C$_{23}$, and a corresponding increase in terrestrial palynomorph counts (section 4.3.2), could be an artefact of a decrease in sedimentation rate. However, LMW n-alkanes show a marked decrease over Mi-1, indicating that a potential lowering of sedimentation rate is not contributing to an increased accumulation of the LMW fraction. This implies that the increase in HMW n-alkanes and n-C$_{23}$ predominantly reflects a real environmental signal. Several potential reasons for an increase in terrestrial n-alkanes at DSDP 270 are considered here.

In the older portion of DSDP 270, the dominant sediment source was likely the proximal Central High and thus vegetation on the Central High probably would have been the primary source for terrestrial n-alkanes, although n-alkanes are also able to be transported long distances by aeolian transport (i.e. Gagosian and Peltzer, 1986, Bendle et al., 2007). Deepening of the paleo-environment from ~250 mbsf may have resulted in a change in transport path for terrestrial material reaching the core site. Potentially, the wider Ross Sea region became the major source for terrestrial material at DSDP 270, reaching the site via suspended sediment load in ocean currents or aeolian transport. An increase in terrestrial n-alkanes above 150 mbsf in DSDP 270 could reflect a shift in either of these transport mechanisms, i.e. a shift in windiness or in the ocean currents crossing the core site would result in a change in n-alkane accumulation.

In a simple explanation, an increase in terrestrial n-alkanes could reflect more vegetation onshore. Certainly, the pollen and spore counts increase above ~150 mbsf in the core. However as this increase occurs over a period of inferred significant ice expansion it would be expected that there would be less available land onshore for vegetation to grow on. Changes to the vegetation assemblage onshore could also result in increases of terrestrial n-alkane accumulation offshore. Different species of plants produce significantly different quantities of n-alkanes (Bush and McInerney, 2013). The shift in vegetation to plants that produce more n-alkanes could also account for an increase in terrestrial n-alkanes at DSDP 270, without

necessarily requiring the actual amount of vegetation onshore to increase. However, palynomorph evidence suggests that there was not a significant overturning in vegetation over Mi-1. While variations in the relative abundances of certain species occurred, the same dominant species were present before, during and after the glacial. A recent study found that in the tropics, plants at higher elevations tend to produce more n-alkanes than lowland plants, a strategy thought to be a response to environmental pressures such as lower temperatures (Feakins et al., 2016). Applying this to DSDP 270, it is possible that more terrestrial n-alkanes offshore could be a result of increasing production of n-alkanes in onshore plants in response to the cold temperatures and harsher climates of the glacial.

Lastly, the expansion of the ice sheets during Mi-1 could have increased erosion and the loss of vegetation onshore, as the growing ice sheets and harsh climate resulted in loss of habitat and devegetation of the continent. This could have resulted in an increased flux of n-alkanes and terrestrial palynomorphs to the core site, especially during the early stages of the glaciation. It is therefore possible that the increase in HMW n-alkanes, n-C$_{23}$, and terrestrial palynomorphs represents a combination of the devegetation of the continent, changes in transport mechanisms such as wind fields and ocean currents, as well as the potential (but as yet not well established) increase in production of n-alkanes at cooler temperatures.

When the HMW and LMW n-alkanes are plotted as a ratio (Figure 4.9), the differences between source inputs becomes even more apparent. HMW n-alkane inputs to the core site slightly predominate over LMW homologues, especially during two peaks in the Late Oligocene. Notably the Mi-1 event is distinguished by an increase in the HMW/LMW ratio by a factor of four. This is mainly a function of major decrease in flux of LMW n-alkanes to the core site, combined with a slight increase in HMW n-alkane flux.

High molecular weight n-alkanes can be characterised by their carbon preference index (CPI) (Eq. 1.1, section 1.8.1). CPI values in DSDP 270 range from 2.4-4.4, with a mean value of 3.3, indicating terrestrial plants are the dominant source of high molecular weight n-alkanes reaching the core site. While there is little trend in CPI through the core, constantly high values are present through Mi-1 (Figure 4.9). Slightly higher CPI during this period could be related to colder temperatures through the glacial, as microbial degradation of n-alkanes proceeds more slowly in cold conditions. In peat bog records, CPI has been used to infer changes in

temperatures, with higher values representing colder periods with less *n*-alkane degradation (i.e. Xie et al., 2004, Zhou et al., 2005, Vogts et al., 2012).

Average chain length (ACL) is also characterised for the HMW *n*-alkanes (Eq. 1.2) (Poynter et al., 1989, Schefuß et al., 2003). At site DSDP 270, ACL varies between ~27.8 and 28 before and after Mi-1, with values decreasing to ~27.6-27.7 during Mi-1 (Figure 4.9). Variation in average chain length is likely a result of either climate-driven plastic response of *n*-alkanes to temperature or aridity within a plant community, or changes to the composition of the plant community in response to climate (Section 3.1.1) (Bush and McInerney, 2013). ACL decreases over Mi-1, and as there is no significant overturning in vegetation over this event, this decrease is considered a response to a colder climate.

4.3.5 n-Alkane δ^{13}C

Carbon isotope ratios were measured on all *n*-alkanes from n-C$_{23}$ to n-C$_{31}$. δ^{13}C ranges from -20.45‰ to -38.13‰, with most values between -25.8‰ and -31.5‰. This study focuses on the n-C$_{23}$ to n-C$_{31}$ odd-numbered *n*-alkanes, as these were consistently the most abundant plant derived *n*-alkanes, yielded clean molecular peaks and produced the most complete compound specific isotopic records (Figure 4.10). One value each for n-C$_{25}$, n-C$_{27}$ and n-C$_{29}$, and three values for n-C$_{31}$ were excluded as outliers, as they were significantly different from adjacent samples by more than 2‰. The late Oligocene is marked by heavier values of δ^{13}C, becoming lighter through the transition into Mi-1, before reaching their lightest values during the early stages of Mi-1. δ^{13}C shifts to slightly heavier values in the Early Miocene, but does not return to the Late Oligocene values. δ^{13}C for n-C$_{23}$ shows a different trend, with values moving slightly lighter during the transition to Mi-1, but then shift slightly heavier over the glacial event. While the HMW *n*-alkanes are all significantly correlated to each other (ranging between r=0.785, p=<0.000 for n-C$_{25}$ and n-C$_{31}$, to r=0.939, p=<0.000 for n-C$_{29}$ and n-C$_{31}$), the HMW *n*-alkanes and n-C$_{23}$ are not correlated (ranging between r=0.130, p=0.564 for n-C$_{23}$ and n-C$_{25}$ and r=0.314, p=0.154 for n-C$_{23}$ and n-C$_{29}$). In order to facilitate comparisons with results from the literature (at variable temporal resolutions) the data is binned into four intervals, Late Oligocene (350-248 mbsf), transition (248-155 mbsf), Mi-1 (155-112 mbsf), and Early Miocene (112-27 mbsf), and values within each bin were averaged. HMW *n*-alkanes show a marked negative carbon isotope excursion across the O/M boundary, with the magnitude

between the Late Oligocene and Mi-1 values varying between -2.5‰ for n-C_{25}, -1.5‰ for n-C_{27}, -3.4‰ for n-C_{29} and -4.8‰ for n-C_{31} (table 4.1).

Table 4.1:Binned $\delta^{13}C$ for odd chained n-alkanes.

$\delta^{13}C$	n-C_{23}	n-C_{25}	n-C_{27}	n-C_{29}	n-C_{31}
L.O.	-28.58	-27.19	-28.79	-27.68	-25.77
Transition	-29.66	-28.16	-29.86	-30.05	-29.52
Mi-1	-28.81	-29.72	-30.32	-31.05	-30.61
E.M.	-29.10	-28.31	-29.63	-30.25	-30.74

4.3.5.1 HMW n-alkane $\delta^{13}C$

The $\delta^{13}C$ values of plant organic matter (and thus leaf waxes) are the result of the isotopic composition of the carbon source, atmospheric CO_2 ($\delta^{13}C_{atm}$), and carbon isotope discrimination by the plant (Farquhar et al., 1989). Plants are depleted in $\delta^{13}C$ relative to $\delta^{13}C_{atm}$ due to enzymatic and physical processes that discriminate against ^{13}C (Marshall et al., 2007). In leaves of C_3 plants, net discrimination (Δ) is described by the relationship:

$$\Delta = a + (b - a) \times p_i/p_a \qquad \text{(Eq. 4.1)}$$

Where a is a fractionation of 4.4‰ caused by the diffusion of CO_2 from the atmosphere into the stomata, b is the photosynthetic fractionation by Rubisco of 27‰, and p_i/p_a is the ratio between the partial pressure of CO_2 in the leaf (p_i) to the atmosphere (p_a) (Farquhar et al., 1989). The p_i/p_a ratio reflects the balance between stomatal conductance and photosynthetic uptake of CO_2 (Farquhar et al., 1989).

The magnitude of carbon isotope discrimination (Δ) across the Mi-1 glaciation can be described by the difference between the $\delta^{13}C_{atm}$, and the $\delta^{13}C$ incorporated into the plant ($\delta^{13}C_{TT}$):

$$\Delta = (\delta^{13}C_{atm} - \delta^{13}C_{TT})/(1 + \delta^{13}C_{TT}/1000)$$
$$\Delta \cong \delta^{13}C_{atm} - \delta^{13}C_{TT} \qquad \text{(Eq. 4.2)}$$

Where $\delta^{13}C_{atm}$ represents the carbon isotopic value of the atmosphere, and $\delta^{13}C_{TT}$ refers to the carbon isotopic value of the total plant tissue (Farquhar et al., 1989). To estimate $\delta^{13}C_{atm}$, two

different methods are followed. The first is described by Smith et al. (2007) which uses planktic foraminifera records of $\delta^{13}C$ ($\delta^{13}C_{pf}$) from ODP site 926 on the Ceara Rise in the equatorial Atlantic, while the second is based on the relationship between $\delta^{13}C_{atm}$ and $\delta^{13}C_{TT}$ in modern C_3 plants (Arens et al., 2000).
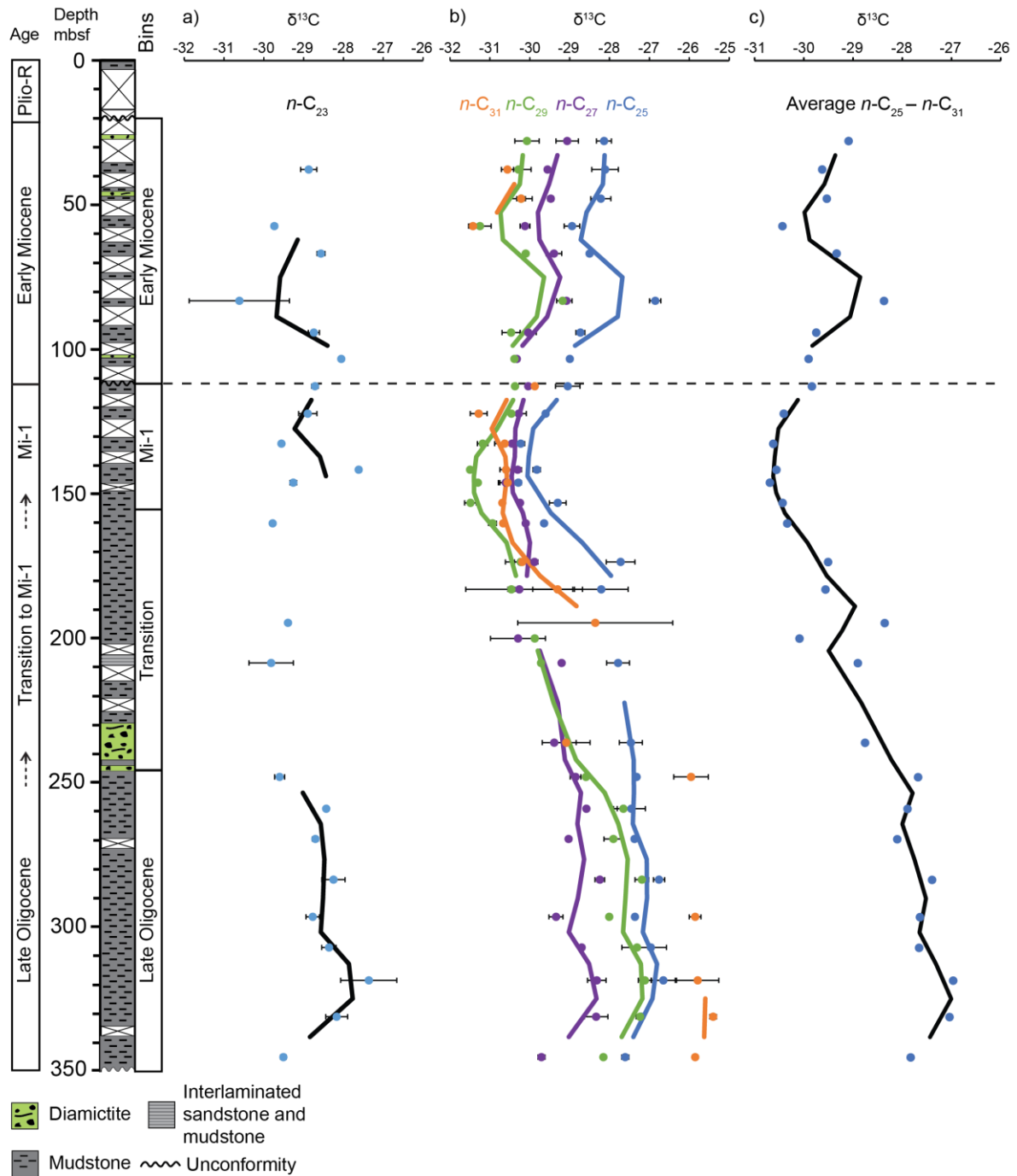
Figure 4.10: Compound specific carbon isotopes on n-alkanes in DSDP 270 (a) n-C₂₃; (b) n-C₂₅, n-C₂₇, n-C₂₉ and n-C₃₁; and c) the averaged δ¹³C of n-C₂₅ - n-C₃₁. Data bins are displayed next to the stratigraphic log. Blue dots represent individual samples, whilst black lines are two point moving averages.

To determine $\delta^{13}C_{atm}$ using the method of Smith et al. (2007), values of $\delta^{13}C_{pf}$ of *Globigerinoides primordius* from ODP site 926 have been binned in averages for Late Oligocene (24.2-23.2 Ma), Mi-1 (23.1-22.9 Ma) and Early Miocene (22.8-21.2 Ma) (Table 4.2) (Paul et al., 2000, Flower et al., 2006, Mawbey and Lear, 2013). Planktic isotope data were too sparse for a transitional bin to be determined. Due to the scarcity of published planktic isotope data covering the Late Oligocene to Early Miocene in an individual core, an Early Miocene average has been derived from slightly older sediment (22.8-21.6 Ma) than is likely sampled in DSDP 270 (~20 Ma). $\delta^{13}C_{atm}$ is calculated assuming isotopic equilibrium between the atmosphere, marine dissolved inorganic carbon, and planktonic foraminifera calcite, using the relationship from Romanek et al. (1992):

$$\varepsilon_{pf-CO_{2(atm)}} = [(\delta^{13}C_{pf} + 1000)/(\delta^{13}C_{atm} + 1000) - 1] \times 10^3 \qquad \text{(Eq. 4.3)}$$

Where $\varepsilon_{pf\text{-}CO_{2(atm)}}$ represents the temperature dependent fractionation factor relating $\delta^{13}C_{pf}$ to $\delta^{13}C_{atm}$ described by:

$$\varepsilon_{pf-CO_{2(atm)}} = 11.98 - 0.12 \times T(°C) \qquad \text{(Eq. 4.4)}$$

Where $T(°C)$ is the sea surface temperature. To calculate sea surface temperatures, oxygen isotopes ($\delta^{18}O_{pf}$) on planktic foraminifera from ODP 926, and the equation from Erez and Luz (1983) is used:

$$T\ (°C) = 16.998 - 4.52\left(\delta^{18}O_{pf} - \delta^{18}O_{sw}\right) \qquad \text{(Eq. 4.5)}$$

Where $\delta^{18}O_{sw}$ represents the $\delta^{18}O$ of sea water. $\delta^{18}O_{sw}$ values are estimated from Mawbey and Lear (2013) (-1‰ for pre-O/M, -0.5‰ for peak-O/M, and -0.8‰ for post-O/M), who determined $\delta^{18}O_{sw}$ using benthic foraminifera from Site 926. $\delta^{13}C_{atm}$ shows a positive excursion over the O/M boundary and Mi-1 glaciation, with values increasing from -7.42‰ to -6.89‰, and returning to -7.11‰ in the earliest Miocene.

Table 4.2: Estimating $\delta^{13}C_{atm}$ using planktic foraminiferal data of G. primordius from ODP site 926 (Paul et al., 2000, Flower et al., 2006, Mawbey and Lear, 2013). $\delta^{18}O_{sw}$ estimated from Mawbey and Lear (2013). L.O. = Late Oligocene, E.M.= Early Miocene, S.D= Standard deviation, $\varepsilon_{pf\text{-}CO_{2(atm)}}$ = the temperature dependent fractionation factor relating $\delta^{13}C_{pf}$ to $\delta^{13}C_{atm}$.

Site 926	$\delta^{13}C$ *G. primordius* (‰)	S.D. (‰)	$\delta^{18}O$ *G. primordius* (‰)	S.D. (‰)	$\delta^{18}O$ sea water (‰)	Temperature from $\delta^{18}O$ (°C)	$\varepsilon_{pf\text{-}CO_{2(atm)}}$	$\delta^{13}C_{atm}$ (‰)
L.O.	1.91	0.25	-1.99	0.19	-1	21.49	9.40	-7.42
Mi-1	2.40	0.14	-1.57	0.16	-0.5	21.88	9.36	-6.89
E.M.	2.29	0.18	-1.66	0.18	-0.8	20.91	9.47	-7.11

An alternative method for obtaining $\delta^{13}C_{atm}$ is to use a regression between $\delta^{13}C_{atm}$ and $\delta^{13}C_{TT}$ derived from late Pleistocene, Holocene, modern and growth chamber relationships in C_3 plants (Arens et al., 2000):

$$\delta^{13}C_{atm} = \frac{\delta^{13}C_{TT} + 18.67}{1.10} \qquad \text{(Eq. 4.6)}$$

Arens et al. (2000) suggests that $\delta^{13}C_{atm}$ accounts for the bulk of variation in $\delta^{13}C_{TT}$ as these values are highly correlated with a linear relationship ($r^2= 0.91$, $p <0.001$).

To calculate the carbon isotopic value of the total plant tissue ($\delta^{13}C_{TT}$), an enrichment factor must be applied to account for isotopic fractionation between plant tissue and individual *n*-alkanes (ε_{lipid}). This is calculated by applying *n*-alkane specific averages from published data (Collister et al., 1994, Chikaraishi and Naraoka, 2003, Diefendorf et al., 2011). The $\delta^{13}C$ of the long chained *n*-alkanes sequestered at site DSDP 270 reflects a catchment integrated signal of the *n*-alkanes produced in the onshore terrestrial biosphere. Published data for temperate C_3 plants is used to calculate ε_{lipid} (Collister et al., 1994, Chikaraishi and Naraoka, 2003, Diefendorf et al., 2011), and ε_{lipid} corrections of 3.28‰ for *n*-C_{25}, 3.46‰ for *n*-C_{27}, 3.90‰ for *n*-C_{29} and 4.17‰ for *n*-C_{31} are applied.

Using the equation of Arens et al. (2000) (Eq. 4.6) determines a different value of $\delta^{13}C_{atm}$ for each *n*-alkane chain length in DSDP 270. Averages for both *n*-C_{25} - *n*-C_{31} as well as *n*-C_{25} - *n*-

C_{29} are displayed in table 4.3, as the Late Oligocene value for $n\text{-}C_{31}$ (-2.66‰) is higher than Cenozoic reconstructed values of $\delta^{13}C_{atm}$ (Tipple et al., 2010). Contrary to what is found when using planktic foraminifera, plant waxes suggest that $\delta^{13}C_{atm}$ becomes more negative over Mi-1 shifting from an average of -4.53‰ ($n\text{-}C_{25}$ - $n\text{-}C_{31}$) or -5.16‰ ($n\text{-}C_{25}$ - $n\text{-}C_{29}$) in the Late Oligocene to -7.32‰ ($n\text{-}C_{25}$ - $n\text{-}C_{31}$) or -7.41‰ ($n\text{-}C_{25}$ - $n\text{-}C_{29}$) during Mi-1. In the Early Miocene, values become slightly higher again, shifting to -6.61‰ ($n\text{-}C_{25}$ - $n\text{-}C_{31}$) or -6.46‰ ($n\text{-}C_{25}$ - $n\text{-}C_{29}$).

Table 4.3: Estimating $\delta^{13}C_{atm}$ using the method of Arens et al. (2000) based on n-alkanes. L.O. = Late Oligocene, E.M.= Early Miocene, S.D= Standard deviation

	$n\text{-}C_{25}$ $\delta^{13}C_{atm}$ (‰)	$n\text{-}C_{27}$ $\delta^{13}C_{atm}$ (‰)	$n\text{-}C_{29}$ $\delta^{13}C_{atm}$ (‰)	$n\text{-}C_{31}$ $\delta^{13}C_{atm}$ (‰)	Average $n\text{-}C_{25}\text{-}n\text{-}C_{31}$ $\delta^{13}C_{atm}$ (‰)	S.D. (‰)	Average $n\text{-}C_{25}\text{-}n\text{-}C_{29}$ $\delta^{13}C_{atm}$ (‰)	S.D. (‰)
L.O	-4.76	-6.06	-4.65	-2.66	-4.53	1.4	-5.16	0.78
Transition	-5.65	-7.02	-6.80	-6.08	-6.39	0.64	-6.49	0.74
Mi-1	-7.06	-7.45	-7.71	-7.06	-7.32	0.32	-7.41	0.33
E.M.	-5.65	-6.77	-6.97	-7.06	-6.61	0.65	-6.46	0.71

These two alternative methods for deriving $\delta^{13}C_{atm}$ show opposite trends, with a positive excursion using planktic foraminifera, and a negative excursion from n-alkanes. Each method however contains its own potential sources of error. Applying the method of Smith et al. (2007) is limited by the use of a single record and a single temperature proxy to estimate $\delta^{13}C_{atm}$, which mean that site, species or proxy specific noise or bias may be included. In their calculation of Paleocene/Eocene Thermal Maximum $\delta^{13}C_{atm}$, Smith et al. (2007) use two different sites and temperature proxies to minimise this effect. Over the Oligocene/Miocene boundary planktic foraminiferal records of $\delta^{13}C$ and temperature are limited, which necessitated the use of a single record and proxy. In particular, using oxygen isotopes for temperature results in warmer temperatures during the maximum of the glacial, the opposite to what would be expected. This is important as decreasing the temperature in this method results in a lower $\delta^{13}C_{atm}$ which could shift the $\delta^{13}C_{atm}$ excursion to negative, rather than positive.

The method of Arens et al. (2000) is also problematic. It is based on the idea that $\delta^{13}C_{TT}$ primarily and linearly reflects shifts in $\delta^{13}C_{atm}$, and also assumes that plants in the geologic past fractionated carbon in the same way as modern and recent geologic plants. Other studies have

questioned some of these assumptions suggesting that this relationship may not be linear, especially during elevated pCO$_2$ concentrations in the geological past (Gröcke, 2002, Lomax et al., 2012). From a physiological viewpoint it has been noted that assuming a constant relationship between $\delta^{13}C_{TT}$ and $\delta^{13}C_{atm}$ is also incorrect, as plants change the way they incorporate carbon depending on environmental conditions (Farquhar et al., 1989, Beerling and Royer, 2002). The regression was also performed on a multi-species database to average out inter-species differences and the biases that may therefore be incorporated, but does not consider how related the input data is (Lomax et al., 2012). Reanalysis of the Arens et al. (2000) dataset does indicate a significant phylogenetic signal in the data (Lomax et al., 2012). As much of the plant waxes analysed from DSDP 270 were sourced from a small range of species, a species specific bias may not be accounted for in the use of the Arens et al. (2000) method. Lomax et al. (2012) also performed growth chamber investigations on the impact of $\delta^{13}C_{atm}$ on $\delta^{13}C_{TT}$, and while it found the two were correlated, it suggests that environmental factors such as water availability play a greater role in determining a plants $\delta^{13}C_{TT}$.

Tipple et al. (2010) developed a long-term Cenozoic record of $\delta^{13}C_{atm}$ using benthic and planktic foraminifera. They suggest that benthic foraminifera may be better indicators of $\delta^{13}C_{atm}$ than planktics, as they are not affected by differences in production depth, photosymbiotes and seasonal variability. However, this record is not ideal for determining $\delta^{13}C_{atm}$ over the Mi-1 event as it applies the same $\delta^{18}O_{sw}$ values for all of the Oligocene and Miocene, and so does not resolve transient glacial events well which could have driven significant variations in $\delta^{18}O_{sw}$ due to large ice volume changes. Planktic-based estimates of $\delta^{13}C_{atm}$ are typically offset from benthic estimates by approximately 1‰, with planktic estimates over the Oligocene/Miocene boundary in a comparable range to the results determined using the method of Smith et al. (2007) in this chapter. Interestingly, a moving average over the Oligocene/Miocene boundary period shows opposite trends in $\delta^{13}C_{atm}$ from planktic and benthic foraminifera, shifting to more negative and more positive values, respectively. It is suggested that offsets between the two may be due to non-equilibrium factors, such as those mentioned above, impacting the planktic foraminifera results (Tipple et al., 2010). The trend to more negative values over the Oligocene/Miocene boundary in planktic foraminifera in the study of Tipple et al. (2010) is opposite to what is determined using planktic foraminifera in this chapter.

The contrasting signals from planktic foraminifera and *n*-alkanes, coupled with the opposing trends in planktic and benthic foraminifera as determined by Tipple et al. (2010) means that it is difficult to confidently establish a trend in $\delta^{13}C_{atm}$ for the Mi-1 event. Estimates of bottom water temperature using benthic foraminifera over Mi-1 indicate a cooling of several degrees prior to and during this glaciation (Lear et al., 2004, Mawbey and Lear, 2013). TEX$_{86}$ estimates from this study suggest a ~5°C cooling coincident with the peak in the excursion of *n*-alkane $\delta^{13}C$ in the Ross Sea. In Quaternary glaciations, equatorial sea surface temperatures are typically cooler by up to 5°C (e.g. Lea et al., 2000). The result determined using $\delta^{18}O_{pf}$ from ODP 926 of a warmer temperature during the peak of the Mi-1 event is therefore surprising. This is potentially the result of either a site-, species- or proxy-specific issue. The results of a positive excursion in $\delta^{13}C_{atm}$ using the method of Smith et al. (2007) may therefore not actually be representative of the trend in $\delta^{13}C_{atm}$ over this glacial. Similarly, the issues associated with using the Arens et al. (2000) method (as highlighted above) mean that this is also a non-ideal way of estimating $\delta^{13}C_{atm}$ and likely overestimates the contribution of $\delta^{13}C_{atm}$ to determining $\delta^{13}C_{TT}$. However, while environmental factors likely play a larger role in a plants $\delta^{13}C$, $\delta^{13}C_{atm}$ still shows a relationship to $\delta^{13}C_{TT}$. With this in mind, we suggest that due to the magnitude of the negative carbon isotope excursion seen in plant waxes over the Mi-1 at DSDP 270 (i.e. up to -4.8‰ for *n*-C$_{31}$), some of this excursion is potentially the result of a negative $\delta^{13}C_{atm}$ excursion.

Negative excursions in $\delta^{13}C_{atm}$ are often described from hyperthermal events such as the Paleocene-Eocene Thermal Maximum, where the injection of light carbon, potentially from the release of sedimentary methane hydrates or permafrost, resulted in a significant lowering of $\delta^{13}C_{atm}$ (e.g. McInerney and Wing, 2011). These events are associated with increases in pCO$_2$ and warming. A negative excursion over a glacial period, where temperatures cooled and pCO$_2$ is expected to be lower, therefore requires a different mechanism. The deep sea benthic foraminifera $\delta^{13}C$ stack from several records spanning different ocean basins becomes more positive in the lead up to Mi-1, coincident with increasing ice volume indicated by increasing benthic foraminifera $\delta^{18}O$ values (Figure 4.1) (Beddow et al., 2016). Foraminiferal $\delta^{13}C$ reaches its maximum at the end of, and during the deglaciation of Mi-1, slightly lagging maximum values in $\delta^{18}O$ (Beddow et al., 2016). This has been suggested to be the result of increased carbon burial due to enhanced productivity in the oceans, in response to global cooling, strengthened atmospheric circulation, and enhanced ocean mixing and upwelling (Diester-Haass et al., 2011, Mawbey and Lear, 2013, Florindo et al., 2015). Enhanced

productivity draws isotopically light carbon into the deep ocean and seafloor sediments, leading to isotopically heavier DIC. $\delta^{13}C_{atm}$ is strongly influenced by $\delta^{13}C$ of DIC, so isotopically heavier values of DIC might be expected to result in more positive $\delta^{13}C_{atm}$. However, various factors can mean that $\delta^{13}C_{atm}$ and the $\delta^{13}C$ of DIC do not always co-vary in a changing climate. The fractionation of carbon between $\delta^{13}C_{atm}$ and DIC can be affected by several factors including ocean pH and SST (Zhang et al., 1995). Higher SSTs translate to heavier $\delta^{13}C_{atm}$ on the order of 0.1‰/1°C (Zhang et al., 1995, Schmitt et al., 2012). A SST cooling exceeding ~5°C at Mi-1 could therefore result in $\delta^{13}C_{atm}$ values ~0.5‰ lighter. Other factors such as the growth and loss of the terrestrial biosphere can also have a strong impact on $\delta^{13}C_{atm}$ (Köhler et al., 2010). As the terrestrial biosphere contains isotopically light carbon, loss of biosphere, for example as the result of extensive ice cover during a glacial, can result in the release of this light carbon to the atmosphere and a reduction in $\delta^{13}C_{atm}$ (Köhler et al., 2010, Schmitt et al., 2012).

The interplay of these impacts described on $\delta^{13}C_{atm}$ have been assessed over Pleistocene glacials using marine records, ice cores and modelling experiments (i.e. Köhler et al., 2010, Schmitt et al., 2012). While the $\delta^{13}C$ of DIC shows distinct glacial/interglacial trends, $\delta^{13}C_{atm}$ does not, as the factors which impact $\delta^{13}C_{atm}$ (i.e terrestrial biosphere, marine DIC, SSTs and ocean circulation) often affect the $\delta^{13}C_{atm}$ in opposing ways, effectively cancelling each other out. An ice core study of the Last Glacial Maximum to present day, shows similar $\delta^{13}C_{atm}$ values at the peak of the glacial, and during the Holocene, suggesting that even though many elements of the climate and carbon cycles were different between these time periods, the relative balance of the opposing factors were the same (Schmitt et al., 2012). However, $\delta^{13}C_{atm}$ showed marked changes during the deglaciation, indicating that the various factors described above had an unbalanced impact on $\delta^{13}C_{atm}$ (Schmitt et al., 2012). The most negative $\delta^{13}C_{atm}$ excursion suggested by *n*-alkane $\delta^{13}C$ occurs at the beginning of Mi-1 and is coeval with coolest reconstructed SSTs and an increased flux of plant waxes reaching the core site (Figures 4.7 and 4.9). It is possible that this excursion is the result of a transient shift in $\delta^{13}C_{atm}$ not reflected in the marine foraminiferal $\delta^{13}C$ record, in response to cool SSTs and a loss of much of Antarctica's terrestrial biosphere as it became covered by ice.

Plant $\delta^{13}C$ is also strongly affected by changes in environmental parameters. Values for $\delta^{13}C_{TT}$ and $\delta^{13}C_{atm}$ from the Arens et al. (2000) and Smith et al. (2007) methods are applied to equation 4.1 to determine carbon isotope discrimination (table 4.4). For the plant wax based method,

averages for $n\text{-}C_{25}$ - $n\text{-}C_{29}$ are applied. Despite differences in the trend of $\delta^{13}C_{atm}$, both methods predict carbon isotope discrimination in plants increased between the Late Oligocene and Mi-1, with the exception of $n\text{-}C_{27}$ using the method of Arens et al. (2000). Using Smith et al. (2007) results in positive shifts in Δ of 3.19‰, 2.15‰, 4.07‰ and 5.59‰ for $n\text{-}C_{25}$, $n\text{-}C_{27}$, $n\text{-}C_{29}$ and $n\text{-}C_{31}$, respectively, whereas the Arens et al., (2000) method shows a shift of 0.33‰, -0.71‰, 1.22‰ and 2.74‰ for $n\text{-}C_{25}$, $n\text{-}C_{27}$, $n\text{-}C_{29}$ and $n\text{-}C_{31}$ respectively. Carbon isotope discrimination values are applied to equation 4.6 to determine p_i/p_a, representing the ratio of the intercellular partial pressure of CO_2 in the leaf to the atmospheric partial pressure of CO_2 (Farquhar et al., 1989) (table 4.4). Over the O/M boundary, the p_i/p_a ratio increases by 14.10%, 9.50%, 17.99% and 24.72% for $n\text{-}C_{25}$, $n\text{-}C_{27}$, $n\text{-}C_{29}$ and $n\text{-}C_{31}$ respectively using Smith et al. (2007). However, for the Arens et al. (2000) method it is 1.48%, -3.13%, 5.38% and 12.13% for $n\text{-}C_{25}$, $n\text{-}C_{27}$, $n\text{-}C_{29}$ and $n\text{-}C_{31}$, respectively.

Table 4.4. Values of Δ and p_i/p_a for different n-alkanes using the methods of Smith et al., 2007 and Arens et al., 2000.

Δ and *pi/pa* (Smith et al., 2007)	$n\text{-}C_{25}\ \Delta$ (‰)	$n\text{-}C_{27}\ \Delta$ (‰)	$n\text{-}C_{29}\ \Delta$ (‰)	$n\text{-}C_{31}\ \Delta$ (‰)	$n\text{-}C_{25}$ *pi/pa* (‰)	$n\text{-}C_{27}$ *pi/pa* (‰)	$n\text{-}C_{29}$ *pi/pa* (‰)	$n\text{-}C_{31}$ *pi/pa* (‰)
L.O.	16.89	18.37	16.76	14.49	0.55	0.62	0.55	0.45
Mi-1	20.08	20.52	20.83	20.08	0.69	0.71	0.73	0.69
E.M.	18.38	19.57	19.75	19.98	0.62	0.67	0.68	0.69
Δ and *pi/pa* (Arens et al., 2000)								
L.O	19.21	20.70	19.08	16.81	0.66	0.72	0.65	0.55
Transition	18.86	20.44	20.19	19.35	0.64	0.71	0.70	0.66
Mi-1	19.55	19.99	20.30	19.55	0.67	0.69	0.70	0.67
E.M.	19.05	20.24	20.43	20.66	0.65	0.70	0.71	0.72

Values of p_i/p_a and Δ are considered to be largely controlled by water availability, with increasing values indicating an increase in water availability (Farquhar et al., 1989, Marshall et al., 2007). Global datasets of Δ show a strong positive correlation with mean annual precipitation (MAP) (Diefendorf et al., 2010, Kohn 2010). The increase in p_i/p_a and Δ over Mi-1 would therefore suggest an increase in MAP. However, several studies indicate that this global relationship may not be the best analogue for use in Antarctica in the

Oligocene/Miocene. A growth chamber and *in situ* study of Δ on *Nothofagus* species from varying latitudes of the southern hemisphere indicated that Δ was most strongly correlated with summer (December to March) rainfall, with higher Δ at lower rainfall, the opposite to the global regression (Read and Farquhar, 1991). They suggest that at high latitudes, *Nothofagus* evolved physiological or morphological mechanisms to allow continued photosynthesis during the warm conditions of summer despite mild water deficit. Following this, a growth chamber study by Read et al. (2010) also found that deciduous *Nothofagus* from summer dry regions maintained high rates of stomatal conductance during the dry summer period in order to maximise photosynthetic opportunities. In contrast, other studies using *in situ* and herbarium *Nothofagus* have described decreased $\delta^{13}C_{TT}$ and thus increased Δ is usually a response to increased precipitation, in line with the global trend (Peri et al., 2012, Griener et al., 2013). *Podocarpidites* spp. is also a persistant component of the vegetation assemblage through DSDP 270 (Figure 4.4). A study of modern Podocarpaceae from New Zealand indicates that $\delta^{13}C$ is positively correlated with vapour pressure deficit, and so Δ would usually decrease in response to less moisture in the air (Brett et al., 2014).

Variable responses of modern *Nothofagus* and Podocarpaceae to distributions of rainfall and moisture in modern environments means that other factors have to be assessed to consider which relationship may be better applied to Antarctic vegetation in the Oligocene/Miocene. Vegetation during this time period would have had to survive different conditions to modern equivalents. In particular, at latitudes below the Antarctic Circle, growth would be restricted to a shorter period during summer when there was sunlight, thawed soil and warmer temperatures for photosynthesis. Similar to the situation described by Read and Farquhar (1991) and Read et al. (2010) a short, restricted growing season may have resulted in plants retaining open stomata to allow continued uptake of CO_2 during this time. During Mi-1, low seasonality and cold temperatures would have further restricted the amount of time each summer when the soil was thawed and temperatures were warm enough for growth. To make the most of this short growing season, plants may have further sacrificed water use efficiency in order to assimilate more CO_2, leading to higher values of carbon isotope discrimination. Support for this lies in case studies of modern high Arctic plants, which indicate that low precipitation is not necessarily restrictive in these environments, as key water sources for plants are snow melt and permafrost thawing at the base of the active soil layer (Gold and Bliss, 1995). Therefore, growth is potentially influenced more by factors such as soil and air temperature and nutrient levels (e.g. Gold and Bliss, 1995, Sturm et al., 2005, Ernakovich et al., 2014).

Altitude also correlates with Δ, with Δ values decreasing at higher elevations (Marshall and Zhang, 1994, Diefendorf et al., 2010, Kohn, 2010). Together with MAP, these two factors can explain 61% of the global variability in Δ (Diefendorf et al., 2010). Lesser influences that can lead to more positive values of Δ include decreasing concentrations of nutrients such as nitrogen, lower levels of irradiance and increased temperatures, although the effects of these can be minor or variable across studies (Marshall et al., 2007, Diefendorf et al., 2010, Kohn, 2010, Cernusak et al., 2013). The correlation with altitude is interesting in the context of DSDP 270, as it would be expected that during a large glacial vegetation may become restricted to coastal regions due to ice advance and climate controls. A shift to more positive Δ could partly reflect a change from vegetation at a range of altitudes to low altitude, coastal vegetation.

Tree height can also control Δ, with Δ declining with increasing tree height in a global dataset (McDowell et al., 2011). This is likely due to several factors, including light availability, differences in atmospheric $\delta^{13}C$ between the ground and canopy, and the impact on hydraulic conductance associated with increasing path length from soil to leaf (McDowell et al., 2011). In a case study of *Nothofagus solandri* in New Zealand, Δ varies with tree height on the order of -0.22‰/m. This relationship that was found to be regionally consistent despite variations in the climate of sampling sites (McDowell et al., 2011). It is likely that during a cold glacial period in Antarctica, tree species like *Nothofagus* would be stunted in their growth, preferably forming shrub like forms similar to Miocene or Pliocene-aged *Nothofagus* fossils preserved at Oliver Bluffs in the Beardmore Glacier region (Francis and Hill, 1996). An increase in Δ (driving plant wax $\delta^{13}C$ to lighter values) could also then potentially result from a shift from more tree-like to more shrub-like forms in the catchment.

Differences in Δ are also apparent across different species and plant functional types. $\delta^{13}C_{alkanes}$ from angiosperms is typically ~3-5‰ more depleted than gymnosperms (Chikaraishi and Naraoka, 2003, Diefendorf et al., 2011). However, pollen records from DSDP 270 do not indicate a significant overturning in the relative abundances of angiosperms (i.e. *Nothofagus*) and gymnosperms (i.e. *Podocarpidites* spp.) over Mi-1. Diefendorf et al. (2010) investigated carbon discrimination between deciduous and evergreen angiosperms and found that globally evergreen angiosperms discriminated against ^{13}C more than deciduous angiosperms, by a Δ value of 1.5‰. However when they separated data by geographic region, or looked at samples

from the same site, this relationship became more variable. Species of *Nothofagus* in Antarctica were likely deciduous (e.g. Francis and Hill, 1996).

In general, p_i/p_a and Δ has not been thought to respond to changes in atmospheric pCO_2 in recent observations, laboratory experiments, or from Cenozoic fossil evidence - although this has been a subject of debate (e.g. Polley et al., 1993, Ehleringer and Cerling, 1995, Arens et al., 2000, Ward et al., 2005, Kohn 2010, Schubert and Jahren, 2012, 2015, Kohn, 2016). For example, a recent Last Glacial Maximum to Holocene global compilation record does suggest a relationship between Δ and pCO_2, with Δ showing an increase with increasing pCO_2 (Schubert and Jahren, 2015). This study suggests a global compilation record averages the effects of local and regional environmental conditions and plant community shifts, and results in a trend which can best be explained by changing pCO_2. However, as DSDP 270 reflects a regional signal it can not be interpreted in these terms. Another recent study disputed the relationship between $\delta^{13}C$ and pCO_2, suggesting that when records are corrected for other factors like MAP, the potential effect of pCO_2 becomes negligible (Kohn, 2016).

In summary, a marked negative $\delta^{13}C$ excursion in HMW *n*-alkanes over Mi-1 is likely the result of several factors, including a potential negative $\delta^{13}C_{atm}$ excursion. Globally, increased carbon isotope discrimination by plants is usually attributed to an increase in MAP. As described above, these global relationships may not be the best analogue for plants living in Antarctica in the Oligocene/Miocene. Instead increased carbon isotope discrimination is attributed to several environmental and physiological changes which would have affected plants during a large glacial event. Namely, the negative plant wax $\delta^{13}C$ excursion could have resulted from a combination of: 1) a shift in climate to colder, shorter growing seasons, 2) a shift in catchment to restricted coastal vegetation, and 3) a shift in vegetation growth form from more tree-like to more shrub-like forms.

4.3.5.2 n-C$_{23}$ $\delta^{13}C$

The *n*-C$_{23}$ in DSDP 270 is inferred to be sourced from mosses and aquatic plants (section 4.3.4). Submerged aquatic plants incorporate carbon differently to emerged plants due to variety of reasons described in section 1.8.2.2. Emergent and semi-emergent bryophytes such as mosses also incorporate carbon differently to vascular plants, as they are non-vascular so do not have stomata to regulate their CO_2 or water uptake (Section 1.8.2.2) (Rice and Giles, 1996, Williams

and Flanagan, 1996). The $\delta^{13}C$ of the n-C_{23} in DSDP 270 does not correlate with the longer carbon chain length n-alkanes, indicating a distinct source with different controlling factors. This lack of correlation is likely a result of the different mechanisms of carbon incorporation employed by both submerged aquatic plants and non-vascular plants, as described in section 1.8.2.2. The n-C_{23} probably reflects a combination of these inputs, although the prominence of *Coptospora* spp., thought to be related to the moss family *Bartramiaceae*, in the palynomorph record suggests that mosses may be a larger contributor than aquatic species. Similar to vascular terrestrial plants, the n-C_{23} is more depleted in $\delta^{13}C$ relative to the bulk organic matter of the plants, on the order of ~10‰ in Sphagnum and freshwater species (Chikaraishi and Naraoka, 2003, Brader et al., 2010). If an enrichment factor of ~10‰ is applied to the binned values for the n-C_{23} from table 4.1, $\delta^{13}C_{TT}$ for bryophytes and submerged aquatic plants is calculated to be -18.58‰ for the Late Oligocene, -19.66‰ for the Transition, -18.81‰ for Mi-1 and -19.10‰ for the Early Miocene. However, it is noted that values for n-C_{23} show more scatter and a less distinct trend as the HMW n-alkanes (Figure 4.10). The values calculated for $\delta^{13}C_{TT}$ are also considerably heavier than the $\delta^{13}C$ of vascular plants. This could be the result of an enrichment factor of 10‰ being too large or incorrect for the vegetation in the catchment of DSDP 270. Heavy $\delta^{13}C$ could result from submerged and semi-submerged vegetation utilising some carbon from HCO_3^-, as this is isotopically heavier than carbon derived from CO_2 (Mook et al., 1974, Maberly and Spence, 1983). If aquatic and semi aquatic plants are drawing their carbon from a more limited pool, such as a standing water in a bog then decreased discrimination can result, producing less negative $\delta^{13}C$.

In mosses, the wetness of the plant is the most important factor in their carbon incorporation, leading to more negative $\delta^{13}C$ results when plants are dryer, the opposite to what usually occurs in vascular terrestrial plants (Farquhar et al., 1989, Rice and Giles, 1996, Williams and Flanagan, 1996). Applying this to n-C_{23} would suggest an increase in moss wetness during Mi-1, as the binned value for Mi-1 is more positive than those for the transition in to the glacial and for the Early Miocene. However, other factors can also contribute to this trend. A strong correlation has also been found between $\delta^{13}C$ of moss tissue cellulose and temperature in certain species in a transect in Poland, with relationships of -1.6‰/°C for *Sphagnum* and -1.5‰/°C for *Polytrichum* (Skrzypek et al., 2007). This suggests that the increase in $\delta^{13}C$ in Mi-1 could instead reflect cooler temperatures. A shift in either the habitat or variation of species throughout the catchment of DSDP 270 that contribute to the n-C_{23} in this core could also result in changes to the $\delta^{13}C$. For instance, a larger contribution from plants occupying wetter habitats

could result in a $\delta^{13}C$ value which appeared to show an increase in moss wetness. The pollen and spore record over Mi-1 does potentially indicate that a boggy, tundra habitat favouring bryophytes and mosses expanded proportionally at the expense of a habitat favouring shrubs and trees such as *Nothofagus* during Mi-1 (section 4.3.2).

4.3.6 n-Alkane δ^2H

Hydrogen isotopes were also measured on odd chain length *n*-alkanes from *n*-C_{23} to *n*-C_{31}, with δ^2H values varying from -143.65‰ to -207.26‰ (Table 4.5) (Figure 4.11). The δ^2H HMW *n*-alkane record shows more variability than the $\delta^{13}C$ record from the same samples. A general increase to heavier values occurs over the Late Oligocene and transition sections of the core, with the exception of lighter values at 173.7 mbsf. δ^2H is still relatively heavy early in Mi-1, but moves towards lighter values through the glacial. Values in the Early Miocene are scattered, and cover a similar range to the rest of the core. The record for *n*-C_{23} shows a slightly different trend, but as abundances of this *n*-alkane were lower the data is sparser. δ^2H moves towards lighter values over the Late Oligocene, followed by a gap in data to the late stages of the transition/early Mi-1. Values are also lighter over this section of the core, reaching lightest values at 112.8 mbsf, before moving towards heavier values in the Early Miocene.

Table 4.5: δ^2H on odd chained n-alkanes, in binned intervals.

δ^2H	*n*-C_{23}	*n*-C_{25}	*n*-C_{27}	*n*-C_{29}	*n*-C_{31}
L.O.	-166.98	-175.50	-185.72	-194.95	-189.12
Transition	-145.69	-167.85	-177.56	-190.04	-184.41
Mi-1	-176.68	-179.11	-180.93	-191.09	-189.53
E.M.	-165.57	-172.01	-177.25	-192.95	-190.22

4.3.6.1 HMW n-alkane δ^2H

The δ^2H of lipids in leaf wax is related to the δ^2H of the plants source water, as water is the primary source of hydrogen for photosynthesising plants and aquatic organisms (Sachse et al., 2012). The δ^2H of lipid biomarkers (δ^2H_l) is highly correlated with, but offset from, the δ^2H of the water source used by the organism which synthesised the lipids, which is usually meteoric water (δ^2H_w) (Sessions et al., 1999, Sauer et al., 2001, Chikaraishi and Naraoka, 2003, Sasche et al., 2004). The isotopic composition of meteoric water varies spatially and temporally

(Section 1.8.2.1). The δ^2H of the HMW n-alkanes measured in DSDP 270 likely reflects meteoric water, but with the added influence of the series of fractionations and variables described in section 1.8.2. To take account of this, δ^2H values are corrected for $\varepsilon_{l/w}$, representing the apparent fractionation between δ^2H_l and δ^2H_w, and incorporating potential fractionations from soil water evaporation, leaf-water transpiration and biosynthetic fractionation (Eq. 1.4) (Sasche et al., 2012).
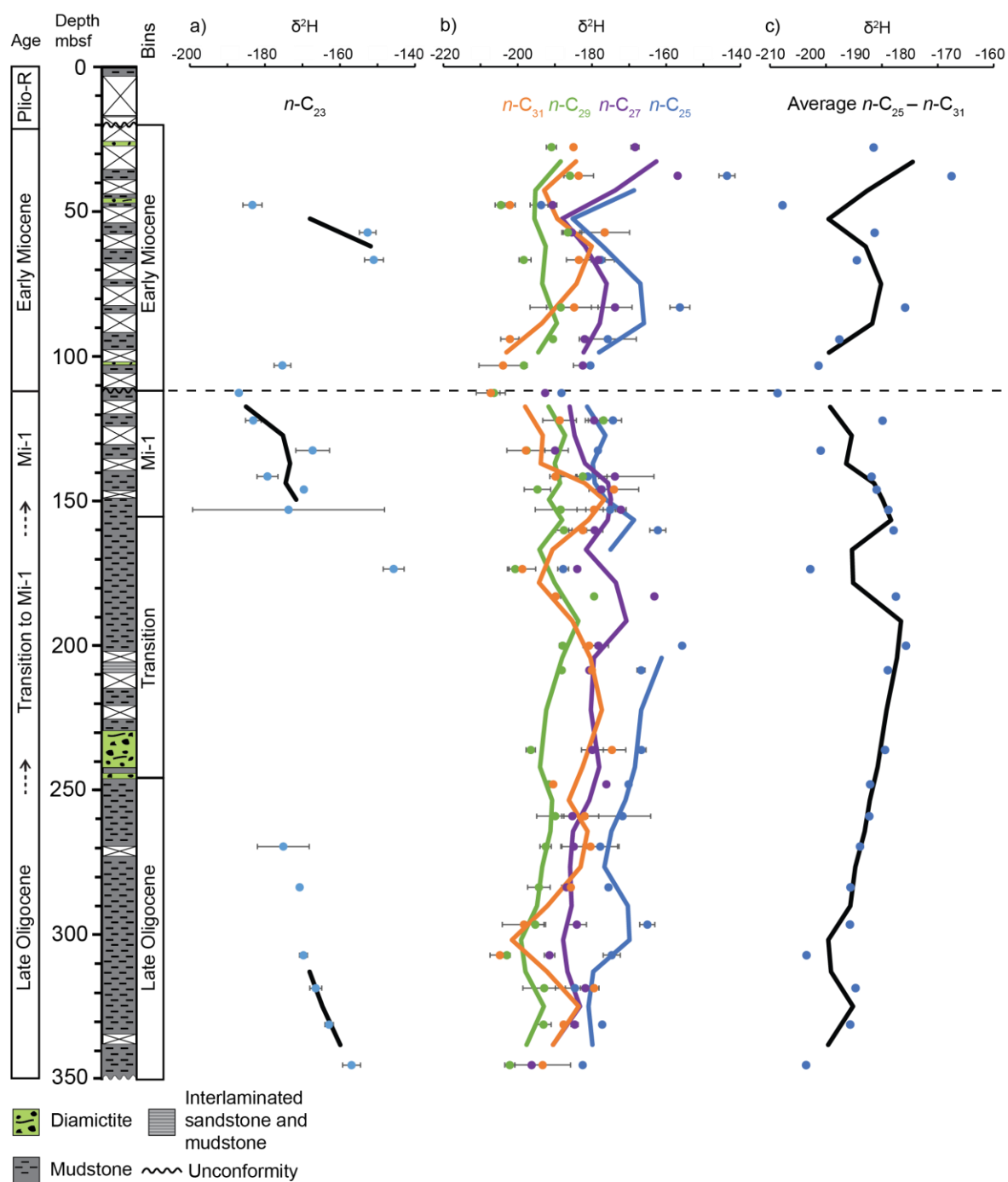
Figure 4.11: Compound specific hydrogen isotopes on n-alkanes in DSDP 270 (a) n-C$_{23}$; (b) n-C$_{25}$, n-C$_{27}$, n-C$_{29}$ and n-C$_{31}$; and c) the averaged δ^{2}H of n-C$_{25}$ - n-C$_{31}$. Blue dots represent individual samples, whilst black lines are two point moving averages.

A compilation study found ε$_{l/w}$ values of -110±27‰ for *n*-C$_{27}$, -113±29‰ for *n*-C$_{29}$, and -111±30‰ for *n*-C$_{31}$ for C$_3$ gymnosperms and angiosperm-dicots (Sachse et al., 2012). However, greenhouse experiments of three species of plants living under 24 hour light conditions found smaller fractionations under continuous light regimes, from -62‰ to -87‰ for *n*-C$_{29}$, attributed to greater water loss during 24 hour transpiration (Yang et al., 2009). *In situ* studies of high latitude plants also support this, suggesting ε$_{l/w}$ can be 20-50‰ smaller than at lower latitudes (Lui and Yang, 2008, Yang et al., 2011). Plant life form also displays an impact on ε$_{l/w}$. For example, in the compilation of Sachse et al. (2012), shrubs and shrubby trees show a smaller average *n*-C$_{27}$ - *n*-C$_{31}$ ε$_{l/w}$ (-101‰) than trees (-114‰). On the other hand, forbs and C$_3$ angiosperm-monocots such as grasses typically display a larger ε$_{l/w}$ than woody plants (-123‰ and -144‰ respectively, averaged across *n*-C$_{27}$ - *n*-C$_{31}$) (Sachse et al., 2012). The magnitude of these differences also varies between *n*-alkane chain lengths. In terms of modern analogues for vegetation present in DSDP 270, a study investigating ε$_{l/w}$ on *Nothofagus menziesii* in New Zealand found ε$_{l/w}$ averaged across *n*-C$_{27}$ to *n*-C$_{31}$ varied from 113.7‰ to 146.1‰, averaging 129.9‰, slightly greater than the global compilation (Zhuang et al. 2015).

The variation in net fractionation between plant species, growth forms and light regimes makes applying an appropriate net fractionation to the δ^{2}H from DSDP 270 difficult, and creates a large source of uncertainty. To account for this, I follow the lead of Feakins et al. (2014) who investigated plant wax δ^{2}H on the Antarctic Peninsula in the Eocene, and assume two end member fractionations. A high net fractionation is based on the mean ε$_{l/w}$ on *Nothofagus menziesii* (130‰) (Zhuang et al., 2015) whilst a low one is based on laboratory experiments of plants living under a 24 hour light regime (70‰) (Yang et al., 2009, Yang et al., 2011). These fractionations are applied to the average δ^{2}H for *n*-C$_{25}$ – *n*-C$_{31}$ through the core to derive average end member paleoprecipitation values for the Ross Sea region during the Late Oligocene/ Early Miocene of -62.1‰ (range of -43.1‰ to -78.9‰) for the high ε$_{l/w}$, and -122.7‰ (range of -104.9‰ to -138.3‰) for the low ε$_{l/w}$ (Figure 4.12).
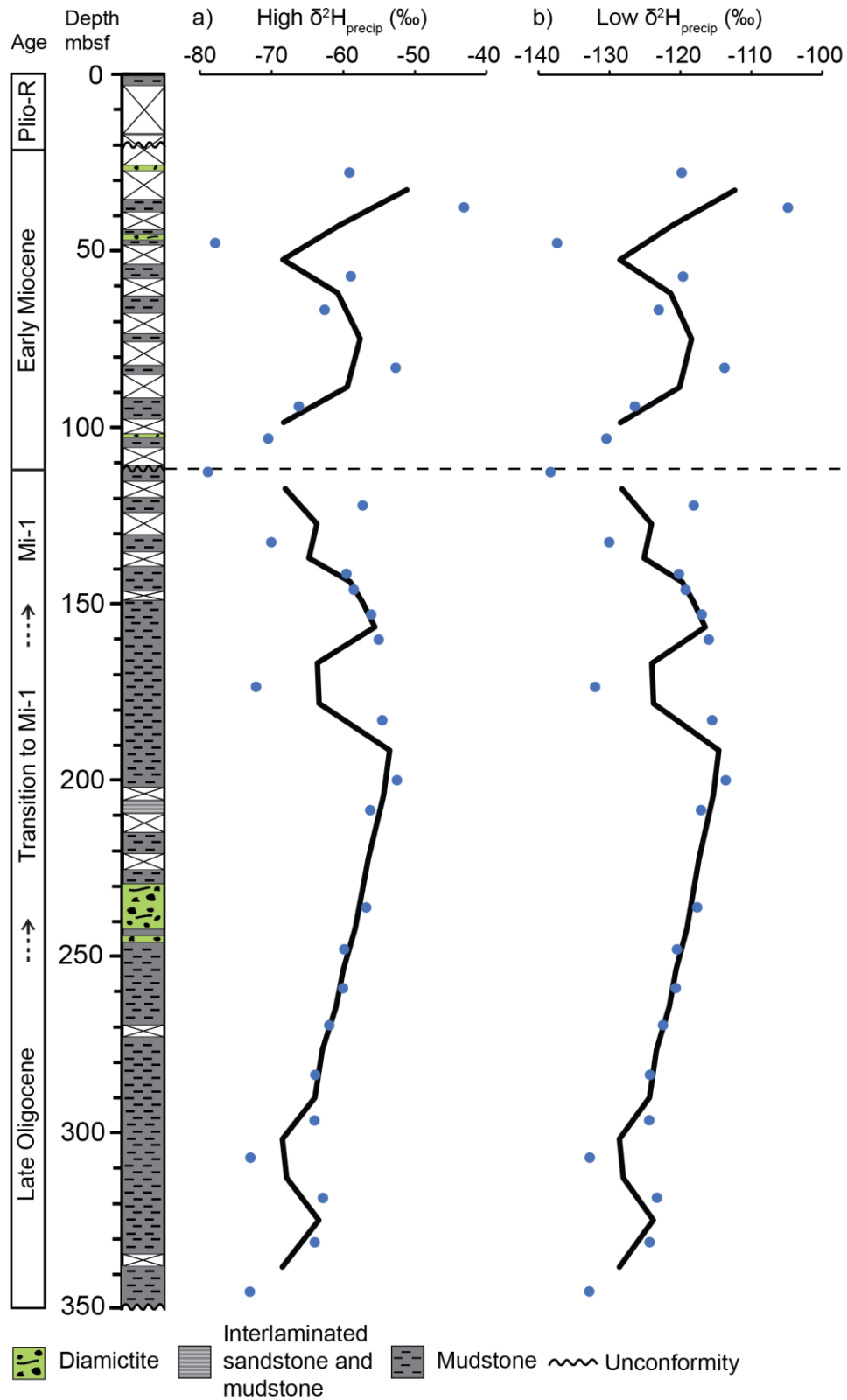
Figure 4.12: δ²H of paleoprecipitation assuming both a) a high net fractionation (ε_l/w) of 130‰ and b) a low net fractionation of 70‰. Blue dots represent individual samples, whilst black lines are two point moving averages.

At mid to high latitudes, δ^2H is strongly associated with temperature gradients (Bowen et al., 2008). In Antarctica, δ^2H of modern snow samples varies from ~-80‰ on the Antarctic Peninsula to ~-450‰ in the interior (Masson-Delmotte et al., 2008). Spatial variations in δ^2H are strongly related to temperature, which is turn is related to the distance from the ocean, latitude, elevation and atmospheric circulation (Masson-Delmotte et al., 2008). Snow pit data from the Western Ross Sea at latitudes of -77°S to -78°S indicate a variable snow δ^2H, but usually in the range of -150‰ to -250‰ (Gooseff et al., 2006, Masson-Delmotte et al., 2008, Bull, 2009). Regardless of whether a high or low fractionation factor is applied to the n-alkane δ^2H from DSDP 270, end member values of -62.1‰ and -122.7‰ are both enriched compared to present day. Following the present day relationship with temperature, this indicates significantly warmer air temperatures in the Ross Sea Region in the Late Oligocene/Early Miocene, which is also supported by MAT_{mrs} temperatures and the presence of onshore vegetation through this time period (sections 4.3.2 and 4.3.3). It is likely that δ^2H demonstrates specifically warmer summer temperatures (MST), as the leaf wax would have been synthesized during summer leaf growth, and plants such as *Nothofagus* were likely deciduous (e.g. Francis and Hill, 1996).

While plant wax δ^2H values have been modelled to reconstruct absolute temperature in the Ross Sea region previously, for the Mid-Miocene (Feakins et al., 2012), there are considerable uncertainties in this approach due to assuming an appropriate fractionation factor and significant variation between n-alkane chain lengths. If the modern Antarctic relationship between δ^2H is used and projected, then high and low paleoprecipitation values from DSDP 270 equate to MST temperatures ranging from -2.6°C to 3.1°C and -11.9°C to -6.7°C, respectively (Figure 4.13). Values reconstructed using both these net fractionations are lower than brGDGT-based MAT_{mrs} MST values of ~10°C, as well as the minimum temperature of ~5°C under which vegetation like *Nothofagus* could have survived (Francis and Hill et al., 1996). This indicates that either assumed $\epsilon_{l/w}$ are too low, or that the modern δ^2H-temperature gradient is not an accurate analogue for gradients in the Late Oligocene/Early Miocene.
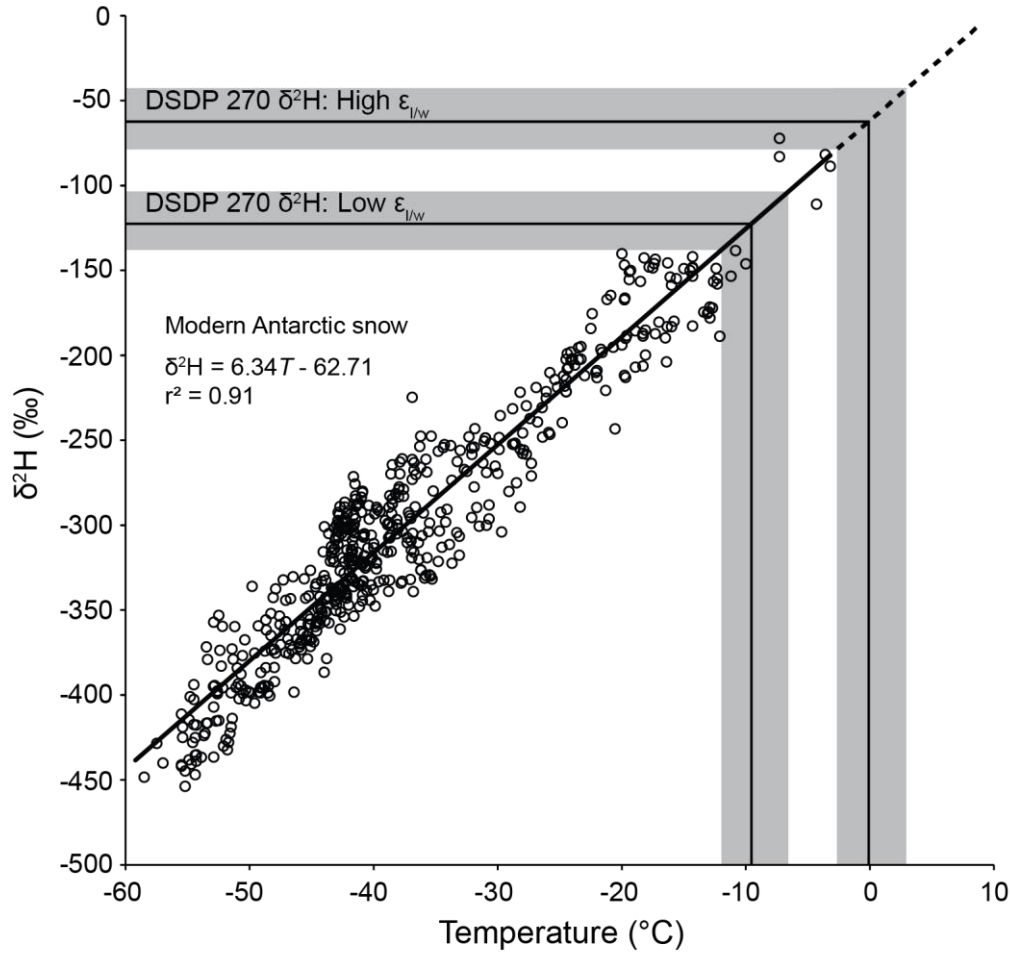
Figure 4.13: Modern δ²H-temperature gradient for Antarctica (black circles and solid black line) (Masson-Delmotte et al., 2008), compared with DSDP 270 paleoprecipitation values reconstructed using both a high (-130‰) and low (-70‰) $\mathcal{E}_{l/w}$ (grey boxes with black line indicating the average value). The modern δ²H-temperature gradient relationship is projected (dashed line) for comparison with samples from DSDP 270 which are higher than modern δ²H in Antarctica.

While a δ²H-temperature gradient for the whole modern continent is applied here to gain some insight into surface temperatures, this gradient does vary spatially due to aspects such as elevation, distance from moisture source and moisture transport pathways (Masson-Delmotte et al., 2008). In the Late Oligocene/Early Miocene, the topography of the Ross Sea region varied compared to present, and Antarctica as a whole was a warmer continent surrounded by warmer oceans. These factors likely resulted in a somewhat different δ²H-temperaure gradient. To account for this problem in a Mid-Miocene Ross Sea setting, Feakins et al. (2012) used isotope enabled modelling to infer that plant wax δ²H during this time period reflected not just

warmer temperatures but also an intensified hydrological cycle driven by a warmer Southern Ocean. Feakins et al. (2012) derived a δ^2H paleoprecipitation value of ~-50‰ for the Mid-Miocene Climate Optimum, inferred to be a period of relative warmth. Even using a high net fractionation value, the majority of paleoprecipitation δ^2H values reconstructed from DSDP 270 are lower than ~-50‰. n-Alkane δ^2H therefore suggests that in the Late Oligocene/Early Miocene the Ross Sea Region was comparatively colder than during the Mid-Miocene Climate Optimum.

4.3.6.2 n-C_{23} δ^2H

Source water is also recorded by the δ^2H of n-C_{23} from submerged wetland plants and peat bogs (Xie et al., 2000, Nichols et al., 2010). In non-arid regions, the n-C_{23} of aquatic plants should faithfully record meteoric water, while in arid regions evaporative processes can reflect temperature and relative humidity (i.e. Xie et al., 2000, Xie et al., 2004). As the n-C_{23} in DSDP 270 is likely sourced from both aquatic plants as well as mosses and other bryophytes, it potentially reflects a mixture of evaporative processes as well as a meteoric water source. The n-C_{23} dataset is lower resolution, but displays similar trends to the HMW n-alkanes through Mi-1 and the Early Miocene (Figure 4.11). In the early Oligocene, it shows a steadily decreasing trend compared to the HMW n-alkanes, which remain fairly stable. A move to more depleted values would suggest either cooling air temperatures or less evaporation, something which could also be driven by cooler temperatures. Potentially the habitats occupied primarily by n-C_{23} producing plants (i.e higher altitudes and more exposed aspects) experienced some cooling during the Late Oligocene, a trend not displayed by the HMW n-alkanes, potentially sourced from plants occupying more sheltered and warmer niches.

4.4 Synthesis

4.4.1 Stratigraphic Setting

While other Late Oligocene/Early Miocene sites around Antarctica show an unconformity over Mi-1 related to a significant ice sheet expansion, DSDP 270 appears to contain a relatively continuous sedimentary sequence (Hambrey et al., 1991, Naish et al., 2001b, Naish et al., 2008, Wilson et al., 2008, Escutia et al., 2011, Kulhanek et al., in prep.). This may be due to the geography of the Ross Sea embayment during this time period, which consisted of subaerial basement highs separated by rapidly subsiding basins (De Santis et al.,1995, De Santis et al., 1999). In particular, seismic evidence suggests that the Central High, proximal to the core site, was a bathymetric high which varied between subaerial and submerged during high and low

stands of sea level, before permanently submerging as the result of glacial erosion and tectonic subsidence at some stage in the Early-Middle Miocene (De Santis et al.,1995, De Santis et al., 1999, Bart and De Santis, 2012). Ice caps on these basement highs would have advanced and retreated into shallow water, but are not thought to have extended across the deeper parts of the marine basins. This is likely due to the lack of the development of a shallow proglacial platform across these basins, as sediment supply was unable to keep pace with rapid tectonic subsidence (De Santis et al.,1995, Bart and De Santis, 2012). During the deposition of DSDP 270 benthic foraminifera suggests the water depth increased, from ~150-300 m in the Late Oligocene section of the core, to ~500 m by the Early Miocene (Leckie and Webb, 1983).

4.4.2 Late Oligocene to Early Miocene climate evolution

DSDP 270 contains a semi-continuous glaciomarine sequence of sediment recording the manifestation of the Mi-1 event in Antarctica, one of the largest transient glaciations of the Cenozoic (Zachos et al., 2001a). This study uses palynomorphs, molecular and isotopic biomarker proxies to assess the evolution of the climate and environment in the Ross Sea region in response to this glaciation, which terminated a period of relative warmth during the Late Oligocene, and was then followed by a return to relative warmth in the Early Miocene. The entire Mi-1 excursion occurs within 400,000 years and its duration has been linked to the long-period eccentricity cycle (Zachos et al., 2001b, Pälike et al., 2006a, Pälike et al., 2006b). The proxy information, underpinned by the stratigraphy and sedimentology of the core (Kraus, 2016), has allowed the DSDP 270 record to be subdivided into 4 broad stratigraphic intervals of environmental change (Figure 4.14).

4.4.2.1 Interval 1 (350-248 mbsf): Late Oligocene- warm equable climate with local glaciers calving at the coastline

Interval 1 contains a Late Oligocene record, prior to the transition in to Mi-1 (Figures 4.14 and 4.15). Foraminiferal evidence indicates that this section of the core was deposited in an outer shelf to upper slope environment (150-300 m water depth) (Leckie and Webb, 1983). The dominance of mudstone deposition with dispersed to common clasts over this interval, suggests an ice distal, low energy marine environment with a steady supply of fine grained terrigenous sediment from a relatively stable coastal ice margin, periodically calving ice bergs (Kraus, 2016). Seismic stratigraphy and sediment provenance studies indicates both IRD and hemipelagic sediment sourced from both Marie Byrd Land and a variably subaerial Central

High (Barrett, 1975, De Santis et al., 1995). Palynology indicates the presence of a low diversity, shrubby tundra, similar to that observed in Cape Roberts 2/2A during this time period (Figure 4.4) (Askin and Raine, 2000, Prebble et al., 2006). The marine palynomorph record is dominated by acritarch *Leiosphaera* spp., suggesting a freshwater input to the site, likely from fluvial and glaciofluvial systems, and/or glacial meltwater sourced from marine calving glaciers originating from the Central High (Figure 4.5). The palynology indicates a low input of pollen and spores over this time period, with the record dominated by marine palynomorphs. However, the ratio between HMW and LMW *n*-alkanes indicates a variable relationship between these two sources with more terrestrially sourced *n*-alkanes reaching the core site than marine *n*-alkanes at several stages through this interval. The Central High was likely a primary source for terrestrial *n*-alkanes due to its proximity, with inputs from the wider Ross Sea region via aeolian processes and ocean currents also a contributing factor.

Absolute and relative ocean temperature estimates via the BAYSPAR subT calibration for TEX_{86} and the RI respectively, indicate that temperatures were warmer during the Late Oligocene in DSDP 270 than the younger sections of the core. While BAYSPAR-subTs demonstrate some fluctuations, temperatures average 7.2°C, indicating significantly warmer ocean temperatures than present day values of ~0 to -2°C in the Ross Sea, and more similar to temperatures currently experienced around the Subantarctic frontal zone (Orsi and Wiederwohl, 2009, Boyer et al., 2013). Relative and absolute estimates of onshore MST from various biomarker proxies (MAT_{mrs} from brGDGTs, compound specific δ^2H from *n*-alkanes, and ACL of *n*-alkanes), suggest that terrestrial air temperatures during the late Oligocene were not markedly warmer than the Early Miocene section of the core (Figure 4.14). Absolute temperatures from MAT_{mrs} indicate an average of 10.3°C, compared with an average for the total core of ~10°C. A value of 10.3°C compares well with Late Oligocene terrestrial palynomorph based temperature reconstructions from Cape Roberts 2/2A (Prebble et al., 2006). However, δ^2H on the *n*-C_{23} *n*-alkane shows a cooling trend through this interval, potentially suggesting that the environmental niches occupied primarily by *n*-C_{23} producing plants, such as higher altitudes and more exposed locations, experienced some cooling during the Late Oligocene. *n*-Alkane $\delta^{13}C$ was consistently less depleted during Interval 1 compared to the rest of the core, potentially indicating vegetation with more tree-like forms, as well as a less restricted growing season and a catchment that likely included both higher and lower altitude vegetation.
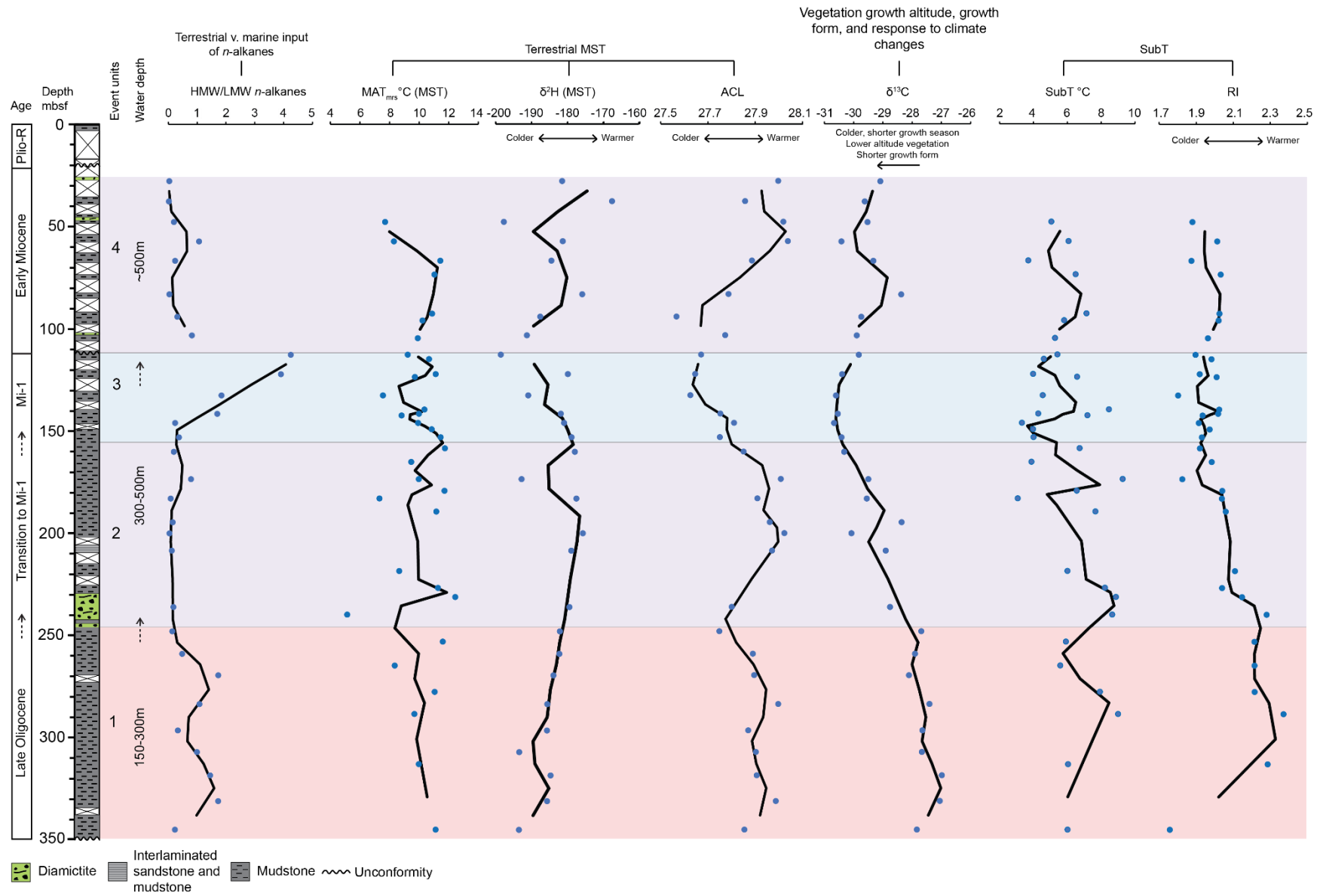
Figure 4.14: Compilation of key datasets for DSDP 270 and stratigraphic intervals. The terrestrial versus marine input of n-alkanes is assessed by the HMW/LMW ratio. Estimates of Mean Summer Temperature are from brGDGT-based MAT$_{mrs}$, and n-alkane based δ^2H and ACL. n-Alkane based $\delta^{13}C$ describes the vegetation response to growth altitude, growth form and climate changes. Subsurface ocean temperatures (SubT) are assessed by BAYSPAR STD SubT and RI. Blue dots represent individual samples, whilst black line are two point moving averages.

4.4.2.2 Interval 2 (248-155 mbsf): Punctuated transition to colder climate and the Mi-1 glaciation of Antarctica

Interval 2 represents sediments encompassing the transition from the Late Oligocene into the Mi-1 glaciation (Figures 4.14 and 4.15). While sediments in Interval 1 indicate deposition under a relatively stable climate and glacial regime, sediments in this interval represent a more dynamic environment. The base of the unit is characterised by an ice proximal stratified diamictite thought to indicate the expansion of grounded marine-based ice from the Central High to nearer the core site (Kraus, 2016). Above this diamictite, rhythmically-stratified cyclopels and cyclopsams, the products of tidally-influenced turbid plume discharge proximal to the grounding line of a tide water glacier, pass up into a more distal mudstone with decreasing IRD concentrations, consistent with retreat of a marine-based ice sheet grounding line from the drillsite vicinity (Powell and Cooper, 2002, Kraus, 2016). However, this glacial retreat is coincident with continuing subsidence of the basin to ~300-500 m water depth (Leckie and Webb, 1983). There are therefore, two possible reasons for this retreat sequence; either ice loss as the result of climate warming, or continued subsidence resulting in a movement of ice from the site, as the ocean temperatures were likely still too warm to sustain a marine-based ice sheet at significant depths.

Ocean subsurface temperatures through this retreat sequence indicate cooling, especially from the less scattered RI record. Foraminifera also indicate cooling above ~200 mbsf, with more polar forms and greater carbonate dissolution, suggested to indicate bottom waters that were colder, more saline and enriched in dissolved carbon dioxide (Leckie and Webb, 1983). This is also supported by n-alkane $\delta^{13}C$, which steadily becomes more depleted over this section, a trend inferred to represent a shift to lower altitude vegetation, more stunted growth forms and shorter growing seasons. While subTs and n-alkane $\delta^{13}C$ would suggest that this period

represents a regional cooling, the terrestrial records of MST show a scattered record from MAT_{mrs}, and steady warming from *n*-alkane δ^2H and ACL. However, these trends could also be explained by the same processes that result in a depletion of *n*-alkane $\delta^{13}C$. If the depletion in *n*-alkane $\delta^{13}C$ and cooling subTs indicates the initiation of a regional cooling and potential build up of ice on land, then this would have led to a change in source for terrestrially derived brGDGTs and *n*-alkanes to lower altitudes, and coastal soils and vegetation. This process would drive *n*-alkane δ^2H to more enriched values, and would also likely increase the ACL, as low altitude plants would be expected to demonstrate a higher ACL due warmer habitat temperatures. Collectively, these proxies would therefore seem to indicate regional climate cooling, rather than warming, through this retreat sequence.

The HMW/LMW *n*-alkane ratio and abundance of HMW *n*-alkanes indicates that LMW *n*-alkanes dominate this part of the record. This is also supported by the dominance of marine palynomorphs in this section of the core. Throughout this section marine palynomorphs indicate a shift from predominantly acritarchs (mainly *Leiosphaera* spp.) to predominantly protoperidinoid dinoflaggellate cysts (Figure 4.5). A reduction in *Leiosphaera* spp. would seem to indicate a reduced freshwater input, with an increase in protoperidinoid dinoflaggellates representing a shift to more favourable deeper marine conditions. Overall, the proxy evidence appears to indicate that Interval 2 represents the initiation of regional cooling and the transition into Mi-1, coupled with ongoing subsidence and water temperatures just warm enough to limit the growth of a large marine-based ice sheet across the continental shelf. Hence, DSDP 270 records grounding-line retreat, where the position of the grounding line is controlled by the tectonically-driven marine transgression.

Proxy evidence from DSDP 270 suggests several factors influenced the initiation of Mi-1, from an Antarctic perspective. Firstly foraminifera indicate that a deepening of the Ross Sea in the lead up to, and during Mi-1, and a cooling in bottom waters (Leckie and Webb, 1983). Subsurface ocean temperatures from this study also begin to cool concurrently with these changes, starting at ~240-230 mbsf (Figure 4.14). An orbital configuration favouring low seasonality and cool temperatures (i.e. Zachos et al., 2001b, Pälike et al., 2006b) would have resulted in colder subTs, and this, coupled with a deepening Ross Sea potentially increased proto-Antarctic bottom water production. Isotopic gradients from ocean basins around the globe indicate that in the Late Oligocene and Early Miocene the production of bottom water from Antarctica varied significantly in intensity, from relatively weak during interglacials, to

more intense during large glacials such as Mi-1 (i.e. Pekar and DeConto, 2006, Pekar et al., 2006). The impact of low seasonality in initiating Mi-1 is also supported by plant wax $\delta^{13}C$, which also starts to show a depletion at ~240 mbsf. It is argued in this study that seasonality potentially has a strong impact on $\delta^{13}C$ in Antarctic plants, as a response to a shorter growing season (section 4.3.5). Thus, the combination of low seasonality, coupled with cool subTs would have promoted the build-up of ice on Antarctica and enhanced bottom water production cooling the margins of the continent. It is interesting that the terrestrial temperature proxies do not also reflect the impact of these influences, only showing cooler temperatures between ~140-112 mbsf, during what is likely the height of the Mi-1 glacial. As mentioned earlier, it is possible that this is due to a change in the catchment altitude for terrestrial *n*-alkanes and brGDGTs during ice build up, from vegetation surviving at a range of altitudes to a primarily coastal vegetation, a process that would also contribute to a depletion in *n*-alkane $\delta^{13}C$.

4.4.2.3 Interval 3: (155-112 mbsf): Ice sheet growth and climate cooling during Mi-1, but no ice grounding at DSDP 270.

Interval 3 spans the Mi-1 glaciation (Figure 4.14 and 4.15). Recent work has made significant progress modelling transient glaciations in the Early to Mid-Miocene (Section 4.1.2) (Gasson et al., 2016). The models provided by Gasson et al. (2016) propose that during the large transient glaciations of the Early Miocene, grounded ice sheets or at least ice shelves would have been present at DSDP 270. However, the stratigraphy of this core indicates ice free conditions at the core site during Mi-1, with grounding line distal mudstones present throughout the section (Kraus, 2016). This suggests that DSDP 270 was not in a grounding line proximal setting during this glaciation. Modelling studies and sediment cores documenting the initiation of large continental scale Antarctic Ice Sheets at the Eocene/Oligocene transition imply that ice-marginal water depths and sea-level changes were highly variable during this extensive glacial event, because of the significant local influence by glacio-hydro isostatic adjustment (GIA) (Stocchi et al., 2013). It is possible that GIA processes may have influenced relative water depth changes at DSDP 270 during Mi-1, which can cause large departures from global eustatic sea-level in the near field of the ice sheet. Somewhat counterintuitively, gravitational field strength in the near-field of a growing ice sheet pulls water towards it with a relative sea-level rise of hundreds of metres. This combined with ongoing tectonic subsidence would have further precluded the advance of a marine grounding line towards DSDP 270. Ocean temperatures derived from this study show that through the Mi-1 interval, the coldest

subTs were ~4°C, ~2-4°C warmer than present, and likely too warm to sustain an ice shelf or marine grounded ice near the core site in the central Ross Sea. However, the lack of IRD through this interval of the core also indicates that debris laden icebergs were not reaching the core site. Potentially cooler temperatures nearer the coast may have sustained a coastal fringing ice shelf, calving 'clean' rather than 'dirty' bergs. The grounding line distal stratigraphy of the core, coupled with minimum subTs of ~4°C indicate that Mi-1 did not manifest as a widespread grounded marine-based ice sheet in the Ross Sea, suggesting that much of the ice volume associated with this event must have been held terrestrially, potentially on a West Antarctica with still extensive areas above or marginally below sea level.

The coldest subTs in Mi-1 occur early in the glaciation, at ~150 mbsf, and while the TEX$_{86}$ record exhibits some scatter, RI indicates that temperatures remained low throughout this interval. At ~150 mbsf, plant wax δ^{13}C values are also at their most depleted, and continue to remain relatively low throughout the rest of the glacial (Figure 4.14). Depleted plant wax δ^{13}C during Mi-1 is considered to indicate a combination of a lowering in the altitude of vegetation and a shift to shorter growth forms, as well as a response to a harsher, shorter growing season (section 4.3.5). A possible negative δ^{13}C$_{atm}$ excursion may also play a role in the depleted plant wax values (section 4.3.5). While subTs and plant wax δ^{13}C reach their most depleted and coldest values respectively at ~150 mbsf, other proxies suggest that peak glacial conditions did not occur until ~130-110 mbsf. In particular, measures of MST still show a decreasing trend at 150 mbsf, reaching their minimum values at ~130-110 mbsf. Absolute values of MST from MAT$_{mrs}$ do not show significantly colder temperatures during this interval compared to the rest of the core, with a lowest temperature of 7.6°C at 132.7 mbsf. Terrestrial palynomorphs and *n*-alkanes indicate that terrestrial vegetation was present throughout Mi-1. Prostrate forms of *Nothofagus* fossils at Oliver Bluffs (85°C) imply a growing season temperature of greater than ~5°C was required for these plants to survive (Francis and Hill et al., 1996). A minimum MAT$_{mrs}$ of 7.6°C therefore aligns well with the survival of plants like *Nothofagus* over this glacial.

ACL values steadily decrease to reach minimum values at ~130 mbsf, before remaining low for the rest of the glacial (Figure 4.14). This likely reflects both colder MSTs as well as proportionally more mid-chain length producing plants, such as mosses and other bryophytes in the catchment. A shift to a more bryophyte dominated environment is also supported by the

palynomorph record which shows a greater proportion of spores are present in the assemblages during Mi-1 than the Late Oligocene and Early Miocene sections of the core (Figure 4.6).

The abundance of HMW *n*-alkanes increases in the early stages of Mi-1 (~150-140 mbsf), coincident with an increase in *n*-C_{23} and terrestrial palynomorphs, and remains relatively high during the glacial (Figure 4.9). As discussed earlier (section 4.3.4), this may relate to a number of processes, including a devegetation signal from loss of habitat and increased erosion as ice expanded onshore, changes in wind and/or ocean current transport paths for *n*-alkanes to the core site, and the potential for increased production of *n*-alkanes at cooler temperatures (i.e. Feakins et al., 2016). However, if the latter was the case, it may be expected that highest abundances of HMW *n*-alkanes would coincide with coldest onshore temperatures. As the increase in HMW *n*-alkanes precedes minimum temperatures, it may be that the former two suggestions are more likely. The ratio between HMW and LMW *n*-alkanes increases markedly over Mi-1, mainly as the result of a significant drop off in the abundance of LMW *n*-alkanes. This suggests conditions were not favourable for the productivity of marine algae and bacteria, as these are the likely source for LMW *n*-alkanes at this core site. This decrease in productivity could be due to a number of reasons including factors like sea ice distribution, ice shelf cover, ocean currents or water temperature and nutrient levels.

4.4.2.4 Interval 4 (112-27 mbsf): Early Miocene

Following a disconformity in the core, Interval 4 contains a sequence of sediments from the Early Miocene (Figures 4.14 and 4.15). Sediments and proxy environmental information indicate a baseline shift in the climate of Antarctica post Mi-1 (Figure 4.14). Sediments are primarily glaciomarine mudstone with varying degrees of glacial proximity, including several thin diamictites (Kraus, 2016). Sediments show evidence for a relatively ice proximal environment, or increased iceberg discharge, during this interval of the core. Foraminifera assemblages in this section of the core are low diversity, polar forms, representing truly polar conditions compare to the Late Oligocene (Leckie and Webb, 1983). TEX_{86}-subTs are on average 1.1°C colder than the Late Oligocene, averaging 5.6°C, a similar range to Early Miocene subTs calculated from the ANDRILL 2A record (Levy et a., 2016, TEX_{86} data re-calibrated to BAYSPAR, see Chapter 5). While the BAYSPAR record does show some scatter, consistently colder temperatures in the Early Miocene are observed from RI values.

Plant wax n-alkane $\delta^{13}C$ values are also consistently more depleted in the Early Miocene, potentially due to a permanent shift to shorter growth forms and a lower altitude of habitation. Terrestrial palynomorph assemblages in this section of the core are similar to other Miocene Antarctic records such as Miocene sediments in Cape Robert 2/2A, and the Miocene or Pliocene Meyer Desert Formation (Askin and Markgraf, 1986, Askin and Raine, 2000, Ashworth and Cantrill 2004). Interestingly, terrestrial temperatures however do not show such a clear shift, with n-alkane δ^2H and MAT_{mrs} both showing relatively comparable temperatures to the rest of the record. ACL also returns to Late Oligocene values in the Early Miocene. Although the overall terrestrial climate in Antarctica was marginally colder than the Late Oligocene, this may just indicate that vegetation has permanently migrated to lower altitudes or at least sites where it can remain within its preferred temperature range and ecological niche. This could be the result of a larger volume of ice remaining onland following the Mi-1 glaciation, or glacial erosion reducing the elevations of the West Antarctic interior.

Age | Depth mbsf

Plio-R

Early Miocene — 4

Mi-1 — 3

Transition to Mi-1 — 2

Late Oligocene — 1

Transition: Late Oligocene to Mi-1

Orbital parameters = cooler summers

Transantarctic Mountains

EAIS

WAIS

Ice volume increases

Vegetation migrates to lower altitudes

Marie Byrd Land

Ross Sea

Sources of sediment and biomarkers for DSDP 270

Cooling ocean

Central High

300-500m

Subsidence

Intensified bottom currents

DSDP 270

Diamictites → cyclopels/cyclopsams → mudstone

Late Oligocene

Transantarctic Mountains

EAIS

WAIS

Marie Byrd Land

Ross Sea

Sources of sediment and biomarkers for DSDP 270

150-300m

Central High

DSDP 270

Glaciomarine mud with IRD

Diamictite

Mudstone

Interlaminated sandstone and mudstone

Unconformity

155

Figure 4.15: Schematic reconstructions of the Ross Sea embayment throughout DSDP 270.

4.5 Conclusions

DSDP 270 contains a proximal Antarctic record of the Mi-1 glaciation, one of the largest transient glacial excursions in the Cenozoic. Biomarker-based proxies and palynomorphs have been interpreted in the context of the lithostratigraphy of the core to determine environment conditions and constraints before, during and after this extensive glaciation. Relatively warm conditions in the Late Oligocene gave way to regional cooling during the transition into Mi-1, in response to orbital parameters which promoted low seasonality and cool summers over Antarctica. Regional subsidence and cooling SSTs may have also driven an intensification in proto-Antarctic bottom water production. The glacial manifested a period of cool temperatures both on and offshore. Short, cold growing seasons drove vegetation to lower altitudes and more stunted growth forms, with mosses and other spore producing plants expanding relative to shrubby trees such as *Nothofagus*. Grounding line distal sediment facies during this period, coupled with SSTs ~6°C warmer than present, indicate that grounded ice did not extend over this section of the Ross Sea. Instead, it is likely that a topographically higher, terrestrial West Antarctica was able to hold a significant amount of the ice volume associated with this glacial, in order to reconcile the magnitude of the $\delta^{18}O$ excursion in deep-sea foraminiferal records. Grounding line distal sediments also indicate that the Central High may not have held an ice cap during this time, suggesting that it was potentially submerged. This could be due to tectonic subsidence or increased relative sea levels as the result of a glacioisostatic adjustment caused by the large volume of ice on land in the West and East Antarcitc interiors. Fringing ice shelves during this time may also explain the lack of ice rafted debris and a reduction in LMW *n*-alkanes. The Early Miocene section of DSDP 270 is represented by periods of glacial proximity and/or increased iceberg discharge from coastal outlets from a WAIS lacking a fringing ice shelf. SSTs were slightly warmer than Mi-1 (by ~0.4°C) but ~1.4°C cooler than the Late Oligocene, while polar benthic foraminiferal assemblages and a tundra like vegetation are similar to other Miocene records around the region. Following the relative warmth of the Late Oligocene, Mi-1 therefore appears to mark the start of period of increasingly polar conditions in the Ross Sea embayment.

Chapter 5: A Cenozoic record of ocean temperature from the Ross Sea region, Antarctica: Implications for the use of isoprenoid GDGT-based proxies in ice-proximal, high latitude settings.

This chapter reconstructs a long-term record of ocean temperature through the Cenozoic from localities in the Ross Sea, Antarctica using proxies based on isoprenoid GDGTs. This chapter aims to understand the evolution of ocean temperature in this key region of Antarctica, as well as the implication of applying isoprenoid GDGT-based proxies in a setting which has undergone significant changes to climate, oceanography and tectonics.

5.1 Introduction

The long-term climate evolution of Antarctica is largely derived from records far removed from the continent. Global stacks of benthic foraminiferal $\delta^{18}O$ reflect both deep-sea temperature and ice volume, and as such have been used to interpret the changes in each of these parameters over the Cenozoic (i.e. Zachos et al., 2001a, 2008, Cramer et al., 2009, De Vleeschouwer et al., 2017). However, evidence from both present day (i.e. Moritz et al., 2002, Vaughan et al., 2003), and the past (i.e. Sluijs et al, 2006, Lunt et al., 2012, Brigham-Grette et al. 2013) show polar amplification of temperature changes, which is attributed to a range of high latitude feedback processes such as snow and sea-ice cover, atmospheric CO_2 levels and changes in atmospheric circulation. High latitude temperature records are therefore important for understanding the process of polar amplification in the past, and the consequences of enhanced polar temperatures for ice sheet volume and extent. In Antarctic sediments, microfossil based methods of reconstructing ocean temperature, such as assemblages and the geochemistry of foraminifera, are challenging due to sparse distribution, low diversity of species, or poor preservation in sediments. Biomarkers therefore have the potential to provide environmental proxy information where other methods are unsuitable. This study use GDGTs to reconstruct and compile ocean temperatures in the Ross Sea region over the Cenozoic. The Ross Sea is a key area for studying the previous extent and behaviour of both the EAIS and WAIS. It is a major drainage area for both Antarctic ice sheets, in particular the WAIS, and models indicate it is sensitive to climate forcings such as ocean heat flux and sea level (De Santis et al., 1999, Pollard and DeConto, 2009, Golledge et al., 2012, Golledge et al., 2013).

5.1.1 Tectonic Setting

Since the late Cretaceous, the Ross Sea embayment has comprised a number of subsiding basins, the Eastern Basin, Central Trough and Victoria Land basin, separated by the structural

highs of the Central High and Coulman High (Section 1.3) (Figures 5.1 and 5.2) (De Santis et al., 1995). The embayment has formed within the WARS and is bordered to the west by the TAM, and the east by Marie Byrd Land (Behrendt et al., 1991). The Central High and Coulman High remained subaerial until at least the Mid Oligocene, and then likely varied between subaerial and submerged during high and low stands of sea level, before permanently submerging as the result of glacial erosion and tectonic subsidence at some stage in the Early-Middle Miocene (De Santis et al.,1995, De Santis et al., 1999, Bart and De Santis, 2012). Millions of years of erosion and sedimentation coupled with thermal subsidence and tectonic plate movement have resulted in substantial changes in topography of the Ross Sea Region (Figure 5.1) (Wilson and Luyendyk, 2009, Wilson et al., 2012). Most significantly, the region has changed from an archipelago of islands separated by seaways with a much more elevated and subaerial West Antarctica, to the present day overdeepened, submerged Ross Sea (Figure 5.1) (i.e. De Santis et al.,1995, De Santis et al., 1999, Wilson and Luyendyk, 2009, Bart and De Santis, 2012, Wilson et al., 2012).
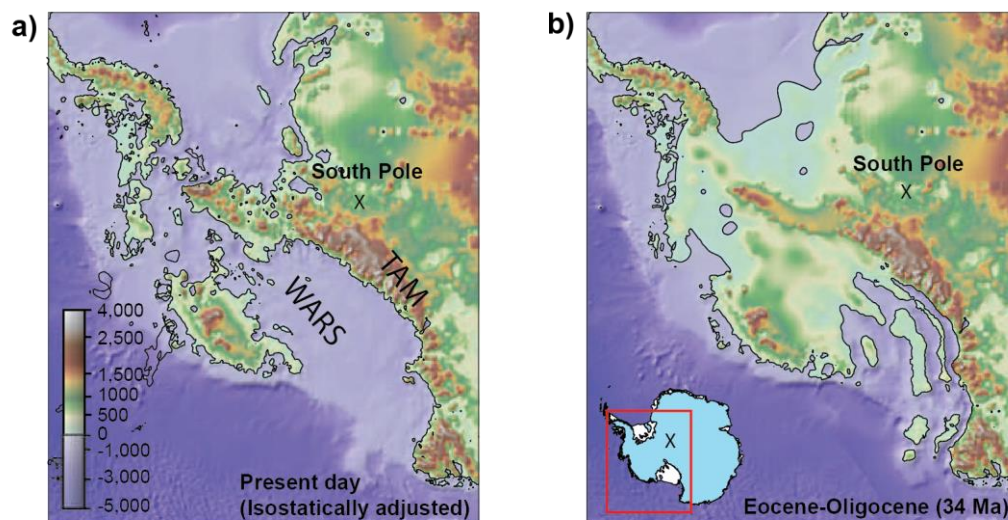
Figure 5.1: Isostatically adjusted topography of present day West Antarctica (a), and modelled topography at the Eocene-Oligocene boundary (~33 Ma) (b), adapted from Studinger and Barrett (2009) and Wilson and Luyendyk (2009). TAM: Tranantarctic Mountains, WARS: West Antarctic Rift System.

5.1.2 Modern Oceanographic Setting and Primary Production

The continental shelf in the Ross Sea embayment has an average water depth of ~530 m, with portions shallowing to above 200 m (Smith et al., 2012). Troughs and banks, carved by ice

streams cross the shelf in a roughly north-south direction, influencing regional circulation (Smith et al., 2012). Sea ice covers most of the region in winter, with reduced ice near the front of the Ross Ice Shelf, while in summer most of the embayment is ice free (Smith et al., 2012).

The surface water mass in the Ross Sea is near-freezing, low salinity Antarctic Surface Water (AASW), with temperatures typically between 0 and -2°C (Orsi and Wiederwohl, 2009). This is underlain by Modified Circumpolar Deepwater, which is slightly warmer, reaching to ~0.5°C (MCDW) (Orsi and Wiederwohl, 2009). Sea ice formation and brine rejection is particularly active in the Ross Sea and Terra Nova Bay polynyas, converting the upper waters into cold (~-2°C), dense Shelf Water (SW) which forms the bottom water on the continental shelf and under the Ross Ice Shelf (Orsi and Wiederwohl, 2009, Smith et al., 2012). SW flows off the continental shelf break and into the deep ocean where it forms Antarctic Bottom Water (AABW) (Orsi and Wiederwohl, 2009). In the deep ocean, seaward of the continental shelf AASW overlies CDW, with AABW below. The clockwise rotating Ross Gyre, entrains CDW from the westerly Antarctic Circumpolar Current further north, and acts to transport these waters southwards towards the continental shelf slope, where circulation becomes dominated by the easterly Antarctic Shelf Current (Orsi and Wiederwohl, 2009).

The Ross Sea has high rates of primary and export production, serving as a major CO_2 sink (Arrigo et al., 2008a, 2008b). The seasonal growth of biomass in the Ross Sea initiates in Late October, coincident with rapidly decreasing sea ice (Smith et al., 2012). The Ross Sea polynya opens up substantially in spring/summer, but remains relatively unstratified as winds drive advection of sea ice away from the polynya before it melts significantly (Arrigo and van Dijken, 2004). The smaller Terra Nova polynya becomes highly stratified in spring/summer due to sea ice melt (Arrigo and van Dijken, 2004). This drives spatial patterns in the species composition of phytoplankton blooms, with the algae *Phaeocystis Antarctica* preferring the more deeply mixed Ross Sea polynya region, while diatoms bloom later in the year in the more stratified region of the Terra Nova Bay polynya (Arrigo et al., 1998, 2000).

This chapter focuses on GDGTs derived from archaea (section 5.1.4). Archaeal abundances around Antarctica exhibit clear temporal and spatial trends. In surface waters around the Antarctic Peninsula, archaea are most abundant during the austral winter and early spring, becoming rare above ~45m water depth in the summer (Murray et al., 1998, Massana et al., 1998, Church et al., 2003, Kalanetra et al., 2009). While in winter their abundances through the water column are more homogenous, maximum abundances in both summer and winter are

typically at ~100m water depth (Murray et al., 1998, Church et al., 2003, Kalanetra et al., 2009). Loss of archaea from surface waters during summer is suggested to be due to photoinhibition (Kalanetra et al., 2009). Studies of the modern distributions of the common phylums of archaea, Thaumarchaeota and Euryarchaeota, around Antarctica indicate that most distributions are dominated by Thaumarchaeota (Church et al., 2003, Alonso-Sáez et al., 2011, Kim et al., 2013). However, a study from the Ross Sea suggests that Euryarchaeota forms a relatively large proportion of the archaeal community in CDW, but not in surface, shelf and thermocline waters (Alonso-Sáez et al., 2011).

5.1.3 Antarctic Cenozoic Ocean and Onshore Temperatures

The climate of Antarctica in the Paleocene (~65-56 Ma) was cool temperate, however by the Early Eocene (~56-49 Ma) the continent was warmer (coastal mean annual air temperatures of ~16±5 °C) and wet, with high atmospheric CO_2 (>1000 ppm) and highly diverse near tropical forests in coastal regions (Anderson et al., 2011, Beerling and Royer, 2011, Passchier et al. 2013, Pross et al. 2012, Masson-Delmotte et al., 2013). The Mid-Eocene marked the beginning of a period of global cooling (Section 1.1) (Zachos et al., 2001a). In Antarctica, SSTs cooled by 2-4°C across the Early-Middle Eocene transition, inferred to be related to the early opening of the Tasmanian Gateway at ~49-50 Ma, resulting in circum-Antarctic surface circulation and regional surface water cooling (Bijl et al., 2013). Onshore, temperatures cooled by ~7°C and a temperate rainforest biome expanded at the expense of near tropical vegetation (Pross et al., 2012). From the Middle to Late Eocene, SSTs continued to decline around Antarctica, related to declining CO_2 and continued expansion of the Tasmanian Gateway (Inglis et al., 2015). TEX_{86} and TEX_{86}^L SST estimates for the Mid-Late Eocene in the Southern Ocean and offshore Wilkes Land range from ~20-25°C (Bijl et al., 2009, Bijl et al., 2013, Inglis et al., 2015). Eocene cooling culminated in the development of large-scale Antarctic ice sheets at the Eocene/Oligocene boundary (~34 Ma) (Section 1.1) (e.g. Pagani et al. 2011, Bijl et al., 2013, Passchier et al., 2013, Galeotti et al., 2016, Anagnostou et al., 2016). While different high latitude sites show different absolute SST estimates, a relative cooling of ~5°C has been proposed over the Eocene/Oligocene transition (Liu et al., 2009).

Continued global cooling during the Oligocene was associated with declining atmospheric CO_2 concentrations (from 600 to 300 ppm) (Pälike et al. 2006b, Pagani et al., 2011). Records from the Ross Sea indicate a mainly subpolar regime in the region during this time, with sediment-laden freshwater input and the presence of sea ice (i.e. Leckie and Webb, 1983, Powell et al.,

2000, Prebble et al., 2006b). Mean spring/summer temperatures at <100m water depth are estimated from stable isotopes on molluscs to be ~5-7°C (Lavelle et al., 2001).

The Oligocene/Miocene boundary at ~23 Myr is marked by the Mi-1 event, coinciding with the expansion of the EAIS to close to, or exceeding present day volume (Chapter 4) (Zachos et al., 1997, Naish et al., 2001b, Zachos et al. 2001a, 2001b, Pekar and DeConto, 2006). TEX_{86} based temperatures from this study indicate subsurface temperatures of ~4°C in the Central Ross Sea during this glaciation (Chapter 4). During the Early to Mid-Miocene the Antarctic ice sheets were highly dynamic, responding to small shifts in CO_2 (Gasson et al., 2016, Levy et al., 2016). SSTs in the Ross Sea vary between ~-2 to 10°C during this time period, as inferred from TEX_{86}^L and carbonate-based clumped isotopes (Levy et al., 2016). The MMCO (~17-15 Ma) manifested as a period of relative warmth in Antarctica, with warmer onshore temperatures and an expansion of vegetation and more tree like forms (Warny et al., 2009, Feakins et al., 2012). During the warmest periods of the MMCO, TEX_{86}^L and carbonate isotopes SSTs indicate temperatures between ~6 and 10°C in the Ross Sea (Levy et al., 2016).

The MMCO was followed by the MMCT, a significant cooling event is characterised by a foraminiferal $\delta^{18}O$ decrease of ~1 ‰ (Section 1.1) (Shackleton and Kennett, 1975, Flower and Kennett, 1994, Zachos et al., 2001a). In the Southern Ocean, surface waters cooled by 6-7°C and deep waters by ~2°C (Shevenell et al., 2004, Shevenell et al., 2008). In the Ross Sea, large hiatuses in continental shelf records indicate expansion of the Antarctic ice sheets across the shelf, leading to widespread erosion surfaces (i.e. De Santis et al., 1999, Bart, 2003).

Cooling following the MMCT was interrupted by a relative warming during the Pliocene between 5-3 Ma. The Pliocene was largely characterised by moderately higher temperatures and CO_2 concentrations than present, and a greatly reduced WAIS during interglacials, but with marine-based ice sheet advances during glacials (Naish et al. 2009, Seki et al. 2010). In the Ross Sea, interglacials during this period were characterised by TEX_{86}^L SSTs of ~5°C and diatom assemblages more typical of modern subantarctic waters (McKay et al., 2012a). Cooling during the Late Pliocene (3.6 to 2.58 Ma) resulted in the development of perennial sea ice in the Southern Ocean, a more expansive WAIS, and the development of continental-scale northern hemisphere ice sheets with TEX_{86}^L SSTs indicating a cooling in the western Ross Sea to between ~0-2°C (McKay et al., 2012a).

5.1.4 GDGTs

Isoprenoid GDGT's (IsoGDGT's) are membrane lipids produced by Thaumarchaeota, a type of archaea found in the ocean and lakes, while branched GDGT's (brGDGT's) are thought to be produced by soil bacteria (Peterse et al., 2010, Sinninghe Damsté et al., 2011, Schouten et al., 2013). IsoGDGTs increase the number of cyclopentane moieties they produce with increasing water temperature, a relationship commonly assessed using the TEX_{86} ratio (Eq.1.8) (Schouten et al., 2002, Schouten et al., 2013).

At high latitudes, core tops show large scatter and a different relationship with temperature to the rest of the global oceans (Kim et al., 2008, Kim et al., 2010, Ho et al., 2014). Early studies found that the relationship between TEX_{86} and SST was linear for temperatures between 5-30°C (Schouten et al., 2002, Kim et al., 2008). However, in the polar ocean where temperatures are below 5°C, variance in TEX_{86} values are relatively minor and have a non-linear relationship with temperature (Schouten et al., 2002, Kim et al., 2008). Kim et al. (2010) developed two different calibrations in order to make TEX_{86} a suitable low temperature proxy method. They found that the regio-isomer of crenarchaeol is strongly correlated with SST at high temperatures, but not at low temperatures. Therefore, one calibration excludes the crenarchaeol regio-isomer for temperatures below 15°C (TEX_{86}^{L}) and one calibration includes it for temperatures above 15°C (TEX_{86}^{H}). Where a temperature record is likely to encompass both temperature ranges, they recommended that TEX_{86}^{L} is used.

$$TEX_{86}^{L} = \log \left(\frac{[GDGT-2]}{[GDGT-1]+[GDGT-2]+[GDGT-3]} \right) \qquad (Eq.\,5.1)$$

and

$$SST = 67.5 \times (TEX_{86}^{L}) + 46.9 \qquad (Eq.\,5.2)$$

$$TEX_{86}^{H} = \log\ (TEX_{86}) \qquad (Eq.\,5.3)$$

and

$$SST = 68.4 \times (TEX_{86}^{H}) + 38.6 \qquad (Eq.\,5.4)$$

The residual standard error for the TEX_{86}^{L} calibration is ±4°C and for TEX_{86}^{H} it is ±2.5°C. However, as TEX_{86}^{L} does not correlate to TEX_{86} its physiological basis remains unclear.

Furthermore, TEX_{86}^L can produce unrealistically low temperatures without a modern analogue (i.e. below -3°C) (section 5.4.3.1). To try to address some of the challenges associated with the use of TEX_{86} at high latitudes several regional specific approaches have been taken. Shevenell et al., (2011) analysed core top samples from the Antarctic Peninsula and integrated this data into the global core top calibration of Kim et al., (2008):

$$TEX_{86} = (0.0125 \times SST) + 0.3038 \qquad \text{(Eq. 5.5)}$$

This calibration has a standard error of ±2.5°C. To account for spatial variance in the response of TEX_{86} to temperature, Tierney and Tingley (2014, 2015) developed BAYSPAR, a Bayesian, spatially-varying regression calibration. BAYSPAR can be used in two modes: 1) a standard mode, which assumes oceanographic conditions are similar enough to present that it is reasonable to use a spatially weighted distribution, and 2) an analogue mode, which instead finds similar TEX_{86} values from various locations throughout the global data set to form a calibration. In standard mode, BAYSPAR applies a local calibration to high latitude sites, taking into account of the distinctive nature of high latitude TEX_{86} relationships.

Debate has centred on whether TEX_{86} reflects a sea surface or subsurface temperature (Section 1.8.3.1). The seasonality of isoGDGT production and export has also been considered a potential bias for TEX_{86}, and suggests that the TEX_{86} value derived from seafloor sediment may be weighted towards a certain season rather than reflecting mean annual temperature (e.g. reviews in Schouten et al., 2013, Taylor et al., 2013). In Antarctica, archaea are most abundant in winter and early spring, with maximum abundances in the subsurface at ~100m (section 5.1.2). Kim et al. (2012) recognised that Thaumarchaeota have elevated abundances in the subsurface offshore Wilkes Land, Antarctica, and proposed an adjustment to the TEX_{86}^L calibration to calibrate it to depth integrated mean annual temperatures from 0-200m water depth.

$$SST = 50.8 \times (TEX_{86}^L) + 36.1 \qquad \text{(Eq. 5.6)}$$

This calibration has an error of ±2.8°C.

Several other factors can impact the robustness of the relationship between TEX_{86} and temperature. In methane-rich environments, archaeal GDGTs can also be produced in sediments post deposition by methanotrophic archaea (Section 1.8.3.1) (Zhang et al., 2011).

The methane index (MI) quantifies the relative contribution of methanotrophic produced GDGTs to those produced in the water column by non-methanotrophic Thaumarcheaota, where values >0.3 indicate a significant contribution from a source other than normal marine sedimentation (Eq. 1.9) (Zhang et al., 2011). Methanogenic Euryarchaeota can also synthesise GDGT-0, and to a lesser extent GDGT-1, GDGT-2 and GDGT-3 (Section 1.8.3.1) (e.g. Pancost et al., 2001, Blaga et al., 2009, Sinninghe Damsté et al., 2012, Inglis et al., 2015). The impact of these archaea is described using %GDGT-0, where values >67% indicate that a sample contains a substantial contribution from methanogenic sourced GDGTs (Eq. 1.10) (Sinninghe Damsté et al., 2012). The BIT index is used to assess the contribution of GDGTs from terrestrial soils, ranging from 0, representing no branched GDGT input, to 1, representing no Crenarchaeol input (Eq. 1.11, section 1.8.3.1) (Hopmans et al., 2004). Oxygen content can also have an important control on TEX_{86} (Section 1.8.3.1) (Qin et al., 2015).

Different strains of archaea have been found to display variable TEX_{86} values, despite having been cultured at the same temperatures (Qin et al., 2015). However, a linear relationship was found between the Ring Index (RI) and temperature across all strains of archaea, indicating that this may be a better proxy for temperature (Qin et al., 2015). The RI as defined by Zhang et al., (2016b) is used in this study, where higher values indicate warmer temperatures (Eq. 1.12, section 1.8.3.1). RI may be a more reliable indicator of temperature at high latitudes, as GDGT-0 and crenarchaeol tend to dominant cold water samples, but are not included in the TEX_{86} index (Section 1.8.3.1). In the modern ocean, TEX_{86} and RI are correlated, and RI can be calculated from TEX_{86} using a regression (Eq. 1.13, section 1.8.3.1). If RI deviates from calculated RI (ΔRI=calculated RI-analysed RI) by more than ± 0.3 RI units then that sample may be influenced by non-thermal factors and may deviate from modern analogues (Section 1.8.3.1)

5.1.5 Sampling Sites

Proximal Antarctic cores usually contain frequent unconformities, which is often the product of ice sheet overriding or other erosional processes in a glaciomarine environment. In order to compile a long-term Cenozoic record of ocean temperatures from the Ross Sea, this has necessitated using multiple sampling sites and core sites from across the region (Figures 1.6 and 5.2).
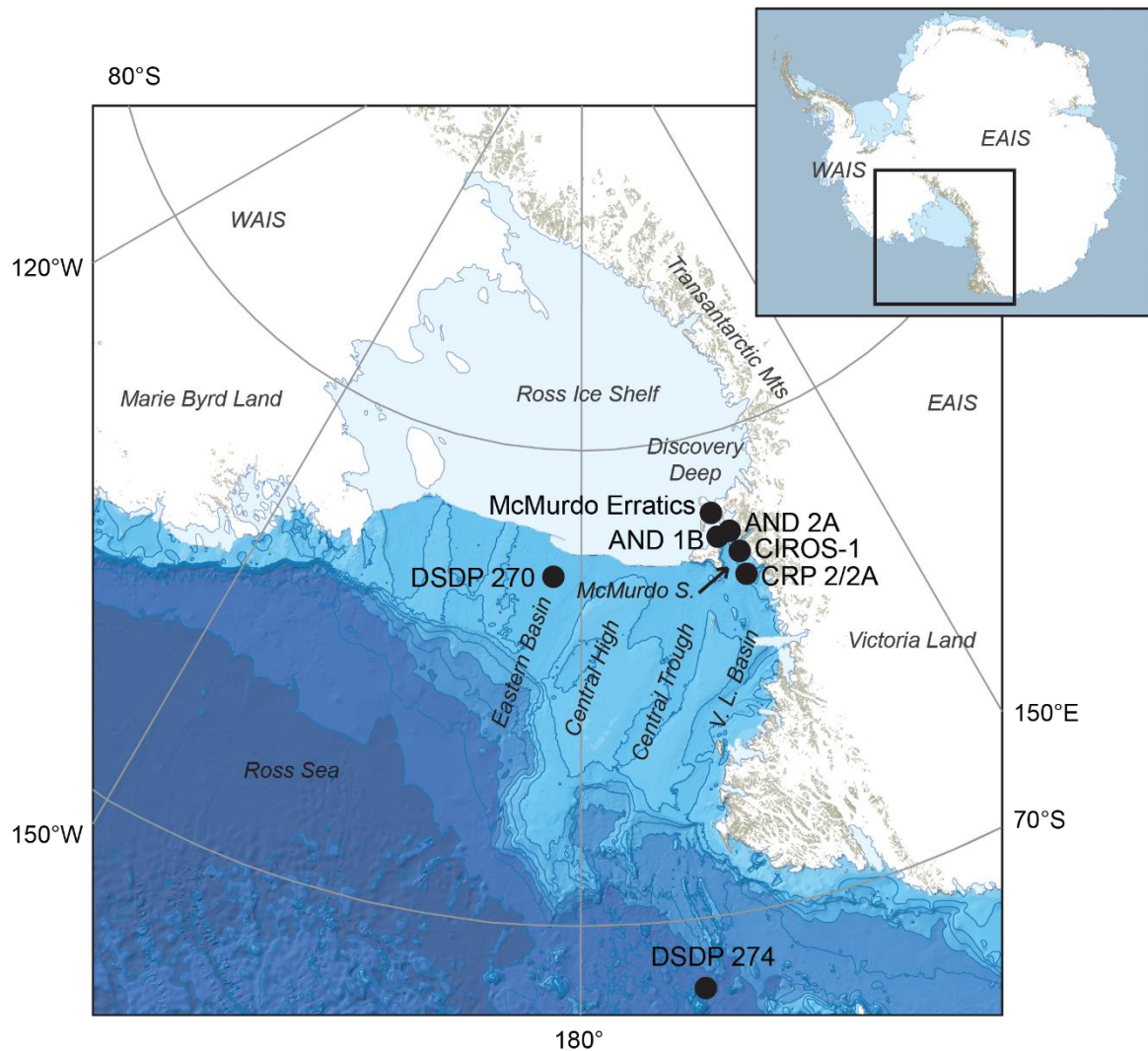
Figure 5.2: Locations for sites sampled in this study. Base map from Quantarctica GIS package, Norwegian Polar Institute.

5.1.5.1 McMurdo Erratics

The oldest sediments used in this compilation are glacial erratics, collected from the Mt Discovery and Minna Bluff region (Figure 5.2, section 1.7.4 and 3.1.3.1) (Harwood and Levy, 2000). The erratics have been eroded from rift-fill sediments in the western Ross Sea and transported by expanded ice sheets during past glacial periods (Harwood and Levy, 2000). The erratics used in this chapter have been dated on basis of microfossils to be mid-late Eocene to mid-late Miocene in age (Harwood and Levy, 2000). Their environment of deposition is interpreted as coastal-terrestrial and nearshore marine, under ice free conditions for the Eocene

samples, while the influence of marine calving glaciers in the form of ice rafted debris is apparent in younger samples (Harwood and Levy, 2000).

5.1.5.2 CIROS-1

The CIROS-1 core was drilled in McMurdo Sound in 1986 (Figure 5.2) (Barrett, 1989). The core consists predominantly of sequences of diamictites, sandstones and mudstones (Hambrey et al., 1989). The upper part of the core (366-0 m) is glacially influenced, recording seven major glacial advances represented by massive and stratified diamictites (Hambrey et al., 1989). Below an unconformity, the lower sequence of the core (702-366 m) displays significantly less subglacial influence, containing marine mudstones and sandstones, but with ice rafted debris throughout indicating the presence of marine terminating glaciers at the coastline (Hambrey et al., 1989). The upper part of the core is Late Oligocene/Early Miocene in age, dated by magnetostratigaphy, biostratigraphy, $^{87}Sr/^{86}Sr$ dating of macrofossils and ^{40}Ar-^{39}Ar radiometric dating (Roberts et al., 2003). The lower part of the core has recently been redated to Late Eocene to Early Oligocene (Prebble et al., in prep.) Samples for this study are derived from unpublished results from Stefan Schouten (NIOZ). Samples were taken at regular intervals throughout nearly all of the core (102-697 m).

5.1.5.3 DSDP 270

DSDP site 270 was recovered from the Eastern Basin of the central Ross Sea (Figure 5.2, sections 1.7.7 and 3.1.3.4) (The Shipboard Scientific Party, 1975a). Samples for this study have been taken from glaciomarine sediments between 387.9-27.8 mbsf. An age model for DSDP 270 is currently in preparation and the key data from this preliminary age model are discussed in Chapter 4 (Kulhanek et al., in prep.). As the focus of this chapter is long term trends, the interpretations are not dependent on a high-resolution age model, and it is accepted there may be hiatuses of ~1 Ma present in the DSDP 270 core. With these caveats in minds, a linear sedimentation rate is assumed between the highest occurrence of *Chiasmolithus altus* at 345.29 mbsf dating to ~25.44 Ma, and the highest occurrence of *Zygrhablithus bijugatus* at 280.25 mbsf, dating to 23.76 Ma. This same sedimentation rate was assumed below the unconformity at 352 mbsf. A linear sedimentation rate was then applied between the highest occurrence of *Zygrhablithus bijugatus* and the highest occurrence of *Dictyococcites bisectus* at 150.65 mbsf, dating to 23.13 Ma. This same rate was applied until an inferred disconformity at 112 mbsf (Chapter 4). Above this point, the sedimentation rate was constrained by lowest occurrence of

Batiacasphaera cooperi at 111.13 mbsf, dating to 20.71 Ma and highest occurrence of *Kisseleviella tricoronata* at 105 mbsf, dating to 20.439 Ma.

5.1.5.4 CRP 2/2A

The Cape Roberts Project recovered CRP 2/2A off the Victoria Land coast of Antarctica (Figure 5.2, sections 1.7.6 and 3.1.3.3) (Cape Roberts Science Team, 1999). This study investigates three glaciomarine sequences in the late Oligocene/early Miocene section of the core (Naish et al., 2001b, Naish et al., 2008). Sequences are correlated to the geomagnetic time scale through an integrated approach using magnetostratigaphy, biostratigraphy, ^{87}Sr/^{86}Sr dating of macrofossils and ^{40}Ar/^{39}Ar radiometric dating (Wilson et al., 2000, Naish et al., 2008). An unconformity between ~23.2 to 21.3 Ma separates Late Oligocene from Early Miocene sediments.

5.1.5.5 AND-2A

The AND-2A core was recovered in 2007 from Southern McMurdo Sound as part of the ANDRILL program (Figure 5.2) (Harwood et al., 2008-2009). Samples for this compilation were collected from the Early Miocene to Mid-Miocene section of the core, and were published as TEX_{86}^{L} values by Levy et al. (2016), calibrated to Kim et al. (2012). The age model for this core is based on magnetostratigraphy, biostratigraphy, ^{87}Sr/^{86}Sr dating of macrofossils and ^{40}Ar/^{39}Ar dating of volcanic clasts and tephra (Levy et al., 2016). Sediments through this section consist of unconformity bound sequences of mudstones, sandstones, and massive and stratified diamictites (Fielding et al., 2008, Levy et al., 2016). These sequences represent ice-distal to ice-proximal, and occasionally subglacial settings, reflecting advance and retreat of grounded ice across the drill site (Fielding et al., 2011, Passchier et al., 2011). Below ~390 mbsf, sediments represent a relatively warm, subpolar regime characterised by larger volumes of sediment-laden glacial meltwater (Fielding et al., 2011, Passchier et al., 2011, Levy et al., 2016). A baseline shift to a colder, more ice-proximal environment occurs between 390 and 259 mbsf (~16-15 Ma) (Fielding et al., 2011, Passchier et al., 2011, Levy et al., 2016)

5.1.5.6 DSDP 274

DSDP 274 was drilled on the lower continental rise in the Northwestern Ross Sea (Figure 5.2; Sections 1.7.8 and 3.1.3.5) (The Shipboard Scientific Party, 1975b). Samples for this study were taken from 156-90 mbsf, spanning an Early Miocene to Late Miocene succession

(McCollum, 1975, Crampton et al., 2016). Ages have been assigned using the relaxed hybrid CONOP model of Crampton et al., (2016). This model however, does not extend below 141.26 mbsf. For samples below this depth the same linear sedimentation rate is assumed as occurs in the CONOP model above 141.26 mbsf, which is constrained by the first appearance of *Denticulopsis maccollumii* at 141.26 mbsf (dated to 17.05 Ma) and the first appearance of *Actinocyclus ingens* at 113.6 mbsf (dated to 15.83 Ma). The continuation of this sedimentation rate is supported by the apparent lack of a hiatus or change in lithology through this interval (The Shipboard Scientific Party, 1975b). The CONOP model of Crampton et al. (2016) assumes a hiatus or reduced sedimentation rate at 113.6 mbsf, which is supported by the presence of ferromanganese nodules (The Shipboard Scientific Party, 1975b). Mid-Late Miocene sediments above this depth also display an abrupt increase in course detritus, considered to indicate an enhanced ice-rafted component (Frakes, 1975).

5.1.5.7 AND-1B

The AND-IB core was drilled in 2006 as part of the ANDRILL McMurdo Ice Shelf project (Figure 5.2, section 1.7.5) (Naish et al., 2007). Samples were collected from two sections of the core. The Late Miocene section of this core, dated to ~9-10 Ma was analysed for this study (Ross et al., 2012). Maximum ages for this section are constrained by ^{40}Ar-^{39}Ar dates on volcanic clasts (Ross et al., 2012). Sediments in this interval are interstratified diamictite and mudstone, representing sequences of advance and retreat of a subpolar ice sheet, with subglacial outwash and glaciofluvial discharge from the EAIS margin providing significant sediment input to the site (McKay et al., 2009). Samples were also compiled from published data from the Plio-Pleistocene section of the core, which is characterised by diatomites with limited terrigenous input, indicating a significant cooling in glacial regime (~4.6-2 Ma) (McKay et al., 2012a). The age model for this section was developed from diatom biostratigraphy, ^{40}Ar-^{39}Ar radiometric ages and magnetostratigraphy (Naish et al., 2009). Pliocene sediments also reflect successions of advance and retreat of the marine-based ice sheet in the Ross Sea, and consist of cycles of diamictite leading up into mudstone and diatomite, bounded by glacial erosion surfaces (McKay et al., 2012a). The presence of diatom oozes in the Plio-Pleistocene interval of AND-1B, rather than glaciomarine mudstones, is interpreted as being indicative of sediment starvation in a glacial regime cooling towards modern polar conditions.

5.2 Methods

Samples from DSDP 270, DSDP 274, Cape Roberts 2/2A and the Miocene section of AND-1B were processed and analysed for this study. Methods for GDGT extraction, separation and analysis are described in Chapter 2.

5.2.1 Other sites included in this study

Samples from ANDRILL 2A were processed at Utrecht University and analysed at the Royal Netherlands Institute for Sea Research (NIOZ) (Levy et al., 2016). Samples for AND-1B were analysed between NIOZ and Yale University, following methods outlined in McKay et al. (2012a). Unpublished samples for CIROS-1 were analysed by Stefan Schouten at NIOZ, and samples from the McMurdo Erratics were analysed by Francesca Sangiorgi and Veronica Willmott at Utrecht University and NIOZ, using methods outlined in Schouten et al. (2007). The original results were compiled and recalibrated for this study.

5.3 Site Results

5.3.1 McMurdo Erratics

The samples from the McMurdo erratics vary considerably in age, from the Middle Eocene to Middle Miocene. All samples contain isoGDGTs but several are absent of brGDGTs. Younger samples typically display lower TEX_{86} values than the Eocene suite (ranging in total from 0.44-0.64), while RI shows a less consistent trend (ranging from 1.8-2.31) (Figures 5.3). BIT is also variable and frequently high. In the samples with brGDGTs present, BIT ranges from 0.03 to 0.55. MI indices are all below the threshold of 0.3 suggested by Zhang et al. (2011) as a lower limit for methanotropic influence, but some samples are still relatively high (ranging from 0.04 to 0.22). All samples are below the threshold of 67% for %GDGT-0 that indicates a methanogenic influence (range of 40.8% to 58.3%) (Sinninghe Damsté et al., 2012) (Figure 5.4).
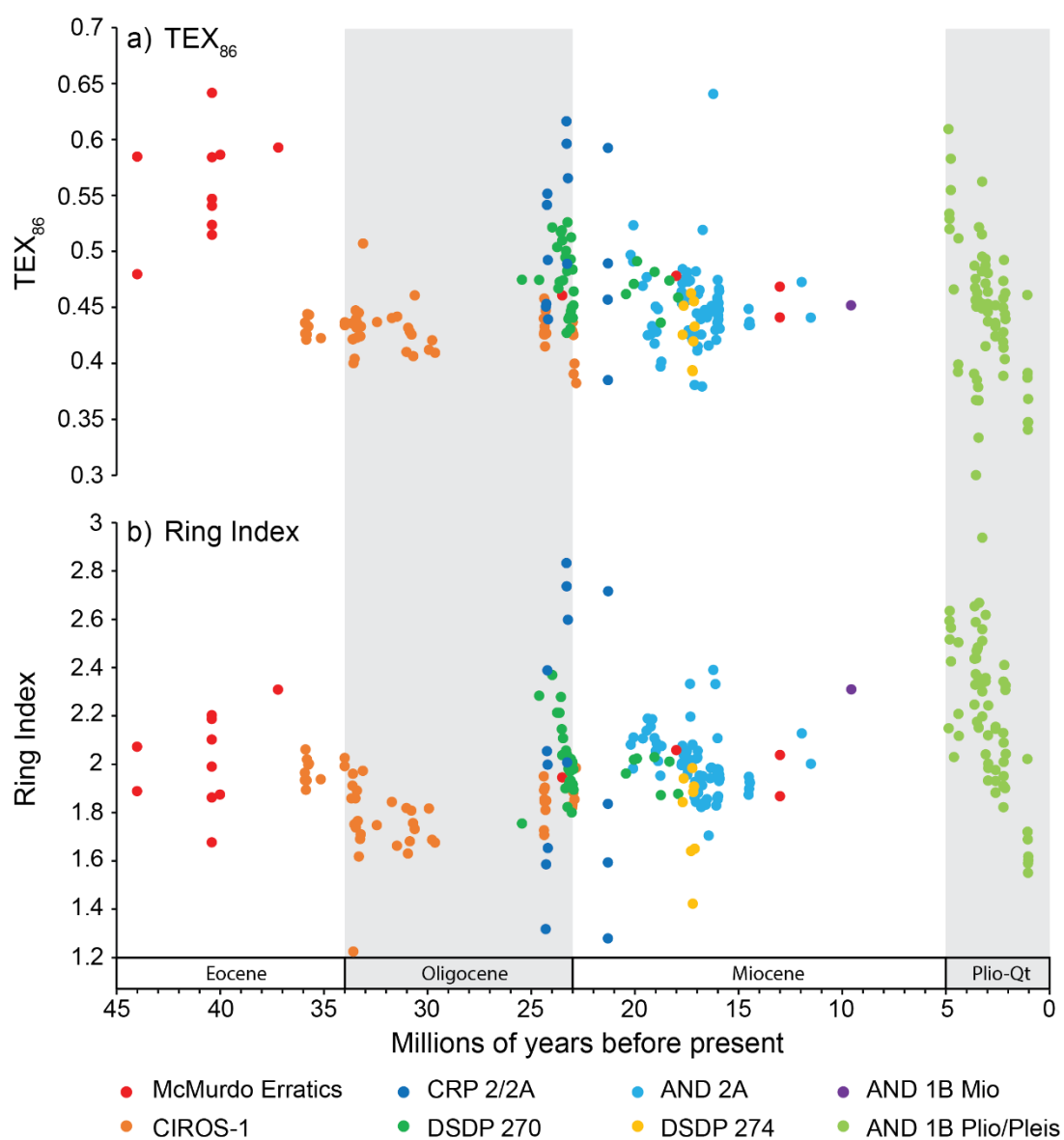
Figure 5.3: a) TEX$_{86}$ and b) Ring Index for Ross Sea region localities over the Cenozoic.
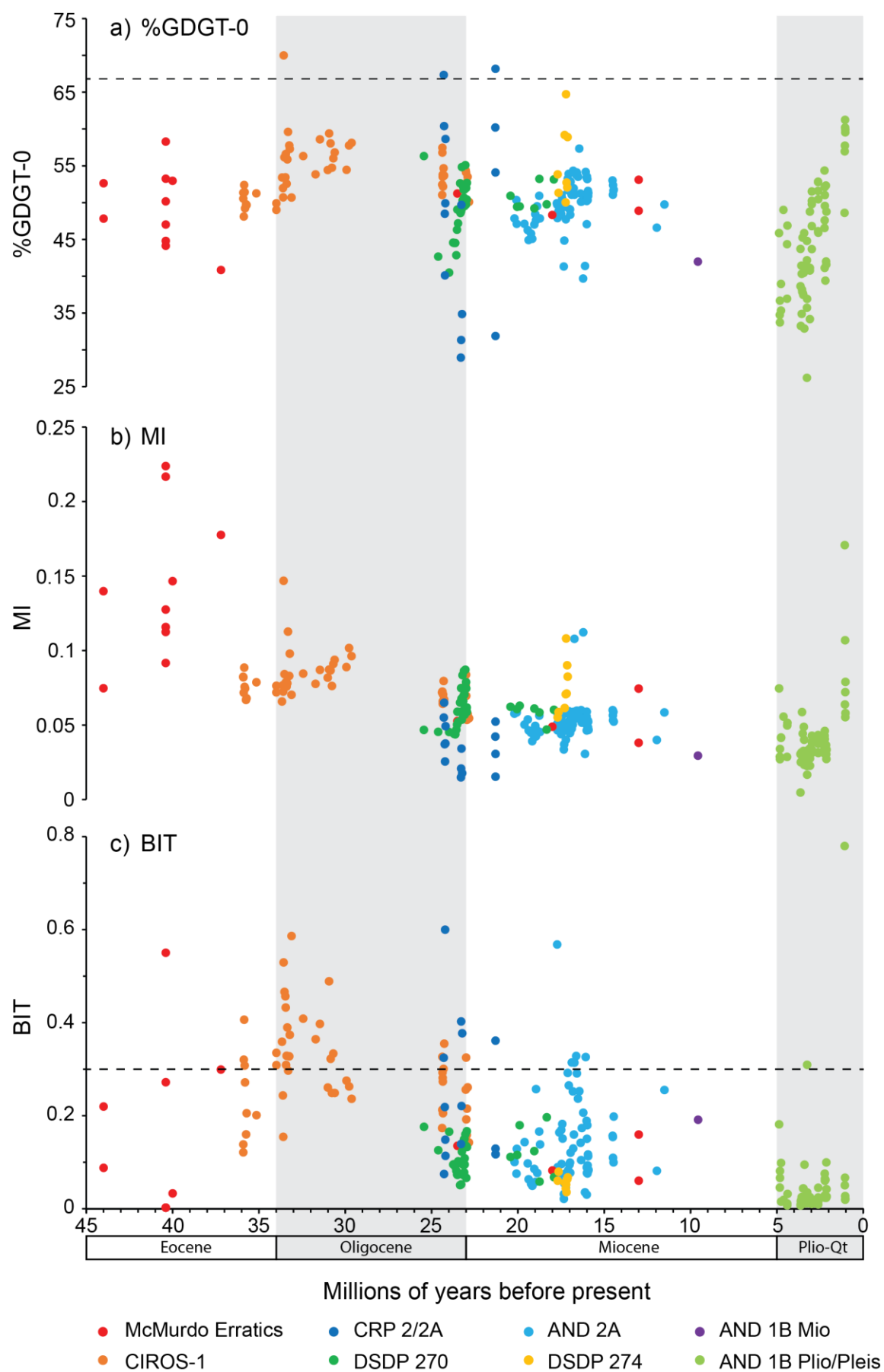
Figure 5.4: a) %GDGT-0, dashed line represents limit above which the GDGT distribution is considered to be influenced by methanogenic archaea, b) Methane Index (MI) and c) Branched and isoprenoid tetraether index (BIT), dashed line represents limit above which a significant amount of terrestrially sourced GDGTs are present.

5.3.2 CIROS-1

Samples from CIROS-1 span the Late Eocene through to the Early Miocene, with all samples containing both iso-GDGTs and brGDGTs. TEX_{86} values range from 0.38 to 0.51 and RI varies between 1.23 and 2.06 (Figure 5.3). BIT values are typically high throughout the sequence and frequently above the value of 0.3 suggested by Weijers et al. (2006b) to signal a significant influence from brGDGTs on TEX_{86} temperatures. While MI is low through the sequence, one sample contains a %GDGT-0 value of 70%, indicating a likely methanogenic influence (Figure 5.4).

5.3.3 DSDP 270

Samples below the unconformity at ~352 mbsf in DSDP 270 contained GDGTs, but in abundances that are too low to integrate, with only GDGT-0 and Crenarchaeol above the detection limit. While the rest of the sampled core still contained a few samples with very low GDGTs, the majority were abundant enough for integration, for which TEX_{86} ranges from 0.43 to 0.53 and RI from 1.80 to 2.37 (Figure 5.3). The TEX_{86} record shows more scatter, while RI demonstrates a clear decreasing trend. BIT values are typically low, varying between 0.04 and 0.19. Indicators of methanogenic or methanotrophic input are both low (Figure 5.4).

5.3.4 CRP 2/2A

GDGTs are present throughout CRP 2/2A, although in some samples abundances are too low to integrate, with the less abundant GDGTs below the detection limit. TEX_{86} values and RI are highly variable, ranging from 0.38 to 0.61 and 1.28 to 2.83 (Figure 5.3). BIT values vary between 0.07 and 0.60, indicating a significant terrestrial influence in several samples. While MI values are low, two samples have %GDGT-0 values above 67%, potentially indicating a contribution from methanogenic archaea (Figure 5.4).

5.3.5 ANDRILL 2A

Miocene samples from ANDRILL 2A contain both iso- and brGDGTs. TEX_{86} and RI values vary from 0.38 to 0.52 and 1.70 to 2.33, with one sample containing higher values of 0.64 and

2.39, respectively (Figure 5.3). BIT values are typically below 0.3, although 5 samples do exceed this - the highest of which contains a value of 0.57. Indicators of methanogenic or methanotrophic input are both low (Figure 5.4)

5.3.6 DSDP 274

Samples taken from Late Miocene sediments in DSDP 274 did not contain any detectable GDGTs. Samples from the Mid-Miocene were more productive, containing GDGTs in sufficient abundance for integration. Samples from this section of the core contained TEX_{86} and RI values ranging from 0.39 to 0.46 and 1.43 to 1.99 (Figure 5.3). BIT and MI values were low in all samples, and %GDGT-0 was below the limit of 67% in all samples (Figure 5.4).

5.3.7 ANDRILL 1B

5.3.7.1 Late Miocene section

GDGTs are present throughout this section but abundances are typically very low. While GDGT-0 and Crenarcheaol are present in most samples, the other GDGTs are usually below the detection limit or if present, are too low to integrate. Only one sample from this section of the core contained GDGTs in great enough abundance for integration (sample depth 1030 mbsf, age 9.6 Ma). This sample derived a TEX_{86} value of 0.45 with a RI of 2.3 (Figure 5.3). Indicators of methanogenic or methanotrophic input and terrestrial input are all low (%GDGT-0 of 50.1%, MI of 0.05 and BIT of 0.14) (Figure 5.4).

5.3.7.2 Pliocene/Pleistocene section

TEX_{86} values through the Plio-Pleistocene section of ANDRILL 1B varied considerably, with a range between 0.30 to 0.61. RI was also similarly variable, ranging between 1.55 and 2.94 (Figure 5.3). Both TEX_{86} and RI showed an overall decreasing trend through the Plio-Pleistocene. %GDGT-0, increases through the Plio-Pleistocene but no samples exceed the methanogenic input limit of 67%. MI is typically low, with some samples in the Pleistocene section showing slightly higher values but still below 0.3. With the exception of two samples. BIT values are low throughout (Figure 5.4).

5.4 Data Compilation and Temperature Calibrations

5.4.1 Ring index
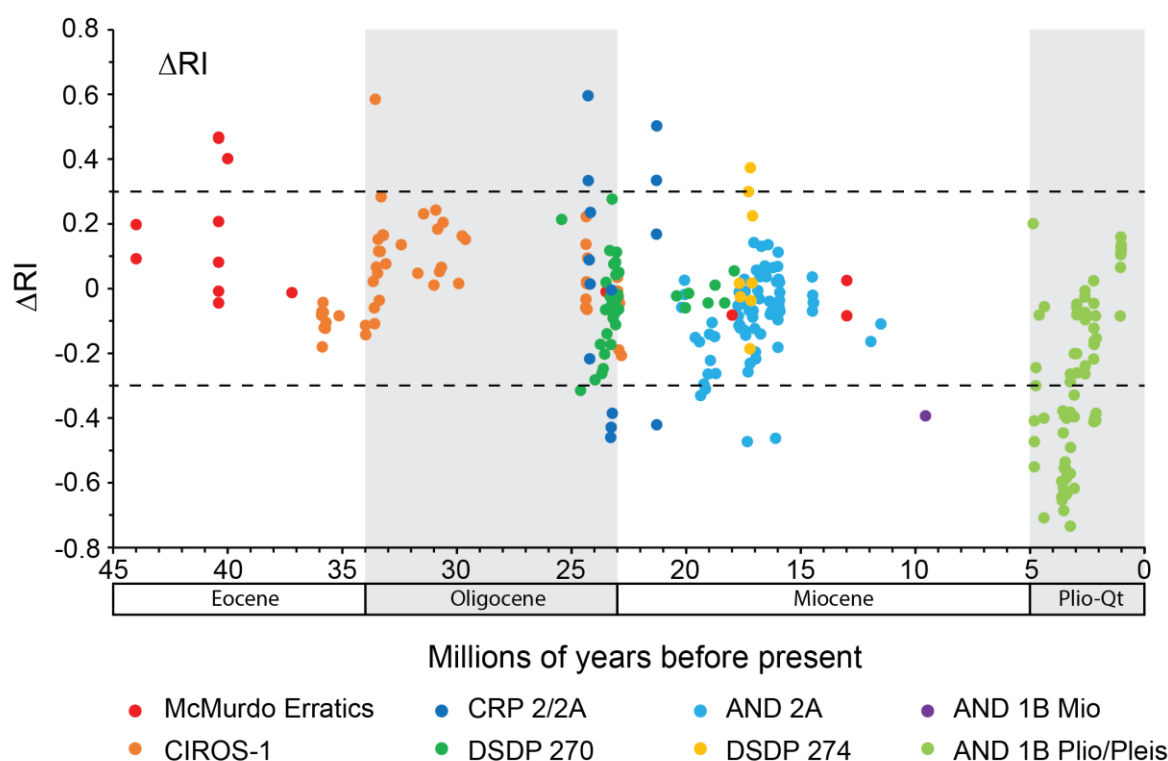
Figure 5.6: ΔRI for Ross Sea region localities, dashed lines indicates ±0.3 range, with values falling within this considered to be controlled by temperature (section 5.1.4).

The RI and TEX_{86} should correlate in samples where temperature is the dominant control, although in certain situations factors other than temperature may have a strong influence on the distribution of GDGTs (Section 1.8.3.1) (Zhang et al., 2016b). Samples demonstrating a ΔRI deviation of greater than ±0.3 potentially indicate a non-thermal influence (Figure 5.6). Interestingly, over the course of the Cenozoic, a long term trend in ΔRI emerges, from more positive values in the Eocene, to more negative in the Plio-Pleistocene.

To assess for some of the common factors that can result in large ΔRI deviations, ΔRI has been compared to BIT, MI and %GDGT-0, representing input from terrestrially derived GDGTs and those sourced from methanotrophic and methanogenic archaea, respectively (Figure 5.7). While several high BIT values are associated with large deviations in ΔRI, there is no clear trend. A trend emerges on a site-by-site basis when MI is compared to ΔRI. While all samples contain MI values lower than 0.3, higher values of MI are associated with larger positive

deviations in ΔRI while lower values have more negative ΔRI deviations. This same trend is more strongly apparent when ΔRI is compared to %GDGT-0. This indicates that in some samples the abundance of GDGT-0 is considerably higher or lower than the modern relationship between TEX_{86} and RI would suggest.
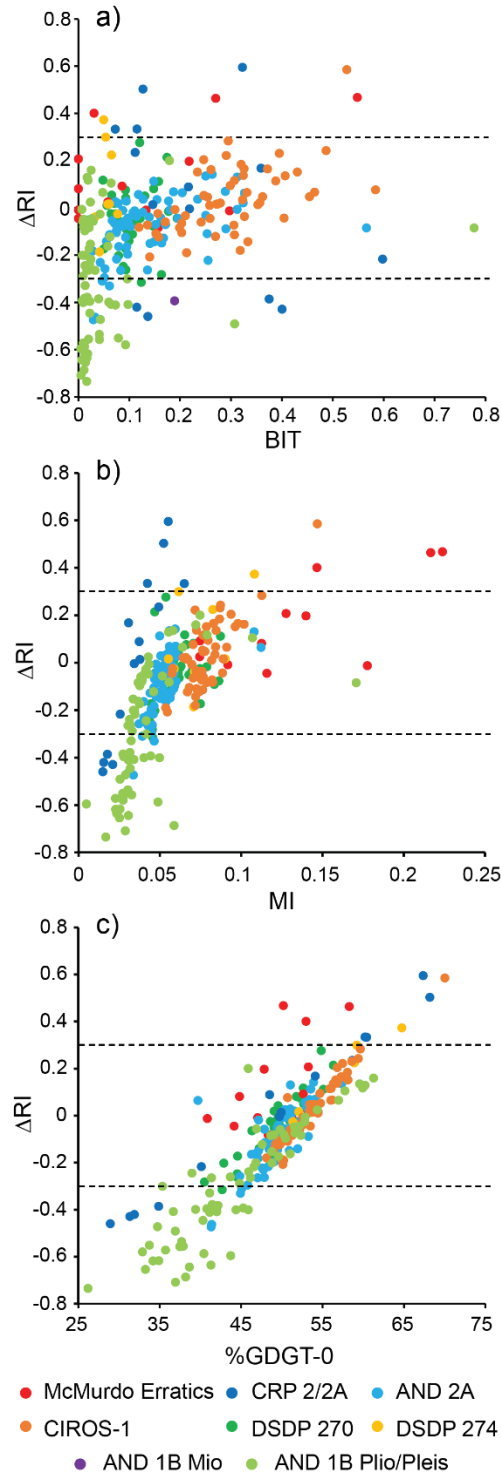
Figure 5.7: Scatter plots of a) ΔRI versus BIT, b) ΔRI versus MI, and c) ΔRI versus %GDGT-0.

5.4.2 Cenozoic TEX₈₆ and RI trend
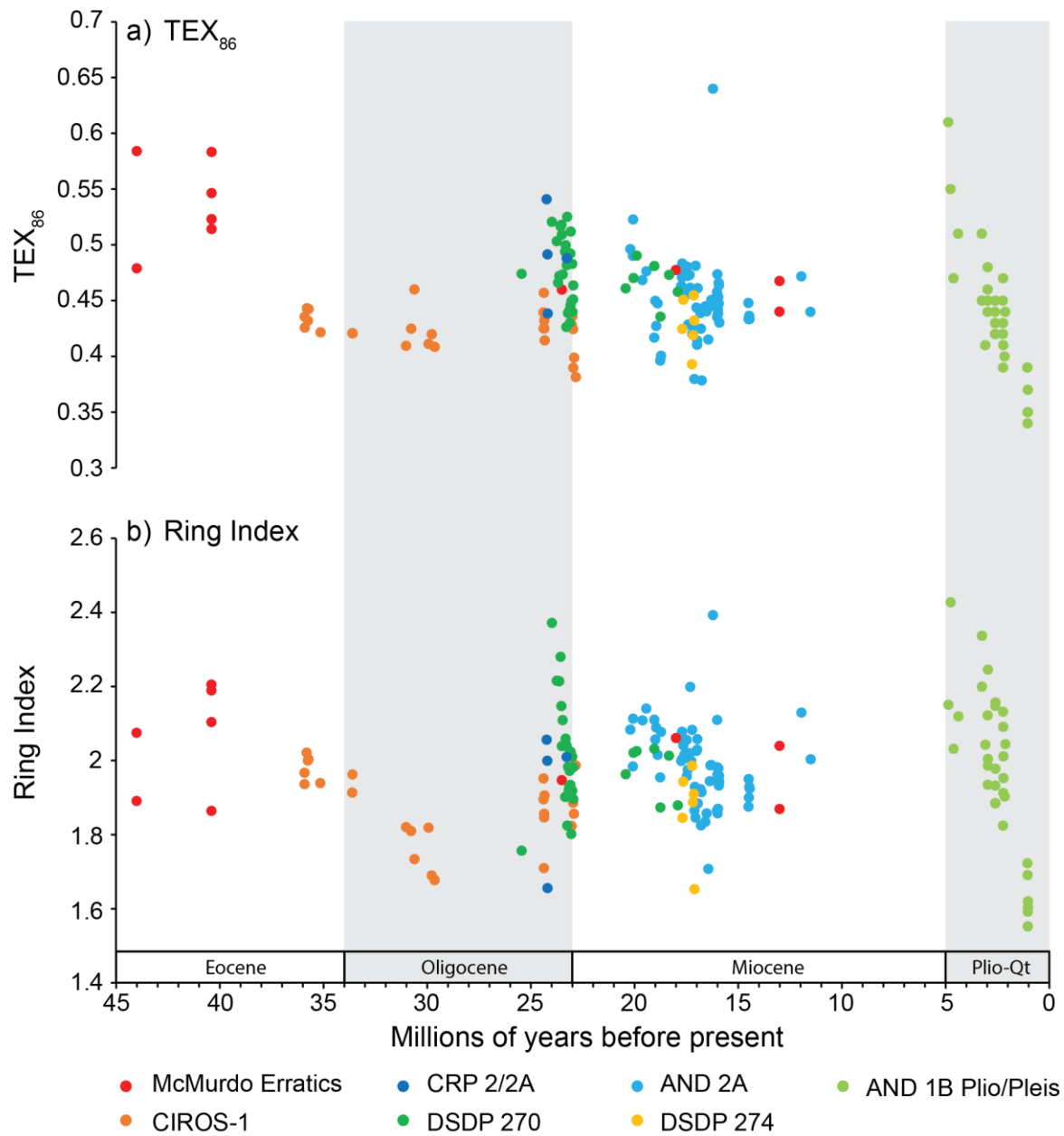
Figure 5.8: a) TEX$_{86}$ and b) RI from Ross Sea region localities, with values associated with high BIT, %GDGT-0 and a large deviation in ΔRI removed.

In order to correct for possible non-thermal influences on TEX$_{86}$ and RI at these core sites, samples which demonstrate high BIT, GDGT-0 or a large deviation in ΔRI have been removed from the long term compilation of TEX$_{86}$ and RI (Figure 5.8). When this is accounted for, higher values of TEX$_{86}$ are apparent in the Mid Eocene, decreasing by the Late Eocene-Early Oligocene. Samples in the Late Oligocene and through the Miocene show more scatter,

particularly between different core sites, but TEX$_{86}$ values are generally lower than the Mid Eocene. Other than a couple of scattered higher values, TEX$_{86}$ decreases through the Plio-Pleistocene. RI shows considerable site specific variation. Values decrease from the Mid Eocene through to the Mid Oligocene before increasing again in the Late Oligocene, with samples from DSDP 270 showing particularly high RI during this time. RI decreases through the Early to Mid-Miocene before increasing once again in the Early Pliocene. Values then subsequently decrease to the lowest values in the record during the Pleistocene.

5.4.3 SST calibrations

Applying a calibration to absolute temperature in a high latitude setting can be challenging, as outlined in section 5.1.4. Here, the TEX$_{86}$ compilation is converted into temperature using several calibrations designed for use in high latitude settings.

5.4.3.1 TEX$_{86}^{L}$

The TEX$_{86}^{L}$ calibration was developed for use in cold environments, where temperatures of less than 15°C might be expected, and is based on a different ratio of GDGTs to TEX$_{86}$ (section 5.1.4) (Kim et al., 2010). This has been commonly applied in polar settings, and was the calibration method used for the published results from AND-1B (Kim et al., 2010 calibration) and AND-2A (Kim et al., 2012 calibration) (McKay et al., 2012a, Levy et al., 2016). When applied to the Ross Sea compilation it determines relatively warm SSTs for the Mid Eocene ranging from ~9.5°C to 20°C (Figure 5.9). By the Late Eocene, temperatures cool to ~5°C. Temperatures are very variable through the Oligocene and Early Miocene, especially over the Oligocene/Miocene boundary where different sites predict considerably different temperatures. Temperatures predominantly vary in a ~10°C temperature range from -2°C to 8°C through the Mid-Late Miocene. With the exception of a few considerably warmer samples, temperatures in the Plio-Pleistocene indicate a cooling trend. However, a distinctive feature of the TEX$_{86}^{L}$ record is the prediction of numerous unrealistically cold values, including a value of -14.1°C for one sample from DSDP 270.

Kim et al. (2012) adjusted the TEX$_{86}^{L}$ calibration to be more suitable for use offshore Antarctica, where Thaumarcheaota typically live in the subsurface (Section 5.1.2). When the Cenozoic record is reconstructed using this calibration the range of temperatures predicted is reduced in

comparison to Kim et al. (2010), i.e. the warmest values become cooler, and the coolest values become warmer (Figure 5.9). Despite this, unrealistically cold temperatures are still predicted at some sites, mostly in DSDP 270.
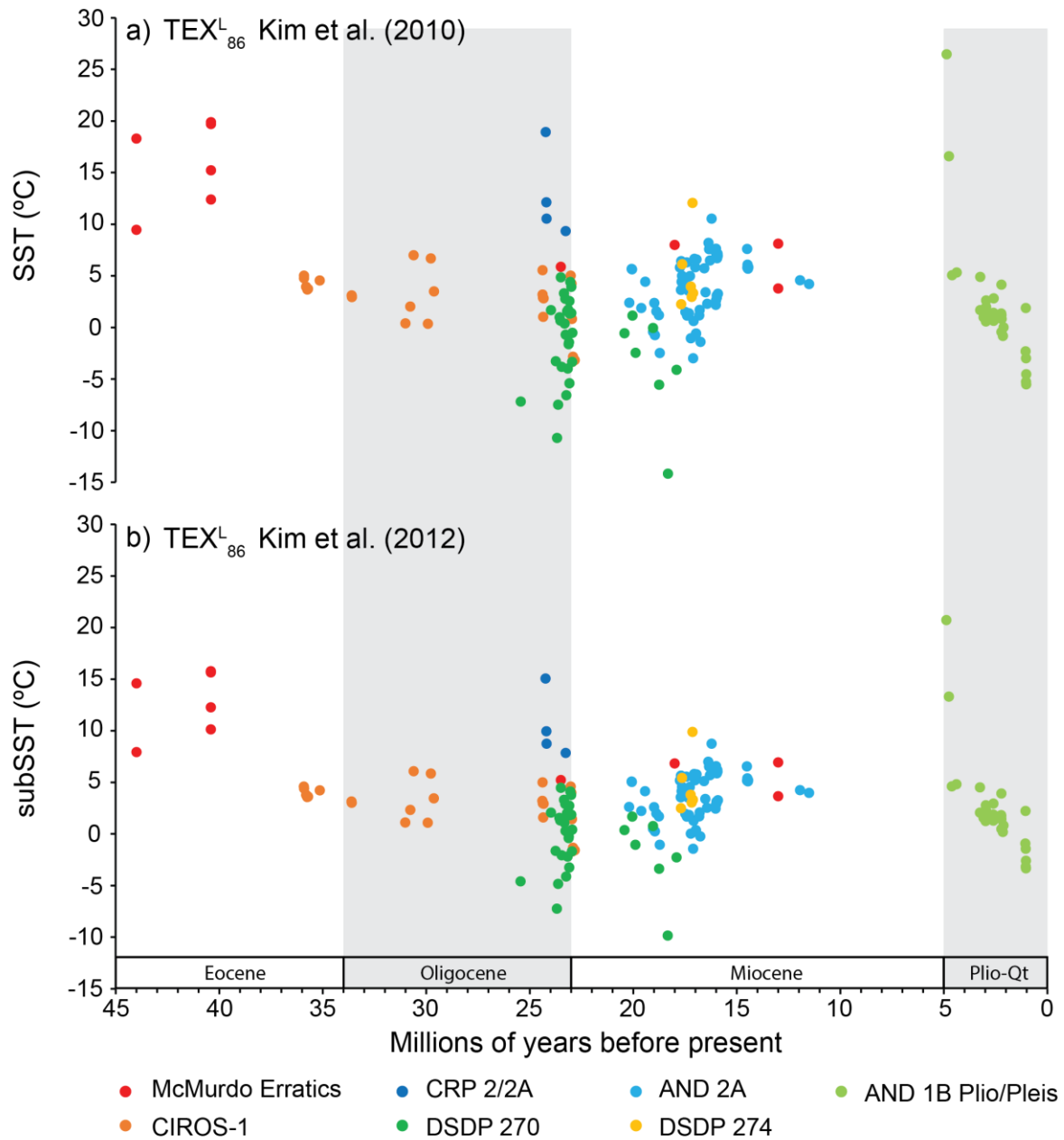
Figure 5.9: TEX_{86}^L temperature calibrations from a) Kim et al. (2010) and b) Kim et al. (2012).

5.4.3.2 Shevenell et al. (2011) calibration

Shevenell et al. (2011) approached the challenges of a high latitude calibration by integrating additional core top data from the Antarctic Peninsula into a global calibration by Kim et al.

(2008) (Section 5.1.4). As this calibration is based on the TEX$_{86}$ index, it derives the same trend as described in section 5.4.2. Predicted temperatures are warmer than the other calibrations, with the exception of BAYSPAR analogue, which predicts similar temperatures (section 5.4.3.3). A range of ~14-22.5°C is determined for Mid-Eocene samples, decreasing to ~10°C during the Late Eocene/Early Oligocene (Figure 5.10). Samples in the Late Oligocene/Early Miocene have a wide range from ~6-18°C, decreasing to ~6-14°C by the Mid-Miocene. Temperatures decrease from ~10-15°C in the Early Pliocene, to ~3-7°C in the Pleistocene.
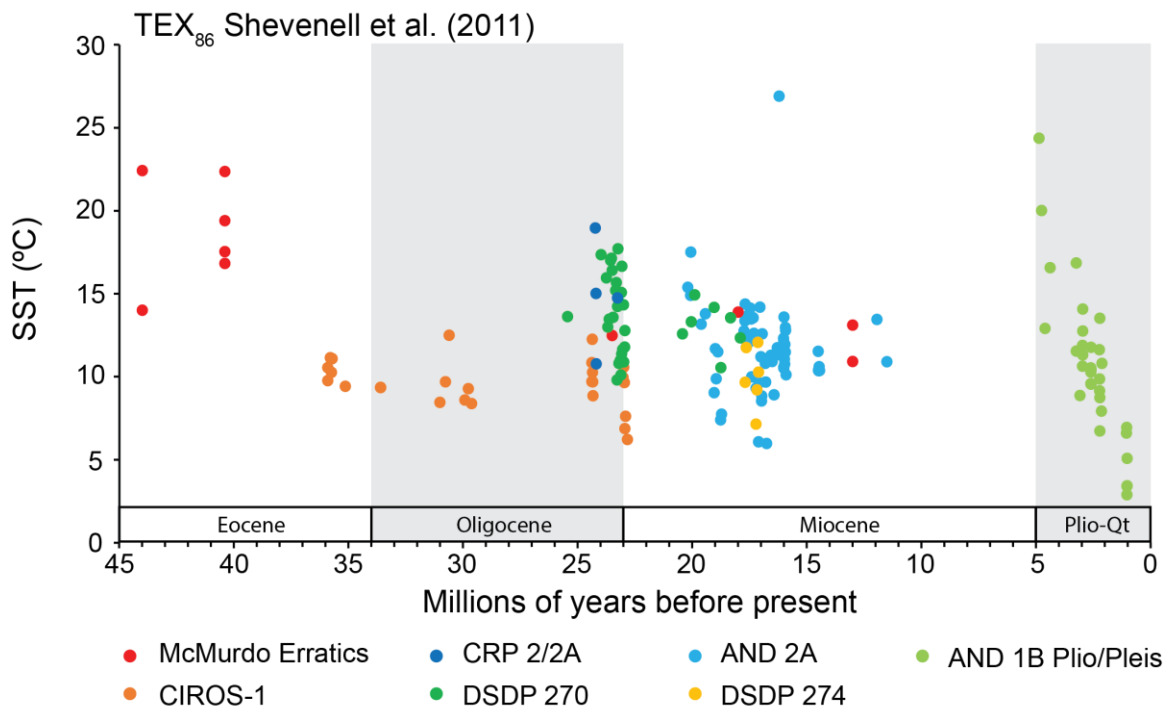
Figure 5.10: SST temperatures using the calibration of Shevenell et al. (2011).

5.4.3.3 BAYSPAR

Tierney and Tingley (2014, 2015) recognised that there is spatial variance in the relationship between TEX$_{86}$ and temperature, and developed the BAYSPAR calibration to take account of this (section 5.1.4). When used in standard mode, BAYSPAR creates a calibration weighted to local TEX$_{86}$-temperature relationships, which makes it an appropriate calibration for high latitude settings. However, BAYSPAR standard assumes that oceanographic conditions are similar to present, an assumption that may not be accurate over the entirety of the Cenozoic record in the Ross Sea region due to the evolution of the climate and tectonic setting, and the noted shifts in glacial meltwater input into the Ross Sea through time (Lewis et al., 2006,

McKay et al., 2009, Chapter 4). If oceanographic conditions are considered substantially different to present day, then BAYSPAR can also be used in analogue mode, where a calibration is created with reference to locations with similar TEX_{86} values in the global data set.
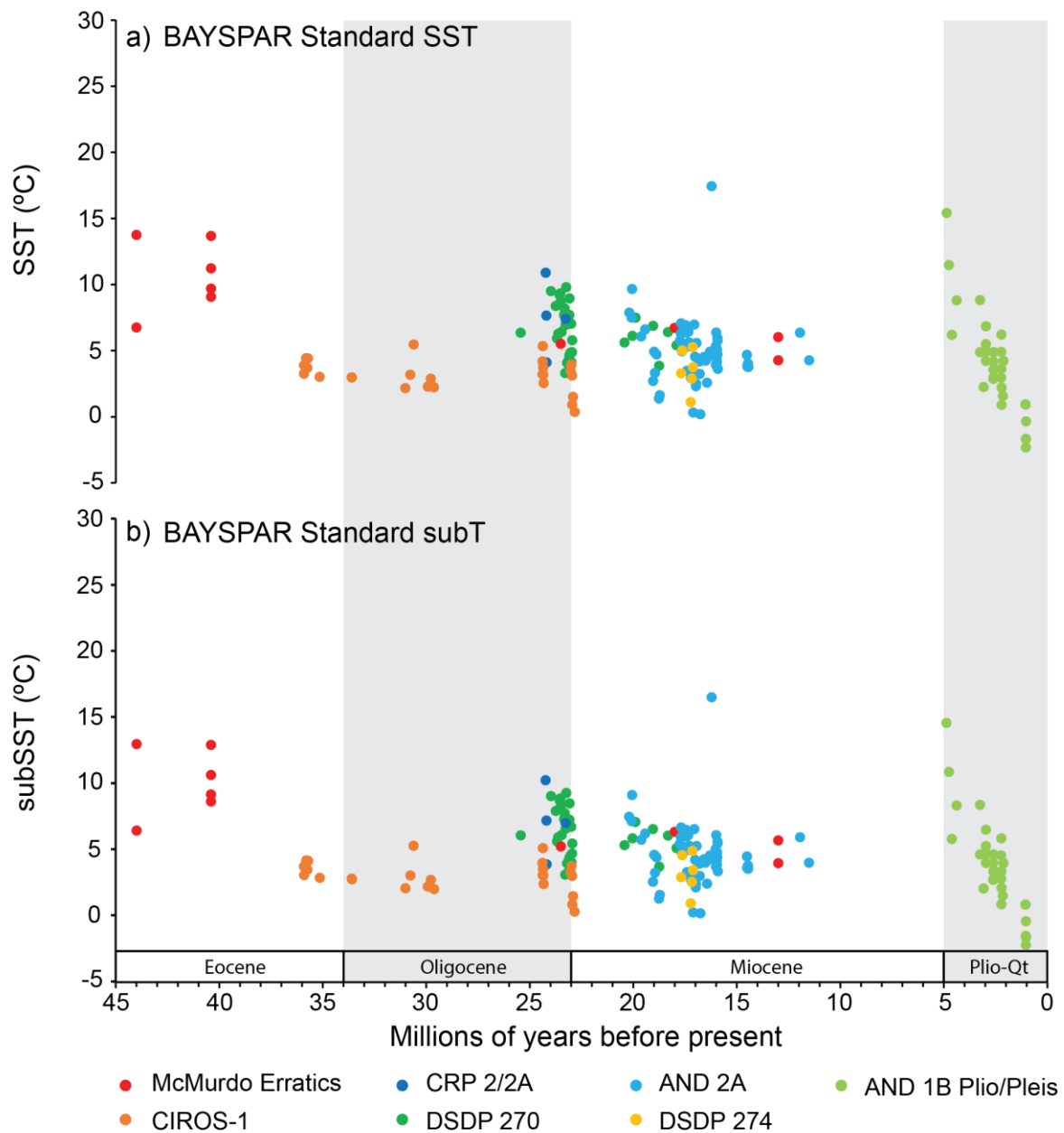
Figure 5.11: BAYSPAR Standard temperatures for a) sea surface and b) subsurface.

Figures 5.11, 5.12 and 5.13 present BAYSPAR in standard mode, in analogue mode, and a combination of the two where analogue mode is used for sites covering the Mid-Eocene to the Earliest Miocene (the Eocene and Oligocene McMurdo erratics, CIROS-1, DSDP 270 and CRP 2/2A), and standard mode is used for younger sites (Miocene erratics, AND-2A, DSDP 274 and AND-1B). This attempts to take into account the shift in oceanographic setting over this time, as the basement highs which separated the Ross Sea into various seaways in the Early Cenozoic are inferred to have permanently submerged by the Early-Mid Miocene (Section 5.1.1)(De Santis et al.,1995, De Santis et al., 1999, Bart and De Santis, 2012). It has also been debated whether TEX$_{86}$ reflects a SST or subsurface signal (section 5.1.4). BAYSPAR takes this in to account by predicting both SSTs and subsurface temperatures. The subsurface calibration used weighted averages for temperatures over 0-200m water depth, weighted towards the shallow subsurface (~50 m) (Tierney and Tingley, 2015). Figures 5.11, 5.12 and 5.13, show predictions for both SST and subsurface temperatures.

As BAYSPAR is derived from the TEX$_{86}$ index, the trend for each calibration is the same as described in section 5.4.2. In standard SST mode, temperatures of ~7-14°C are predicted for the Mid-Eocene, decreasing to ~3-4°C through the Late-Eocene/Oligocene. Late Oligocene to Early Miocene temperatures vary between 0 and 10°C, and between 0 and 7°C for the Mid Miocene. Aside from several warmer temperatures in the Early Pliocene, Pliocene temperatures range from 2.2°C to 8.8°C, cooling to 0.9° to -2.3° in the Mid-Pleistocene. (Figure 5.11). Analogue SST mode predicts temperatures that are on average 5-10°C warmer than standard mode, and are similar to those indicated by the calibration of Shevenell et al. (2011), as both these methods are predominantly based on the global TEX$_{86}$-temperature relationship (Figure 5.12).

Due to the large difference in temperature between standard and analogue mode, splitting the record into analogue mode for samples older than then Earliest Miocene, and standard mode for those younger than the Early Miocene, results in an apparent significant cooling over this time period (Figure 5.13). The difference between SST and subsurface calibrations is minor in standard mode, with subsurface predictions typically less than 0.5°C cooler than SSTs (Figure 5.11). The difference is slightly larger in analogue mode, with subsurface temperatures ~2.5°C cooler (Figure 5.12). 90% confidence intervals using BAYSPAR are large, averaging ±6.3-7.1°C for standard SST mode, ±5.8-6.3°C for standard subsurface mode, ±6.7-8.5°C for

analogue SST mode and 6.7-8.6°C for analogue subsurface mode. In part, this may be due to the scarcity of core tops from this area in the global dataset.
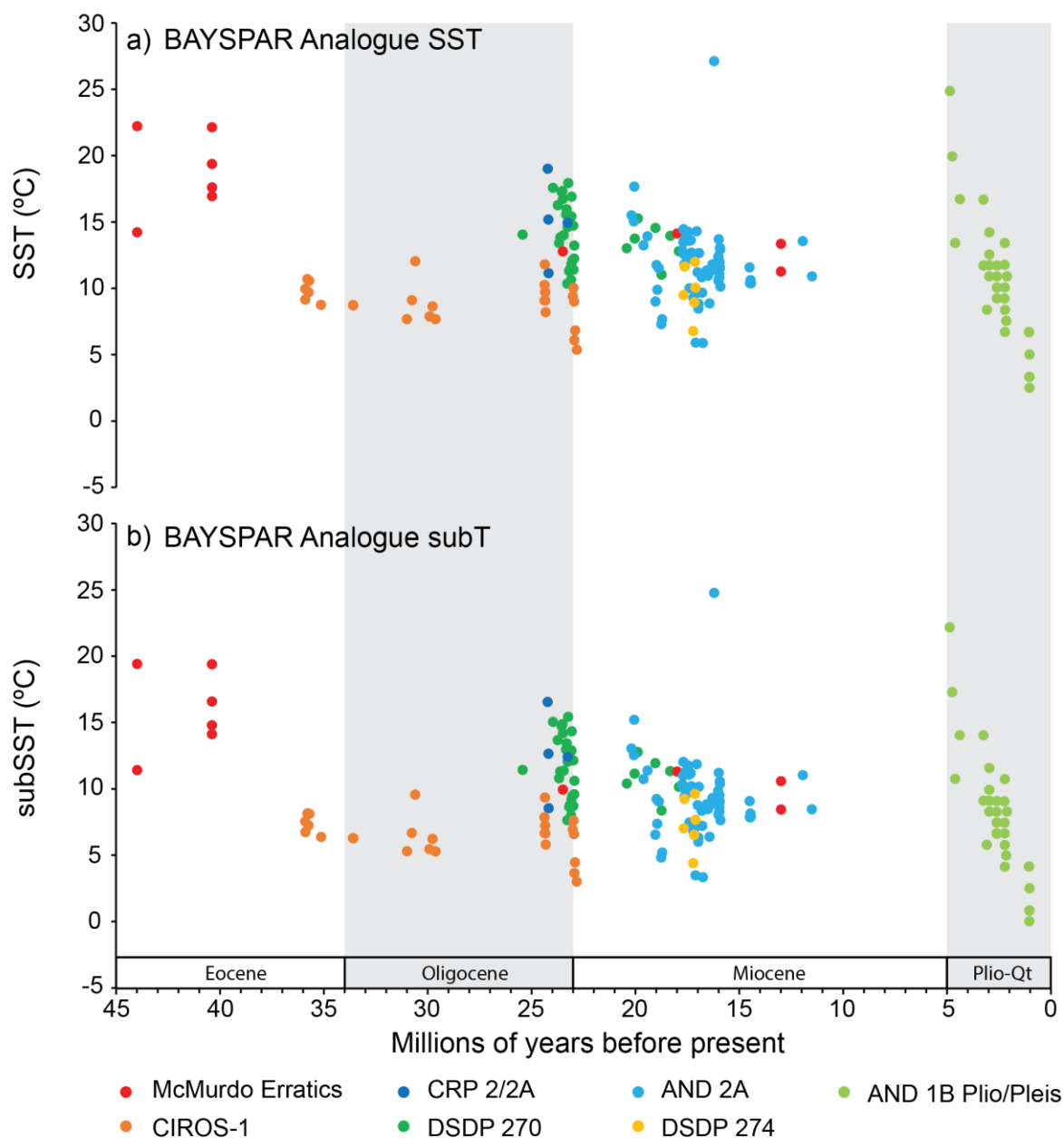
Figure 5.12: BAYSPAR Analogue temperatures for a) sea surface and b) subsurface.
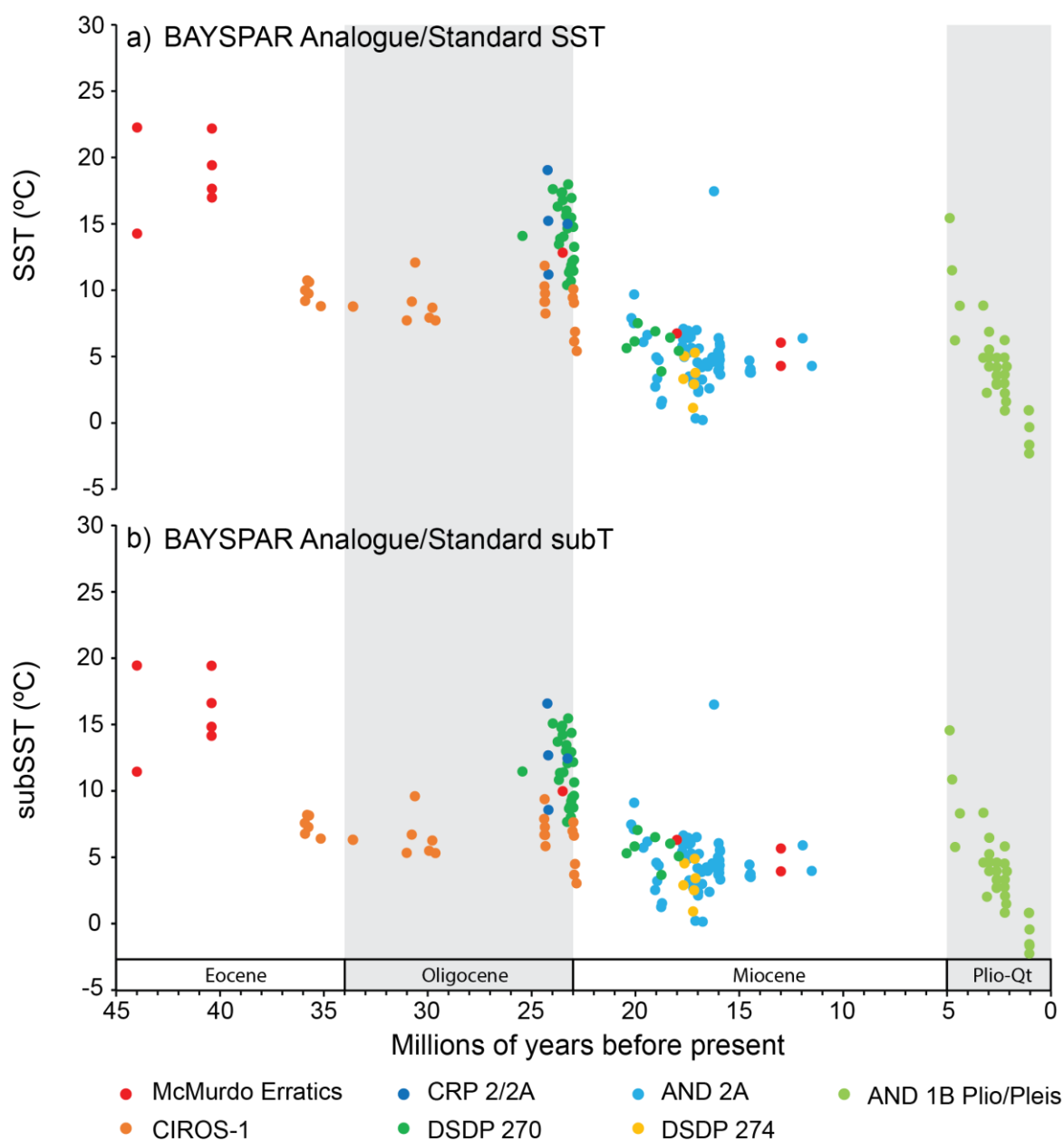
Figure 5.13: BAYSPAR Analogue/Standard temperatures for a) sea surface and b) subsurface, splitting from the analogue to standard calibration in the Early Miocene (see text for details).

5.5 Synthesis

5.5.1 Cenozoic BIT trend
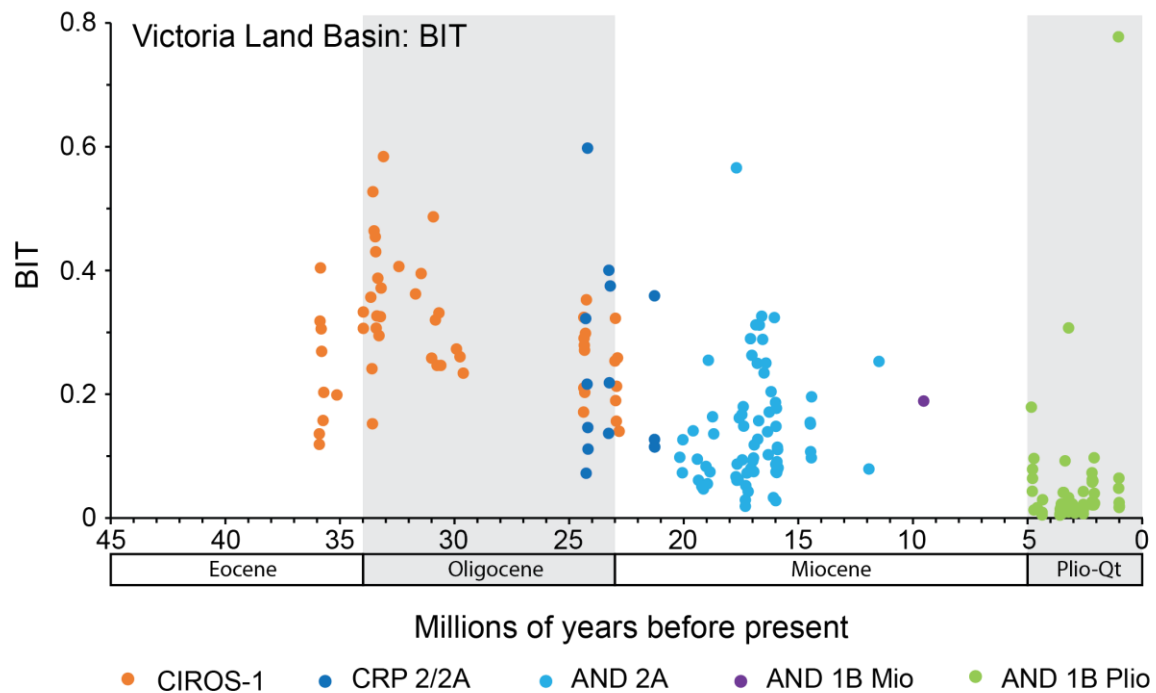
Figure 5.14: BIT values from core sites in the Victoria Land Basin.

Over the course of the Cenozoic, a long-term trend of decreasing BIT values is apparent (Figure 5.4). This trend is especially clear when just the core sites from McMurdo Sound and the Victoria Land basin are compared (Figure 5.14). As well as being proximal to one another, these sites have remained continuously close to land, and the Transantarctic Mountains, over the course of the Cenozoic. The McMurdo erratics are not included in this figure, as their source location is not precisely known (Harwood and Levy, 2000). Decreasing BIT values over the Cenozoic indicate a decrease in the contribution of terrestrially sourced brGDGTs to the core sites. The chemical index of alteration and clay mineralogy on the Cape Roberts Project cores and CIROS-1 indicate a shift from chemical weathering to dominantly physical weathering over the course of the Late Eocene to Miocene, associated with cooling and drying in the region (Krissek and Kyle, 1998, Ehrmann et al., 2005, Passchier and Krissek, 2008). This cold, dry climate with a limited chemical weathering has led to very slow soil development. In some cases, soils at high elevations of the Transantarctic Mountains that have remained dry and without a well-formed saturated active layer since the Mid-Miocene (Lewis et al., 2007). In marine sediments, BIT primarily represents the relative input of fluvially-transported soil

organic matter, as the transport of brGDGTs is not considered to have a strong aeolian component (Schouten et al., 2013). Lower BIT also likely indicates increasingly less active glaciofluvial systems as the region becomes progressively more arid. The decline in BIT over the Cenozoic is therefore interpreted to reflect a shift to a more limited brGDGT source in response to reduced soil development and a decrease in the available ice-free land for soils to form on, coupled with less active glaciofluvial systems to transport the brGDGTs offshore. The MMCO (~17-15 Ma) displays several higher BIT values, suggesting this period of relative warmth also likely resulted in a return to more chemical weathering with greater active soil development on land, and more glacioactive fluvial transport enhancing the supply of brGDGTs to the core site. The lack of samples between the MMCT and the Miocene/Pliocene boundary makes constraining the timing of the shift to increasingly hyper-arid conditions difficult. However, by the Early Pliocene BIT is very low in most samples.

5.5.2 Cenozoic ΔRI, MI and %GDGT-0 trend

As outlined in section 5.4.1, a trend from more positive to more negative ΔRI emerges over the Cenozoic. Scatter plots indicate correlations between GDGT-0 and MI with ΔRI (Figure 5.7). A larger relative abundance of GDGT-0, resulting in a positive ΔRI deviation, could indicate a larger contribution from Euryarchaeota to the GDGT distribution in seafloor sediment, as these archaea predominantly synthesise GDGT-0 (e.g. Pancost et al., 2001, Blaga et al., 2009, Sinninghe Damsté et al., 2012, Inglis et al., 2015). The trend towards positive ΔRI values in the earlier Cenozoic may indicate the methanogenic Euryarchaeota formed a greater proportion of the archaeal community in the Ross Sea region during this time. Similarly, the trend in MI may also indicate a larger contribution from methanotrophic archaea during the early to mid Cenozoic. This is supported by higher MI values during this time, which steadily decline over the course of the Cenozoic (Figure 5.4). Both methanogenic and methanotrophic archaea thrive in anoxic water and sediment (Valentine, 2002). These conditions can develop along continental margins or in stratified, restricted basins with a high export of organic matter (Demaison and Moore, 1980). The Paleogene Ross Sea is thought to have consisted of several basins and seaways (Figure 5.1), an arrangement which may have favoured the development of sub-oxic or anoxic ocean floor conditions, particularly if a more active hydrological cycle in a warmer environment resulted in high input of nutrients, encouraging surface ocean productivity. As climate cooled and rifting induced subsidence continued through the Cenozoic, the Ross Sea became less restricted, and stronger bottom water currents developed

alongside decreasing terrestrial input (sections 5.1 and 5.3 and Chapter 4). This would likely have resulted in a more oxygenated seafloor, unfavourable conditions for methanogenic and methanotrophic archaea. The negative ΔRI values in the younger portion of the record indicate that GDGT-0 is relatively less abundant than would be predicted from the modern TEX_{86}-RI relationship. Interestingly, unlike MI, %GDGT-0 does not show a strong long-term Cenozoic trend. This is likely due to %GDGT-0 reflecting both a thermal signal as well as a contribution of Euryarchaeota, i.e. %GDGT-0 also increases with decreasing water temperature.

In the modern ocean, high latitude distributions of TEX_{86} are offset from the global relationship between TEX_{86} and temperature (i.e. Kim et al., 2008, Kim et al., 2010). Both positive and negative deviations in ΔRI over the Cenozoic indicate that high latitude GDGT distributions have also been offset from the global TEX_{86}-RI relationship during this time. The long-term trend from more positive to more negative ΔRI deviations through the Cenozoic could reflect a shift in archaeal community composition and/or a change in the relationship between TEX_{86} and temperature in the Ross Sea. It is also worth noting that oxygen content can have a strong impact on TEX_{86}, with apparent TEX_{86} derived temperatures increasing with O_2 limitation (Qin et al., 2015). A potential shift in Ross Sea oxygenation suggested by MI could therefore also impact TEX_{86} temperatures.

5.5.3 Cenozoic temperature compilation

Section 5.4.3 outlined the various applicable GDGT calibrations to absolute temperature, based on TEX_{86} and TEX_{86}^{L}. To assess which calibration is the most appropriate to apply to the Cenozoic in the Ross Sea, the validity of numerous assumptions have to be assessed, namely whether the temperatures predicted are reasonable in the context of other environmental evidence from the core sites.

Independent estimates of temperature for comparison with GDGT estimates are rare at high latitudes due to poor species diversity, sparse distribution or poor preservation. This has required the use of other evidence to inform whether a GDGT temperature reconstruction is reasonable, such as the presence or absence of grounded marine-based ice sheets or microfossils found in sea-ice. However, in the Middle Eocene however, independent assessments of SSTs at relatively high latitudes do exist, using the $U^{K'}_{37}$ index from alkenones and the $\delta^{18}O$ of planktic foraminifera (Burgess et al., 2008, Liu et al., 2009). These estimates

suggest temperatures in the region of ~16-25°C (Burgess et al., 2008, Liu et al., 2009). BAYSPAR analogue (SST mode) and the calibration of Shevenell et al. (2011) align with these estimations, although the McMurdo erratics were eroded from strata located in a more southerly latitude than the sites sampled by Burgess et al. (2008) and Liu et al. (2009). It is therefore suggested that temperatures predicted by these calibrations may be too warm, with all other calibrations suggesting slightly cooler temperatures.

To determine the most reasonable calibration in the younger portion of the record, the temperatures have been compared to the Pliocene record of ANDRILL 1B, where the stratigraphy and diatom assemblages both indicate the frequent presence of grounded marine ice sheets, ice shelves and/or sea-ice cover in the vicinity of the core site (Naish et al., 2009, McKay et al., 2012a). Diatom assemblages vary from 'subantarctic', to 'polar- open ocean to sea-ice tolerant' to 'sea ice' species, and as such expected temperatures would range between ~8 to -1.5°C (McKay et al., 2012a). BAYSPAR analogue (SST mode) and the calibration of Shevenell et al. (2011) predict temperatures through this period ranging as high as ~20°C. Temperatures in BAYSPAR analogue (subsurface mode) are also too warm through this period, suggesting ~10-15°C (Figure 5.12). The calibrations which best fit for the Pliocene are therefore the TEX_{86}^L calibrations of both Kim et al. 2010 and Kim et al. 2012, and BAYSPAR in standard mode.

A further consideration to take into account is the changing tectonic setting over this time period. Using BAYSPAR in standard mode requires the assumption that the oceanographic conditions in the past were similar to present day, which in the Ross Sea region is almost certainly not the case during the course of the Cenozoic (Section 5.1.1). Section 5.5.2 has also outlined what appears to be a shift in the archaeal community and/or the GDGT-temperature relationship over the Cenozoic, which may be related to changes in both climate and oceanographic setting. In an attempt to demonstrate the sensitivity of this calibration to this assumption, I split the older portion of the record into analogue mode, and the younger portion into standard mode at the Earliest Miocene, resulting in a large jump in temperature. In the absence of other independent water mass indicators, this is a somewhat arbitrary approach. As such, a case could be made to assign the split to later climatic events such as the MMCT when stratigraphic and geomorphic evidence from the Tranantarctic Mountains indicates the onset of increasingly hyperarid conditions and reduced meltwater input to the Ross Sea (Lewis et al., 2006), or during the Pliocene when marine based ice sheets transitioned to a polar glacial

regime and ice shelves developed (McKay et al., 2009). As discussed above, even in the Eocene analogue mode likely predicts temperatures which are too warm. Given the current state of knowledge, it is therefore considered most appropriate for the same calibration to be applied over the course of the record, despite the changes in environmental setting complicating the archaeal-temperature relationships.

Modern archaea around Antarctica are most abundant in the subsurface, at ~100m water depth (section 5.1.2). While their depth relationship as far back as the Eocene is uncertain, recent analysis from Ho and Laepple (2016) does suggest a subsurface source for archaea in the Eocene is also reasonable. With this in mind, preference is given to the two calibrations which take this into account; BAYSPAR subsurface (standard mode) and the TEX_{86}^L adjustment of Kim et al. (2012). Both these calibrations are compared to the Cenozoic compilations of deep sea benthic oxygen isotopes and atmospheric CO_2 concentration, alongside the ring index for a further relative measure of temperature change (Figure 5.15).

Both absolute calibrations of BAYSPAR standard subT and the TEX_{86}^L adjustment of Kim et al. (2012) provide relatively reasonable temperature estimates for a high latitude polar environment over the course of the record, as constrained by the Pacific ocean benthic $\delta^{18}O$ stack of Cramer et al. (2009) (Figure 5.15). The single basin Pacific stack is used as the deep Pacific is fed by bottom water formation in the Ross Sea, and Cramer et al. (2009, 2011) show that the $\delta^{18}O$ of the deep ocean basins becomes heterogeneous from the Oligocene and younger. The spatial and temporal distribution of global data set is considered too sporadic for a meaningful global average over these heterogeneous basins, with the Pacific therefore suggested as the most representative of a true deep water signal (Cramer et al., 2011). Both BAYSPAR and TEX_{86}^L calibrations display a cooling from the Mid Eocene towards the E/O boundary glaciation event, a trend mirrored in the deep sea $\delta^{18}O$ record. In fact, temperature estimates from CIROS-1 indicate cool temperatures of ~3.6-4.6°C (TEX_{86}^L Kim et al. 2012) or 3.2-4.4°C (BAYSPAR) were already present up to 2 million years prior to the E/O glaciation at this core site, with temperatures during the glacial event not markedly colder (~3°C from both calibrations). An increase in high latitude radiolarian fauna ~3 Ma prior to the E/O glacial, during the Priabonian Oxygen Isotope Maximum, is also seen at high latitude site DSDP 277 on the Campbell Plateau and interpreted as related to an expansion of the cold water Ross Gyre (Pascher et al., 2015). Temperatures remain relatively uniform through most of the Oligocene

despite a decrease in atmospheric CO_2. However, a large disparity in temperatures both between sites and calibrations becomes apparent in the Late Oligocene during the lead up to the Mi-1 event at the Oligocene/Miocene boundary, especially in the TEX_{86}^L record. For example, CIROS-1 displays warmer temperatures than DSDP 270 using TEX_{86}^L, but cooler temperatures from BAYSPAR, a discrepancy discussed further below.

Temperatures from TEX_{86}^L show steady warming through the Early to Mid Miocene and into the MMCO, similar to that displayed in the benthic $\delta^{18}O$ record (Figure 5.15). This warming is not so apparent in the BAYSPAR reconstruction, although temperatures are less scattered during the MMCO than the Early Miocene - i.e. while maximum temperatures are not as warm in the MMCO, minimum temperatures are not as cold. Therefore, while TEX_{86}^L supports the MMCO as a period of ocean warmth around Antarctica compared to the Early Miocene, BAYSPAR suggests that temperatures in general were more moderate, and not as variable as observed during the Early Miocene. Regardless, temperatures during the MMCO appear significantly warmer than present, varying between ~2.4 to 6°C using BAYSPAR and between 2.3 to 10.6°C using TEX_{86}^L. BAYSPAR values are comparable to SST model estimates of You et al. (2009) of ~0 to 5°C for high southern latitudes. Similarly, the anomaly from present is comparable (to slightly higher) than the ~4-5°C indicated by Shevenell et al (2004) using planktic foraminifera Mg/Ca on two subantarctic core sites (situated at ~55°S in the MMCO). These studies suggest that temperatures of >10°C, as predicted by TEX_{86}^L, are probably too warm. Unfortunately values during and following the MMCT are too sparse for trends to be determined. Despite a couple of outliers, both calibrations show a clear trend to cooler temperatures over the Plio-Pleistocene, coincident with decreasing CO_2, cooler global bottom water temperatures and increased ice-volume with the initiation of Northern Hemisphere Ice Sheets (e.g. Sosdian and Rosenthal, 2009, Bartoli et al., 2011, McKay et al., 2012a).

a) Ring Index

b) BAYSPAR Standard subT

c) TEX$^L_{86}$ Kim et al. (2012)

e) Ice Volume + Deep Sea Temperature

warmer/less ice ↑

cooler/more ice ↓

d) Atmospheric CO_2 Concentration

Legend:
- McMurdo Erratics
- CIROS-1
- CRP 2/2A
- DSDP 270
- AND 2A
- DSDP 274
- AND 1B Plio/Pleis

- Phytoplankton
- Stomata
- Boron
- Paleosols

RI: 2.6, 2.4, 2.2, 2, 1.8, 1.6, 1.4

SubT (°C): 20, 15, 10, 5, 0, -5

SubT (°C): 25, 20, 15, 10, 5, 0, -5, -10

Benthic δ^{18}O (‰): 0, 1, 2, 3

CO^2 (ppm): 2000, 1000, 500, 200

MMCO, MMCT, NHG, E/O, O/M

Eocene, Oligocene, Miocene, Plio-Qt

40, 30, 20, 10, 0

Millions of years before present

192

Figure 5.15: Summary of Ross Sea GDGT-based temperature proxies over the Cenozoic; a) Ring Index, b) sub surface temperatures from BAYSPAR standard, c) subsurface temperatures from the TEX_{86}^L calibration of Kim et al. (2012), d) atmospheric CO_2 concentrations based off Beerling and Royer (2011) and e) the deep-sea benthic foraminiferal $\delta^{18}O$ record from Cramer et al. (2009). Shaded bars indicate significant climate events; E/O= Eocene/Oligocene boundary, O/M= Oligocene/Miocene boundary, MMCO= Mid-Miocene Climate Optimum, MMCT= Mid-Miocene Climate Transition, NHG= Northern Hemisphere glaciation.

The RI appears to vary much more significantly between localities, potentially due to the combined impact of site specific archaeal community distributions and temperature on GDGT-0. This means that RI is likely not a good indicator of long-term temperature change over the Cenozoic, but may still be an appropriate temperature indicator for individual sites. For example, the RI declines from the Late Eocene into the Oligocene in CIROS-1, before increasing again in the Late Oligocene, mirroring the cooling to warming trend displayed by benthic $\delta^{18}O$ (Figure 5.15). RI values at DSDP 270 show a decreasing trend towards low values over the Oligocene/Miocene transition, potentially reflecting significant cooling into the Mi-1 glaciation (Chapter 4). However, as mentioned in Chapter 4, subsidence in the region means the depositional environment of DSDP 270 is deepening over this time, complicating interpretations. Taylor et al. (2013) showed that the ratio of GDGT-2 to GDGT-3 typically increased with depth, with deeper water settings (>1000 m) displaying a GDGT-2/GDGT-3 value in excess of 5. In DSDP 270, GDGT-2/GDGT-3 is lower in the deeper Early Miocene sediments than the shallower Late Oligocene section, suggesting depth is not a dominant impact on this ratio at this site. Potentially this shift in environment could also have resulted in a shift in archaeal community, a factor which could impact RI values. RI decreases over the Early to Mid-Miocene in ANDRILL 2A, in contrast to apparent warming displayed in benthic $\delta^{18}O$, suggesting that trends in RI at this core site may be reflecting site specific shifts in the ocean thermal regime and/or archaeal-temperature relationship. ANDRILL 1B shows declining RI over the Plio-Pleistocene, aligning with the cooling displayed in the benthic $\delta^{18}O$ over this time.

There are numerous caveats to this compilation approach in the Ross Sea, as a long term record from multiple sites could lead to site specific biases, including those regarding RI discussed above. In particular, depositional environments can vary greatly between sites, and within an individual record. Most of the sample localities were deposited in glaciomarine settings, where

marine conditions vary from ice-proximal to open water, with variable sea ice, melt water inputs and associated changes in water column stratification (i.e. Hambrey et al., 1989, Naish et al., 2001a, McKay et al., 2012a, Levy et al., 2016). These factors could influence the GDGT distributions as there may be variation in archaeal communities and depth of GDGT export between different environments. Furthermore, while this chapter focuses on long-term Cenozoic trends, superimposed on these trends are regular glacial/interglacial cycles. As samples have been taken from sediments representing both glacials and interglacials, this could account for the wide range of temperatures displayed through the record. Temperature variations through an individual cycle may also not necessarily follow a simple pattern of coldest at peak glacial and warmest at peak interglacial either. For example, McKay et al. (2012a) suggests that in the Pliocene record of ANDRILL 1B, temperatures in sediments representing the deglacial sequence are occasionally warmer than at the height of an interglacial. This is attributed to enhanced stratification warming the upper water column, the result of increased glacial meltwater input during a marine ice sheet collapse event, and increased seasonal melt of coastal sea ice (McKay et al., 2012a).

A large discrepancy between core sites occurs over the Late Oligocene/Early Miocene (Figure 5.15). In particular, cooler temperatures at DSDP 270 compared to CIROS-1 are predicted by the TEX_{86}^{L} adjustment of Kim et al. (2012), but BAYSPAR suggests the opposite. A large difference is also apparent in RI between the core sites, especially in the Late Oligocene. CIROS-1 and DSDP 270 were deposited in the Victoria Land Basin and Eastern Basin, respectively, which in the Late Oligocene/Early Miocene were likely isolated seaways separated by variable subaerial basement highs (Figure 5.1). These discrepancies imply that archaeal communities or GDGT-temperature relationships were not consistent throughout the region, and depending on which calibration or GDGT ratio is used the apparent trends between sites will differ. This further highlights some of the complications involved in compiling a long-term record from different core sites across a region which has seen significant changes to the oceanographic and tectonic setting.

Other biomarkers in the Ross Sea region display a variable contribution from reworked material, particularly in more ice-proximal depositional environments (Chapter 3). As outlined in Chapter 3, it is unlikely that GDGTs have been reworked from pre-Cenozoic sedimentary rocks in the region, but it is possible that GDGTs from earlier Cenozoic rift-fill sediments could be incorporated into younger material. This could potentially explain some of the large ΔRI

deviations, as the GDGT distribution could be reflecting a mixed source (i.e. derived from both contemporaneous and reworked material). Reworking may also account for occasional samples which display a markedly different temperature than adjacent samples. For example, two samples in the Early Pliocene of ANDRILL 1B, and a sample from 16.22 Ma in ANDRILL 2A (which exhibits a TEX_{86} of 0.64, when other close samples are typified by values of ~0.42 to 0.46) (Figure 5.15).

With these caveats in mind, an ideal sampling strategy for a long-term Ross Sea temperature record would aim to be restricted to a minimal number of sites within the same depositional basin, sampling where possible from ice-distal facies at a similar stage in each glacial/interglacial cycle. Potential for reworked input could also be minimised by focusing on sites where other biomarkers or micro- and macrofossils indicate limited reworking has occurred. This study primarily consists of sites within McMurdo Sound, simply as this is where the majority of drilling in the region has taken place. However many of these sites represent ice-proximal regimes with significant shifts in the environment of deposition over glacial/interglacial timescales, often also associated with large levels of reworking (i.e. see discussion of CRP 2/2A in Chapter 3). In this compilation, DSDP 270 in the Eastern Basin provides a good example of many of the more ideal features, as facies analysis indicates that it is relatively continuously deposited, usually in an ice-distal setting with no clear evidence for ice sheet over-riding, and other biomarkers and microfossils indicate limited contribution from recycled material (Chapter 3 and 4).

5.6 Conclusion

Isoprenoid GDGTs provide a means of reconstructing long-term ocean temperature records in the Ross Sea Region, where other methods of deriving ocean temperatures are either not possible or challenging to apply. Calibrating GDGT ratios to temperature in a high latitude setting can be difficult, as high latitude GDGT distributions are offset from the global relationship, and abundances of key GDGTs are frequently very low. Comparing calibrations designed for use at high latitude sites to other proxy indicators of climate, coupled with a preferred subsurface depth range for modern archaea in this region, indicates that the TEX_{86}^{L} calibrations of Kim et al. (2012) and BAYSPAR in standard subT mode derive the most appropriate temperatures. Despite slight differences in trends between calibrations, ocean temperatures appear to have cooled prior to the E/O transition and remained relatively cool

through the Cenozoic, with the exception of short periods of relative warmth, or at least warmer minimum temperatures, during the Late Oligocene and MMCO. The Ross Sea further cooled over the Plio-Pleistocene, with temperatures of 0 to -3°C by the mid-Pleistocene, comparable to present. RI appears to be strongly influenced by site-specific differences in archaeal communities and/or archaea-temperature relationships and is thus suboptimal for a long-term record of trends, but still potentially appropriate for identifying trends within an individual site. Changes in these parameters may also be responsible for a shift in ΔRI from more positive to more negative deviations over the Cenozoic. This is supported by a decline in MI over the Cenozoic, a trend that may be related to a shift to a more oxygenated seafloor as the Ross Sea deepened and bottom currents became more active. A change in climate is also exhibited in the decline in the BIT index over the Cenozoic, reflecting a decrease in the transfer of soil derived brGDGTs offshore, likely reflecting a change to less active glaciofluvial system, coupled with limited soil development on less ice-free land. A lack of data over the MMCT makes the timing of this shift to hyper arid conditions difficult to constrain, but certainly BIT is almost constantly low by the start of the Pliocene. This study highlights some of the considerations and challenges in developing long-term ocean temperature records in a setting which has undergone significant changes in climate, oceanography and tectonics.

Chapter 6: Synthesis

The Cenozoic Era in Antarctica has been marked by the transition from a warm, ice free continent with diverse vegetation to the permanent ice sheets and sparse macroflora of present. Biomarkers can provide important environmental proxy data in a region where other methods can be unsuitable due to low species diversity, sparse distribution and poor preservation. This study has applied to apply biomarker-based proxies to reconstruct environmental conditions in Antarctica during the Cenozoic, to further our understanding of the climatic drivers of major transitions in the Antarctic ice sheets. This study addressed two research questions:

Research Question 1: How do biomarkers vary across a range of sedimentary facies and ages in Antarctic sediments?

Biomarker-based climate proxies are often founded on relatively novel techniques, and as such have had limited application in Antarctic sediments. These methods have the potential to be extensively used in this region, where other approaches are challenging or unsuitable. However, much of the Antarctic Cenozoic record consists of widely varying lithologies deposited in rapidly changing settings. Previous sedimentological and micro-fossil studies have indicated that reworking of older material is a significant issue in Antarctic sediments, highlighting the need for biomarkers to also be investigated in this context.

Chapter 3 assessed the distribution and abundances of *n*-alkanes between a range of depositional settings in Oligocene and Miocene aged sediments. A terrestrial locality (Mt Boreas), two glaciomarine cores (CRP-2/2A and DSDP 270) and an ice-distal deep marine core (DSDP 274) were evaluated using several different parameters; the carbon preference index, average chain length, the ratio of n-C_{29}/n-C_{27} and the total abundance of *n*-alkanes. *n*-Alkanes are near ubiquitous at these sites, and represent a mix of autochthonous and allochthonous inputs. Key sources for *n*-alkanes are from contemporaneous material, as well as reworked early Cenozoic and pre Cenozoic sediments. To establish what a reworked signal may look like, Eocene aged glacial erratics were also analysed, and comparisons were made with published data from pre Cenozoic sedimentary rocks of the Beacon Super Group.

Sites sampling the Late Eocene and Early Oligocene document a shift in dominant chain length from n-C_{29} to n-C_{27}. This is considered a response to a significant climate cooling between these time periods, resulting in a shift in plant community composition as well as climate-driven plastic response of *n*-alkanes to temperature. In Oligocene and Miocene samples, a

variable contribution from both contemporary and reworked sources is displayed. Samples primarily containing contemporary material exhibit high CPIs, and low ACLs and n-C_{29}/n-C_{27} values, supplied by the sparse tundra vegetating Antarctica during this time. Reworked samples are characterised by low CPI, and high ACL and n-C_{29}/n-C_{27}, likely due to a mixed contribution of earlier Cenozoic material, as well as input from the Beacon Supergroup which has varying levels of thermal alteration.

Importantly, this chapter highlighted that particular environments of deposition are more disposed to containing either a reworked or contemporary n-alkane distribution. Reworked n-alkanes are more likely to be deposited in glaciofluvial environments onshore, and subglacial and ice-proximal environments offshore, due to the more erosive processes inherent in these settings. Lacustrine environments onshore, and ice-distal environments offshore, are more likely to reflect contemporary n-alkane input. These findings emphasise the need for caution when applying and interpreting n-alkane-based proxies in glacially influenced settings, with implications for the application of other biomarker-based proxies. Ideally an integrated sedimentological, paleontological and geochemical approach should be present to ensure that contemporary rather than reworked biomarkers are being evaluated in paleoclimate studies.

Research Question 2: What can biomarkers tell us about climate conditions during key periods in the development of the Antarctic ice sheets?

Chapters 4 and 5 address this research question, by focusing on a large glacial event (Chapter 4) and a long-term Cenozoic compilation record (Chapter 5).

In Chapter 3, DSDP 270 is identified as containing a predominantly contemporary n-alkane distribution, indicating that this site is appropriate for detailed paleoclimate investigation. DSDP 270 contains a relatively continuous record of the Late Oligocene warmth through to the Mi-1 glaciation, and following a disconformity, a sequence of Early Miocene sediments. The Mi-1 event is one of the largest transient glaciations of the Cenozoic, and as such is a key time period for investigating climate thresholds and ice sheet sensitivity in a warmer, higher CO_2 world. DSDP 270 is situated in the central Ross Sea, a major drainage area for the WAIS, and a region considered sensitive to climate forcings. This chapter applies a range of proxies based on n-alkanes, GDGTs and palynomorphs, to reconstruct vegetation, climate, glacial and marine conditions in the Ross Sea during the Late Oligocene to Early Miocene.

The Late Oligocene is marked by relatively warm and stable conditions, in a Ross Sea embayment which likely contained several subaerial basement highs separated by seaways. Subsurface sea temperatures were warmer during this time period than the rest of the drillcore, averaging ~7.2°C, while onshore mean summer temperatures average ~10.3°C. Vegetation was a low diversity tundra, but more enriched n-alkane $\delta^{13}C$ values suggest potentially some tree-like growth forms were present, a growing season that was not too restricted, and likely a contribution from both high- and low-altitude plants. Regional cooling then initiated the transition towards Mi-1, thought to be driven by a combination of orbital parameters favouring low seasonality and cool summers, with an uncertain contribution from atmospheric CO_2. A cooling and deepening Ross Sea may also have driven an intensification in proto-Antarctic bottom water production.

Mi-1 manifested in the Ross Sea as a regionally cool period both onshore and offshore. A significant negative n-alkane $\delta^{13}C$ excursion is interpreted as a vegetation response to cold, restricted growing seasons, with plants driven to lower altitudes and more stunted growth forms. Mosses and spore-producing plants expanded relative to shrubby trees such as *Nothofagus*. However, the sedimentology of the core shows grounding line distal sediments, indicating that ice did not over-ride the core site. This is likely due a near field sea-level rise (~100m) caused by instantaneous gravitational field influences, and ocean temperatures still being too warm for a marine-based ice sheet to ground in the deeper basins of the Ross Sea continental shelf, a hypothesis that is supported by the temperature estimates presented in this thesis. Instead, some of the large ice volume associated with this event in global benthic $\delta^{18}O$ records was probably held on a higher, more extensive terrestrial West Antarctica. It is likely there was marine based ice in the shallower parts of the continental shelf, as the relative lack of ice rafted debris and reduced LMW n-alkanes from marine algae are consistent with the presence of large-fringing ice shelf whose basal layers are free of sediment – as is the case with the modern Ross Ice Shelf.

The Early Miocene in DSDP 270 displays a warming relative to the Mi-1 glaciation interval, but exhibits a baseline change towards a cooler climate relative to the Late Oligocene. Sediments are characterised by periods of either ice proximity or increased iceberg discharge from outlet glaciers into the Ross Sea in the absence of the ice shelves that were proposed to have been present during the Mi-1 glaciation. This interval was on average 1.4°C cooler than the late Oligocene. Polar benthic foraminiferal assemblages and a tundra vegetation comparable to other Miocene localities from the Ross Sea region indicate a period of

increasingly polar conditions in the Ross Sea embayment. This chapter described the climate drivers and response of the Ross Sea region to the large, transient Mi-1 glaciation, and highlights the effectiveness of integrating biomarkers with sedimentology and micropaleontology in an Antarctic record.

Ocean temperatures around Antarctica have proved challenging to reconstruct, as approaches based on microfossil assemblages are difficult to apply in deep time due to a lack of extant species and modern analogues, while the geochemistry of foraminifera are unsuitable in this region due to sporadic carbonate preservation. Isoprenoid GDGTs sourced from marine archaea can therefore provide a method of reconstructing polar ocean temperatures, which are important for understanding past ice sheet volume and extent, and the magnitude of polar amplification. Chapter 5 used GDGTs to compile a long-term Cenozoic record of ocean temperatures in the Ross Sea.

Calibrating GDGT distributions to temperatures at high latitudes can be challenging as the polar ocean displays a different relationship between GDGT ratios and temperature than the rest of the global ocean. This chapter assesses numerous ways in which different studies have tried to combat this issue. Comparing calibration results to other proxy indicators of high latitude climate, coupled with the modern distribution of archaea around Antarctica skewed to the subsurface, suggests that the TEX_{86}^{L} calibrations of Kim et al. (2012) and BAYSPAR TEX_{86} in standard subT mode predict the most appropriate temperatures for the Ross Sea. While trends differ slightly between calibrations, ocean temperatures cool prior to the E/O transition, and with the exception of short periods of relative warmth in the Late Oligocene and MMCO, remain cool for the rest of the Cenozoic.

This chapter also investigated how several other GDGT ratios can provide environmental information. While RI should relate to temperature, in the Ross Sea this ratio appears strongly site specific, making it a suboptimal proxy for a long-term compilation record. This is likely due to variable archaea communities between sites which strongly impact the abundance of GDGT-0, a compound not included in TEX_{86} and TEX_{86}^{L}. At individual sites, RI may describe valid temperature trends. ΔRI can be used to indicate a non-thermal influence on the GDGT distribution within a sample. In the Ross Sea, a shift from more positive to more negative ΔRI deviations occurs over the Cenozoic. This is correlated strongly with %GDGT-0, and also relates to a long-term decreasing trend in MI. These changes suggest that in the earlier Cenozoic, methanogenic and methanotrophic archaea contributed to the archaea community.

As both these groups thrive in anoxic water masses and sediments, it is suggested that the oceanographic setting of seaways and basins separated by basement highs may have resulted in conditions favouring the development of an anoxic or sub-oxic sea floor. As the Ross Sea subsided and opened up, and bottom currents became more active, the seafloor may shifted to more oxygenated conditions.

The transfer of soil organic matter offshore can be reconstructed using the BIT index. This index shows a long-term decline over the Cenozoic, particularly in sites from the Victoria Land basin. This is interpreted to reflect a change to less active glaciofluvial systems and therefore reduced transport of terrestrial material offshore. This would have occurred alongside reduced soil development and less ice-free land, as conditions cooled and became increasingly hyper-arid and ice covered. This chapter highlights the caveats to compiling a long term GDGT-temperature record in an area which has undergone substantial tectonic, oceanographic and climatic changes. These factors have likely affected the archaeal communities in the region, and potentially the relationship between these communities and ocean temperature.

6.1 Implications of this study

This thesis aimed to investigate the use of biomarkers in Antarctic sediments, and apply biomarker-based proxies to key transitional periods of climate through the Cenozoic. In achieving these aims, this study provides a framework for the use of biomarkers in Antarctica and other high latitude, glacially-influenced settings. Importantly, while this study does emphasise that issues such as variable depositional environments or reworking must be taken into consideration, a clear biomarker signal can be derived from Antarctic sites to investigate past aspects of climate such as temperature, vegetation, and the hydrological and climate cycles. This shows the substantial potential biomarker-based methods have for reconstructing past climate in Antarctica. A critical component of this research assessed the applicability of biomarker proxies in this region, in particular addressing whether standard interpretations of these of proxies based on global data sets were appropriate in this distinctive high latitude setting. For example, Chapter 4 highlighted how global trends in plant wax carbon isotopes may not necessarily be applicable in Antarctica, where light availability and temperature restrictions play a crucial role in plant growth. This was again emphasised with the use of GDGTs in Chapter 5 for reconstructing ocean temperatures, as global calibrations typically produce unreasonable numbers in the southern high latitudes, necessitating the use of a region-specific calibration.

Much of our understanding of global climate over the Cenozoic has been developed from far-field sites in the mid- and low-latitudes where proxies based on geochemistry and assemblages of microfossils are readily able to be analysed. As such, a key tool in understanding Cenozoic climate has been the benthic foraminiferal δ^{18}O stack (i.e. Zachos et al., 2001, 2008, Cramer et al., 2009, 2011). However, benthic δ^{18}O incorporates a signal that reflects both shifts in ice volume and deep-sea temperature. Attributing the relative contribution from each of these two factors is challenging, making it essential to investigate temperature changes at the high southern latitudes where much of the global ocean deep water is formed. Chapter 5 provides the first attempt to reconstruct a long-term Cenozoic temperature record from the Ross Sea, that can be compared with far-field proxy records such as with the deep Pacific benthic δ^{18}O record of Cramer (2009). As the surface water masses that form in the Ross Sea feed directly into the deep Pacific, this thesis attempts to make a direct link between high latitude surface temperatures and deep oceanic proxies of temperature and ice volume. While absolute temperatures differ between the two high latitude calibrations used, temperature trends are generally comparable to the deep Pacific record. Evidence from the past and present day, as well as models of future warming, suggest that temperature changes at the poles are amplified relative to the global mean (i.e. Vaughan et al., 2003, Lunt et al., 2012, Masson-Delmotte et al., 2013). As proxy temperature reconstructions from high latitudes are limited through the Cenozoic, and climate models tend to underestimate the equator to pole gradient during past periods of global warmth, the temperature compilation presented here provides an Antarctic end-member for constraints on the magnitude of polar amplification in the geological past. It also highlights time periods where this critical data is absent, particularly following the MMCT and during Late Miocene – which are both periods of large-scale inferred cooling in the Antarctic during which its sparse tundra vegetation disappeared.

This study was also motivated by the need to further understand the concept of ice-sheet hysteresis, whereby Antarctic ice sheet models have previously struggled to grow and melt continental scale ice sheets while accommodating the magnitude of ice volume change suggested by the benthic foraminiferal record (i.e. Pollard and DeConto, 2005). Critical to investigating this problem is the need for proximal Antarctic proxy records which can be used to provide climate boundary conditions to ground truth models and assess the sensitivity of the ice sheets to changes in climate. This thesis addresses this problem over the Mi-1 glaciation at the Oligocene/Miocene boundary, by providing higher-resolution Antarctic temperature and environmental constraints from DSDP site 270 over this large transient glacial event. This core

revealed marine grounded ice or ice shelves did not advance across the central Ross Sea during Mi-1, suggesting that the majority of the ice volume associated with this glacial was held shoreward of DSDP site 270. This indicates that marine-based ice did not advance to the continental shelf edge in Antarctica and terrestrial terminating ice may have been susceptible to dramatic changes in volume in a warmer, higher CO_2 world. These findings have implications for the behaviour of the Antarctic Ice Sheets in response to present day climate change, and the potential impact that their melt may have on global sea level.

This study intended to investigate the decline of vegetation in Antarctica between the MMCT and the Pliocene, as the timing of vegetation extinction has implications for the future response of Antarctic biota in a warmer world. However, in building a sample set for this project it was noted that there was a lack of high quality records through this critical time period. Terrestrial records from the Mid to Late Miocene have recently been drilled from the Friis Hills in the Dry Valleys, and more continuous strata are the target for the upcoming IODP Expedition 374 in the central Ross Sea in early 2018. While a lack of available sediment meant this thesis was unable to achieve this goal, it put forward and tested a methodology in Chapter 3 to identify contemporaneous and reworked plant waxes in Antarctic sediments, which will be applied in future to these sample sites to identify the demise of Antarctic vegetation. Critically, it also identified the central Ross Sea as an ideal region to apply to biomarker based proxies as it is less influenced by reworking issues than more coastal sites.

6.2 Conclusion

This thesis aimed to assess and apply biomarker-based proxies in Cenozoic Antarctic sediments, to further understanding of Antarctica's climate during the development the ice sheets. Two environmental reconstructions are presented: 1) an investigation of the onshore and offshore climate of the Ross Sea region prior to and during the Mi-1 glaciation, with inferences as to the drivers and climatic response to this major glacial event, and 2) the use of GDGTs to determine temperatures and temperature trends in the Ross Sea over the Cenozoic, emphasising the caveats that must be taken into account in using these proxy methods in a high latitude, glacially influenced setting. The study also highlights that the distinctive nature of high latitude depositional settings can result in significant reworking of biomarkers. This indicates that while biomarkers can be a powerful method of determining past climate in Antarctica, it is important to understand the variable environments of deposition and how these

factors can impact proxy interpretations. Ideally a multi-proxy approach is ideal, taking into consideration the geochemistry, sedimentology and micropaleontology of a sample site.

6.3 Future work and sites not included in Chapters 3 to 5

6.3.1 Sample sites not included in Chapters 3 to 5

As part of this thesis, small sample runs of biomarkers were also initially analysed from the Sirius Group at Beardmore Glacier and Friis Hills in the Dry Valleys, and the Pagodroma Group and Marine Plain in Prydz Bay (Chapter 1). As the thesis progressed, these sites were not included in Chapter 3 to 5, as the focus was moved to concentrate on more continuous stratigraphic records, rather than these 'snapshot' outcrops. This was due to it being recognised that biomarker trends rather than spot measurements of absolute numbers can sometimes provide more meaningful information. This is particularly important in a region where only limited biomarker-based work has been done to draw comparison to. As analytical processing for biomarkers can be time intensive, priority in second and third sample runs was given to increasing data resolution in the more stratigraphically continuous records.

It is hoped that some of these analyses may be included in future work. For example, drill cores were recovered from the Friis Hills in 2016/2017, which when analysed will allow a broader stratigraphic frame work for outcrop records to tie into. This study also progressed to focus on the Ross Sea region, which contributed to limited samples from the Prydz Bay sites not being included. However, if sample resolution was increased these sites also have the potential to provide important proxy climate data from a geographically distinct region on the opposite margin of the EAIS.

6.3.2 Future work

Initial future work will be focused on developing and interpreting two data sets also collected as part of this thesis. While compound specific isotopes from DSDP 270 are described in Chapter 4, all other studied sites have also been analysed for isotopes. Unfortunately, laboratory delays resulted in this data only being received shortly before thesis submission, requiring it to form a component of future work instead of being included within this PhD. These areas of research will be:

- A compound specific approach using *n*-alkanes to investigating biomarker reworking in the Ross Sea region. Facies-specific differences in the incorporation of reworked material were recognised in Chapter 3. It is intended to use compound specific isotopes

to investigate if samples identified as incorporating significant reworked material (i.e. demonstrating a low CPI, and high ACL and n-C_{29}/n-C_{27}), also include isotopic values offset from those considered contemporaneous.

- A reconstruction of Mid-Miocene climate from a high altitude terrestrial locality (Mt Boreas) and a deep-marine Ross Sea drill core (DSDP 274). n-Alkane compound specific isotopes of $\delta^{13}C$ and δ^2H and brGDGT-based soil temperatures have been obtained from Mt Boreas, and will be used to reconstruct temperature, plant carbon incorporation and the hydrological cycle at this site. These results will be compared to compound specific isotopes and isoGDGT-based ocean temperatures during this same time period in the Ross Sea. This will require additional samples to be analysed from DSDP 274 to increase sampling resolution over this time period.

This thesis has highlighted several areas where further biomarker work could be focused in Antarctica. Long-term stratigraphic records allow for trends in biomarker proxies to be assessed over time. However, in Antarctica these records are frequently complicated by rapidly changing depositional environments and significant input of reworked material. It is suggested that biomarker work in this region would benefit from being focused on more ice-distal records, or ice-distal facies within a record, where subglacial erosion and high reworked input has a lesser impact. Stratigraphically continuous, long-term records of biomarkers proxies such as n-alkane compound specific isotopes would provide important insights into the evolution of climate and vegetation in this region, as well as a context for 'snapshot' records, such as those in the Sirius Group at Beardmore Glacier, to be compared to. This study indicates that in Antarctica n-alkane $\delta^{13}C$ appears to be primarily influenced by different factors than those suggested by global data sets (i.e. where mean annual precipitation plays the most significant role) (Chapter 4). Further study is required to investigate whether these inferences also apply over other periods of the Cenozoic. Chapter 5 highlights the complications with applying isoGDGT-based temperature proxies in this region, emphasising the importance of an extensive regional assessment of the modern relationship between archaea and temperature. This chapter also indicates that a more meaningful long-term record could be derived by focusing on stratigraphically continuous, ice-distal sediments within a single depositional basin. Significantly, this thesis highlights the need to apply an integrated approach when studying proxy records in Antarctica, with consideration of the depositional setting of the sediments.

7. Reference List

Aislabie, J., McLeod, M., & Fraser, R. (1998). Potential for biodegradation of hydrocarbons in soil from the Ross Dependency, Antarctica. *Applied Microbiology and Biotechnology*, *49*(2), 210-214.

Allibone, A. H., Cox, S. C., Graham, I. J., Smillie, R. W., Johnstone, R. D., Ellery, S. G., & Palmer, K. (1993a). Granitoids of the Dry Valleys area, southern Victoria Land, Antarctica: plutons, field relationships, and isotopic dating. *New Zealand journal of geology and geophysics*, *36*(3), 281-297.

Allibone, A. H., Cox, S. C., & Smillie, R. W. (1993b). Granitoids of the Dry Valleys area, southern Victoria Land: geochemistry and evolution along the early Paleozoic Antarctic Craton margin. *New Zealand journal of geology and geophysics*, *36*(3), 299-316.

Allis, R. G., Barrett, P. J., and Christoffel, D. A. (1975). A paleomagnetic stratigraphy for Oligocene and Early Miocene marine glacial sediments at Site 270, Ross Sea, Antarctica. *Initial Reports of the Deep Sea Drilling Project, 28,* 879-884.

Alonso, B., Anderson, J. B., Díaz, J. I., & Bartek, L. R. (1992). Pliocene-Pleistocene Seismic Stratigraphy of the Ross Sea: Evidence for Multiple Ice Sheet Grounding Episodes. In D. H. Elliot (Ed), *Contributions to Antarctic Research III* (pp. 93-103). Washington, D. C: American Geophysical Union.

Alonso-Sáez, L., Andersson, A., Heinrich, F., & Bertilsson, S. (2011). High archaeal diversity in Antarctic circumpolar deep waters. *Environmental microbiology reports*, *3*(6), 689-697.

Anagnostou, E., John, E. H., Edgar, K. M., Foster, G. L., Ridgwell, A., Inglis, G. N., Pancost, R. D., Lunt, D. J., & Pearson, P. N. (2016). Changing atmospheric CO2 concentration was the primary driver of early Cenozoic climate. *Nature*, *533*(7603), 380-384.

Anderson, J. B., Warny, S., Askin, R. A., Wellner, J. S., Bohaty, S. M., Kirshner, A. E., Livsey, D. N., Simms, A. R., Smith, T. R., Ehrmann, W., Lawyer, L. A., Barbeau, D., Wise, S. W., Kulhanek, D. K., Weaver, F. M., & Majewski, W. (2011). Progressive Cenozoic cooling and the demise of Antarctica's last refugium. *Proceedings of the National Academy of Sciences*, *108*(28), 11356-11360.

Arens, N. C., Hope Jahren, A., & Amundson, R. (2000). Can C3 plants faithfully record the carbon isotopic composition of atmospheric carbon dioxide?. *Paleobiology*, *26*(1), 137-164.

Arrigo, K. R., Robinson, D. H., Worthen, D. L., Schieber, B., & Lizotte, M. P. (1998). Bio-optical properties of the southwestern Ross Sea. *Journal of Geophysical Research: Oceans*, *103*(C10), 21683-21695.

Arrigo, K. R., DiTullio, G. R., Dunbar, R. B., Robinson, D. H., VanWoert, M., Worthen, D. L., & Lizotte, M. P. (2000). Phytoplankton taxonomic variability in nutrient utilization and primary production in the Ross Sea. *Journal of Geophysical Research: Oceans*, *105*(C4), 8827-8846.

Arrigo, K. R., & van Dijken, G. L. (2004). Annual changes in sea-ice, chlorophyll a, and primary production in the Ross Sea, Antarctica. *Deep Sea Research Part II: Topical Studies in Oceanography*, *51*(1), 117-138.

Arrigo, K. R., van Dijken, G. L., & Bushinsky, S. (2008). Primary production in the Southern Ocean, 1997–2006. *Journal of Geophysical Research: Oceans*, *113*, C08004, doi:10.1029/2007JC004551.

Arrigo, K. R., van Dijken, G., & Long, M. (2008). Coastal Southern Ocean: A strong anthropogenic CO2 sink. *Geophysical Research Letters*, *35*, L21602, doi:10.1029/2008GL035624.

Ashworth, A. C. & Cantrill, D. J. (2004). Neogene vegetation of the Meyer Desert Formation (Sirius Group) Transantarctic Mountains, Antarctica. *Palaeogeography, Palaeoclimatology, Palaeoecology*, *213*(1), 65-82.

Askin, R. A., & Markgraf, V. (1986). Palynomorphs from the Sirius Formation, Dominion Range, Antarctica. *Antarctic Journal of the United States*, *21*(5), 34-35.

Askin, R. A. (1998). Palynological investigations of Mount Feather Sirius Group samples: recycled Triassic assemblages. In G. S. Wilson & J. Barron (Eds.), *Mount Feather Sirius Group Core Workshop and Collaborative Sample Analysis. Byrd Polar Research Center Report No. 14.* (pp. 59-65). Columbus, Ohio: Byrd Polar Research Center, The Ohio State University.

Askin, R. A. (2000). Spores and pollen from the McMurdo Sound erratics, Antarctica. In J. D. Stilwel & R. M. Feldman (Eds.), *Paleobiology and Paleoenvironments of Eocene Rocks: McMurdo Sound, East Antarctica*, (pp. 161-181). Washington D. C: American Geophysical Union.

Askin, R. A., & Raine, J. I. (2000). Oligocene and Early Miocene terrestrial palynology of the Cape Roberts Drillhole CRP-2/2A, Victoria Land Basin, Antarctica. *Terra Antartica*, *7*(4), 493-501.

Baas, M., Pancost, R., van Geel, B., & Sinninghe Damsté, J.S. (2000). A comparative study of lipids in *Sphagnum* species. *Organic Geochemistry*, *31*(6), 535-541.

Badger, M. P., Lear, C. H., Pancost, R. D., Foster, G. L., Bailey, T. R., Leng, M. J., & Abels, H. A. (2013). CO2 drawdown following the middle Miocene expansion of the Antarctic Ice Sheet. *Paleoceanography*, *28*(1), 42-53.

Barrett, P. J. (1975). Characteristics of pebbles from Cenozoic marine glacial sediments in the Ross Sea (DSDP sites 270-274) and the south Indian Ocean (Site 268). *Initial Reports of the Deep Sea Drilling Project, 28,* 769-784.

Barrett, P. J. (1981). History of the Ross Sea region during the deposition of the Beacon Supergroup 400-180 million years ago. *Journal of the Royal Society of New Zealand*, *11*(4), 447-458.

Barrett, P. J., Elliot, D. H., & Lindsay, J. F. (1986). The Beacon Supergroup (Devonian-Triassic) and Ferrar Group (Jurrasic) in the Beardmore Glacier Area, Antarctica. In M.

D. Turner & J. E. Splettstoesser (Eds.), *Geology of the central Transantarctic Mountains* (pp. 339-428). Washington, D. C: American Geophysical Union.

Barrett, P. J. (Ed). (1989). *Antarctic Cenozoic history from the CIROS-1 drillhole, McMurdo Sound*. Wellington, New Zealand: DSIR Publishing.

Barrett, P. J. (2013). Resolving views on Antarctic Neogene glacial history–the Sirius debate. *Earth and Environmental Science Transactions of the Royal Society of Edinburgh*, *104*(0), 31-53.

Bart, P. J. (2003). Were West Antarctic ice sheet grounding events in the Ross Sea a consequence of East Antarctic ice sheet expansion during the middle Miocene?. *Earth and Planetary Science Letters*, *216*(1), 93-107.

Bart, P. J., & De Santis, L. (2012). Glacial intensification during the Neogene: A review of seismic stratigraphic evidence from the Ross Sea, Antarctica, continental shelf. *Oceanography, 25*(3), 166-183.

Bartoli, G., Hönisch, B., & Zeebe, R. E. (2011). Atmospheric CO_2 decline during the Pliocene intensification of Northern Hemisphere glaciations. *Paleoceanography*, *26*(4).

Beddow, H. M., Liebrand, D., Sluijs, A., Wade, B. S., & Lourens, L. J. (2016). Global change across the Oligocene-Miocene transition: High-resolution stable isotope records from IODP Site U1334 (equatorial Pacific Ocean). *Paleoceanography, 31,* 81-97.

Beerling, D. J., & Royer, D. L. (2002). Fossil plants as indicators of the Phanerozoic global carbon cycle. *Annual Review of Earth and Planetary Sciences*, *30*(1), 527-556.

Beerling, D.J., & Royer, D.L. (2011). Convergent Cenozoic CO_2 history. *Nature Geoscience, 4,* 418-420.

Behrendt, J. C., LeMasurier, W. E., Cooper, A. K., Tessensohn, F., Trehu, A., & Damaske, D. (1991). The West Antarctic rift system: a review of geophysical investigations. In D. H. Elliot (Ed), *Contributions to Antarctic research II* (pp. 67-112). Washington, D. C: American Geophysical Union.

Bej, A. K., Saul, D., & Aislabie, J. (2000). Cold-tolerant alkane-degrading *Rhodococcus* species from Antarctica. *Polar Biology*, *23*(2), 100-105.

Bendle, J., Kawamura, K., Yamazaki, K., & Niwai, T. (2007). Latitudinal distribution of terrestrial lipid biomarkers and n-alkane compound-specific stable carbon isotope ratios in the atmosphere over the western Pacific and Southern Ocean. *Geochimica et Cosmochimica Acta*, *71*(24), 5934-5955.

Benz, V., Esper, O., Gersonde, R., Lamy, F., & Tiedemann, R. (2016). Last Glacial Maximum sea surface temperature and sea-ice extent in the Pacific sector of the Southern Ocean. *Quaternary Science Reviews*, *146*, 216-237.

Berthe-Corti, L., & Fetzner, S. (2002). Bacterial Metabolism of n-Alkanes and Ammonia under Oxic, Suboxic and Anoxic Conditions. *Engineering in Life Sciences*, *22*(3-4), 299-336.

Bijl, P. K., Schouten, S., Sluijs, A., Reichart, G. J., Zachos, J. C., & Brinkhuis, H. (2009). Early Palaeogene temperature evolution of the southwest Pacific Ocean. *Nature*, *461*(7265), 776-779.

Bijl, P. K., Bendle, J. A., Bohaty, S. M., Pross, J., Schouten, S., Tauxe, L. Stickley, C. E., McKay, R. M., Röhl, U., Olney, M., Sluijs, A., Escutia, C., Brinkhuis, H., & Expedition 318 Scientists (2013). Eocene cooling linked to early flow across the Tasmanian Gateway. *Proceedings of the National Academy of Sciences*, *110*(24), 9645-9650.

Billups, K., Pälike, H., Channell, J. E. T., Zachos, J. C., & Shackleton, N. J. (2004). Astronomic calibration of the late Oligocene through early Miocene geomagnetic polarity time scale. *Earth and Planetary Science Letters*, *224*(1), 33-44.

Bingham, E. M., McClymont, E. L., Väliranta, M., Mauquoy, D., Roberts, Z., Chambers, F. M., Pancost, R.D., & Evershed, R. P. (2010). Conservative composition of *n*-alkane biomarkers in *Sphagnum* species: implications for palaeoclimate reconstruction in ombrotrophic peat bogs. *Organic Geochemistry*, *41*(2), 214-220.

Birkenmajer, K., & Zastawniak, E. (1989). Late Cretaceous-early Tertiary floras of King George Island, West Antarctica: their stratigraphic distribution and palaeoclimatic significance. *Geological Society, London, Special Publications*, *47*(1), 227-240.

Blaga, C. I., Reichart, G. J., Heiri, O., & Sinninghe Damsté, J. S. (2009). Tetraether membrane lipid distributions in water-column particulate matter and sediments: a study of 47 European lakes along a north–south transect. *Journal of Paleolimnology*, *41*(3), 523-540.

Bohaty, S. M., & Zachos, J. C. (2003). Significant Southern Ocean warming event in the late middle Eocene. *Geology*, *31*(11), 1017-1020.

Bohaty, S. M., Zachos, J. C., Florindo, F., & Delaney, M. L. (2009). Coupled greenhouse warming and deep-sea acidification in the middle Eocene. *Paleoceanography*, *24*, PA2207, doi:10.1029/2008PA001676.

Borg, S. G., Stump, E., & Holloway, J. R. (1986). Granitoids of northern Victoria Land, Antarctica: A reconnaissance study of field relations, petrography, and geochemistry. In E. Stump (Ed), *Geological Investigations in Northern Victoria Land* (pp. 115-188). Washington, D.C: American Geophysical Union.

Bowen, G. J. (2008). Spatial analysis of the intra-annual variation of precipitation isotope ratios and its climatological corollaries. *Journal of Geophysical Research: Atmospheres*, *113*, D05113, doi:10.1029/2007JD009295.

Boyer, T.P., Antonov, J. I., Baranova, O. K., Coleman, C., Garcia, H. E., Grodsky, A., Johnson, D. R., Locarnini, R. A., Mishonov, A. V., O'Brien, T. D., Paver, C., R., Reagan, J. R., Seidov, D., Smolyar, I. V., & Zweng, M. M. (2013). World Ocean Database 2013. In S. Levitus (Ed.), A. Mishonov, (Technical Ed.). *NOAA Atlas NESDIS 72* (pp. 1-209). Silver Spring, MD.

Brader, A. V., van Winden, J. F., Bohncke, S. J., Beets, C. J., Reichart, G. J., & de Leeuw, J. W. (2010). Fractionation of hydrogen, oxygen and carbon isotopes in n-alkanes and cellulose of three Sphagnum species. *Organic Geochemistry*, *41*(12), 1277-1284.

Bradshaw, M. A. (2013). The Taylor Group (Beacon Supergroup): the Devonian sediments of Antarctica. *Geological Society, London, Special Publications*, *381*(1), 67-97.

Bramley-Alves, J., Wanek, W., French, K., & Robinson, S. A. (2015). Moss δ^{13}C: an accurate proxy for past water environments in polar regions. *Global change biology*, *21*(6), 2454-2464.

Bramley-Alves, J., Wanek, W., & Robinson, S. A. (2016). Moss δ^{13}C: Implications for subantarctic palaeohydrological reconstructions. *Palaeogeography, Palaeoclimatology, Palaeoecology*, *453*, 20-29.

Brancolini, G., Cooper, A. K., & Coren, F. (1995). Seismic facies and glacial history in the western Ross Sea (Antarctica). In A. K. Cooper, P. F. Barker & G. Brancolini (Eds.), *Geology and Seismic Stratigraphy of the Antarctic Margin* (pp. 209-233). Washington, D. C: American Geophysical Union.

Bray, E.E., & Evans, E.D. (1961). Distribution of *n*-paraffins as a clue to recognition of source beds. *Geochimica et Cosmochimica Acta, 22*(1), 2-15.

Brett, M. J., Baldini, J. U., & Gröcke, D. R. (2014). Environmental controls on stable isotope ratios in New Zealand Podocarpaceae: Implications for palaeoclimate reconstruction. *Global and Planetary Change*, *120*, 38-45.

Brigham-Grette, J., Melles, M., Minyuk, P., Andreev, A., Tarasov, P., DeConto, R., Koenig, S., Nowaczyk, N., Wennrich, V., Rosén, P., Haltia, E., Cook, T., Gebhardt, C., Meyer-Jacob, C., Snyder, J., & Herzschuh (2013). Pliocene warmth, polar amplification, and stepped Pleistocene cooling recorded in NE Arctic Russia. *Science*, *340*(6139), 1421-1427.

Brooks, J. D., & Smith, J. W. (1967). The diagenesis of plant lipids during the formation of coal, petroleum and natural gas—I. Changes in the n-paraffin hydrocarbons. *Geochimica et Cosmochimica Acta*, *31*(12), 2389-2397.

Bücker, C. J., Wonik, T., & Jarrard, R. (2001). The temperature and salinity profile in CRP-2/2A, Victoria Land Basin, Antarctica. *Terra Antartica*, *7*(3), 255-259.

Bücker, C., Jarrard, R. D., & Wonik, T. (2001). Downhole temperature, radiogenic heat production, and heat flow from the CRP-3 drillhole, Victoria Land Basin, Antarctica. *Terra Antartica*, *8*(3), 151-160.

Bull, J. R. (2009). *Stable isotope, major and trace element chemistry of modern snow from Evans Piedmont Glacier, Antarctica: insights into potential source regions and relationship of glaciochemistry to atmospheric circulation and vigour.* (Unpublished Masters Thesis). Victoria University of Wellington, New Zealand.

Burgess, C. E., Pearson, P. N., Lear, C. H., Morgans, H. E., Handley, L., Pancost, R. D., & Schouten, S. (2008). Middle Eocene climate cyclicity in the southern Pacific: Implications for global ice volume. *Geology*, *36*(8), 651-654.

Burrington, P. (2015). *How to be a Prehistoric Weatherman: Using n-alkanes as a Proxy for Holocene Climate and Hydrology, Southwest South Island, New Zealand* (Unpublished Masters Thesis). University of Otago, New Zealand.

Bush, R. T., & McInerney, F. A. (2013). Leaf wax n-alkane distributions in and across modern plants: implications for paleoecology and chemotaxonomy. *Geochimica et Cosmochimica Acta*, *117*, 161-179.

Bush, R. T., & McInerney, F. A. (2015). Influence of temperature and C_4 abundance on *n*-alkane chain length distributions across the central USA. *Organic Geochemistry*, *79*, 65-73.

Calvo, E., Pelejero, C., Logan, G. A., & De Deckker, P. (2004). Dust-induced changes in phytoplankton composition in the Tasman Sea during the last four glacial cycles. *Paleoceanography*, *19*, PA2020, doi:10.1029/2003PA000992.

Canuel, E. A., & Martens, C. S. (1996). Reactivity of recently deposited organic matter: Degradation of lipid compounds near the sediment-water interface. *Geochimica et cosmochimica acta*, *60*(10), 1793-1806.

Cape Roberts Science Team (1999). Studies from the Cape Roberts Project, Ross Sea Antarctica, Initial report on CRP-2/2A. *Terra Antartica*, *6*(1), 1-173.

Castañeda, I. S., Mulitza, S., Schefuß, E., dos Santos, R. A. L., Sinninghe Damsté, J. S., & Schouten, S. (2009). Wet phases in the Sahara/Sahel region and human migration patterns in North Africa. *Proceedings of the National Academy of Sciences*, *106*(48), 20159-20163.

Castañeda, I.S., & Schouten, S. (2011). A review of molecular organic proxies for examining modern and ancient lacustrine environments. *Quaternary Science Reviews*, *30*(21), 2851-2891.

Cerling, T. E., Wang, Y., & Quade, J. (1993). Expansion of C4 ecosystems as an indicator of global ecological change in the late Miocene. *Nature*, *361*(6410), 344-345.

Cernusak, L. A., Ubierna, N., Winter, K., Holtum, J. A., Marshall, J. D., & Farquhar, G. D. (2013). Environmental and physiological determinants of carbon isotope discrimination in terrestrial plants. *New Phytologist*, *200*(4), 950-965.

Chikaraishi, Y., & Naraoka, H. (2003). Compound-specific δD–δ 13 C analyses of n-alkanes extracted from terrestrial and aquatic plants. *Phytochemistry*, *63*(3), 361-371.

Church, M. J., DeLong, E. F., Ducklow, H. W., Karner, M. B., Preston, C. M., & Karl, D. M. (2003). Abundance and distribution of planktonic Archaea and Bacteria in the waters west of the Antarctic Peninsula. *Limnology and Oceanography*, *48*(5), 1893-1902.

Clark Jr, R. C., & Blumer, M. (1967). Distribution of n-paraffins in marine organisms and sediment. *Limnology and Oceanography, 12*(1), 79-87.

Claypool, G. E., & Kvenvolden, K. A. (1983). Methane and other hydrocarbon gases in marine sediment. *Annual Review of Earth and Planetary Sciences*, *11*(1), 299-327.

Collinson, J. W. (1997). Paleoclimate of Permo-Triassic Antarctica. *International Symposium on Antarctic Earth Sciences, 7,* 1029-1034.

Collister, J. W., Rieley, G., Stern, B., Eglinton, G., & Fry, B. (1994). Compound-specific δ 13C analyses of leaf lipids from plants with differing carbon dioxide metabolisms. *Organic Geochemistry*, *21*(6-7), 619-627.

Cook, R. A., & Woolhouse, A. D. (1989). Hydrocarbon residue. In P. J. Barrett (Ed), *Antarctic Cenozoic history from the CIROS-1 drillhole, McMurdo Sound*, (pp. 211-217). Wellington, New Zealand: DSIR Publishing.

Cook, C. P., Van De Flierdt, T., Williams, T., Hemming, S. R., Iwai, M., Kobayashi, M., Jimenez-Espejo, F. J., Escutia, C., González, J. J., Khim, B. –K., McKay, R. M., Passchier, S., Bohaty, S. M., Riesselman, C. R., Tauxe, L., Sugisaki, S., Galindo, A. L., Patterson, M. O., Sangiorgi, F., Pierce, E. L., Brinkhuis, H., Klaus, A., Fehr, A., Bendle, J. A. P., Bijl, P. K., Carr, S. A., Dunbar, R. B., Flores, J. A., Hayden, T. G., Katsuki, K., Kong, G. S., Nakai, M., Olney, M. P., Pekar, S. F., Pross, J., Röhl, U., Sakai, T., Shrivastava, P. K., Stickley, C. E., Tuo, S., Welsh, K., & Yamane, M. (2013). Dynamic behaviour of the East Antarctic ice sheet during Pliocene warmth. *Nature Geoscience*, *6*(9), 765-769.

Cooper, A. K., Davey, F. J., & Behrendt, J. C. (1987). Seismic stratigraphy and structure of the Victoria Land basin, western Ross Sea, Antarctica. In A. K. Cooper & F. J. Davey (Eds.), *The Antarctic Continental Margin: Geology and Geophysics of the Western Ross Sea* (pp. 27-65). Houston, T.X: Circumpacific Council for Energy and Mineral Resources.

Coulon, F., Pelletier, E., Gourhant, L., & Delille, D. (2005). Effects of nutrient and temperature on degradation of petroleum hydrocarbons in contaminated sub-Antarctic soil. *Chemosphere*, *58*(10), 1439-1448.

Cox, S., Turnbull, I., Isaac, M., Townsend, D., & Smith Lyttle, B. (2012). Geology of Southern Victoria Land, Antarctica. *Geology of Southern Victoria Land, Antarctica: New Zealand Institute of Geological and Nuclear Sciences Geologic Map*, *22*.

Coxall, H. K., Wilson, P. A., Pälike, H., Lear, C. H., & Backman, J. (2005). Rapid stepwise onset of Antarctic glaciation and deeper calcite compensation in the Pacific Ocean. *Nature*, *433*(7021), 53-57.

Cramer, B. S., Toggweiler, J. R., Wright, J. D., Katz, M. E., & Miller, K. G. (2009). Ocean overturning since the Late Cretaceous: Inferences from a new benthic foraminiferal isotope compilation. *Paleoceanography*, *24*, PA4216, doi:10.1029/2008PA001683.

Cramer, B. S., Miller, K. G., Barrett, P. J., & Wright, J. D. (2011). Late Cretaceous–Neogene trends in deep ocean temperature and continental ice volume: Reconciling records of benthic foraminiferal geochemistry (δ18O and Mg/Ca) with sea level history. *Journal of Geophysical Research: Oceans*, *116,* C12023, doi:10.1029/2011JC007255.

Crampton, J. S., Cody, R. D., Levy, R., Harwood, D., McKay, R., & Naish, T. R. (2016). Southern Ocean phytoplankton turnover in response to stepwise Antarctic cooling over the past 15 million years. *Proceedings of the National Academy of Sciences*, *113*(25), 6868-6873.

Cranwell, P. A., Eglinton, G., & Robinson, N. (1987). Lipids of aquatic organisms as potential contributors to lacustrine sediments—II. *Organic Geochemistry*, *11*(6), 513-527.

Cúneo, N. R., Isbell, J., Taylor, E. L., & Taylor, T. N. (1993). The Glossopteris flora from Antarctica: taphonomy and paleoecology. *Comptes Rendus XII ICC-P*, *2*, 13-40.

Cúneo, N. R., Taylor, E. L., Taylor, T. N., & Krings, M. (2003). In situ fossil forest from the upper Fremouw Formation (Triassic) of Antarctica: paleoenvironmental setting and paleoclimate analysis. *Palaeogeography, Palaeoclimatology, Palaeoecology*, *197*(3), 239-261.

Dawson, T. E., & Pate, J. S. (1996). Seasonal water uptake and movement in root systems of Australian phraeatophytic plants of dimorphic root morphology: a stable isotope investigation. *Oecologia*, *107*(1), 13-20.

Decesari, R. C., Sorlien, C. C., Luyendyk, B. P., Wilson, D. S., Bartek, L. R., Diebold, J., & Hopkins, S. E. (2007). Regional seismic stratigraphic correlations of the Ross Sea: implications for the tectonic history of the West Antarctic Rift System. In A. K. Cooper, C. R. Raymond & 10th ISAES Editorial Team (Eds.), *Antarctica: A Keystone in a Changing World- Online Proceedings of the 10th ISAES*, 2007-1047, USGS Open-File Report, Short Research Paper 052, 4p.

DeConto, R. M., & Pollard, D. (2003). Rapid Cenozoic glaciation of Antarctica induced by declining atmospheric CO_2. *Nature*, *421*(6920), 245-249.

DeConto, R.M., Pollard, D., Wilson, P.A., Pälike, H., Lear, C.A. & Pagani, M. (2008). Thresholds for Cenozoic bipolar glaciations. *Nature, 455,* 652-656.

DeConto, R. M., & Pollard, D. (2016). Contribution of Antarctica to past and future sea-level rise. *Nature*, *531*(7596), 591-597.

Denton, G. H., Sugden, D. E., Marchant, D. R., Hall, B. L., & Wilch, T. I. (1993). East Antarctic Ice Sheet sensitivity to Pliocene climatic change from a Dry Valleys perspective. *Geografiska Annaler. Series A. Physical Geography, 74*(4), 155-204.

Denton, G. H., & Sugden, D. E. (2005). Meltwater features that suggest Miocene ice-sheet overriding of the Transantarctic Mountains in Victoria Land, Antarctica. *Geografiska Annaler: Series A, Physical Geography*, *87*(1), 67-85.

De Jonge, C., Hopmans, E. C., Stadnitskaia, A., Rijpstra, W. I. C., Hofland, R., Tegelaar, E., & Sinninghe Damsté, J. S. (2013). Identification of novel penta-and hexamethylated branched glycerol dialkyl glycerol tetraethers in peat using HPLC–MS 2, GC–MS and GC–SMB-MS. *Organic geochemistry*, *54*, 78-82.

De Jonge, C., Hopmans, E. C., Zell, C. I., Kim, J. H., Schouten, S., & Sinninghe Damsté, J. S. (2014). Occurrence and abundance of 6-methyl branched glycerol dialkyl glycerol

tetraethers in soils: Implications for palaeoclimate reconstruction. *Geochimica et Cosmochimica Acta*, *141*, 97-112.

Demaison, G. J., & Moore, G. T. (1980). Anoxic environments and oil source bed genesis. *Organic Geochemistry*, *2*(1), 9-31.

De Santis, L., Anderson, J. B., Brancolini, G., & Zayatz, I. (1995). Seismic record of late Oligocene through Miocene glaciation on the central and eastern continental shelf of the Ross Sea. In A. K. Cooper, P. F. Barker & G. Brancolini (Eds.), *Geology and Seismic Stratigraphy of the Antarctic Margin* (pp. 235-260). Washington, D. C: American Geophysical Union.

De Santis, L., Prato, S., Brancolini, G., Lovo, M., & Torelli, L. (1999). The Eastern Ross Sea continental shelf during the Cenozoic: implications for the West Antarctic ice sheet development. *Global and Planetary Change*, *23*(1), 173-196.

De Vleeschouwer, D., Vahlenkamp, M., Crucifix, M., & Pälike, H. (2017). Alternating Southern and Northern Hemisphere climate response to astronomical forcing during the past 35 my. *Geology*, *45*(4), 375-378.

Didyk, B. M., Simoneit, B. R. T., Brassell, S. C., and Eglinton, G. (1978). Organic geochemical indicators of palaeoenvironmental conditions of sedimentation. *Nature*, *272*, 216-222.

Diefendorf, A. F., Mueller, K. E., Wing, S. L., Koch, P. L., & Freeman, K. H. (2010). Global patterns in leaf ^{13}C discrimination and implications for studies of past and future climate. *Proceedings of the National Academy of Sciences*, *107*(13), 5738-5743.

Diefendorf, A. F., Freeman, K. H., Wing, S. L., & Graham, H. V. (2011). Production of n-alkyl lipids in living plants and implications for the geologic past. *Geochimica et Cosmochimica Acta*, *75*(23), 7472-7485.

Diefendorf, A. F., Leslie, A. B., & Wing, S. L. (2015). Leaf wax composition and carbon isotopes vary among major conifer groups. *Geochimica et Cosmochimica Acta*, *170*, 145-156.

Diester-Haass, L., Billups, K., & Emeis, K. (2011). Enhanced paleoproductivity across the Oligocene/Miocene boundary as evidenced by benthic foraminiferal accumulation rates. *Palaeogeography, Palaeoclimatology, Palaeoecology*, *302*(3), 464-473.

Dirks, P. H. G. M., & Wilson, C. J. L. (1995). Crustal evolution of the East Antarctic mobile belt in Prydz Bay: continental collision at 500 Ma? *Precambrian Research*, *75*(3-4), 189-207.

Dodd, R. S., Rafii, Z. A., & Power, A. B. (1998). Ecotypic adaptation in *Austrocedrus chilensis* in cuticular hydrocarbon composition. *New Phytologist*, *138*(4), 699-708.

Dodd, R. S., & Afzal-Rafii, Z. (2000). Habitat-related adaptive properties of plant cuticular lipids. *Evolution*, *54*(4), 1438-1444.

Dowsett, H. J. (2007). The PRISM palaeoclimate reconstruction and Pliocene sea-surface temperature. In M. Williams, A. M. Haywood, F. J. Gregory & D. N. Schmidt (Eds.), *Deep-time perspectives on climate change: Marrying the signal from computer*

models and biological proxies (pp. 459-480). London: The Geological Society for The Micropalaeontological Society.

Eglinton, G., and Hamilton, R. J. (1963). The distribution of alkanes. *Chemical plant taxonomy*, *187*, 217.

Eglinton, G., and Hamilton, R. J. (1967). Leaf epicuticular waxes. *Science*, *156*(3780), 1322-1335.

Eglinton, T. I., & Eglinton, G. (2008). Molecular proxies for paleoclimatology. *Earth and Planetary Science Letters*, *275*(1), 1-16.

Ehleringer, J. R., & Cerling, T. E. (1995). Atmospheric CO_2 and the ratio of intercellular to ambient CO_2 concentrations in plants. *Tree Physiology*, *15*(2), 105-111.

Ehrmann, W., Setti, M., & Marinoni, L. (2005). Clay minerals in Cenozoic sediments off Cape Roberts (McMurdo Sound, Antarctica) reveal palaeoclimatic history. *Palaeogeography, Palaeoclimatology, Palaeoecology*, *229*(3), 187-211.

Erez, J., & Luz, B. (1983). Experimental paleotemperature equation for planktonic foraminifera. *Geochimica et Cosmochimica Acta*, *47*(6), 1025-1031.

Ernakovich, J. G., Hopping, K. A., Berdanier, A. B., Simpson, R. T., Kachergis, E. J., Steltzer, H., & Wallenstein, M. D. (2014). Predicted responses of arctic and alpine ecosystems to altered seasonality under climate change. *Global Change Biology*, *20*(10), 3256-3269.

Escutia, C., Brinkhuis, H., & Klaus, A. (2011). IODP Expedition 318: From Greenhouse to Icehouse at the Wilkes Land Antarctic Margin. *Scientific Drilling*, *12*, 15-23.

Farquhar, G. D., Ehleringer, J. R., & Hubick, K. T. (1989). Carbon isotope discrimination and photosynthesis. *Annual review of plant biology*, *40*(1), 503-537.

Feakins, S. J., Warny, S., & Lee, J. E. (2012). Hydrologic cycling over Antarctica during the middle Miocene warming. *Nature Geoscience*, *5*(8), 557-560.

Feakins, S. J., Warny, S., & DeConto, R. M. (2014). Snapshot of cooling and drying before onset of Antarctic Glaciation. *Earth and Planetary Science Letters*, *404*, 154-166.

Feakins, S. J., Peters, T., Wu, M. S., Shenkin, A., Salinas, N., Girardin, C. A., Bentley, L. P., Blonder, B., Enquist, B. J., Martin, R. E., Asner, G. P., & Asner, G. P. (2016). Production of leaf wax n-alkanes across a tropical forest elevation transect. *Organic Geochemistry*, *100*, 89-100.

Feng, X., Simpson, A. J., Gregorich, E. G., Elberling, B., Hopkins, D. W., Sparrow, A. D., Novis, P. M., Greenfield, L. G., & Simpson, M. J. (2010). Chemical characterization of microbial-dominated soil organic matter in the Garwood Valley, Antarctica. *Geochimica et Cosmochimica Acta*, *74*(22), 6485-6498.

Ficken, K. J., Li, B., Swain, D. L., & Eglinton, G. (2000). An *n*-alkane proxy for the sedimentary input of submerged/floating freshwater aquatic macrophytes. *Organic Geochemistry*, *31*(7), 745-749.

Fielding, C. R., & Webb, J. A. (1995). Sedimentology of the Permian Radok Conglomerate in the Beaver Lake area of MacRobertson Land, East Antarctica. *Geological Magazine*, *132*(01), 51-63.

Fielding, C. R., Naish, T. R., Woolfe, K., & Lavelle, M. (2000). Facies analysis and sequence stratigraphy of CRP-2/2A, Victoria Land Basin, Antarctica. *Terra Antartica*, *7*(3), 323-338.

Fielding, C. R., Naish, T. R., & Woolfe, K. (2001). Facies architecture of the CRP-3 drillhole, Victoria Land Basin, Antarctica. *Terra Antarctica*, *8*(3), 217-224.

Fielding, C. R., Henrys, S. A., & Wilson, T. J. (2006). Rift history of the western Victoria Land Basin: a new perspective based on integration of cores with seismic reflection data. In D. K. Fütterer, D. Damaske, G. Kleinschmidt, H. Miller & F. Tessensohn (Eds.), *Antarctica* (pp. 309-318). Berlin Heidelberg: Springer.

Fielding, C. R., Atkins, C. B., Bassett, K. N., Browne, G. H., Dunbar, G. B., Field, B. D., Frank, T. D., Krissek, L. A., Panter, K. S., Passchier, S., Pekar, S. F., Sandroni, S., & Talarico, F. (2008). Sedimentology and stratigraphy of the AND-2A core, ANDRILL Southern McMurdo Sound project, Antarctica. *Terra Antarctica, 15*(1), 77-112.

Fielding, C. R., Browne, G. H., Field, B., Florindo, F., Harwood, D. M., Krissek, L. A., Levy, R. H., Panter, K. S., Passchier, S., & Pekar, S. F. (2011). Sequence stratigraphy of the ANDRILL AND-2A drillcore, Antarctica: A long-term, ice-proximal record of Early to Mid-Miocene climate, sea-level and glacial dynamism. *Palaeogeography, Palaeoclimatology, Palaeoecology*, *305*(1), 337-351.

Fielding, C. R., Harwood, D. M., Winter, D. M., & Francis, J. E. (2012). Neogene stratigraphy of Taylor Valley, Transantarctic Mountains, Antarctica: evidence for climate dynamism and a vegetated early Pliocene coastline of McMurdo Sound. *Global and Planetary Change*, *96-97*, 97-104.

Fitzgerald, P. G. (1994). Thermochronologic constraints on post-Paleozoic tectonic evolution of the central Transantarctic Mountains, Antarctica. *Tectonics*, *13*(4), 818-836.

Florindo, F., Gennari, R., Persico, D., Turco, E., Villa, G., Lurcock, P. C., Roberts, A. P., Winkler, A., Carter, L., & Pekar, S. F. (2015). New magnetobiostratigraphic chronology and paleoceanographic changes across the Oligocene-Miocene boundary at DSDP Site 516 (Rio Grande Rise, SW Atlantic). *Paleoceanography*, *30*(6), 659-681.

Flower, B. P., & Kennett, J. P. (1994). The middle Miocene climatic transition: East Antarctic ice sheet development, deep ocean circulation and global carbon cycling. *Palaeogeography, palaeoclimatology, palaeoecology*, *108*(3), 537-555.

Flower, B. P., Zachos, J. C. & Pearson, P. N. (2006). Astronomic and oceanographic influences on global carbon cycling across the Oligocene/Miocene boundary. In: D. K. Sinha (Ed.), *Micropaleontology: Application in Stratigraphy and Paleoceanography*, New Delhi: Narosa Publishing House

Frakes, L. A. (1975). Paleoclimatic significance of some sedimentary components at Site 274. *Initial Reports of the Deep Sea Drilling Project*, *28*, 785-787.

Francis, J. E., Woolfe, K. J., Arnott, M. J., & Barrett, P. J. (1994). Permian climates of the southern margins of Pangea: evidence from fossil wood in Antarctica. *Pangea: Global Environments and Resources- Memoir 17,* 275-282.

Francis, J.E., & Hill, R.S. (1996). Fossil plants from the Pliocene Sirius Group, Transantarctic Mountains: Evidence for climate from growth rings and fossil leaves. *Palaios, 11,* 389-396.

Francis, J. E. (2000). Fossil Wood from Eocene High Latitude Forests: Mcmurdo Sound, Antarctica. In J. D. Stilwel & R. M. Feldman (Eds.), *Paleobiology and Paleoenvironments of Eocene Rocks: McMurdo Sound, East Antarctica*, (pp. 253-260). Washington D. C: American Geophysical Union.

Francis, J. E., Ashworth, A., Cantrill, D. J., Crame, J. A., Howe, J., Stephens, R., Tosolini, A.-M., & Thorn, V. (2008). 100 million years of Antarctic climate evolution: evidence from fossil plants. In A. K. Cooper, P. J. Barrett, H. Stagg, B. Storey, E. Stump, W. Wise & the 10th ISAES editorial team (Eds.), *Antarctica: a keystone in a changing world*, (pp. 19-28). Washington, D. C: The National Academies Press.

Fretwell, P., Pritchard, H., Vaughan, D., Bamber, J., Barrand, N., Bell, R., Bianchi, C., Bingham, R., Blankenship, D., Casassa, G., Catania, G., Callens, D., Conway, H., Cook, A., Corr, H., Damaske, D., Damm, V., Ferraccioli, F., Forsberg, R., Fujita, S., Gim, Y., Gogineni, P., Griggs, J. A., Hindmarsh, R. C. A., Holmlund, P., Holt, J. W., Jacobel, R. W., Jenkins, A., Jokat, W., Jordan, T., King, E. C., Kohler, J., Krabill, W., Riger-Kusk, M., Langley, K. A., Leitchenkov, G., Leuschen, C., Luyendyk, B. P., Matsuoka, K., Mouginot, J., Nitsche, F. O., Nogi, Y., Nost, O. A., Popov, S. V., Rignot, E., Rippen, D. M., Rivera, A., Roberts, J., Ross, N., Siegert, M. J., Smith, A. M., Steinhage, D., Studinger, M., Sun, B., Tinto, B. K., Welch, B. C., Wilson, D., Young, D. A., Xiangbin, C., & Zirizzotti A. (2013). Bedmap2: improved ice bed, surface and thickness datasets for Antarctica. *Cryosphere, 7*(1), 375-393.

Ford, A. B., & Barrett, P. J. (1975). Basement rocks of the south-central Ross Sea, Site 270, DSDP Leg 28. *Initial Reports of the Deep Sea Drilling Project, 28,* 861-868.

Foster, G. L., Lear, C. H. & Rae, J. W. B. (2012). The evolution of pCO_2, ice volume and climate during the middle Miocene. *Earth and Planetary Science Letters, 341-344,* 243-254.

Foster, G. L., & Rohling, E. J. (2013). Relationship between sea level and climate forcing by $CO2$ on geological timescales. *Proceedings of the National Academy of Sciences*, *110*(4), 1209-1214.

Foster, L. C., Pearson, E. J., Juggins, S., Hodgson, D. A., Saunders, K. M., Verleyen, E., & Roberts, S. J. (2016). Development of a regional glycerol dialkyl glycerol tetraether (GDGT)–temperature calibration for Antarctic and sub-Antarctic lakes. *Earth and planetary science letters*, *433*, 370-379.

Funaki, M. (1984). Paleomagnetic Investigation of McMurdo Sound Region, Southern Victoria Land, Antarctica. *Memoirs of National Institute of Polar Research. Ser. C, Earth sciences*, *16*, 1-81.

Gagosian, R. B., & Peltzer, E. T. (1986). The importance of atmospheric input of terrestrial organic material to deep sea sediments. *Organic Geochemistry*, *10*(4-6), 661-669.

Galeotti, S., DeConto, R., Naish, T., Stocchi, P., Florindo, F., Pagani, M., Barrett, P., Bohaty, S. M. Lanci, L., Pollard, D., Sandroni, S. Talarico, F. M., & Zachos, J. C. (2016). Antarctic Ice Sheet variability across the Eocene-Oligocene boundary climate transition. *Science*, *352*(6281), 76-80.

Gasson, E., DeConto, R. M., Pollard, D., & Levy, R. H. (2016). Dynamic Antarctic ice sheet during the early to mid-Miocene. *Proceedings of the National Academy of Sciences*, *113*(13), 3459-3464.

Gersonde, R., Crosta, X., Abelmann, A., & Armand, L. (2005). Sea-surface temperature and sea ice distribution of the Southern Ocean at the EPILOG Last Glacial Maximum—a circum-Antarctic view based on siliceous microfossil records. *Quaternary Science Reviews*, *24*(7), 869-896.

Gold, W. G., & Bliss, L. C. (1995). Water limitations and plant community development in a polar desert. *Ecology*, *76*(5), 1558-1568.

Golledge, N. R., Fogwill, C. J., Mackintosh, A. N., & Buckley, K. M. (2012). Dynamics of the last glacial maximum Antarctic ice-sheet and its response to ocean forcing. *Proceedings of the National Academy of Sciences*, *109*(40), 16052-16056.

Golledge, N. R., Levy, R. H., McKay, R. M., Fogwill, C. J., White, D. A., Graham, A. G., Smith, J. A., Hillenbrand, C. –D., Licht, K. J., Denton, G. H., Ackert Jr., R. P., Maas, S. M., & Hall, B. L. (2013). Glaciology and geological signature of the Last Glacial Maximum Antarctic ice sheet. *Quaternary Science Reviews*, *78*, 225-247.

Golledge, N. R., Levy, R. H., McKay, R. M., & Naish, T. R. (2017). East Antarctic ice sheet most vulnerable to Weddell Sea warming. *Geophysical Research Letters, 44,* doi:10.1002/2016GL072422.

Goodge, J. W., Myrow, P., Williams, I. S., & Bowring, S. A. (2002). Age and provenance of the Beardmore Group, Antarctica: constraints on Rodinia supercontinent breakup. *The Journal of geology*, *110*(4), 393-406.

Gooseff, M. N., Lyons, W. B., McKnight, D. M., Vaughn, B. H., Fountain, A. G., & Dowling, C. (2006). A stable isotopic investigation of a polar desert hydrologic system, McMurdo Dry Valleys, Antarctica. *Arctic, Antarctic, and Alpine Research*, *38*(1), 60-71.

Gough, M. A., & Rowland, S. J. (1990). Characterization of unresolved complex mixtures of hydrocarbons in petroleum. *Nature*, *344*(6267), 648-650.

Gough, M. A., Rhead, M. M., & Rowland, S. J. (1992). Biodegradation studies of unresolved complex mixtures of hydrocarbons: model UCM hydrocarbons and the aliphatic UCM. *Organic Geochemistry*, *18*(1), 17-22.

Greenop, R., Foster, G. L., Wilson, P. A., & Lear, C. H. (2014). Middle Miocene climate instability associated with high-amplitude CO_2 variability. *Paleoceanography*, *29*(9), 845-853.

Griener, K. W., Nelson, D. M., & Warny, S. (2013). Declining moisture availability on the Antarctic Peninsula during the Late Eocene. *Palaeogeography, Palaeoclimatology, Palaeoecology*, *383*, 72-78.

Grimalt, J., Albaigés, J., Al-Saad, H. T., & Douabul, A. A. Z. (1985). n-Alkane distributions in surface sediments from the Arabian Gulf. *Naturwissenschaften*, *72*(1), 35-37.

Grimalt, J., & Albaigés, J. (1987). Sources and occurrence of C_{12}-C_{22} *n*-alkane distributions with even carbon-number preference in sedimentary environments. *Geochimica et Cosmochimica Acta*, *51*(6), 1379-1384.

Gröcke, D. R. (2002). The carbon isotope composition of ancient CO_2 based on higher-plant organic matter. *Philosophical Transactions of the Royal Society of London A: Mathematical, Physical and Engineering Sciences*, *360*(1793), 633-658.

Hambrey, M. J., Barrett, P. J., & Robinson, P. H. (1989). Stratigraphy. In P. J. Barrett (Ed.) *Antarctic Cenozoic history from the CIROS-1 drillhole, McMurdo Sound,* (pp. 23-48) *Antarctic Cenozoic history from the CIROS-1 drillhole, McMurdo Sound.* Wellington, New Zealand: DSIR Publishing.

Hambrey, M.J., Ehrmann, W.U., & Larsen, B. (1991). Cenozoic glacial record of the Prydz Bay continental shelf, East Antarctica. In J. Barron and B. Larsen (Eds), *Proceeding of the Ocean Drilling Program, Scientific. Results, 119* (pp. 77-132). College Station, TX: Ocean Drilling Program.

Hambrey, M. J., & McKelvey, B. (2000a). Neogene fjordal sedimentation on the western margin of the Lambert Graben, East Antarctica. *Sedimentology*, *47*(3), 577-607.

Hambrey, M. J., & McKelvey, B. (2000b). Major Neogene fluctuations of the East Antarctic ice sheet: Stratigraphic evidence from the Lambert Glacier region. *Geology*, *28*(10), 887-890.

Hambrey, M. J., & Barrett, P. J. (1993). Cenozoic sedimentary and climatic record, Ross Sea region, Antarctica. In J.P. Kennett and D.A. Warnke (Eds.) *The Antarctic Paleoenvironment: A Perspective on Global Change: Part Two*, (pp. 91-124). Washington, D.C: American Geophysical Union.

Han, J., & Calvin, M. (1969). Hydrocarbon distribution of algae and bacteria, and microbiological activity in sediments. *Proceedings of the National Academy of Sciences*, *64*(2), 436-443.

Hannah, M. J. (2006). The palynology of ODP Site 1165, Prydz Bay, East Antarctica: a record of Miocene glacial advance and retreat. *Palaeogeography, Palaeoclimatology, Palaeoecology*, *231*(1), 120-133.

Harland, R., & Pudsey, C. J. (1999). Dinoflagellate cysts from sediment traps deployed in the Bellingshausen, Weddell and Scotia seas, Antarctica. *Marine Micropaleontology*, *37*(2), 77-99.

Hart, K. M., Szpak, M. T., Mahaney, W. C., Dohm, J. M., Jordan, S. F., Frazer, A. R., Allen, C. C. R., & Kelleher, B. P. (2011). A bacterial enrichment study and overview of the extractable lipids from paleosols in the Dry Valleys, Antarctica: implications for future Mars reconnaissance. *Astrobiology*, *11*(4), 303-321.

Harwood, D. M. (1983). Diatoms from the Sirius Formation, Transantarctic Mountains. *Antarctic Journal of the United States*, *18*(5), 98-100.

Harwood, D. M., & Levy, R. H. (2000). The McMurdo Erratics: introduction and overview. In J. D. Stilwel & R. M. Feldman (Eds.), *Paleobiology and Paleoenvironments of Eocene Rocks: McMurdo Sound, East Antarctica*, (pp. 1-18). Washington D. C: American Geophysical Union.

Harwood, D. M., McMinn, A., & Quilty, P. G. (2000). Diatom biostratigraphy and age of the Pliocene Sørsdal Formation, Vestfold Hills, East Antarctica. *Antarctic Science*, *12*(04), 443-462.

Harwood, D. M., Florindo, F., Talarico, F., & Levy, R. H. (Eds.). (2008-2009). Studies from the ANDRILL Southern McMurdo Sound Project, Antarctica. Initial Science Report on AND-2A. *Terra Antarctica, 15*(1), 1-235.

Helby, R. J., & McElroy, C. T. (1969). Microfloras from the Devonian and triassic of the Beacon Group, Antarctica. *New Zealand Journal of Geology and Geophysics*, *12*(2-3), 376-382.

Herbert, T. D., Lawrence, K. T., Tzanova, A., Peterson, L. C., Caballero-Gill, R., & Kelly, C. S. (2016). Late Miocene global cooling and the rise of modern ecosystems. *Nature Geoscience, 9,* 843-847.

Hill, R. S. (1989). Fossil leaf. In P. J. Barrett (Ed), *Antarctic Cenozoic history from the CIROS-1 drillhole, McMurdo Sound*, (pp. 143-144). Wellington, New Zealand: DSIR Publishing.

Ho, S. L., Mollenhauer, G., Fietz, S., Martínez-Garcia, A., Lamy, F., Rueda, G., Schipper, K., Méheust, M., Rosell-Melé, Stein, R., & Tiedemann, R. (2014). Appraisal of TEX 86 and thermometries in subpolar and polar regions. *Geochimica et Cosmochimica Acta*, *131*, 213-226.

Ho, S. L., & Laepple, T. (2016). Flat meridional temperature gradient in the early Eocene in the subsurface rather than surface ocean. *Nature Geoscience*, *9*(8), 606-610.

Holbourn, A., Kuhnt, W., Lyle, M., Schneider, L., Romero, O., & Andersen, N. (2014). Middle Miocene climate cooling linked to intensification of eastern equatorial Pacific upwelling. *Geology*, *42*(1), 19-22.

Holbourn, A., Kuhnt, W., Kochhann, K. G., Andersen, N., & Meier, K. S. (2015). Global perturbation of the carbon cycle at the onset of the Miocene Climatic Optimum. *Geology*, *43*(2), 123-126.

Hopmans, E. C., Weijers, J. W., Schefuß, E., Herfort, L., Sinninghe Damsté, J. S., & Schouten, S. (2004). A novel proxy for terrestrial organic matter in sediments based on branched and isoprenoid tetraether lipids. *Earth and Planetary Science Letters*, *224*(1), 107-116.

Huguet, C., Kim, J. H., Sinninghe Damsté, J. S., & Schouten, S. (2006). Reconstruction of sea surface temperature variations in the Arabian Sea over the last 23 kyr using organic proxies (TEX_{86} and $U_{37}^{K'}$). *Paleoceanography*, *21*, PA3003, doi:10.1029/2005PA001215.

Inglis, G. N., Farnsworth, A., Lunt, D., Foster, G. L., Hollis, C. J., Pagani, M., Jardine, P. E., Pearson, P. N., Markwick, P., Galsworthy, A. M. J., Raynham, L., Taylor, K. W. R., & Pancost, R. D. (2015). Descent toward the Icehouse: Eocene sea surface cooling inferred from GDGT distributions. *Paleoceanography*, *30*(7), 1000-1020.

Jacobs, S. S., Giulivi, C. F., & Mele, P. A. (2002). Freshening of the Ross Sea during the late 20th Century. *Science, 297*, 386-389.

Jansen, E., Fronval, T., Rack, F., & Channell, J. E. (2000). Pliocene-Pleistocene ice rafting history and cyclicity in the Nordic Seas during the last 3.5 Myr. *Paleoceanography*, *15*(6), 709-721.

John, C. M., Karner, G. D., Browning, E., Leckie, R. M., Mateo, Z., Carson, B., & Lowery, C. (2011). Timing and magnitude of Miocene eustasy derived from the mixed siliciclastic-carbonate stratigraphic record of the northeastern Australian margin. *Earth and Planetary Science Letters*, *304*(3), 455-467.

Jones, R. S., Mackintosh, A. N., Norton, K. P., Golledge, N. R., Fogwill, C. J., Kubik, P. W., Christl, M., & Greenwood, S. L. (2015). Rapid Holocene thinning of an East Antarctic outlet glacier driven by marine ice sheet instability. *Nature communications*, *6*, 8910, doi:10.1038/ncomms9910.

Kahmen, A., Schefuß, E., & Sachse, D. (2013a). Leaf water deuterium enrichment shapes leaf wax n-alkane δD values of angiosperm plants I: Experimental evidence and mechanistic insights. *Geochimica et Cosmochimica Acta*, *111*, 39-49.

Kahmen, A., Hoffmann, B., Schefuß, E., Arndt, S. K., Cernusak, L. A., West, J. B., & Sachse, D. (2013b). Leaf water deuterium enrichment shapes leaf wax n-alkane δD values of angiosperm plants II: Observational evidence and global implications. *Geochimica et Cosmochimica Acta*, *111*, 50-63.

Kalanetra, K. M., Bano, N., & Hollibaugh, J. T. (2009). Ammonia-oxidizing Archaea in the Arctic Ocean and Antarctic coastal waters. *Environmental microbiology*, *11*(9), 2434-2445.

Kawamura, K., Ishimura, Y., & Yamazaki, K. (2003). Four years' observations of terrestrial lipid class compounds in marine aerosols from the western North Pacific. *Global Biogeochemical Cycles*, *17*(1).

Keeley, J. E., & Sandquist, D. R. (1992). Carbon: freshwater plants. *Plant, Cell & Environment*, *15*(9), 1021-1035.

Kemp, E. M. (1975). Palynology of Leg 28 drill sites, Deep Sea Drilling Project. *Initial Reports of the Deep Sea Drilling Project, 28,* 599-623.

Kemp, E. M., & Barrett, P. J. (1975). Antarctic glaciation and early Tertiary vegetation. *Nature, 258,* 507-508.

Kim, J. H., Schouten, S., Hopmans, E. C., Donner, B., & Sinninghe Damsté, J. S. (2008). Global sediment core-top calibration of the TEX_{86} paleothermometer in the ocean. *Geochimica et Cosmochimica Acta*, *72*(4), 1154-1173.

Kim, J. H., Van der Meer, J., Schouten, S., Helmke, P., Willmott, V., Sangiorgi, F., Koç, H., Hopmans, E. C., & Sinninghe Damsté, J. S. (2010). New indices and calibrations derived from the distribution of crenarchaeal isoprenoid tetraether lipids: Implications for past sea surface temperature reconstructions. *Geochimica et Cosmochimica Acta*, *74*(16), 4639-4654.

Kim, J. H., Crosta, X., Willmott, V., Renssen, H., Bonnin, J., Helmke, P., Schouten, S., & Sinninghe Damsté, J. S. (2012). Holocene subsurface temperature variability in the eastern Antarctic continental margin. *Geophysical Research Letters*, *39*(6), L06705, doi:10.1029/2012GL051157.

Kim, J. G., Park, S. J., Quan, Z. X., Jung, M. Y., Cha, I. T., Kim, S. J., Kim, K. H., Kim, Y. N., Lee, S. H., & Rhee, S. K. (2014). Unveiling abundance and distribution of planktonic Bacteria and Archaea in a polynya in Amundsen Sea, Antarctica. *Environmental microbiology*, *16*(6), 1566-1578.

Kim, J. H., Schouten, S., Rodrigo-Gámiz, M., Rampen, S., Marino, G., Huguet, C., Helmke, P., Buscail, R., Hopmans, E. C., Pross, J., & Sangiorgi, F. (2015). Influence of deep-water derived isoprenoid tetraether lipids on the paleothermometer in the Mediterranean Sea. *Geochimica et Cosmochimica Acta*, *150*, 125-141.

Kohn, M. J. (2010). Carbon isotope compositions of terrestrial C3 plants as indicators of (paleo) ecology and (paleo) climate. *Proceedings of the National Academy of Sciences*, *107*(46), 19691-19695.

Kohn, M. J. (2016). Carbon isotope discrimination in C3 land plants is independent of natural variations in pCO2. *Geochemical Perspectives Letters*, *2*(1), 35-43.

Köhler, P., Fischer, H., & Schmitt, J. (2010). Atmospheric $\delta^{13}CO_2$ and its relation to pCO_2 and deep ocean $\delta^{13}C$ during the late Pleistocene. *Paleoceanography*, *25*, PA1213, doi:10.1029/2008PA001703.

Kraus, C. (2016). *Oligocene to early Miocene glacimarine sedimentation of the central Ross Sea, and implications for the evolution of the West Antarctic Ice Sheet* (Unpublished Masters Thesis). Victoria University of Wellington, New Zealand.

Krissek, L. A., & Kyle, P. R. (1998). Geochemical indicators of weathering and Cenozoic palaeoclimates in sediments from CRP-1 and CIROS-1, McMurdo Sound, Antarctica. *Terra Antartica*, *5*(3), 673-680.

Kürschner, W. M., Kvaček, Z., & Dilcher, D. L. (2008). The impact of Miocene atmospheric carbon dioxide fluctuations on climate and the evolution of terrestrial ecosystems. *Proceedings of the National Academy of Sciences*, *105*(2), 449-453.

Kvenvolden, K. A., Rapp, J. B., Golan-Bac, M., & Hostettler, F. D. (1987). Multiple sources of alkanes in Quaternary oceanic sediment of Antarctica. *Organic geochemistry*, *11*(4), 291-302.

Kyle, R. A. (1977). Devonian palynomorphs from the basal Beacon Supergroup of South Victoria Land, Antarctica (Note). *New Zealand Journal of Geology and Geophysics*, *20*(6), 1147-1150.

Kyle, P. R., & Muncy, H. L. (1989). Geology and geochronology of McMurdo Volcanic Group rocks in the vicinity of Lake Morning, McMurdo Sound, Antarctica. *Antarctic Science*, *1*(4), 345-350.

Laskar, J., Robutel, P., Joutel, F., Gastineau, M., Correia, A. C. M., & Levrard, B. (2004). A long-term numerical solution for the insolation quantities of the Earth. *Astronomy & Astrophysics*, *428*(1), 261-285.

Laskar, J., Fienga, A., Gastineau, M., & Manche, H. (2011). La2010: a new orbital solution for the long-term motion of the Earth. *Astronomy & Astrophysics*, *532*, A89.

Lavelle, M., Fielding, C. R., & Hall, M. (2001). Molluscan stable isotope temperature estimates of the southwestern Ross Sea during the early Oligocene and early Miocene, CRP-2/2A and CRP-3, Victoria Land Basin, Antarctica. *Terra Antartica*, *8*(4), 439-444.

Lea, D. W., Pak, D. K., & Spero, H. J. (2000). Climate impact of late Quaternary equatorial Pacific sea surface temperature variations. *Science*, *289*(5485), 1719-1724.

Lear, C. H., Rosenthal, Y., Coxall, H. K., & Wilson, P. A. (2004). Late Eocene to early Miocene ice sheet dynamics and the global carbon cycle. *Paleoceanography*, *19*, PA4015, doi:10.1029/2004PA001039.

Lear, C. H., Bailey, T. R., Pearson, P. N., Coxall, H. K., & Rosenthal, Y. (2008). Cooling and ice growth across the Eocene-Oligocene transition. *Geology*, *36*(3), 251-254.

Leckie, R. M., & Webb, P. N. (1983). Late Oligocene–early Miocene glacial record of the Ross Sea, Antarctica: Evidence from DSDP site 270. *Geology*, *11*(10), 578-582.

Lehtonen, K., & Ketola, M. (1993). Solvent-extractable lipids of Sphagnum, Carex, Bryales and Carex-Bryales peats: content and compositional features vs peat humification. *Organic Geochemistry*, *20*(3), 363-380.

Levy, R. H., & Harwood, D. M. (2000). Tertiary marine palynomorphs from the McMurdo Sound erratics, Antarctica. In J. D. Stilwel & R. M. Feldman (Eds.), *Paleobiology and Paleoenvironments of Eocene Rocks: McMurdo Sound, East Antarctica*, (pp. 183-242). Washington D. C: American Geophysical Union.

Levy, R., Cody, R., Crampton, J., Fielding, C., Golledge, N., Harwood, D., Henrys, S., McKay, R., Naish, T., Ohneiser, C., Wilson, G., Wilson, T., & Winter, D. (2012). Late Neogene climate and glacial history of the Southern Victoria Land coast from integrated drill core, seismic and outcrop data. *Global and Planetary Change*, *80-81*, 61-84.

Levy, R., Harwood, D., Florindo, F., Sangiorgi, F., Tripati, R., von Eynatten, H., Gasson, E., Kuhn. G., Tripati, A., DeConto, R., Fielding, C., Field, B., Golledge, N., McKay, R., Naish, T., Olney, M., Pollard, D., Schouten, S., Talarico, F., Warny, S., Willmott, V., Acton, G., Panter, K., Paulsen, T., Taviani, M., & SMS Science Team (2016). Antarctic ice sheet sensitivity to atmospheric CO_2 variations in the early to mid-Miocene. *Proceedings of the National Academy of Sciences*, *113*(13), 3453-3458.

Lewis, A. R., Marchant, D. R., Kowalewski, D. E., Baldwin, S. L., & Webb, L. E. (2006). The age and origin of the Labyrinth, western Dry Valleys, Antarctica: Evidence for extensive middle Miocene subglacial floods and freshwater discharge to the Southern Ocean. *Geology*, *34*(7), 513-516.

Lewis, A. R., Marchant, D. R., Ashworth, A. C., Hemming, S. R., & Machlus, M. L. (2007). Major middle Miocene global climate change: Evidence from East Antarctica and the Transantarctic Mountains. *Geological Society of America Bulletin*, *119*(11-12), 1449-1461.

Lewis, A.R., Marchant, D. R., Ashworth, A. C., Hedenäs, L., Hemming, S. R, Johnson, J. V., Leng, M. J., Machlus, M. L., Newton, A. E., Raine, J. I., Willenbring, J. K., Williams, M., & Wolfe, A. P. (2008). Mid-Miocene cooling and the extinction of tundra in continental Antarctica. *Proceedings of the National Academy of Sciences, 105*(31), 10676-10680.

Lewis, A. R., & Ashworth, A. C. (2016). An early to middle Miocene record of ice-sheet and landscape evolution from the Friis Hills, Antarctica. *Geological Society of America Bulletin*, *128*(5-6), 719-738.

Liebrand, D., Lourens, L. J., Hodell, D. A., De Boer, B., Van de Wal, R. S. W., & Pälike, H. (2011). Antarctic ice sheet and oceanographic response to eccentricity forcing during the early Miocene. *Climate of the Past*, *7*(3), 869-880.

Lisiecki, L. E., & Raymo, M. E. (2005). A Pliocene-Pleistocene stack of 57 globally distributed benthic δ18O records. *Paleoceanography*, *20*(1), PA1003, doi:10.1029/2004PA001071.

Liu, W., & Yang, H. (2008). Multiple controls for the variability of hydrogen isotopic compositions in higher plant n-alkanes from modern ecosystems. *Global Change Biology*, *14*(9), 2166-2177.

Liu, Z., Pagani, M., Zinniker, D., DeConto, R., Huber, M., Brinkhuis, H., Shah, S. R., Leckie, M. & Pearson, A. (2009). Global cooling during the Eocene-Oligocene climate transition. *Science*, *323*(5918), 1187-1190.

Lomax, B. H., Knight, C. A., & Lake, J. A. (2012). An experimental evaluation of the use of C3 δ13C plant tissue as a proxy for the paleoatmospheric δ13CO2 signature of air. *Geochemistry, Geophysics, Geosystems*, *13*, Q0AI03, doi:10.1029/2012GC004174.

Lunt, D. J., Haywood, A. M., Schmidt, G. A., Salzmann, U., Valdes, P. J., Dowsett, H. J., & Loptson, C. A. (2012). On the causes of mid-Pliocene warmth and polar amplification. *Earth and Planetary Science Letters*, *321*, 128-138.

Luyendyk, B. P., Sorlien, C. C., Wilson, D. S., Bartek, L. R., & Siddoway, C. S. (2001). Structural and tectonic evolution of the Ross Sea rift in the Cape Colbeck region, Eastern Ross Sea, Antarctica. *Tectonics*, *20*(6), 933-958.

Maberly, S. C., & Spence, D. H. N. (1983). Photosynthetic inorganic carbon use by freshwater plants. *The Journal of ecology*, 705-724.

Madureira, L. A., & Piccinini, A. (1999). Lipids as indicators of paleoclimatic changes, II: terrestrial biomarkers. *Revista Brasileira de Oceanografia*, *47*(2), 115-125.

Marchant, D. R., & Denton, G. H. (1996). Miocene and Pliocene paleoclimate of the Dry Valleys region, southern Victoria Land: a geomorphological approach. *Marine Micropaleontology*, *27*(1-4), 253-271.

Marchant, D.R., Denton, G.H., Swisher, C.C., & Potter, N. (1996). Late Cenozoic Antarctic paleoclimate reconstructed from volcanic ashes in the Dry Valleys region of southern Victoria Land. *Geological Society of America Bulletin, 108*(2), 181-194.

Marchant, D. R., Lewis, A. R., Phillips, W. M., Moore, E. J., Souchez, R. A., Denton, G. H., Sugden, D.E., Potter Jr. N., & Landis, G. P. (2002). Formation of patterned ground and sublimation till over Miocene glacier ice in Beacon Valley, southern Victoria Land, Antarctica. *Geological Society of America Bulletin*, *114*(6), 718-730.

Marret, F., & de Vernal, A. (1997). Dinoflagellate cyst distribution in surface sediments of the southern Indian Ocean. *Marine Micropaleontology*, *29*(3-4), 367-392.

Marshall, J. D., & Zhang, J. (1994). Carbon Isotope Discrimination and Water-Use Efficiency in Native Plants of the North-Central Rockies. *Ecology*, *75*(7), 1887-1895.

Marshall, J. D., Brooks, J. R., & Lajtha, K. (2007). Sources of variation in the stable isotopic composition of plants. In R. Michener & K Lajtha (Eds), *Stable isotopes in ecology and environmental science* (pp. 22-60). Oxford: Blackwell Publishing.

Martin, A. P., Cooper, A. F., & Dunlap, W. J. (2010). Geochronology of Mount Morning, Antarctica: two-phase evolution of a long-lived trachyte-basanite-phonolite eruptive center. *Bulletin of Volcanology*, *72*(3), 357-371.

Maslin, M. A., Li, X. S., Loutre, M. F., & Berger, A. (1998). The contribution of orbital forcing to the progressive intensification of Northern Hemisphere glaciation. *Quaternary Science Reviews*, *17*(4-5), 411-426.

Massana, R., Taylor, L. T., Murray, A. E., Wu, K. Y., Jeffrey, W. H., & DeLong, E. F. (1998). Vertical distribution and temporal variation of marine planktonic archaea in the Gerlache Strait, Antarctica, during early spring. *Limnology and Oceanography*, *43*(4), 607-617.

Masson-Delmotte, V., Hou, S., Ekaykin, A., Jouzel, J., Aristarain, A., Bernardo, R. T., Bromwich, D., Cattani, O., Delmotte, M., Falourd, S., Frezzotti, M., Gallée, H., Genoni, L., Isaksson, E., Landais, A., Helsen, M. M., Hoffmann, G., Lopez, J., Morgan, V.,

Motoyama, H., Noone, D., Oerter, H., Petit, J. R., Royer, A., Uemura, R., Schmidt, G. A., Schlosser, E., Simões, J. C., Steig, E. J., Stenni, B., Stievenard, M., van den Broeke, M. R., van de Wal, R. S., van de Berg, W. J., Vimeux, F., & White, J. W. C., (2008). A review of Antarctic surface snow isotopic composition: Observations, atmospheric circulation, and isotopic modeling. *Journal of Climate*, *21*(13), 3359-3387.

Masson-Delmotte, V., Schulz, M., Abe-Ouchi, A., Beer, J., Ganopolski, A., González Rouco, J. F., Jansen, E., Lambeck, K., Luterbacher, J., Naish, T., Osborn, T., Otto-Bliesner, B., Quinn, T., Ramesh, R., Rojas, M., Shao X., & Timmermann, A. (2013). Information from Paleoclimate Archives. In T. F., Stocker, D. Qin, G. -K. Plattner, M. Tignor, S. K. Allen, J. Boschung, A. Nauels, Y. Xia, V. Bex & P. M. Midgley (Eds.). *Climate Change 2013: The Physical Science Basis. Contribution of Working Group I to the Fifth Assessment Report of the Intergovernmental Panel on Climate Change*. Cambridge, United Kingdom and New York, NY: Cambridge University Press.

Matsumoto, G., Torii, T., & Hanya, T. (1981). High abundances of long-chain normal alkanoic acids in Antarctic soil. *Nature*, *290*(5808), 688-690.

Matsumoto, G. I., Watanuki, K., & Torii, T. (1985). Fatty acids in the Beacon Group of southern Victoria Land in Antarctica. *Memoirs of National Institute of Polar Research. Special issue*, *37*, 201-210.

Matsumoto, G. I., Funaki, M., Machihara, T., & Watanuki, K. (1986). Alkanes and alkanoic acids in the Beacon Supergroup samples from the Allan Hills and the Carapace Nunatak in Antarctica. *Memoirs of National Institute of Polar Research. Special issue*, *43*, 149-158.

Matsumoto, G. I., Machihara, T., Suzuki, N., Funaki, M., & Watanuki, K. (1987). Steranes and triterpanes in the Beacon Supergroup samples from southern Victoria Land in Antarctica. *Geochimica et Cosmochimica Acta*, *51*(10), 2663-2671.

Matsumoto, G. I., Akiyama, M., Watanuki, K., & Torii, T. (1990a). Unusual distributions of long-chain n-alkanes and n-alkenes in Antarctic soil. *Organic Geochemistry*, *15*(4), 403-412.

Matsumoto, G. I., Hirai, A., Hirota, K., & Watanuki, K. (1990b). Organic geochemistry of the McMurdo dry valleys soil, Antarctica. *Organic Geochemistry*, *16*(4-6), 781-791.

Matsumoto, G. I., Komori, K., Enomoto, A., Imura, S., Takemura, T., Ohyama, Y., & Kanda, H. (2006). Environmental changes in Syowa Station area of Antarctica during the last 2300 years inferred from organic components in lake sediment cores. *Polar bioscience*, *19*, 51-62.

Matsumoto, G. I., Honda, E., Sonoda, K., Yamamoto, S., & Takemura, T. (2010). Geochemical features and sources of hydrocarbons and fatty acids in soils from the McMurdo Dry Valleys in the Antarctic. *Polar Science*, *4*(2), 187-196.

Mawbey, E. M., & Lear, C. H. (2013). Carbon cycle feedbacks during the Oligocene-Miocene transient glaciation. *Geology*, *41*(9), 963-966.

McCollum, D. W. (1975). Diatom stratigraphy of the Southern Ocean. *Initial Reports of the Deep Sea Drilling Project*, *28*, 515-571.

McDowell, N. G., Bond, B. J., Dickman, L. T., Ryan, M. G., & Whitehead, D. (2011). Relationships between tree height and carbon isotope discrimination. In F. C. Meinzer, B. Lachenbruch & T. E. Dawson (Eds). *Size-and age-related changes in tree structure and function* (pp. 255-286). The Netherlands: Springer Netherlands.

McInerney, F. A., & Wing, S. L. (2011). The Paleocene-Eocene Thermal Maximum: a perturbation of carbon cycle, climate, and biosphere with implications for the future. *Annual Review of Earth and Planetary Sciences*, *39*, 489-516.

McIntyre, D. J., & Wilson, G. J. (1966). Preliminary palynology of some Antarctic Tertiary erratics. *New Zealand journal of botany*, *4*(3), 315-321.

McIver, R. D. (1975). Hydrocarbon gases in canned core samples from Leg 28 Sites 271, 272, and 273, Ross Sea. *Initial Reports of the Deep Sea Drilling Project, 28,* 815-817.

McKay, R. M., Barrett, P. J., Harper, M. A. & Hannah, M. J. (2008). Atmospheric transport and concentration of diatoms in surficial and glacial sediments of the Allan Hills, Transantarctic Mountains. *Palaeogeography, Palaeoclimatology, Palaeoecology*, *260*(1), 168-183.

McKay, R., Browne, G., Carter, L., Cowan, E., Dunbar, G., Krissek, L., Naish, T., Powell, R., Reed, J., Talarico, F., & Wilch, T. (2009). The stratigraphic signature of the late Cenozoic Antarctic Ice Sheets in the Ross Embayment. *Geological Society of America Bulletin*, *121*(11-12), 1537-1561.

McKay, R., Naish, T., Carter, L., Riesselman, C., Dunbar, R., Sjunneskog, C., Winter, D., Sangiorgi, F., Warren, C., Pagini, M., Schouten, S., Willmott, V., Levy, R., DeConto R., & Powell, R. D. (2012a). Antarctic and Southern Ocean influences on Late Pliocene global cooling. *Proceedings of the National Academy of Sciences, 109*(17), 6423-6428.

McKay, R., Naish, T., Powell, R., Barrett, P., Scherer, R., Talarico, F., Kyle, P., Monien, D., Kuhn, G., Jackolski, C., & Williams, T. (2012b). Pleistocene variability of Antarctic ice sheet extent in the Ross embayment. *Quaternary Science Reviews*, *34*, 93-112.

McKay, R. M., Barrett, P. J., Levy, R. S., Naish, T. R., Golledge, N. R., & Pyne, A. (2016). Antarctic Cenozoic climate history from sedimentary records: ANDRILL and beyond. *Philosophical Transactions of the Royal Society A*, *374*(2059), 20140301.

McKay, R.M., De Santis, L., & Kulhanek, D.K., (in press). Ross Sea West Antarctic Ice Sheet History: Ocean-ice sheet interactions and West Antarctic Ice Sheet vulnerability: Clues from the Neogene and Quaternary record of the outer Ross Sea continental margin. *IODP Science Prospectus, 374*. doi:10.2204/iodp.sp.374.2017

McLoughlin, S., & Drinnan, A. N. (1997a). Revised stratigraphy of the Permian Bainmedart Coal Measures, northern Prince Charles Mountains, East Antarctica. *Geological Magazine*, *134*(03), 335-353.

McLoughlin, S., & Drinnan, A. N. (1997b). Fluvial sedimentology and revised stratigraphy of the Triassic Flagstone Bench Formation, northern Prince Charles Mountains, East Antarctica. *Geological Magazine*, *134*(06), 781-806.

McMinn, A., & Harwood, D. (1995). Biostratigraphy and palaeoecology of early Pliocene diatom assemblages from the Larsemann Hills, eastern Antarctica. *Antarctic Science*, *7*(1), 115-116.

Ménot, G., & Burns, S. J. (2001). Carbon isotopes in ombrogenic peat bog plants as climatic indicators: calibration from an altitudinal transect in Switzerland. *Organic Geochemistry*, *32*(2), 233-245.

Ménot-Combes, G., Combes, P. P., & Burns, S. J. (2004). Climatic information from $\delta^{13}C$ in plants by combining statistical and mechanistic approaches. *The Holocene*, *14*(6), 931-939.

Meyers, P. A., & Ishiwatari, R. (1993). Lacustrine organic geochemistry—an overview of indicators of organic matter sources and diagenesis in lake sediments. *Organic geochemistry*, *20*(7), 867-900.

Mildenhall, D. C. (1989). Terrestrial palynology. In P. J. Barrett (Ed), *Antarctic Cenozoic history from the CIROS-1 drillhole, McMurdo Sound*, (pp. 119-127). Wellington, New Zealand: DSIR Publishing.

Miller, M. C., McCave, I. N., & Komar, P. (1977). Threshold of sediment motion under unidirectional currents. *Sedimentology*, *24*(4), 507-527.

Miller, K. G., Wright, J. D., & Fairbanks, R. G. (1991). Unlocking the ice house: Oligocene-Miocene oxygen isotopes, eustasy, and margin erosion. *Journal of Geophysical Research: Solid Earth*, *96*(B4), 6829-6848.

Miller, K. G., Kominz, M. A., Browning, J. V., Wright, J. D., Mountain, G. S., Katz, M. E., Sugarman, P. J., Cramer, B. S., Christie-Blick, N., & Pekar, S. F. (2005). The Phanerozoic record of global sea-level change. *Science*, *310*(5752), 1293-1298.

Miller, K. G., Wright, J. D., Browning, J. V., Kulpecz, A., Kominz, M., Naish, T. R., Cramer, B. S., Rosenthal, Y., Peltier, W. R., & Sosdian, S. (2012). High tide of the warm Pliocene: Implications of global sea level for Antarctic deglaciation. *Geology*, *40*(5), 407-410.

Mook, W. G., Bommerson, J. C., & Staverman, W. H. (1974). Carbon isotope fractionation between dissolved bicarbonate and gaseous carbon dioxide. *Earth and Planetary Science Letters*, *22*(2), 169-176.

Moossen, H., Bendle, J., Seki, O., Quillmann, U., & Kawamura, K. (2015). North Atlantic Holocene climate evolution recorded by high-resolution terrestrial and marine biomarker records. *Quaternary Science Reviews*, *129*, 111-127.

Morin, R. H., Williams, T., Henrys, S. A., Magens, D., Niessen, F., & Hansaraj, D. (2010). Heat flow and hydrologic characteristics at the AND-1B borehole, ANDRILL McMurdo Ice Shelf Project, Antarctica. *Geosphere*, *6*(4), 370-378.

Moritz, R. E., Bitz, C. M., & Steig, E. J. (2002). Dynamics of recent climate change in the Arctic. *Science*, *297*(5586), 1497-1502.

Mudelsee, M., Bickert, T., Lear, C. H., & Lohmann, G. (2014). Cenozoic climate changes: A review based on time series analysis of marine benthic δ18O records. *Reviews of Geophysics*, *52*(3), 333-374.

Mudie, P. J. (1992). Circum-Arctic Quaternary and Neogene marine palynofloras: paleoecology and statistical analysis. In M. J. Head & Wrenn, J. H. (Eds.), *Neogene and Quaternary dinoflagellate cysts and acritarchs* (pp. 347-390). Dallas: American Association of Stratigraphic Palynologists Foundation.

Murray, A. E., Preston, C. M., Massana, R., Taylor, L. T., Blakis, A., Wu, K., & DeLong, E. F. (1998). Seasonal and spatial variability of bacterial and archaeal assemblages in the coastal waters near Anvers Island, Antarctica. *Applied and Environmental Microbiology*, *64*(7), 2585-2595.

Naish, T. R., Barrett, P. J., Dunbar, G. B., Woolfe, K. J., Dunn, A. G., Henrys, S. A., Claps, M., Powell, R. D., & Fielding, C. R. (2001a). Sedimentary cyclicity in CRP drillcore, Victoria Land Basin, Antarctica. *Terra Antarctica, 8*(3), 225-244.

Naish, T. R., Woolfe, K. J., Barrett, P. J., Wilson, G. S., Atkins, C., Bohaty, S. M., Bücker, C.J., Claps, M., Davey, F.J., Dunbar, G.B., Dunn, A.G., Fielding, C.R., Florindo, F., Hannah, M.J., Harwood, D.M., Henrys, S.A., Krissek, L.A., Lavelle, M., van der Meer, J., McIntosh, W.C., Niessen, F., Passchier, S., Powell, R.D., Roberts, A.P., Sagnotti, L., Scherer, R.P., Strong, C.P., Talarico, F., Verosub, K.L., Villa, G., Watkins, D.K., Webb, P.-N., & Wonik, T. (2001b). Orbitally induced oscillations in the East Antarctic ice sheet at the Oligocene/Miocene boundary. *Nature*, *413*(6857), 719-723.

Naish, T., Powell, R., Levy, R., Florindo, F., Harwood, D., Kuhn, G., Niessen, F., Talarico, F., & Wilson, G. (2007). A record of Antarctic climate and ice sheet history recovered. *Eos, Transactions American Geophysical Union*, *88*(50), 557-558.

Naish, T. R., Wilson, G. S., Dunbar, G. B., & Barrett, P. J. (2008). Constraining the amplitude of Late Oligocene bathymetric changes in western Ross Sea during orbitally-induced oscillations in the East Antarctic Ice Sheet:(2) Implications for global sea-level changes. *Palaeogeography, Palaeoclimatology, Palaeoecology*, *260*(1), 66-76.

Naish, T., Powell, R., Levy, R., Wilson, G., Scherer, R., Talarico, F., Krissek, L., Niessen, F., Pompilio, M., Wilson, T., Carter, L., DeConto, R., Huybers, P., McKay, R., Pollard, D., Ross, J., Winter, D., Barrett, P., Browne, G., Cody, R., Cowan, E., Crampton, J., Dunbar, G., Dunbar, N., Florindo, F., Gebhardt, C., Graham, I., Hannah, M., Hansaraj, D., Harwood, D., Helling, D., Henrys, S., Hinnov, L., Kuhn, G., Kyle, P., Läufer, A., Maffioli, P., Magens, D., Mandernack, K., McIntosh, W., Millan, C., Morin R., Ohneiser, C., Paulsen, T., Persico, D., Raine, I., Reed, J., Riesselman, C., Sagnotti, L., Schmitt, D., Sjunneskog, C., Strong, P., Taviani, M., Vogel, S., Wilch T., & Williams, T. (2009). Obliquity-paced Pliocene West Antarctic ice sheet oscillation. *Nature, 458,* 322-328.

Nichols, J. E., Booth, R. K., Jackson, S. T., Pendall, E. G., & Huang, Y. (2006). Paleohydrologic reconstruction based on *n*-alkane distributions in ombrotrophic peat. *Organic Geochemistry*, *37*(11), 1505-1513.

Nott, C. J., Xie, S., Avsejs, L. A., Maddy, D., Chambers, F. M., & Evershed, R. P. (2000). n-Alkane distributions in ombrotrophic mires as indicators of vegetation change related to climatic variation. *Organic Geochemistry*, *31*(2), 231-235.

Orsi, A. H., & Wiederwohl, C. L. (2009). A recount of Ross Sea waters. *Deep Sea Research Part II: Topical Studies in Oceanography*, *56*(13), 778-795.

Pagani, M., Zachos, J. C., Freeman, K. H., Tipple, B., & Bohaty, S. (2005). Marked decline in atmospheric carbon dioxide concentrations during the Paleogene. *Science*, *309*(5734), 600-603.

Pagani, M., Huber, M., Liu, Z., Bohaty, S. M., Hendericks, J., Sijp, W., Krishnan, S., & DeConto R. M. (2011). The role of carbon dioxide during the onset of Antarctic Glaciation. *Science, 334*(6060), 1261-1264.

Pälike, H., Frazier, J., & Zachos, J. C. (2006a). Extended orbitally forced palaeoclimatic records from the equatorial Atlantic Ceara Rise. *Quaternary Science Reviews*, *25*(23), 3138-3149.

Pälike, H., Norris, R.D., Herrie, J.O., Wilson, P.A., Coxall, H.K., Lear, C.H., Shackleton, N.J., Tripati, A.K., & Wade, B.S. (2006b). The heartbeat of the Oligocene climate system, *Science, 314*(5807), 1894-1898.

Pancost, R. D., Hopmans, E. C., & Sinninghe Damsté, J. S. and The MEDINAUT Shipboard Scientific Party (2001). Archaeal lipids in Mediterranean cold seeps: molecular proxies for anaerobic methane oxidation. *Geochimica et Cosmochimica Acta*, *65*(10), 1611-1627.

Pancost, R. D., Baas, M., van Geel, B., & Sinninghe Damsté, J. S. (2002). Biomarkers as proxies for plant inputs to peats: an example from a sub-boreal ombrotrophic bog. *Organic Geochemistry*, *33*(7), 675-690.

Pancost, R. D., Baas, M., van Geel, B., & Sinninghe Damsté, J. S. (2003). Response of an ombrotrophic bog to a regional climate event revealed by macrofossil, molecular and carbon isotopic data. *The Holocene*, *13*(6), 921-932.

Pascher, K. M., Hollis, C. J., Bohaty, S. M., Cortese, G., McKay, R. M., Seebeck, H., Suzuki, N., & Chiba, K. (2015). Expansion and diversification of high-latitude radiolarian assemblages in the late Eocene linked to a cooling event in the Southwest Pacific. *Climate of the Past*, *11*(12), 1599-1620.

Passchier, S., & Krissek, L. A. (2008). Oligocene–Miocene Antarctic continental weathering record and paleoclimatic implications, Cape Roberts drilling project, Ross Sea, Antarctica. *Palaeogeography, Palaeoclimatology, Palaeoecology*, *260*(1), 30-40.

Passchier, S., Browne, G., Field, B., Fielding, C. R., Krissek, L. A., Panter, K., & Pekar, S. F. (2011). Early and middle Miocene Antarctic glacial history from the sedimentary facies

distribution in the AND-2A drill hole, Ross Sea, Antarctica. *Geological Society of America Bulletin*, *123*(11-12), 2352-2365.

Passchier, S., Bohaty, S. M., Jiménez-Espejo, F., Pross, J., Röhl, U., van de Flierdt, T., Escutia, C., & Brinkhuis, H. (2013). Early Eocene to middle Miocene cooling and aridification of East Antarctica. *Geochemistry, Geophysics, Geosystems, 14*(5), 1399-1410.

Patterson, M. O., McKay, R., Naish, T., Escutia, C., Jimenez-Espejo, F. J., Raymo, M. E., Meyers, S. R., Tauxe, L., Brinkhuis, H., & IODP Expedition 318 Scientists (2014). Orbital forcing of the East Antarctic ice sheet during the Pliocene and Early Pleistocene. *Nature Geoscience*, *7*(11), 841-847.

Paul, H. A., Zachos, J. C., Flower, B. P., & Tripati, A. (2000). Orbitally induced climate and geochemical variability across the Oligocene/Miocene boundary. *Paleoceanography*, *15*(5), 471-485.

Pearson, A., Huang, Z., Ingalls, A. E., Romanek, C. S., Wiegel, J., Freeman, K. H., Smittenberg, R. H., & Zhang, C. L. (2004). Nonmarine crenarchaeol in Nevada hot springs. *Applied and Environmental Microbiology*, *70*(9), 5229-5237.

Pearson, P. N., Foster, G. L., & Wade, B. S. (2009). Atmospheric carbon dioxide through the Eocene–Oligocene climate transition. *Nature*, *461*(7267), 1110-1113.

Pearson, E. J., Juggins, S., Talbot, H. M., Weckström, J., Rosén, P., Ryves, D. B., Roberts, S. J., & Schmidt, R. (2011). A lacustrine GDGT-temperature calibration from the Scandinavian Arctic to Antarctic: Renewed potential for the application of GDGT-paleothermometry in lakes. *Geochimica et Cosmochimica Acta*, *75*(20), 6225-6238.

Peat, H. J., Clarke, A., & Convey, P. (2007). Diversity and biogeography of the Antarctic flora. *Journal of biogeography, 34,* 132-146.

Pekar, S. F., & DeConto, R. M. (2006). High-resolution ice-volume estimates for the early Miocene: Evidence for a dynamic ice sheet in Antarctica. *Palaeogeography, Palaeoclimatology, Palaeoecology*, *231*(1), 101-109.

Pekar, S. F., DeConto, R. M., & Harwood, D. M. (2006). Resolving a late Oligocene conundrum: deep-sea warming and Antarctic glaciation. *Palaeogeography, Palaeoclimatology, Palaeoecology*, *231*(1), 29-40.

Peri, P. L., Ladd, B., Pepper, D. A., Bonser, S. P., Laffan, S. W., & Amelung, W. (2012). Carbon (δ13C) and nitrogen (δ15N) stable isotope composition in plant and soil in Southern Patagonia's native forests. *Global Change Biology*, *18*(1), 311-321.

Peterse, F., Kim, J. H., Schouten, S., Kristensen, D. K., Koç, N., & Sinninghe Damsté, J. S. (2009). Constraints on the application of the MBT/CBT palaeothermometer at high latitude environments (Svalbard, Norway). *Organic Geochemistry*, *40*(6), 692-699.

Peterse, F., Nicol, G. W., Schouten, S., & Sinninghe Damsté, J. S. (2010). Influence of soil pH on the abundance and distribution of core and intact polar lipid-derived branched GDGTs in soil. *Organic Geochemistry*, *41*(10), 1171-1175.

Peterse, F., van der Meer, J., Schouten, S., Weijers, J. W., Fierer, N., Jackson, R. B., Kim, J. H., & Sinninghe Damsté, J. S.(2012). Revised calibration of the MBT–CBT paleotemperature proxy based on branched tetraether membrane lipids in surface soils. *Geochimica et Cosmochimica Acta*, *96*, 215-229.

Petit, J. R., Jouzel, J., Raynaud, D., Barkov, N. I., Barnola, J. M., Basile, I., Bender, M., Chappellaz, J., Davis, M., Delaygue, G., Delmotte, M., Kotlyakov, V. M., Legrand, M., Lipenkov, V. Y., Lorius, C., Pépin, L., Ritz, C., Saltzman, E., & Stievenard, M. (1999). Climate and atmospheric history of the past 420,000 years from the Vostok ice core, Antarctica. *Nature*, *399*(6735), 429-436.

Pitcher, A., Wuchter, C., Siedenberg, K., Schouten, S., & Sinninghe Damsté, J. S. (2011). Crenarchaeol tracks winter blooms of ammonia-oxidizing Thaumarchaeota in the coastal North Sea. *Limnology and Oceanography*, *56*(6), 2308-2318.

Pole, M., Hill, B., & Harwood, D. (2000). Eocene plant macrofossils from erratics, McMurdo Sound, Antarctica. In J. D. Stilwel & R. M. Feldman (Eds.), *Paleobiology and Paleoenvironments of Eocene Rocks: McMurdo Sound, East Antarctica*, (pp. 243-251). Washington D. C: American Geophysical Union.

Polissar, P. J., Freeman, K. H., Rowley, D. B., McInerney, F. A., & Currie, B. S. (2009). Paleoaltimetry of the Tibetan Plateau from D/H ratios of lipid biomarkers. *Earth and Planetary Science Letters*, *287*(1), 64-76.

Pollard, D. & DeConto, R.M. (2005). Hysteresis in Cenozoic Antarctic ice-sheet variations. *Global and Planetary Change*, *45*(1), 9-21.

Pollard, D., & DeConto, R. M. (2009). Modelling West Antarctic ice sheet growth and collapse through the past five million years. *Nature, 458*(7236), 329-332.

Pollard, D., DeConto, R. M., & Alley, R. B. (2015). Potential Antarctic Ice Sheet retreat driven by hydrofracturing and ice cliff failure. *Earth and Planetary Science Letters*, *412*, 112-121.

Polley, H. W., Johnson, H. B., Marino, B. D., & Mayeux, H. S. (1993). Increase in C3 plant water-use efficiency and biomass over Glacial to present CO_2 concentrations. *Nature*, *361*, 61-64.

Powell, R., Krissek, L. A., & Van der Meer, J. (2000). Preliminary depositional environmental analysis of CRP-2/2A, Victoria Land Basin, Antarctica: palaeoglaciological and palaeoclimatic inferences. *Terra Antartica*, *7*(3), 313-322.

Powell, R. D., & Cooper, J. M. (2002). A glacial sequence stratigraphic model for temperate, glaciated continental shelves. *Geological Society, London, Special Publications*, *203*(1), 215-244.

Powell, R.D., & Domack, E.W. (2002). Modern glacimarine environments. In J. Menzies (Ed.), *Modern and Past Glacial Environments* (pp. 361-390). Boston: Butterworth-Heinemann.

Poynter, J. G., Farrimond, P., Robinson, N., & Eglinton, G. (1989). Aeolian-derived higher plant lipids in the marine sedimentary record: Links with palaeoclimate. In M. Leinen &

M. Sarnthein (Eds.) *Paleoclimatology and paleometeorology: modern and past patterns of global atmospheric transport* (pp. 435-462). Springer Netherlands.

Prebble, J. G., Raine, J. I., Barrett, P. J., & Hannah, M. J. (2006a). Vegetation and climate from two Oligocene glacioeustatic sedimentary cycles (31 and 24 Ma) cored by the Cape Roberts Project, Victoria Land Basin, Antarctica. *Palaeogeography, Palaeoclimatology, Palaeoecology, 23,* 41-57.

Prebble, J. G., Hannah, M. J., & Barrett, P. J. (2006b). Changing Oligocene climate recorded by palynomorphs from two glacio-eustatic sedimentary cycles, Cape Roberts Project, Victoria Land Basin, Antarctica. *Palaeogeography, Palaeoclimatology, Palaeoecology*, *231*(1), 58-70.

Prebble et al. (in prep.). Title to be confirmed.

Pross, J., Contreras, L., Bijl, P. K., Greenwood, D. R., Bohaty, S. M., Schouten, S., Bendle, J. A., Röhl, U., Tauxe, L., Raine, J. I., Huck, C. E., van de Flierdt, T., Jamieson, S. S. R., Stickley, C. E., van de Scootbrugge, B., Escutia, C., Brinkhuis, H., & Integrated Ocean Drilling Program Expedition 318 Scientists (2012). Persistent near-tropical warmth on the Antarctic continent during the early Eocene epoch. *Nature*, *488*(7409), 73-77.

Qin, W., Carlson, L. T., Armbrust, E. V., Devol, A. H., Moffett, J. W., Stahl, D. A., & Ingalls, A. E. (2015). Confounding effects of oxygen and temperature on the TEX$_{86}$ signature of marine Thaumarchaeota. *Proceedings of the National Academy of Sciences*, *112*(35), 10979-10984.

Quilty, P. G., Lirio, J. M., & Jillett, D. (2000). Stratigraphy of the Pliocene Sørsdal Formation, Marine Plain, Vestfold Hills, East Antarctica. *Antarctic Science*, *12*(02), 205-216.

Raine, J. I. (1998). Terrestrial palynomorphs from Cape Roberts Project drillhole CRP-1, Ross Sea, Antarctica. *Terra Antartica*, *5*(3), 539-548.

Raine, J. I., & Askin, R. A. (2001). Terrestrial palynology of Cape Roberts Project Drillhole CRP-3, Victoria Land Basin, Antarctica. *Terra Antartica*, *8*(4), 389-400.

Read, J., & Farquhar, G. (1991). Comparative studies in Nothofagus (Fagaceae). I. Leaf carbon isotope discrimination. *Functional Ecology, 5*(5), 684-695.

Read, J., Hill, R. S., & Hope, G. S. (2010). Contrasting responses to water deficits of Nothofagus species from tropical New Guinea and high-latitude temperate forests: can rainfall regimes constrain latitudinal range?. *Journal of biogeography*, *37*(10), 1962-1976.

Ribecai, C. (2007). Early Jurassic miospores from Ferrar Group of Carapace Nunatak, South Victoria Land, Antarctica. *Review of Palaeobotany and Palynology*, *144*(1-2), 3-12.

Rice, S. K., & Giles, L. (1996). The influence of water content and leaf anatomy on carbon isotope discrimination and photosynthesis in Sphagnum. *Plant, Cell & Environment*, *19*(1), 118-124.

Roberts, A. P., Wilson, G. S., Harwood, D. M., & Verosub, K. L. (2003). Glaciation across the Oligocene–Miocene boundary in southern McMurdo Sound, Antarctica: new chronology

from the CIROS-1 drill hole. *Palaeogeography, Palaeoclimatology, Palaeoecology, 198*(1), 113-130.

Robinson, S. A., Ruhl, M., Astley, D. L., Naafs, B. D. A., Farnsworth, A. J., Bown, P. R., Jenkyns, H. C., Lunt, D. J., O'Brien, C., Pancost, R. D., & Markwick, P. J. (2016). Early Jurassic North Atlantic sea-surface temperatures from TEX$_{86}$ palaeothermometry. *Sedimentology, 64*(1), 215-230.

Rocchi, S., LeMasurier, W. E., & Di Vincenzo, G. (2006). Oligocene to Holocene erosion and glacial history in Marie Byrd Land, West Antarctica, inferred from exhumation of the Dorrel Rock intrusive complex and from volcano morphologies. *Geological Society of America Bulletin, 118*(7-8), 991-1005.

Romanek, C. S., Grossman, E. L., & Morse, J. W. (1992). Carbon isotopic fractionation in synthetic aragonite and calcite: effects of temperature and precipitation rate. *Geochimica et Cosmochimica Acta, 56*(1), 419-430.

Ross, J. I., McIntosh, W. C., & Dunbar, N. W. (2012). Development of a precise and accurate age–depth model based on 40 Ar/39 Ar dating of volcanic material in the ANDRILL (1B) drill core, Southern McMurdo Sound, Antarctica. *Global and Planetary Change, 96*, 118-130.

Sachse, D., Radke, J., & Gleixner, G. (2004). Hydrogen isotope ratios of recent lacustrine sedimentary n-alkanes record modern climate variability. *Geochimica et Cosmochimica Acta, 68*(23), 4877-4889.

Sachse, D., Radke, J., & Gleixner, G. (2006). δD values of individual n-alkanes from terrestrial plants along a climatic gradient–Implications for the sedimentary biomarker record. *Organic Geochemistry, 37*(4), 469-483.

Sachse, D., Billault, I., Bowen, G. J., Chikaraishi, Y., Dawson, T. E., Feakins, S. J., Freeman, K. H., Magill, C. R., McInerney, F. A., van der Meer, M. T. J., Polissar, P., Robins, R. J., Sachs, J. P., Schmidt, H. -L., Sessions, A. L., White, J. W. C., West, J. B., & Kahmen, A. (2012). Molecular paleohydrology: Interpreting the hydrogen-isotopic composition of lipid biomarkers from photosynthesizing organisms. *Annual Review of Earth and Planetary Sciences, 40,* 221-249.

Sackett, W. M., Poag, C. W., & Eadie, B. J. (1974). Kerogen recycling in the Ross sea, Antarctica. *Science, 185*(4156), 1045-1047.

Sandroni, S., & Talarico, F. (2004). Petrography and provenance of basement clasts in CIROS-1 core, McMurdo Sound, Antarctica. *Terra Antartica, 11*, 93-114.

Sandroni, S., & Talarico, F. M. (2011). The record of Miocene climatic events in AND-2A drill core (Antarctica): Insights from provenance analyses of basement clasts. *Global and Planetary Change, 75*(1), 31-46.

Sauer, P. E., Eglinton, T. I., Hayes, J. M., Schimmelmann, A. & Sessions, A. L. (2001). Compound-specific D/H ratios of lipid biomarkers from sediments as a proxy for

environmental and climatic conditions. *Geochimica et Cosmochimica Acta*, *65*(2), 213-222.

Scalan, E. S., & Smith, J. E. (1970). An improved measure of the odd-even predominance in the normal alkanes of sediment extracts and petroleum. *Geochimica et Cosmochimica Acta*, *34*(5), 611-620.

Schefuß, E., Ratmeyer, V., Stuut, J. B. W., Jansen, J. H. F., & Sinninghe Damsté, J. S. (2003). Carbon isotope analyses of *n*-alkanes in dust from the lower atmosphere over the central eastern Atlantic. *Geochimica et Cosmochimica Acta*, *67*(10), 1757-1767.

Schefuß, E., Schouten, S., & Schneider, R. R. (2005). Climatic controls on central African hydrology during the past 20,000 years. *Nature*, *437*(7061), 1003-1006.

Scher, H. D., Bohaty, S. M., Smith, B. W., & Munn, G. H. (2014). Isotopic interrogation of a suspected late Eocene glaciation. *Paleoceanography*, *29*(6), 628-644.

Scher, H. D., Whittaker, J. M., Williams, S. E., Latimer, J. C., Kordesch, W. E., & Delaney, M. L. (2015). Onset of Antarctic Circumpolar Current 30 million years ago as Tasmanian Gateway aligned with westerlies. *Nature*, *523*(7562), 580-583.

Schmitt, J., Schneider, R., Elsig, J., Leuenberger, D., Lourantou, A., Chappellaz, J., Köhler, P., Joos, F., Stocker, T. F., Leuenberger, M., & Fischer, H. (2012). Carbon isotope constraints on the deglacial CO2 rise from ice cores. *Science*, *336*(6082), 711-714.

Schoof, C. (2007). Ice sheet grounding line dynamics: Steady states, stability, and hysteresis. *Journal of Geophysical Research: Earth Surface*, *112*, F03S28, doi:10.1029/2006JF000664

Schouten, S., Hopmans, E. C., Schefuß, E., & Sinninghe Damsté, J. S. (2002). Distributional variations in marine crenarchaeotal membrane lipids: a new tool for reconstructing ancient sea water temperatures? *Earth and Planetary Science Letters*, *204*(1), 265-274.

Schouten, S., Hopmans, E. C., & Sinninghe Damsté, J. S. (2004). The effect of maturity and depositional redox conditions on archaeal tetraether lipid palaeothermometry. *Organic Geochemistry*, *35*(5), 567-571.

Schouten, S., Huguet, C., Hopmans, E. C., Kienhuis, M. V., & Sinninghe Damsté, J. S. (2007). Analytical methodology for TEX86 paleothermometry by high-performance liquid chromatography/atmospheric pressure chemical ionization-mass spectrometry. *Analytical Chemistry*, *79*(7), 2940-2944.

Schouten, S., Hopmans, E. C., & Sinninghe Damsté, J. S. (2013). The organic geochemistry of glycerol dialkyl glycerol tetraether lipids: a review. *Organic geochemistry*, *54*, 19-61.

Schröder, H., Paulsen, T., & Wonik, T. (2011). Thermal properties of the AND-2A borehole in the southern Victoria Land Basin, McMurdo Sound, Antarctica. *Geosphere*, *7*(6), 1324-1330.

Schubert, B. A., & Jahren, A. H. (2012). The effect of atmospheric CO_2 concentration on carbon isotope fractionation in C3 land plants. *Geochimica et Cosmochimica Acta*, *96*, 29-43.

Schubert, B. A., & Jahren, A. H. (2015). Global increase in plant carbon isotope fractionation following the Last Glacial Maximum caused by increase in atmospheric pCO$_2$. *Geology*, *43*(5), 435-438.

Seki, O., Meyers, P. A., Kawamura, K., Zheng, Y., & Zhou, W. (2009). Hydrogen isotopic ratios of plant wax n-alkanes in a peat bog deposited in northeast China during the last 16kyr. *Organic Geochemistry*, *40*(6), 671-677.

Seki, O., Foster, G.L., Schmidt, D.N., Mackensen, A., Kawamura, K., & Pancost, R.D. (2010). Alkenone and boron-based Pliocene *p*CO$_2$ records. *Earth and Planetary Science Letters, 292*(1-2)*, 201-211.

Seki, O., Bendle, J. A., Harada, N., Kobayashi, M., Sawada, K., Moossen, H., Inglis, G. N., Nagao, S., & Sakamoto, T. (2014). Assessment and calibration of TEX$_{86}$ paleothermometry in the Sea of Okhotsk and sub-polar North Pacific region: Implications for paleoceanography. *Progress in Oceanography*, *126*, 254-266.

Sessions, A. L., Burgoyne, T. W., Schimmelmann, A., & Hayes, J. M. (1999). Fractionation of hydrogen isotopes in lipid biosynthesis. *Organic Geochemistry*, *30*(9), 1193-1200.

Shackleton, N. J., & Kennett, J. P. (1975). Paleotemperature history of the Cenozoic and the initiation of Antarctic glaciation: oxygen and carbon isotope analyses in DSDP Sites 277, 279, and 281. *Initial reports of the deep sea drilling project*, *29*, 743-755.

Shevenell, A. E., Kennett, J. P., & Lea, D. W. (2004). Middle Miocene southern ocean cooling and Antarctic cryosphere expansion. *Science*, *305* (5691), 1766-1770.

Shevenell, A. E., & Kennett, J. P. (2007). Cenozoic Antarctic cryosphere evolution: Tales from deep-sea sedimentary records. *Deep Sea Research Part II: Topical Studies in Oceanography*, *54*(21), 2308-2324.

Shevenell, A. E., Kennett, J. P., & Lea, D. W. (2008). Middle Miocene ice sheet dynamics, deep-sea temperatures, and carbon cycling: A Southern Ocean perspective. *Geochemistry, Geophysics, Geosystems*, *9*(2), Q02006, doi:10.1029/2007GC001736.

Shevenell, A. E., Ingalls, A. E., Domack, E. W., & Kelly, C. (2011). Holocene Southern Ocean surface temperature variability west of the Antarctic Peninsula. *Nature*, *470*(7333), 250-254.

Sinninghe Damsté, J. S., Rijpstra, W. I. C., Hopmans, E. C., Weijers, J. W., Foesel, B. U., Overmann, J., & Dedysh, S. N. (2011). 13, 16-Dimethyl octacosanedioic acid (iso-diabolic acid), a common membrane-spanning lipid of Acidobacteria subdivisions 1 and 3. *Applied and Environmental Microbiology*, *77*(12), 4147-4154.

Sinninghe Damsté, J. S., Ossebaar, J., Schouten, S., & Verschuren, D. (2012). Distribution of tetraether lipids in the 25-ka sedimentary record of Lake Challa: extracting reliable TEX$_{86}$ and MBT/CBT palaeotemperatures from an equatorial African lake. *Quaternary Science Reviews*, *50*, 43-54.

Sjunneskog, C., & Scherer, R. P. (2005). Mixed diatom assemblages in glacigenic sediment from the central Ross Sea, Antarctica. *Palaeogeography, Palaeoclimatology, Palaeoecology*, *218*(3), 287-300.

Skrzypek, G., Kałużny, A., Wojtuń, B., & Jędrysek, M. O. (2007). The carbon stable isotopic composition of mosses: a record of temperature variation. *Organic geochemistry*, *38*(10), 1770-1781.

Sluijs, A., Schouten, S., Pagani, M., Woltering, M., Brinkhuis, H., Sinninghe Damsté, J. S., Dickens, G. R., Huber, M., Reichart, G. –J., Stein, R., Matthiessen, J., Lourens, L. J., Pedentchouk, N., Backman, J., Moran, K., & the Expedition 302 Scientists (2006). Subtropical Arctic Ocean temperatures during the Palaeocene/Eocene thermal maximum. *Nature*, *441*(7093), 610-613.

Smellie, J. L. (2000). Erosional history of the Transantarctic Mountains deduced from sand grain detrital modes in CRP-2/2A, Victoria Land Basin, Antarctica. *Terra Antartica*, *7*(4), 545-552.

Smellie, J. L. (2001). History of Oligocene erosion, uplift and unroofing of the Transantarctic Mountains deduced from sandstone detrital modes in CRP-3 drillcore, Victoria Land Basin, Antarctica. *Terra Antartica*, *8*(4), 481-490.

Smith, B. N., & Epstein, S. (1971). Two categories of ^{13}C/^{12}C ratios for higher plants. *Plant physiology*, *47*(3), 380-384.

Smith, F. A., Wing, S. L., & Freeman, K. H. (2007). Magnitude of the carbon isotope excursion at the Paleocene–Eocene thermal maximum: the role of plant community change. *Earth and Planetary Science Letters*, *262*(1), 50-65.

Smith, W. O., Sedwick, P. N., Arrigo, K. R., Ainley, D. G., & Orsi, A. H. (2012). The Ross Sea: In a Sea of Change. *Oceanography*, *25*(3), 90-103.

Sorlien, C. C., Luyendyk, B. P., Wilson, D. S., Decesari, R. C., Bartek, L. R., & Diebold, J. B. (2007). Oligocene development of the West Antarctic Ice Sheet recorded in eastern Ross Sea strata. *Geology*, *35*(5), 467-470.

Sosdian, S., & Rosenthal, Y. (2009). Deep-sea temperature and ice volume changes across the Pliocene-Pleistocene climate transitions. *Science*, *325*(5938), 306-310.

Stocchi, P., Escutia, C., Houben, A. J., Vermeersen, B. L., Bijl, P. K., Brinkhuis, H., DeConto, R. M., Galeotti, S., Passchier, S., Pollard, D., Brinkhuis, H., Escutia, C., Klaus, A., Fehr, A., Williams, T., Bendle, J. A. P., Bijl, P. K., Bohaty, S. M., Carr, S. A., Dunbar, R. B., Flores, J. A., Gonzàlez, J. J., Hayden, T. G., Iwai, M., Jimenez-Espejo, F. J., Katsuki, K., Kong, G. S., McKay, R. M., Nakai, M., Olney, M. P., Passchier, S., Pekar, S. F., Pross, J., Riesselman, C., Röhl, U., Sakai, T., Shrivastava, P. K., Stickley, C. E., Sugisaki, S., Tauxe, L., Tuo, S., van de Flierdt, T., Welsh, K., & Masako Yamane & (2013). Relative sea-level rise around East Antarctica during Oligocene glaciation. *Nature Geoscience*, *6*(5), 380-384.

Studinger, M., & Barrett, P. (2009). Tectonics: Antarctica sinking. *Nature Geoscience*, *2*(10), 671-672.

Sturm, M., Schimel, J., Michaelson, G., Welker, J. M., Oberbauer, S. F., Liston, G. E., Fahnestock, J., & Romanovsky, V. E. (2005). Winter biological processes could help convert arctic tundra to shrubland. *Bioscience*, *55*(1), 17-26.

Sugden, D. E., Marchant, D. R., & Denton, G. H. (1993). The case for a stable East Antarctic ice sheet: the background. *Geografiska Annaler. Series A. Physical Geography, 75*(4), 151-154.

Sugden, D. E., Marchant, D. R., Potter Jr, N., Souchez, R. A., Denton, G. H., Swisher III, C. C., & Tison, J. L. (1995). Preservation of Miocene glacier ice in East Antarctica. *Nature*, *376*(6539), 412-414.

Sugden, D., & Denton, G. (2004). Cenozoic landscape evolution of the Convoy Range to Mackay Glacier area, Transantarctic Mountains: onshore to offshore synthesis. *Geological Society of America Bulletin*, *116*(7-8), 840-857.

Talarico, F., Sandroni, S., Fielding, C. R., & Atkins, C. (2000). Variability, petrography and provenance of basement clasts in core from CRP-2/2A, Victoria Land Basin, Antarctica. *Terra Antartica*, *7*(4), 529-544.

Talarico, F. M., & Sandroni, S. (2009). Provenance signatures of the Antarctic Ice Sheets in the Ross Embayment during the Late Miocene to Early Pliocene: the ANDRILL AND-1B core record. *Global and Planetary Change*, *69*(3), 103-123.

Taylor, K. W., Huber, M., Hollis, C. J., Hernandez-Sanchez, M. T., & Pancost, R. D. (2013). Re-evaluating modern and Palaeogene GDGT distributions: Implications for SST reconstructions. *Global and Planetary Change*, *108*, 158-174.

The Shipboard Scientific Party (1975a). Shipboard Site Reports: Sites 270, 271, 272. *Initial Reports of the Deep Sea Drilling Project*, *28*, 211-334.

The Shipboard Scientific Party (1975b). Shipboard Site Reports: Site 274. *Initial Reports of the Deep Sea Drilling Project*, *28*, 369-433.

Thorn, V. C., & DeConto, R. (2006). Antarctic climate at the Eocene/Oligocene boundary— climate model sensitivity to high latitude vegetation type and comparisons with the palaeobotanical record. *Palaeogeography, Palaeoclimatology, Palaeoecology*, *231*(1), 134-157.

Tierney, J. E., & Tingley, M. P. (2014). A Bayesian, spatially-varying calibration model for the TEX_{86} proxy. *Geochimica et Cosmochimica Acta*, *127*, 83-106.

Tierney, J. E., & Tingley, M. P. (2015). A TEX_{86} surface sediment database and extended Bayesian calibration. *Scientific data*, *2*, 150029, doi:10.1038/sdata.2015.29.

Tingey, R.J., (1991). The regional geology of Archaean and Proterozoic rocks in Antarctica. In R. J. Tingey (Ed.), *The Geology of Antarctica* (pp. 1-73). Oxford: Oxford University Press.

Tipple, B. J., Meyers, S. R., & Pagani, M. (2010). Carbon isotope ratio of Cenozoic CO2: A comparative evaluation of available geochemical proxies. *Paleoceanography*, *25*, PA3202, doi:10.1029/2009PA001851.

Tissot, B. P., & Welte, D.H. (1984). *Petroleum Formation and Occurance* (2nd ed.). Berlin Heidelberg: Springer-Verlag.

Troedson, A. L., & Riding, J. B. (2002). Upper Oligocene to lowermost Miocene strata of King George Island, South Shetland Islands, Antarctica: stratigraphy, facies analysis, and implications for the glacial history of the Antarctic Peninsula. *Journal of Sedimentary Research*, *72*(4), 510-523.

Truswell, E. M., & Drewry, D. J. (1984). Distribution and provenance of recycled palynomorphs in surficial sediments of the Ross Sea, Antarctica. *Marine Geology*, *59*(1-4), 187-214.

Turner, B. R., & Padley, D. (1991). Lower Cretaceous coal-bearing sediments from Prydz Bay, East Antarctica. *Proceedings of the Ocean Drilling Program, Scientific Results, 119,* 57-60.

Valentine, D. L. (2002). Biogeochemistry and microbial ecology of methane oxidation in anoxic environments: a review. *Antonie van Leeuwenhoek*, *81*(1), 271-282.

Vaughan, D. G., Marshall, G. J., Connolley, W. M., Parkinson, C., Mulvaney, R., Hodgson, D. A., King, J. C., Pudsey, C. J., & Turner, J. (2003). Recent rapid regional climate warming on the Antarctic Peninsula. *Climatic change*, *60*(3), 243-274.

Venkatesan, M. I. (1988). Organic geochemistry of marine sediments in Antarctic region: marine lipids in McMurdo Sound. *Organic Geochemistry*, *12*(1), 13-27.

Vogts, A., Moossen, H., Rommerskirchen, F., & Rullkötter, J. (2009). Distribution patterns and stable carbon isotopic composition of alkanes and alkan-1-ols from plant waxes of African rain forest and savanna C_3 species. *Organic Geochemistry*, *40*(10), 1037-1054.

Vogts, A., Schefuß, E., Badewien, T., & Rullkötter, J. (2012). n-Alkane parameters from a deep sea sediment transect off southwest Africa reflect continental vegetation and climate conditions. *Organic Geochemistry*, *47*, 109-119.

Waelbroeck, C., Paul, A., Kucera, M., Rosell-Melé, A., Weinelt, M., Schneider, R., Mix, A. C., Abelmann, A., Armand, L., Bard, E., Barker, S., Barrows, T. T., Benway, H., Cacho, I., Chen, M. T., Cortijo, E., Crosta, X., de Vernal, A., Dokken, T., Duprat, J., Elderfield, H., Eynaud, F., Gersonde, R., Hayes, A., Henry, M., Hillaire-Marcel, C., Huang, C. C., Jansen, E., Juggins, S., Kallel, N., Kiefer, T., Kienast, M., Labeyrie, L., Leclaire, H., Londeix, L., Mangin, S., Matthiessen, J., Marret, F., Meland, M., Morey, A. E., Mulitza, S., Pflaumann, U., Pisias, N. G., Radi, T., Rochon, A., Rohling, E. J., Sbaffi, L., Schafer-Neth, C., Solignac, S., Spero, H., Tachikawa, K., Turon, J. -L. M.P. (2009). Constraints on the magnitude and patterns of ocean cooling at the Last Glacial Maximum. *Nature Geoscience*, *2*(2), 127-132.

Ward, J. K., Harris, J. M., Cerling, T. E., Wiedenhoeft, A., Lott, M. J., Dearing, M. D., Coltrain, J. B. & Ehleringer, J. R. (2005). Carbon starvation in glacial trees recovered from the La Brea tar pits, southern California. *Proceedings of the National Academy of Sciences of the United States of America*, *102*(3), 690-694.

Warny, S., Wrenn, J. H., Bart, P. J., & Askin, R. (2006). Palynology of the NBP03-01A transect in the Northern Basin, western Ross Sea, Antarctica: a late Pliocene record. *Palynology*, *30*(1), 151-182.

Warny, S., Askin, R. A., Hannah, M. J., Mohr, B. A., Raine, J. I., Harwood, D. M., & Florindo, F. (2009). Palynomorphs from a sediment core reveal a sudden remarkably warm Antarctica during the middle Miocene. *Geology*, *37*(10), 955-958.

Webb, P. N., Harwood, D. M., McKelvey, B. C., Mercer, J. H., & Stott, L. D. (1984). Cenozoic marine sedimentation and ice-volume variation on the East Antarctic craton. *Geology*, *12*(5), 287-291.

Webb, P. N., Harwood, D. M., Mabin, M. G. C., & McKelvey, B. C. (1996). A marine and terrestrial Sirius Group succession, middle Beardmore Glacier-Queen Alexandra Range, Transantarctic Mountains, Antarctica. *Marine Micropaleontology*, *27*(1-4), 273-297.

Wei, L. J., Raine, J. I., & Liu, X. H. (2014). Terrestrial palynomorphs of the Cenozoic Pagodroma Group, northern Prince Charles Mountains, East Antarctica. *Antarctic Science*, *26*(01), 69-79.

Weijers, J. W., Schouten, S., Hopmans, E. C., Geenevasen, J. A., David, O. R., Coleman, J. M., Pancost, R. D., & Sinninghe Damsté, J. S. (2006a). Membrane lipids of mesophilic anaerobic bacteria thriving in peats have typical archaeal traits. *Environmental Microbiology*, *8*(4), 648-657.

Weijers, J. W., Schouten, S., Spaargaren, O. C., & Sinninghe Damsté, J. S. (2006b). Occurrence and distribution of tetraether membrane lipids in soils: implications for the use of the TEX 86 proxy and the BIT index. *Organic Geochemistry*, *37*(12), 1680-1693.

Weijers, J. W., Schouten, S., van den Donker, J. C., Hopmans, E. C., & Sinninghe Damsté, J. S. (2007). Environmental controls on bacterial tetraether membrane lipid distribution in soils. *Geochimica et Cosmochimica Acta*, *71*(3), 703-713.

Weijers, J. W., Schouten, S., Sluijs, A., Brinkhuis, H., & Sinninghe Damsté, J. S. (2007b). Warm arctic continents during the Palaeocene–Eocene thermal maximum. *Earth and Planetary Science Letters*, *261*(1), 230-238.

Whitehead, J. M., Quilty, P. G., Harwood, D. M., & McMinn, A. (2001). Early Pliocene paleoenvironment of the Sørsdal Formation, Vestfold Hills, based on diatom data. *Marine Micropaleontology*, *41*(3), 125-152.

Whitehead, J. M., Harwood, D. M., & McMinn, A. (2003). Ice-distal Upper Miocene marine strata from inland Antarctica. *Sedimentology*, *50*(3), 531-552.

Whitehead, J. M., Harwood, D. M., McKelvey, B. C., Hambrey, M. J., & McMinn, A. (2004). Diatom biostratigraphy of the Cenozoic glaciomarine Pagodroma Group, northern Prince

Charles Mountains, East Antarctica. *Australian Journal of Earth Sciences*, *51*(4), 521-547.

Whitehead, J. M., Quilty, P. G., McKelvey, B. C., & O'Brien, P. E. (2006). A review of the Cenozoic stratigraphy and glacial history of the Lambert Graben—Prydz Bay region, East Antarctica. *Antarctic Science*, *18*(01), 83-99.

Whittaker, J. M., & Müller, R. D. (2006). Seismic stratigraphy of the Adare Trough area, Antarctica. *Marine geology*, *230*(3-4), 179-197.

Williams, T. G., & Flanagan, L. B. (1996). Effect of changes in water content on photosynthesis, transpiration and discrimination against $^{13}CO_2$ and $C^{18}O^{16}O$ in Pleurozium and Sphagnum. *Oecologia*, *108*(1), 38-46.

Wilson, G. S., Florindo, F., Sagnotti, L., Verosub, K. L., & Roberts, A. P. (2000). Magnetostratigraphy of Oligocene-Miocene glaciomarine strata from CRP-2/2A, Victoria Land Basin, Antarctica. *Terra Antartica*, *7*(4), 631-646.

Wilson, G. S., Pekar, S. F., Naish, T. R., Passchier, S., & DeConto, R. (2008). The Oligocene–Miocene Boundary–Antarctic Climate Response to Orbital Forcing. *Developments in Earth and Environmental Sciences*, *8*, 369-400.

Wilson, D. S., & Luyendyk, B. P. (2009). West Antarctic paleotopography estimated at the Eocene-Oligocene climate transition. *Geophysical Research Letters*, *36*(16), L16302, doi:10.1029/2009GL039297.

Wilson, D. S., Jamieson, S. S., Barrett, P. J., Leitchenkov, G., Gohl, K., & Larter, R. D. (2012). Antarctic topography at the Eocene–Oligocene boundary. *Palaeogeography, Palaeoclimatology, Palaeoecology*, *335*, 24-34.

Wilson, D. S., Pollard, D., DeConto, R. M., Jamieson, S. S., & Luyendyk, B. P. (2013). Initiation of the West Antarctic Ice Sheet and estimates of total Antarctic ice volume in the earliest Oligocene. *Geophysical Research Letters*, *40*(16), 4305-4309.

Wuchter, C., Schouten, S., Wakeham, S. G., & Sinninghe Damsté, J. S. (2005). Temporal and spatial variation in tetraether membrane lipids of marine Crenarchaeota in particulate organic matter: implications for TEX86 paleothermometry. *Paleoceanography*, *20*, PA3013, doi:10.1029/2004PA001110.

Xie, S., Nott, C. J., Avsejs, L. A., Volders, F., Maddy, D., Chambers, F. M., ... & Evershed, R. P. (2000). Palaeoclimate records in compound-specific δD values of a lipid biomarker in ombrotrophic peat. *Organic Geochemistry*, *31*(10), 1053-1057.

Xie, S., Nott, C. J., Avsejs, L. A., Maddy, D., Chambers, F. M., & Evershed, R. P. (2004). Molecular and isotopic stratigraphy in an ombrotrophic mire for paleoclimate reconstruction. *Geochimica et Cosmochimica Acta*, *68*(13), 2849-2862.

Yang, H., Pagani, M., Briggs, D. E., Equiza, M. A., Jagels, R., Leng, Q., & LePage, B. A. (2009). Carbon and hydrogen isotope fractionation under continuous light: implications for paleoenvironmental interpretations of the High Arctic during Paleogene warming. *Oecologia*, *160*(3), 461-470.

Yang, H., Liu, W., Leng, Q., Hren, M. T., & Pagani, M. (2011). Variation in n-alkane δD values from terrestrial plants at high latitude: Implications for paleoclimate reconstruction. *Organic Geochemistry*, *42*(3), 283-288.

You, Y., Huber, M., Müller, R.D., Poulsen, C.J. and Ribbe, J. (2009) Simulation of the Middle Miocene Climate Optimum. *Geophysical Research Letters, 36*(4), L04702, doi:10.1029/2008GL036571.

Zachos, J. C., Flower, B. P., & Paul, H. (1997). Orbitally paced climate oscillations across the Oligocene/Miocene boundary. *Nature*, *388*(6642), 567-570.

Zachos, J., Pagani, M., Sloan, L., Thomas, E., & Billups, K. (2001a). Trends, rhythms and aberrations in global climate 65 Ma to present. *Science, 292*(5517), 686-693.

Zachos, J. C., Shackleton, N. J., Revenaugh, J. S., Pälike, H., & Flower, B. P. (2001b). Climate response to orbital forcing across the Oligocene-Miocene boundary. *Science*, *292*(5515), 274-278.

Zachos, J. C., Dickens, G. R., & Zeebe, R. E. (2008). An early Cenozoic perspective on greenhouse warming and carbon-cycle dynamics. *Nature*, *451*(7176), 279-283.

Zamaloa, M. D. C. (2004). Miocene algae and spores from Tierra del Fuego, Argentina. *Alcheringa, 28*(1), 205-227.

Zhang, J., Quay, P. D., & Wilbur, D. O. (1995). Carbon isotope fractionation during gas-water exchange and dissolution of CO_2. *Geochimica et Cosmochimica Acta*, *59*(1), 107-114.

Zhang, G., Sheng, G., Peng, P. A., & Zheng, H. (2000). Molecular organic geochemical peculiarities of lacustrine core sediments in Fildes Peninsula, King George Island, Antarctica. *Chinese science bulletin*, *45*(1), 67-70.

Zhang, Y. G., Zhang, C. L., Liu, X. L., Li, L., Hinrichs, K. U., & Noakes, J. E. (2011). Methane Index: a tetraether archaeal lipid biomarker indicator for detecting the instability of marine gas hydrates. *Earth and Planetary Science Letters*, *307*(3), 525-534.

Zhang, Y. G., Pagani, M., Liu, Z., Bohaty, S. M., & DeConto, R. (2013). A 40-million-year history of atmospheric CO_2. *Philosophical Transactions of the Royal Society A*, *371*, 20130096.

Zhang, Y. G., Pagani, M., & Liu, Z. (2014). A 12-million-year temperature history of the tropical Pacific Ocean. *Science*, *344*(6179), 84-87.

Zhang, Z., Smittenberg, R. H., & Bradley, R. S. (2016a). GDGT distribution in a stratified lake and implications for the application of TEX86 in paleoenvironmental reconstructions. *Scientific Reports*, *6*, 34465, doi:10.1038/srep34465.

Zhang, Y. G., Pagani, M., & Wang, Z. (2016b). Ring Index: A new strategy to evaluate the integrity of TEX_{86} paleothermometry. *Paleoceanography, 31*(2), 220-232.

Zhou, W., Xie, S., Meyers, P. A., & Zheng, Y. (2005). Reconstruction of late glacial and Holocene climate evolution in southern China from geolipids and pollen in the Dingnan peat sequence. *Organic Geochemistry*, *36*(9), 1272-1284.

Zhuang, G., Pagani, M., Chamberlin, C., Strong, D., & Vandergoes, M. (2015). Altitudinal shift in stable hydrogen isotopes and microbial tetraether distribution in soils from the Southern Alps, NZ: Implications for paleoclimatology and paleoaltimetry. *Organic Geochemistry*, *79*, 56-64.

Zink, K. G., Vandergoes, M. J., Mangelsdorf, K., Dieffenbacher-Krall, A. C., & Schwark, L. (2010). Application of bacterial glycerol dialkyl glycerol tetraethers (GDGTs) to develop modern and past temperature estimates from New Zealand lakes. *Organic Geochemistry*, *41*(9), 1060-1066.

Zink, K. –G., Vandergoes, M. J., Bauersachs, T., Newnham, R. M., Rees, A. B. H., & Schwark, L. (2016). A refined paleotemperature calibration for New Zealand limnic environments using differentiation of branched glycerol dialkyl glycerol tetraether (brGDGT) sources. *Journal of Quaternary Science*, *31*(7), 823-835.

8. Appendices

Appendix 1: Data used in Chapter 3

Table A1.1 Data for the McMurdo Erratics, used in Chapter 3.

Sample Name	BMC Number	Age	TOC (wt%)	CPI	ACL	n-C$_{29}$/n-C$_{27}$	µg n-alkanes/g TOC	Lithofacies
D1	67	Mid-Late Eocene	0.26	2.64	28.68	1.58	813.38	mwb
E214	69	Mid-Late Eocene	0.23	1.84	28.04	1.02	3632.69	mmb
E215	70	Mid-Late Eocene	0.28	1.87	28.02	1.11	390.47	sw
MB245	71	Mid-Late Eocene	0.92	3.14	27.91	1.18	930.03	mmb
MTD95	72	Mid Eocene	0.89	2.12	28.46	1.64	737.91	sw
E219	73	Late-Mid to Mid Eocene	0.69	5.46	28.01	1.01	1533.14	mmb

Table A1.2 Data for Mt Boreas, used in Chapter 3.

Sample Name	BMC Number	TOC (wt%)	CPI	ACL	n-C$_{29}$/n-C$_{27}$	µg n-alkanes/g TOC	Facies Number
ALS-05-21E	101	0.18	1.75	26.98	0.97	157.30	2
ALS-05-21G	100	0.30	2.60	27.05	0.69	280.83	2
ALS-05-04F	102	0.09	2.03	26.79	0.69	6.57	1
ALS-05-21H	99	1.55	3.30	27.23	0.74	761.95	1
ALS-05-04E	103	0.31	2.66	26.69	0.55	4.53	1
ALS-05-04C	104	1.15	2.66	27.20	0.37	373.33	1
ALS-05-21K	113	1.47	3.90	26.76	0.38	366.56	1
ALS-05-21N	111	0.89	3.94	26.53	0.49	102.54	1

ALS-05-04A	105	1.15	5.88	26.80	0.15	195.95	1
ALS-05 21O	112	0.11	2.33	26.71	0.62	74.23	1
ALS -05-58	108	1.04	3.39	27.37	0.51	82.59	1
ALS-05-57	110	5.06	5.80	26.17	0.49	72.13	1

Table A1.3 Data for CRP-2/2A, used in Chapter 3.

Sample Depth (mbsf)	BMC Number	TOC (wt%)	CPI	ACL	n-C_{29}/n-C_{27}	µg n-alkanes/g TOC	Facies Number
108.99	123	0.32	2.73	27.24	0.48	29.35	7
110.96	131	0.11	1.33	27.80	0.69	112.22	9
115.99	129	0.26	1.96	26.73	0.65	48.32	7
120.03	127	0.27	1.21	27.95	0.74	545.80	7
123.97	133	0.21	2.70	27.93	0.68	36.32	3
127.98	128	0.34	2.85	27.73	0.60	16.80	4
134.98	130	0.33	3.24	27.41	0.58	16.53	7
139.98	119	0.36	3.36	27.73	0.61	34.56	7
150.36	116	0.19	4.56	27.30	0.33	285.71	8
159.98	121	0.41	1.40	28.39	0.84	217.13	8
170.01	115	0.29	2.40	27.37	0.68	58.10	8
180.04	124	0.49	3.92	27.72	0.62	36.04	8
244.95	118	0.96	1.72	28.29	0.89	22.45	6
249.96	132	0.42	2.31	27.32	0.62	47.98	6
259.89	117	0.58	3.66	27.36	0.72	141.01	8
269.98	114	0.25	1.29	28.48	0.94	70.82	6

280.56	120	0.11	5.53	27.19	0.25	1892.95	6
290.00	122	0.12	1.67	28.00	0.79	32.54	6
299.94	125	0.35	1.20	28.73	1.02	101.82	3

Table A1.4 Data for DSDP 270, used in Chapter 3.

Sample Depth (mbsf)	BMC Number	TOC (wt%)	CPI	ACL	n-C_{29}/n-C_{27}	µg n-alkanes/g TOC	Facies Number
27.8	413	0.66	2.65	28.00	0.86	1760.92	4
37.7	424	0.78	3.69	27.86	0.76	1982.23	8
47.8	406	0.57	2.81	28.02	0.82	580.83	8
57.3	426	0.60	3.64	28.04	0.85	139.41	8
66.8	400	0.66	3.08	27.89	0.79	515.22	3
83.2	409	0.33	3.16	27.79	0.76	4387.74	3
94.2	414	0.55	3.25	27.57	0.69	573.53	8
103.3	427	0.64	4.36	27.77	0.78	166.91	8
112.8	411	0.54	3.27	27.67	0.72	207.61	8
122.3	403	0.31	3.61	27.65	0.71	450.97	8
132.7	420	0.39	4.32	27.63	0.69	168.42	8
141.7	405	0.50	4.12	27.75	0.74	805.81	8
146.2	404	0.54	3.63	27.81	0.76	791.68	8
153.2	401	0.51	3.46	27.75	0.73	2021.40	8
160.3	423	0.52	3.96	27.85	0.67	338.44	8
173.7	412	0.46	2.75	28.01	0.85	258.72	8
183.2	415	0.39	2.47	27.91	0.78	530.55	8

194.8	462	0.22	4.10	27.96	0.69	656.05	8
200.2	421	0.45	3.47	28.02	0.75	844.59	8
208.7	429	0.52	3.63	27.97	0.74	344.66	5
236.3	410	0.38	2.49	27.80	0.67	666.08	4
248.2	428	0.57	4.21	27.75	0.71	669.57	8
259.2	399	0.51	3.02	27.89	0.76	289.62	8
269.7	402	0.48	2.57	27.90	0.75	249.32	8
283.8	422	0.60	3.59	28.00	0.82	154.09	8
296.7	419	0.56	3.74	27.87	0.76	390.57	8
307.3	418	0.63	2.36	27.90	0.77	192.33	8
318.7	416	0.53	2.57	27.91	0.78	198.77	8
331.3	417	0.66	3.17	27.99	0.82	222.58	8
345.3	408	0.59	2.86	27.85	0.74	488.83	8
355.7	398	0.39	3.48	28.10	0.84	2921.00	7
369.7	396	0.44	4.25	27.97	0.69	452.15	7
379.7	397	0.57	4.78	28.04	0.65	846.38	7
384.1	163	0.53				326.29	7
384.51	161	0.57				435.09	8
384.9	162	0.56	3.96	27.99	0.82	6.94	8

Table A1.5 Data for DSDP 274, used in Chapter 3.

Sample Depth (mbsf)	BMC Number	TOC (wt%)	CPI	ACL	$n\text{-}C_{29}/n\text{-}C_{27}$	µg n-alkanes/g TOC	Facies Number
90.2	449	0.39	0.946473	28.01069	1.044231	81.22149	11

91.2	458	0.43	0.953879	27.23319	0.848183	25.25441	11
93.2	442	0.38	1.234695	28.98348	1.101076	5.305313	11
97.7	454	0.22	1.03501	28.91599	1.287677	14.62978	11
99.7	460	0.16	0.942545	28.05965	0.922141	283.6366	11
100.72	448	0.42	1.023719	28.44838	1.37465	5.152237	11
106.2	434	0.34	1.009018	28.84774	1.000941	28.96254	11
107.2	450	0.41	0.90303	29.55966	1.128556	19.06055	11
108.3	461	0.36	1.234225	30.98948		8.385015	11
109.2	445	0.36	0.568692	25.93065		34.81354	11
110.2	447	0.38	0.640302	25		189.8211	11
110.7	430	0.31	0.78344	27.86602	1.1236	75.36291	11
111.3	456	0.37	0.986717	27.99127	1.218371	9.786409	11
111.7	455	0.34	1.119419	28.05935	0.893155	2.655549	11
112.2	443	0.36	1.321123	29.09415	1.117265	1.968058	11
113.2	451	0.34	1.057845	29.65469	1.326095	4.926357	11
115.3	154	0.19	1.369679	27.26344	0.495522	113.7032	11
119.72	159	0.28	1.483986	27.04244	0.628242	31.69623	11
124.78	150	0.52	3.001775	27.37513	0.499216	186.6633	10
129.23	157	0.62	2.797462	27.27092	0.547992	313.9364	10
134.75	158	0.51	2.583291	27.30731	0.516562	316.6175	10
139.27	155	0.61	2.792462	27.11466	0.497526	154.2349	10
142.7	453	0.4	2.583782	27.57062	0.580046	47.74667	10
143.3	444	0.7	2.27644	27.70269	0.588149	26.39599	10
143.7	433	0.6	1.949448	27.64326	0.547954	39.8443	10
144.2	452	0.62	2.325223	27.44277	0.52055	18.43228	10

144.8	457	0.6	2.074098	27.78592	0.630494	36.55773	10		
145.2	446	0.57	1.729866	27.39751	0.631142	42.90946	10		
145.7	437	0.51	1.748149	27.48093	0.567754	29.10519	10		
146.7	459	2.36	2.534629	27.5886	0.587539	4.792842	10		
153.7	438	0.68	1.988462	27.22035	0.552766	87.89355	10		
154.7	431	0.67	2.091311	27.5276	0.563523	81.1082	10		
155.8	436	0.81	2.02388	27.3482	0.543843	75.3325	10		

Appendix 2: Data used in Chapter 4

Palynomorph data was processed and counted by Dr Joe Prebble and is available on request.

Table A2.1 GDGT data for DSDP 270 used in Chapter 4.

Sample Depth (mbsf)	BMC Number	TEX$_{86}$	RI	Calculated RI (Zhang et al. 2016b)	ΔRI	BAYSPAR subT STD 5th percentile (°C)	BAYSPAR subT STD 50th percentile (°C)	BAYSPAR subT STD 95th percentile (°C)	MAT$_{mrs}$ (°C)
47.80	406	0.46	1.88	1.93	0.05	-0.72	5.06	11.21	7.69
57.30	426	0.47	2.01	1.97	-0.04	0.21	6.07	12.19	8.29
66.80	400	0.44	1.87	1.88	0.01	-2.11	3.70	9.74	11.43
73.53	1473	0.48	2.03	1.99	-0.04	0.77	6.49	12.63	11.03
92.69	1472	0.49	2.03	2.01	-0.01	1.25	7.14	13.38	10.88
96.06	1471	0.47	2.02	1.96	-0.06	0.02	5.81	12.00	10.22
104.71	1470	0.46	1.96	1.94	-0.02	-0.52	5.27	11.39	9.90
112.80	411	0.46	1.90	1.95	0.05	-0.46	5.41	11.50	9.22
114.96	1469	0.45	1.98	1.92	-0.06	-1.24	4.62	10.76	10.66

122.30	403	0.44	1.92	1.89	-0.02	-1.86	3.98	10.01	11.11
123.72	1468	0.48	2.01	1.99	-0.02	0.84	6.57	12.81	9.71
132.70	420	0.45	1.80	1.91	0.11	-1.28	4.55	10.59	7.55
139.65	1467	0.51	2.02	2.07	0.04	2.73	8.46	14.55	10.35
141.70	405	0.45	2.02	1.91	-0.11	-1.56	4.28	10.48	9.99
142.53	1466	0.49	1.93	2.02	0.08	1.34	7.19	13.41	8.81
146.20	404	0.43	1.91	1.87	-0.04	-2.64	3.32	9.40	9.92
149.33	1465	0.44	1.97	1.89	-0.08	-1.88	3.97	10.04	10.84
153.20	401	0.44	1.93	1.90	-0.03	-1.84	4.01	10.03	11.45
158.61	1464	0.48	1.92	2.00	0.08	0.89	6.73	12.92	11.74
165.28	1463	0.44	1.98	1.89	-0.09	-1.87	3.88	9.91	9.46
173.70	412	0.53	1.82	2.10	0.28	3.40	9.27	15.64	9.97
179.41	1462	0.48	2.04	1.99	-0.05	0.74	6.56	12.73	11.71
183.20	415	0.43	2.04	1.87	-0.17	-2.75	3.07	9.05	7.31
189.60	1460	0.50	2.06	2.03	-0.02	1.85	7.66	13.95	11.15
218.69	1459	0.47	2.11	1.97	-0.14	0.19	6.01	12.16	8.65
226.95	1458	0.51	2.04	2.06	0.02	2.41	8.22	14.42	11.27
231.42	1457	0.52	2.15	2.08	-0.06	3.07	8.87	15.09	12.44
240.05	1456	0.52	2.28	2.08	-0.20	2.79	8.65	14.97	5.14
253.27	1455	0.47	2.21	1.97	-0.25	0.07	5.92	12.12	11.59
264.98	1454	0.47	2.21	1.95	-0.26	-0.32	5.58	11.73	8.35
277.85	1453	0.50	2.22	2.04	-0.17	2.11	7.93	14.14	11.05
288.70	1452	0.52	2.37	2.09	-0.28	3.22	9.00	15.32	9.68
313.26	1451	0.47	2.29	1.97	-0.31	0.30	6.05	12.20	9.97
345.30	408	0.47	1.76	1.97	0.21	0.36	6.01	12.26	11.11

Table A2.2 n-Alkane data for DSDP 270 used in Chapter 4.

Sample Depth (mbsf)	BMC Number	CPI	ACL	HMW/LMW	HMW *n*-alkanes µg/g TOC	LMW *n*-alkanes µg/g TOC	*n*-C$_{23}$ µg/g TOC
27.8	413	2.65	28.00	0.04	90.52	1496.83	8.03
37.7	424	3.69	27.86	0.02	55.41	1641.86	6.18
47.8	406	2.81	28.02	0.20	117.65	379.51	9.21
57.3	426	3.64	28.04	1.07	70.11	43.26	6.03
66.8	400	3.08	27.89	0.24	115.76	313.54	10.65
83.2	409	3.16	27.79	0.04	209.91	3440.18	26.12
94.2	414	3.25	27.57	0.31	154.14	306.40	19.80
103.3	427	4.36	27.77	0.82	79.33	65.04	9.12
112.8	411	3.27	27.67	4.25	159.57	24.40	15.98
122.3	403	3.61	27.65	3.91	236.00	39.60	39.11
132.7	420	4.32	27.63	1.84	105.93	40.37	9.11
141.7	405	4.12	27.75	1.70	527.11	211.72	51.15
146.2	404	3.63	27.81	0.24	182.20	512.01	16.05
153.2	401	3.46	27.75	0.37	162.99	281.66	18.49
160.3	423	3.96	27.85	0.19	58.59	208.25	4.94
173.7	412	2.75	28.01	0.79	108.67	85.04	10.59
183.2	415	2.47	27.91	0.08	48.85	330.18	6.61
194.8	462	4.10	27.96	0.16	96.66	404.73	11.28
200.2	421	3.47	28.02	0.04	42.52	635.81	5.26
208.7	429	3.63	27.97	0.12	43.91	237.07	4.10
236.3	410	2.49	27.80	0.18	111.18	367.07	12.61
248.2	428	4.21	27.75	0.14	98.70	478.01	11.11

259.2	399	3.02	27.89	0.48	103.51	139.14	8.91
269.7	402	2.57	27.90	1.73	163.64	58.76	13.71
283.8	422	3.59	28.00	1.08	84.19	52.49	7.14
296.7	419	3.74	27.87	0.33	108.39	218.68	10.12
307.3	418	2.36	27.90	0.99	104.21	63.73	8.85
318.7	416	2.57	27.91	1.45	123.36	53.04	10.25
331.3	417	3.17	27.99	1.73	138.09	52.62	11.15
345.3	408	2.86	27.85	0.23	110.43	308.83	9.61

Table A2.3 n-Alkane δ²H data for DSDP 270 used in Chapter 4.

	BMC: 396			BMC: 397				BMC: 398			
	Sample depth (mbsf): 368.2			Sample depth (mbsf): 379.7				Sample depth (mbsf): 355.7			
n-alkane	Rep 1 δ²H	Rep 2 δ²H	Mean δ²H	Rep 1 δ²H	Rep 2 δ²H	Rep 3 δ²H	Mean δ²H	Rep 1 δ²H	Rep 2 δ²H	Rep 3 δ²H	Mean δ²H
C23	-165.28	-177.28	-171.28	N/A	N/A	N/A		N/A	N/A	N/A	
C24	-183.56	-169.82	-176.69	N/A	N/A	N/A		N/A	N/A	N/A	
C25	-187.94	-181.08	-184.51	-177.65	-179.57	-162.70	-173.31	-155.92	-150.69	-146.16	-150.92
C26	-136.54	-155.89	-146.21	-181.15	N/A	N/A	-181.15	N/A	N/A	N/A	
C27	-191.37	-187.61	-189.49	-196.27	-192.12	-194.56	-194.32	-172.76	-157.87	-157.82	-162.82
C28	-180.26	-191.49	-185.87	-171.86	N/A	N/A	-171.86	N/A	N/A	-171.15	-171.15
C29	-198.18	-201.05	-199.61	-181.93	-172.96	-188.42	-181.10	-179.10	-182.52	-171.12	-177.58
C30	-178.03	-184.44	-181.23	N/A	N/A	N/A		N/A	N/A	N/A	
C31	-207.47	-170.45	-188.96	-187.01	-150.86	-177.96	-171.94	-174.13	-190.94	-165.06	-176.71

	BMC: 399				BMC: 400				BMC: 401		
	Sample depth (mbsf): 259.2				Sample depth (mbsf): 66.8				Sample depth (mbsf): 153.2		
n-alkane	Rep 1 δ²H	Rep 2 δ²H	Rep 3 δ²H	Mean δ²H	Rep 1 δ²H	Rep 2 δ²H	Rep 3 δ²H	Mean δ²H	Rep 1 δ²H	Rep 2 δ²H	Mean δ²H
C23	N/A	N/A	N/A		-148.38	-153.47	-151.14	-151.00	-199.30	-148.11	-173.71
C24	N/A	N/A	N/A		-179.36	-173.17	-171.28	-174.60	-177.65	N/A	-177.65
C25	-181.29	-164.17	-169.85	-171.77	-175.87	-182.95	-174.00	-177.61	-173.25	-176.99	-175.12
C26	N/A	N/A	-167.71	-167.71	-199.20	-190.38	-165.73	-185.10	-183.66	-169.38	-176.52
C27	-187.58	-187.16	-181.18	-185.31	-178.33	-180.04	-176.51	-178.29	-173.68	-170.79	-172.23
C28	N/A	N/A	-184.81	-184.81	N/A	-152.45	-161.12	-156.79	N/A	-151.74	-151.74
C29	-191.98	-182.87	-194.89	-189.91	-199.65	-199.19	-196.41	-198.41	-181.65	-195.27	-188.46
C30	N/A	N/A	N/A		N/A	-189.11	N/A	-189.11	N/A	N/A	
C31	-179.58	-178.21	-188.14	-181.98	-180.21	N/A	-186.87	-183.54	-174.91	-184.02	-179.46

	BMC: 402			BMC: 403			BMC: 404		
	Sample depth (mbsf): 269.7			Sample depth (mbsf): 122.3			Sample depth (mbsf): 146.2		
n-alkane	Rep 1 δ^2H	Rep 2 δ^2H	Mean δ^2H	Rep 1 δ^2H	Rep 2 δ^2H	Mean δ^2H	Rep 1 δ^2H	Rep 2 δ^2H	Mean δ^2H
C23	-182.02	-168.21	-175.11	-185.21	-181.04	-183.12	-169.64	N/A	-169.64
C24	-171.57	-176.56	-174.06	-190.31	-192.09	-191.20	-169.12	-168.32	-168.72
C25	-182.43	-173.13	-177.78	-174.43	-174.33	-174.38	-176.86	-177.87	-177.36
C26	-151.42	-147.44	-149.43	-150.34	-155.98	-153.16	-164.34	-159.82	-162.08
C27	-181.49	-188.36	-184.92	-177.87	-180.98	-179.43	-177.57	-177.51	-177.54
C28	-156.46	-173.29	-164.88	-179.02	N/A	-179.02	-176.35	-183.37	-179.86
C29	-190.97	-193.99	-192.48	-172.02	-181.80	-176.91	-191.14	-198.25	-194.70
C30	N/A	N/A		N/A	N/A		N/A	N/A	
C31	-172.72	-188.12	-180.42	-184.20	-193.25	-188.73	-167.43	-180.78	-174.11
	BMC: 405			BMC: 406			BMC: 408		
	Sample depth (mbsf): 141.7			Sample depth (mbsf): 47.8			Sample depth (mbsf): 345.3		
n-alkane	Rep 1 δ^2H	Rep 2 δ^2H	Mean δ^2H	Rep 1 δ^2H	Rep 2 δ^2H	Mean δ^2H	Rep 1 δ^2H	Rep 2 δ^2H	Mean δ^2H
C23	-182.13	-176.54	-179.34	-185.89	-180.80	-183.34	-154.53	-159.29	-156.91
C24	-198.86	-168.75	-183.81	-185.96	-193.49	-189.72	-170.31	-170.89	-170.60
C25	-184.06	-178.20	-181.13	-196.65	-190.77	-193.71	-182.24	-182.79	-182.51
C26	-159.00	-170.40	-164.70	-160.22	-167.41	-163.81	-177.97	-176.49	-177.23
C27	-163.33	-184.35	-173.84	-189.45	-191.83	-190.64	-196.47	-196.07	-196.27
C28	-155.84	-175.73	-165.79	-186.32	-172.53	-179.42	-179.11	-195.06	-187.09
C29	-175.94	-189.00	-182.47	-206.10	-203.02	-204.56	-200.81	-203.48	-202.15
C30	N/A	N/A		N/A	N/A		N/A	N/A	
C31	-191.34	-188.35	-189.85	-203.56	-200.71	-202.13	-200.81	-185.75	-193.28

	BMC: 409			BMC: 410			BMC: 411		
	Sample depth (mbsf): 83.2			Sample depth (mbsf): 236.3			Sample depth (mbsf): 112.8		
n-alkane	Rep 1 δ^2H	Rep 2 δ^2H	Mean δ^2H	Rep 1 δ^2H	Rep 2 δ^2H	Mean δ^2H	Rep 1 δ^2H	Rep 2 δ^2H	Mean δ^2H
C23	N/A	N/A		N/A	N/A		-186.33	-187.63	-186.98
C24	N/A	N/A		N/A	N/A		-181.90	-179.93	-180.92
C25	-159.00	-153.66	-156.33	-165.46	-167.95	-166.70	-188.25	-188.20	-188.23
C26	N/A	N/A		-166.70	-182.90	-174.80	-173.18	-160.42	-166.80
C27	-178.39	-169.20	-173.80	-182.85	-176.97	-179.91	-192.61	-192.63	-192.62
C28	-172.51	-197.16	-184.84	N/A	N/A		-175.16	-175.51	-175.34
C29	-196.67	-180.15	-188.41	-197.71	-195.25	-196.48	-208.04	-204.79	-206.41
C30	N/A	N/A		N/A	N/A		N/A	N/A	
C31	-177.37	-192.26	-184.81	-170.91	-178.31	-174.61	-211.18	-203.33	-207.26
	BMC: 412			BMC: 413			BMC: 414		
	Sample depth (mbsf): 173.7			Sample depth (mbsf): 27.8			Sample depth (mbsf): 94.2		
n-alkane	Rep 1 δ^2H	Rep 2 δ^2H	Mean δ^2H	Rep 1 δ^2H	Rep 2 δ^2H	Mean δ^2H	Rep 1 δ^2H	Rep 2 δ^2H	Mean δ^2H
C23	-148.48	-142.90	-145.69	N/A	N/A		N/A	N/A	
C24	-171.25	-156.98	-164.12	N/A	N/A		N/A	N/A	
C25	-189.23	-186.31	-187.77	N/A	N/A		-183.42	-168.05	-175.74
C26	-179.31	-173.59	-176.45	N/A	N/A		-166.67	-160.07	-163.37
C27	-183.15	-184.77	-183.96	-167.33	-169.48	-168.41	-180.99	-183.00	-182.00
C28	-162.34	-187.40	-174.87	N/A	N/A		N/A	N/A	
C29	-202.76	-198.67	-200.71	-192.27	-189.60	-190.94	-191.19	-189.86	-190.53
C30	-197.28	-197.95	-197.62	N/A	N/A		N/A	N/A	
C31	-202.33	-195.19	-198.76	-184.88	-185.14	-185.01	-199.68	-204.54	-202.11

n-alkane	BMC: 415 Sample depth (mbsf): 183.2			BMC: 416 Sample depth (mbsf): 318.7			BMC: 417 Sample depth (mbsf): 331.3		
	Rep 1 δ^2H	Rep 2 δ^2H	Mean δ^2H	Rep 1 δ^2H	Rep 2 δ^2H	Mean δ^2H	Rep 1 δ^2H	Rep 2 δ^2H	Mean δ^2H
C23	N/A	N/A		-164.85	-168.06	-166.46	-164.02	-161.79	-162.91
C24	N/A	N/A		-168.38	-160.34	-164.36	-168.18	-171.52	-169.85
C25	N/A	N/A		-189.89	-179.35	-184.62	-177.28	-177.25	-177.27
C26	N/A	N/A		-165.23	-185.81	-175.52	-178.28	-175.33	-176.81
C27	-163.15	-163.23	-163.19	-180.45	-183.12	-181.79	-185.61	-183.70	-184.66
C28	-181.17	N/A	-181.17	-174.91	-171.96	-173.44	-178.44	-160.94	-169.69
C29	-179.70	-179.16	-179.43	-187.15	-198.61	-192.88	-191.01	-195.10	-193.06
C30	N/A	N/A		N/A	N/A		N/A	N/A	
C31	-191.15	-188.45	-189.80	-178.12	-180.78	-179.45	-187.14	-188.17	-187.66
n-alkane	BMC: 418 Sample depth (mbsf): 307.3			BMC: 419 Sample depth (mbsf): 296.7			BMC: 420 Sample depth (mbsf): 132.7		
	Rep 1 δ^2H	Rep 2 δ^2H	Mean δ^2H	Rep 1 δ^2H	Rep 2 δ^2H	Mean δ^2H	Rep 1 δ^2H	Rep 2 δ^2H	Mean δ^2H
C23	-170.79	-168.71	-169.75	N/A	N/A		-162.78	-171.79	-167.28
C24	-180.64	-182.31	-181.48	-162.31	-158.24	-160.28	-172.19	-176.29	-174.24
C25	-177.01	-172.37	-174.69	-163.05	-167.14	-165.10	-178.18	-178.68	-178.43
C26	-190.08	-164.42	-177.25	-170.46	-170.26	-170.36	-161.64	-171.44	-166.54
C27	-190.03	-192.85	-191.44	-181.51	-186.66	-184.09	-186.38	-193.49	-189.94
C28	-194.88	-192.23	-193.55	-169.30	-171.70	-170.50	-173.62	-175.50	-174.56
C29	-202.04	-203.86	-202.95	-192.91	-197.64	-195.28	-196.89	-198.33	-197.61
C30	N/A	N/A		N/A	N/A		N/A	N/A	
C31	-202.21	-207.44	-204.83	-204.16	-192.49	-198.32	-202.91	-192.67	-197.79

	BMC: 421			BMC: 422			BMC: 423		
	Sample depth (mbsf): 200.2			Sample depth (mbsf): 283.8			Sample depth (mbsf): 160.3		
n-alkane	Rep 1 δ²H	Rep 2 δ²H	Mean δ²H	Rep 1 δ²H	Rep 2 δ²H	Mean δ²H	Rep 1 δ²H	Rep 2 δ²H	Mean δ²H
C23	N/A	N/A		-170.26	-171.27	-170.76	N/A	N/A	
C24	N/A	N/A		-177.01	-180.17	-178.59	N/A	N/A	
C25	-156.16	-155.30	-155.73	-175.38	-175.75	-175.56	-164.40	-160.14	-162.27
C26	N/A	N/A		-173.90	-178.35	-176.12	-180.26	-153.43	-166.85
C27	-175.58	-180.99	-178.29	-185.49	-188.19	-186.84	-177.10	-181.48	-179.29
C28	-164.57	-169.18	-166.87	-190.40	-189.88	-190.14	-177.92	-178.70	-178.31
C29	-187.03	-188.81	-187.92	-191.25	-197.34	-194.30	-185.35	-189.81	-187.58
C30	N/A	N/A		N/A	N/A		N/A	N/A	
C31	-182.43	-179.11	-180.77	-185.98	-185.43	-185.71	-186.22	-178.71	-182.46
	BMC: 424			BMC: 425			BMC: 426		
	Sample depth (mbsf): 37.7			Sample depth (mbsf): 16.7			Sample depth (mbsf): 57.3		
n-alkane	Rep 1 δ²H	Rep 2 δ²H	Mean δ²H	Rep 1 δ²H	Rep 2 δ²H	Mean δ²H	Rep 1 δ²H	Rep 2 δ²H	Mean δ²H
C23	N/A	N/A		N/A	N/A		-154.83	-150.40	-152.61
C24	N/A	N/A		N/A	N/A		-154.31	-158.07	-156.19
C25	-145.79	-141.51	-143.65	N/A	N/A		-177.23	-176.04	-176.63
C26	N/A	N/A		N/A	N/A		-163.00	-161.21	-162.10
C27	-156.76	-157.08	-156.92	-150.47	-152.00	-151.24	-182.76	-188.13	-185.44
C28	-153.15	-149.88	-151.51	N/A	N/A		-163.19	-151.35	-157.27
C29	-185.78	-186.09	-185.94	-152.30	-151.88	-152.09	-187.74	-185.24	-186.49
C30	N/A	N/A		N/A	N/A		N/A	N/A	
C31	-179.59	-187.59	-183.59	-149.23	-150.52	-149.87	-183.26	-169.87	-176.56

	BMC: 427			BMC: 428			BMC: 429		
	Sample depth (mbsf): 103.3			Sample depth (mbsf): 248.2			Sample depth (mbsf): 208.7		
n-alkane	Rep 1 δ^2H	Rep 2 δ^2H	Mean δ^2H	Rep 1 δ^2H	Rep 2 δ^2H	Mean δ^2H	Rep 1 δ^2H	Rep 2 δ^2H	Mean δ^2H
C23	-173.13	-177.56	-175.34	N/A	N/A		N/A	N/A	
C24	-177.11	-172.91	-175.01	N/A	N/A		-157.10	-155.73	-156.41
C25	-180.76	-180.11	-180.44	-170.53	-169.81	-170.17	-165.71	-167.88	-166.79
C26	-179.10	-188.88	-183.99	-151.72	-150.63	-151.17	-154.24	-163.40	-158.82
C27	-184.98	-180.00	-182.49	-176.66	-175.62	-176.14	-181.22	-180.19	-180.70
C28	-185.18	-164.22	-174.70	-161.34	-162.11	-161.72	-170.16	-167.19	-168.67
C29	-199.07	-197.65	-198.36	-192.17	-190.94	-191.55	-187.88	-188.40	-188.14
C30	N/A	N/A		N/A	N/A		N/A	N/A	
C31	-197.46	-210.47	-203.96	-190.89	-190.02	-190.46	-179.26	-180.83	-180.04

Table A2.4 n-Alkane δ^{13}C data for DSDP 270 used in Chapter 4.

	BMC: 396			BMC: 397			BMC: 398		
	Sample depth (mbsf): 368.2			Sample depth (mbsf): 379.7			Sample depth (mbsf): 355.7		
n-alkane	Rep 1 δ^{13}C	Rep 2 δ^{13}C	Mean δ^{13}C	Rep 1 δ^{13}C	Rep 2 δ^{13}C	Mean δ^{13}C	Rep 1 δ^{13}C	Rep 2 δ^{13}C	Mean δ^{13}C
C23	-29.13	-28.98	-29.06	-29.95	-30.05	-30.00	N/A	N/A	
C24	-27.32	-27.17	-27.24	-26.47	-29.28	-27.87	N/A	N/A	
C25	-27.36	-27.68	-27.52	-28.49	-27.87	-28.18	-28.07	-27.81	-27.94
C26	-29.76	-28.29	-29.02	-30.67	-30.19	-30.43	-26.73	-26.50	-26.62
C27	-29.19	-28.80	-29.00	-30.19	-29.96	-30.08	-28.20	-27.77	-27.98
C28	-28.14	-28.93	-28.53	-32.59	-30.55	-31.57	-27.33	-26.20	-26.76
C29	-29.14	-28.90	-29.02	-29.84	-30.28	-30.06	-27.30	-26.66	-26.98
C30	-23.96	-24.06	-24.01	N/A	N/A		N/A	N/A	
C31	-29.11	-27.97	-28.54	-30.06	-29.60	-29.83	-26.48	-25.19	-25.83

n-alkane	BMC: 399 Sample depth (mbsf): 259.2			BMC: 400 Sample depth (mbsf): 66.8			BMC: 401 Sample depth (mbsf): 153.2		
	Rep 1 δ^{13}C	Rep 2 δ^{13}C	Mean δ^{13}C	Rep 1 δ^{13}C	Rep 2 δ^{13}C	Mean δ^{13}C	Rep 1 δ^{13}C	Rep 2 δ^{13}C	Mean δ^{13}C
C23	-28.44	-28.43	-28.43	-28.47	-28.66	-28.56	N/A	N/A	
C24	-28.35	-28.42	-28.39	-28.67	-28.05	-28.36	-28.30	-29.14	-28.72
C25	-27.10	-27.81	-27.45	-28.44	-28.56	-28.50	-29.09	-29.51	-29.30
C26	-27.41	-27.27	-27.34	-28.71	-29.80	-29.25	-29.42	-29.87	-29.65
C27	-28.58	-28.58	-28.58	-29.20	-29.59	-29.40	-30.26	-30.24	-30.25
C28	-27.25	-26.59	-26.92	-29.74	-30.14	-29.94	-29.96	-30.68	-30.32
C29	-27.40	-27.90	-27.65	-30.16	-30.04	-30.10	-31.34	-31.64	-31.49
C30	N/A	N/A		N/A	N/A		-24.67	-25.54	-25.10
C31	N/A	N/A		N/A	N/A		-30.68	-30.70	-30.69

n-alkane	BMC: 402 Sample depth (mbsf): 269.7			BMC: 403 Sample depth (mbsf): 122.3			BMC: 404 Sample depth (mbsf): 146.2		
	Rep 1 δ^{13}C	Rep 2 δ^{13}C	Mean δ^{13}C	Rep 1 δ^{13}C	Rep 2 δ^{13}C	Mean δ^{13}C	Rep 1 δ^{13}C	Rep 2 δ^{13}C	Mean δ^{13}C
C23	-28.78	-28.63	-28.71	-28.67	-29.12	-28.90	-29.18	-29.34	-29.26
C24	-28.49	-28.36	-28.42	-29.04	-29.69	-29.36	-29.70	-29.20	-29.45
C25	-27.34	-27.41	-27.37	-29.55	-29.66	-29.60	-30.21	-30.36	-30.29
C26	-28.02	-27.36	-27.69	-29.28	-30.03	-29.65	-29.00	-29.37	-29.19
C27	-29.05	-29.01	-29.03	-30.09	-30.47	-30.28	-30.45	-30.75	-30.60
C28	-28.82	-28.22	-28.52	N/A	N/A		-30.67	-30.46	-30.57
C29	-28.14	-27.67	-27.90	-30.51	-30.41	-30.46	-31.31	-31.30	-31.31
C30	N/A	N/A		N/A	N/A		-23.95	-24.48	-24.22
C31	N/A	N/A		-31.49	-31.07	-31.28	-30.32	-30.79	-30.56

n-alkane	BMC: 405 Sample depth (mbsf): 141.7			BMC: 406 Sample depth (mbsf): 47.8			BMC: 408 Sample depth (mbsf): 345.3		
	Rep 1 $\delta^{13}C$	Rep 2 $\delta^{13}C$	Mean $\delta^{13}C$	Rep 1 $\delta^{13}C$	Rep 2 $\delta^{13}C$	Mean $\delta^{13}C$	Rep 1 $\delta^{13}C$	Rep 2 $\delta^{13}C$	Mean $\delta^{13}C$
C23	-27.68	-27.56	-27.62	N/A	N/A		-29.44	-29.58	-29.51
C24	-29.05	-29.05	-29.05	-28.24	-28.94	-28.59	-27.37	-27.99	-27.68
C25	-29.73	-29.92	-29.83	-27.97	-28.47	-28.22	-27.52	-27.70	-27.61
C26	-29.61	-29.09	-29.35	-28.07	-28.74	-28.41	-27.42	-27.72	-27.57
C27	-30.41	-30.21	-30.31	-29.55	-29.40	-29.48	-29.62	-29.80	-29.71
C28	-31.38	-31.39	-31.38	-28.72	-29.49	-29.11	-28.35	-28.84	-28.59
C29	-31.46	-31.54	-31.50	-30.33	-30.11	-30.22	-28.17	-28.14	-28.16
C30	N/A	N/A		N/A	N/A		N/A	N/A	
C31	-30.44	-30.75	-30.60	-30.50	-29.94	-30.22	-25.83	-25.87	-25.85

n-alkane	BMC: 409 Sample depth (mbsf): 83.2			BMC: 410 Sample depth (mbsf): 236.3			BMC: 411 Sample depth (mbsf): 112.8		
	Rep 1 $\delta^{13}C$	Rep 2 $\delta^{13}C$	Mean $\delta^{13}C$	Rep 1 $\delta^{13}C$	Rep 2 $\delta^{13}C$	Mean $\delta^{13}C$	Rep 1 $\delta^{13}C$	Rep 2 $\delta^{13}C$	Mean $\delta^{13}C$
C23	-29.36	-31.88	-30.62	N/A	N/A		-28.80	-28.63	-28.72
C24	-27.05	-26.92	-26.98	N/A	N/A		-28.59	-30.46	-29.53
C25	-26.71	-27.00	-26.85	-27.18	-27.75	-27.46	-29.35	-28.74	-29.05
C26	-33.06	-30.55	-31.81	-27.83	N/A	-27.83	-30.87	-30.90	-30.89
C27	-29.22	-28.94	-29.08	-29.36	-29.41	-29.39	-30.03	-30.05	-30.04
C28	N/A	-27.31	-27.31	-28.80	-28.33	-28.56	-29.42	-30.27	-29.85
C29	-29.32	-29.03	-29.18	-29.33	-28.84	-29.09	-30.33	-30.41	-30.37
C30	N/A	N/A		N/A	N/A		N/A	N/A	
C31	N/A	N/A		-28.49	-29.69	-29.09	-29.83	-29.93	-29.88

n-alkane	BMC: 412 Sample depth (mbsf): 173.7			BMC: 413 Sample depth (mbsf): 27.8			BMC: 414 Sample depth (mbsf): 94.2		
	Rep 1 δ^{13}C	Rep 2 δ^{13}C	Mean δ^{13}C	Rep 1 δ^{13}C	Rep 2 δ^{13}C	Mean δ^{13}C	Rep 1 δ^{13}C	Rep 2 δ^{13}C	Mean δ^{13}C
C23	N/A	N/A		N/A	N/A		-28.61	-28.88	-28.74
C24	-27.41	-26.99	-27.20	N/A	N/A		-28.75	-29.41	-29.08
C25	-27.36								

	BMC: 418			BMC: 419			BMC: 420		
	Sample depth (mbsf): 307.3			Sample depth (mbsf): 296.7			Sample depth (mbsf): 132.7		
n-alkane	Rep 1 δ^{13}C	Rep 2 δ^{13}C	Mean δ^{13}C	Rep 1 δ^{13}C	Rep 2 δ^{13}C	Mean δ^{13}C	Rep 1 δ^{13}C	Rep 2 δ^{13}C	Mean δ^{13}C
C23	-28.55	-28.18	-28.37	-28.61	-28.94	-28.77	-29.51	-29.61	-29.56
C24	-28.10	-28.23	-28.17	-28.40	-27.76	-28.08	-32.44	-30.27	-31.35
C25	-26.57	-27.36	-26.96	-27.33	-27.39	-27.36	-30.33	-30.13	-30.23
C26	-27.69	-27.93	-27.81	-28.86	-28.21	-28.54	-30.00	-30.18	-30.09
C27	-28.63	-28.77	-28.70	-29.52	-29.17	-29.34	-30.30	-30.60	-30.45
C28	-26.46	-27.72	-27.09	-29.46	-29.13	-29.29	-31.17	-30.63	-30.90
C29	-26.93	-27.69	-27.31	-27.98	-28.04	-28.01	-31.31	-31.05	-31.18
C30	N/A	N/A		-20.31	-20.60	-20.45	-28.21	-28.03	-28.12
C31	N/A	N/A		-25.70	-26.00	-25.85	-30.88	-30.38	-30.63
	BMC: 421			BMC: 422			BMC: 423		
	Sample depth (mbsf): 200.2			Sample depth (mbsf): 283.8			Sample depth (mbsf): 160.3		
n-alkane	Rep 1 δ^{13}C	Rep 2 δ^{13}C	Mean δ^{13}C	Rep 1 δ^{13}C	Rep 2 δ^{13}C	Mean δ^{13}C	Rep 1 δ^{13}C	Rep 2 δ^{13}C	Mean δ^{13}C
C23	N/A	N/A		-28.54	-27.96	-28.25	-29.73	-29.83	-29.78
C24	N/A	N/A		-28.69	-27.31	-28.00	-29.88	-28.81	-29.35
C25	N/A	N/A		-26.90	-26.61	-26.76	-29.61	-29.68	-29.64
C26	N/A	-26.80	-26.80	-27.40	-27.74	-27.57	-30.28	-30.64	-30.46
C27	-30.99	-29.61	-30.30	-28.36	-28.12	-28.24	-30.05	-30.16	-30.10
C28	-29.82	-29.23	-29.52	-28.05	-28.18	-28.11	-30.56	-30.34	-30.45
C29	-29.81	-29.95	-29.88	-27.36	-27.02	-27.19	-31.04	-30.84	-30.94
C30	N/A	N/A		N/A	N/A		-25.82	-25.83	-25.83
C31	N/A	N/A		-32.59	-32.84	-32.72	-30.70	-30.64	-30.67

n-alkane	BMC: 424 Sample depth (mbsf): 37.7			BMC: 425 Sample depth (mbsf): 16.7			BMC: 426 Sample depth (mbsf): 57.3		
	Rep 1 $\delta^{13}C$	Rep 2 $\delta^{13}C$	Mean $\delta^{13}C$	Rep 1 $\delta^{13}C$	Rep 2 $\delta^{13}C$	Mean $\delta^{13}C$	Rep 1 $\delta^{13}C$	Rep 2 $\delta^{13}C$	Mean $\delta^{13}C$
C23	-28.67	-29.08	-28.87	N/A	N/A		-29.67	-29.81	-29.74
C24	-29.01	-29.85	-29.43	N/A	N/A		-28.10	-28.43	-28.26
C25	-27.78	-28.44	-28.11	-26.94	-26.97	-26.95	-29.14	-28.75	-28.94
C26	-29.02	-30.27	-29.65	-29.21	-29.15	-29.18	-27.73	-29.61	-28.67
C27	-29.50	-29.61	-29.56	-28.99	-29.18	-29.09	-30.00	-30.24	-30.12
C28	-30.30	-30.87	-30.59	-29.49	-29.24	-29.36	-30.93	-31.47	-31.20
C29	-29.97	-30.60	-30.28	-29.75	-30.49	-30.12	-30.97	-31.54	-31.25
C30	N/A	N/A		N/A	-27.21	-27.21	-26.12	-25.81	-25.96
C31	-30.41	-30.72	-30.56	-30.23	-30.15	-30.19	-31.35	-31.50	-31.43
n-alkane	BMC: 427 Sample depth (mbsf): 103.3			BMC: 428 Sample depth (mbsf): 248.2			BMC: 429 Sample depth (mbsf): 208.7		
	Rep 1 $\delta^{13}C$	Rep 2 $\delta^{13}C$	Mean $\delta^{13}C$	Rep 1 $\delta^{13}C$	Rep 2 $\delta^{13}C$	Mean $\delta^{13}C$	Rep 1 $\delta^{13}C$	Rep 2 $\delta^{13}C$	Mean $\delta^{13}C$
C23	-28.01	-28.10	-28.06	-29.73	-29.48	-29.60	-29.26	-30.37	-29.82
C24	-29.25	-30.05	-29.65	-29.47	-27.72	-28.59	-27.21	-28.73	-27.97
C25	-28.97	-29.02	-29.00	-27.27	-27.37	-27.32	-28.07	-27.50	-27.79
C26	-28.91	-28.88	-28.89	-26.47	-28.30	-27.39	-26.30	-26.50	-26.40
C27	-30.31	-30.35	-30.33	-28.72	-28.99	-28.85	-29.20	-29.21	-29.20
C28	-31.48	-32.06	-31.77	-27.21	-28.45	-27.83	-27.53	-29.45	-28.49
C29	-30.34	-30.43	-30.39	-28.56	-28.62	-28.59	-29.68	-29.76	-29.72
C30	N/A	N/A		N/A	N/A		-25.86	-26.08	-25.97
C31	N/A	N/A		-25.52	-26.39	-25.95	-33.55	-34.03	-33.79

| n-alkane | BMC: 462 | | |
| | Sample depth (mbsf): 194.8 | | |
	Rep 1 $\delta^{13}C$	Rep 2 $\delta^{13}C$	Mean $\delta^{13}C$
C23	-29.37	-29.43	-29.40
C24	-32.81	-30.37	-31.59
C25	-30.66	-31.12	-30.89
C26	-31.51	-30.52	-31.02
C27	-27.69	-27.38	-27.53
C28	-29.46	-28.73	-29.09
C29	-27.59	-27.74	-27.67
C30	-36.22	-35.56	-35.89
C31	-26.41	-30.30	-28.36

Appendix 3: Data used in Chapter 5

This appendix contains data for Chapter 5. Individual GDGT integrations available on request. For access to unpublished data for the McMurdo erratics and CIROS-1 please contact Richard Levy: R.Levy@gns.cri.nz.

Table A3.1 GDGT data for DSDP 270 used in Chapter 5

BMC number	Sample depth (mbsf)	Age (Ma)	TEX_{86}	RI	Calculated RI (Zhang et al. 2016b)	ΔRI	MI	%GDGT-0	BIT	GDGT-2 /GDGT-3	TEX_{86}^L (°C)	Shevenell et al. 2011 (°C)	Kim et al., 2012 (°C)
406	47.80	17.91	0.46	1.88	1.93	0.05	0.06	53.17	0.07	1.59	-4.10	12.34	-2.29
426	57.30	18.33	0.47	2.01	1.97	-0.04	0.05	49.78	0.19	0.86	-14.16	13.55	-9.85
400	66.80	18.75	0.44	1.87	1.88	0.01	0.06	53.25	0.06	1.58	-5.54	10.54	-3.37

1473	73.53	19.05	0.48	2.03	1.99	-0.04	0.06	49.24	0.12	1.97	-0.05	14.18	0.77
1472	92.69	19.89	0.49	2.03	2.01	-0.01	0.06	49.50	0.18	1.82	-2.46	14.93	-1.05
1471	96.06	20.04	0.47	2.02	1.96	-0.06	0.06	49.45	0.11	2.01	1.16	13.31	1.67
1470	104.71	20.43	0.46	1.96	1.94	-0.02	0.06	50.95	0.11	1.83	-0.56	12.58	0.38
411	112.80	22.95	0.46	1.90	1.95	0.05	0.06	52.69	0.13	1.69	-0.51	12.79	0.42
1469	114.96	22.96	0.45	1.98	1.92	-0.06	0.06	50.45	0.16	1.58	-3.32	11.78	-1.69
403	122.30	22.99	0.44	1.92	1.89	-0.02	0.07	52.02	0.06	2.39	1.40	10.89	1.86
1468	123.72	23.00	0.48	2.01	1.99	-0.02	0.08	49.76	0.13	2.29	3.96	14.34	3.78
420	132.70	23.04	0.45	1.80	1.91	0.11	0.09	55.11	0.16	3.09	4.41	11.64	4.12
1467	139.65	23.08	0.51	2.02	2.07	0.04	0.06	49.56	0.09	1.92	1.33	16.65	1.81
405	141.70	23.09	0.45	2.02	1.91	-0.11	0.06	49.54	0.11	1.74	-5.40	11.37	-3.26
1466	142.53	23.09	0.49	1.93	2.02	0.08	0.07	51.79	0.15	1.96	2.57	15.07	2.73
404	146.20	23.11	0.43	1.91	1.87	-0.04	0.07	52.18	0.08	2.60	-1.44	10.10	-0.28
1465	149.33	23.12	0.44	1.97	1.89	-0.08	0.09	50.69	0.15	2.42	-1.61	10.93	-0.41
401	153.20	23.14	0.44	1.93	1.90	-0.03	0.07	51.76	0.07	3.22	1.72	10.99	2.10
1464	158.61	23.17	0.48	1.92	2.00	0.08	0.07	52.23	0.09	1.48	-3.98	14.43	-2.20
1463	165.28	23.20	0.44	1.98	1.89	-0.09	0.08	50.30	0.09	2.28	1.58	10.81	1.99
412	173.70	23.24	0.53	1.82	2.10	0.28	0.05	54.86	0.12	1.46	-6.57	17.71	-4.14
1462	179.41	23.27	0.48	2.04	1.99	-0.05	0.07	49.05	0.10	2.03	-0.69	14.24	0.28
415	183.20	23.29	0.43	2.04	1.87	-0.17	0.07	48.80	0.05	2.53	2.79	9.81	2.90
1460	189.60	23.32	0.50	2.06	2.03	-0.02	0.06	48.59	0.07	1.83	0.39	15.67	1.09
462	194.80	23.34	0.49	1.90	2.02	0.12	0.07	52.66	0.05	2.47	3.31	15.21	3.30
1459	218.69	23.46	0.47	2.11	1.97	-0.14	0.05	47.22	0.10	1.38	-3.82	13.57	-2.07
1458	226.95	23.50	0.51	2.04	2.06	0.02	0.06	49.06	0.07	2.15	4.86	16.42	4.46
1457	231.42	23.52	0.52	2.15	2.08	-0.06	0.05	46.34	0.07	1.57	0.67	17.14	1.31

266

1456	240.05	23.56	0.52	2.28	2.08	-0.20	0.05	42.88	0.08	1.79	0.99	17.01	1.55
1455	253.27	23.63	0.47	2.21	1.97	-0.25	0.04	44.53	0.09	1.10	-7.49	13.47	-4.83
1454	264.98	23.69	0.47	2.21	1.95	-0.26	0.04	44.52	0.09	1.04	-10.70	12.99	-7.25
1453	277.85	23.75	0.50	2.22	2.04	-0.17	0.04	44.58	0.09	1.47	-3.27	15.95	-1.65
1452	288.70	23.98	0.52	2.37	2.09	-0.28	0.05	40.52	0.16	1.84	1.68	17.35	2.06
1451	313.26	24.61	0.47	2.29	1.97	-0.31	0.05	42.68	0.12	0.79			
408	345.30	25.44	0.47	1.76	1.97	0.21	0.05	56.33	0.17	1.28	-7.17	13.62	-4.59

Table A3.2 BAYSPAR temperature data for DSDP 270. 5th, 50th and 95th refer to percentiles.

			BAYSPAR SST STD (°C)			BAYSPAR SubT STD (°C)			BAYSPAR SST Analogue (°C)			BAYSPAR SubT Analogue (°C)		
BMC number	Sample depth (mbsf)	Age (Ma)	5th	50th	95th	5th	50th	95th	5th	50th	95th	5th	50th	95th
406	47.80	17.91	-1.45	5.38	12.26	-0.85	5.06	11.20	6.00	12.79	19.46	3.39	10.17	17.04
426	57.30	18.33	-0.43	6.37	13.25	0.13	6.01	12.28	7.21	13.95	20.71	4.67	11.35	18.38
400	66.80	18.75	-3.00	3.83	10.69	-2.18	3.65	9.74	3.93	11.02	17.59	1.56	8.37	15.18
1473	73.53	19.05	0.04	6.85	13.81	0.64	6.50	12.65	7.87	14.56	21.50	5.16	11.95	19.00
1472	92.69	19.89	0.62	7.47	14.43	1.16	7.04	13.30	8.69	15.26	22.34	5.97	12.78	19.91
1471	96.06	20.04	-0.71	6.09	13.11	-0.01	5.81	11.91	7.01	13.74	20.46	4.39	11.16	18.22
1470	104.71	20.43	-1.23	5.59	12.49	-0.56	5.28	11.28	6.23	13.02	19.71	3.65	10.41	17.27
411	112.80	22.95	-1.06	5.77	12.72	-0.40	5.41	11.50	6.54	13.23	19.95	3.89	10.63	17.57
1469	114.96	22.96	-1.88	4.86	11.78	-1.22	4.66	10.67	5.39	12.24	18.79	2.88	9.62	16.37
403	122.30	22.99	-2.73	4.11	11.04	-1.86	3.99	10.08	4.35	11.41	17.83	1.97	8.73	15.44
1468	123.72	23.00	0.12	7.01	13.97	0.83	6.68	12.91	8.12	14.72	21.61	5.40	12.16	19.29

420	132.70	23.04	-2.11	4.81	11.71	-1.36	4.49	10.60	5.18	12.11	18.66	2.63	9.48	16.29
1467	139.65	23.08	1.96	8.92	15.99	2.72	8.44	14.75	10.37	16.90	24.34	7.67	14.36	21.88
405	141.70	23.09	-2.24	4.60	11.47	-1.57	4.31	10.38	4.87	11.83	18.46	2.46	9.22	16.07
1466	142.53	23.09	0.77	7.68	14.64	1.44	7.22	13.43	8.79	15.42	22.46	6.07	12.90	20.08
404	146.20	23.11	-3.32	3.49	10.49	-2.55	3.33	9.38	3.53	10.65	17.14	1.17	8.01	14.67
1465	149.33	23.12	-2.70	4.21	11.26	-1.86	3.99	9.97	4.41	11.43	17.94	2.00	8.80	15.54
401	153.20	23.14	-2.52	4.20	11.23	-1.82	4.06	10.16	4.47	11.50	18.00	2.10	8.84	15.64
1464	158.61	23.17	0.10	7.02	14.09	0.88	6.76	12.91	8.17	14.78	21.72	5.51	12.20	19.38
1463	165.28	23.20	-2.78	4.06	11.06	-1.98	3.91	10.01	4.25	11.30	17.84	1.89	8.65	15.43
412	173.70	23.24	2.83	9.78	16.89	3.45	9.24	15.52	11.51	17.93	25.58	8.64	15.44	23.12
1462	179.41	23.27	0.00	6.92	13.94	0.74	6.53	12.74	7.98	14.62	21.59	5.29	12.05	19.11
415	183.20	23.29	-3.55	3.28	10.32	-2.83	3.05	9.03	3.18	10.34	16.76	0.80	7.66	14.38
1460	189.60	23.32	1.31	8.16	15.18	1.92	7.70	13.92	9.41	15.96	23.20	6.64	13.43	20.75
462	194.80	23.34	0.96	7.68	14.77	1.48	7.27	13.56	8.96	15.56	22.61	6.29	12.98	20.23
1459	218.69	23.46	-0.43	6.39	13.38	0.28	6.06	12.25	7.24	13.99	20.83	4.60	11.38	18.37
1458	226.95	23.50	1.67	8.69	15.81	2.49	8.25	14.61	10.14	16.74	24.10	7.30	14.20	21.64
1457	231.42	23.52	2.35	9.30	16.43	3.01	8.83	15.12	10.88	17.33	24.78	8.08	14.90	22.38
1456	240.05	23.56	2.14	9.20	16.40	2.93	8.69	15.01	10.83	17.29	24.68	7.96	14.73	22.20
1455	253.27	23.63	-0.64	6.26	13.30	0.18	5.89	11.95	7.16	13.83	20.68	4.52	11.34	18.30
1454	264.98	23.69	-1.04	5.90	12.95	-0.22	5.57	11.75	6.57	13.41	20.14	4.11	10.81	17.68
1453	277.85	23.75	1.40	8.36	15.40	2.02	7.88	14.16	9.79	16.25	23.48	6.95	13.69	20.96
1452	288.70	23.98	2.44	9.47	16.60	3.27	9.00	15.29	11.14	17.57	25.15	8.38	15.06	22.66
408	345.30	25.44	-0.36	6.33	13.42	0.23	6.03	12.19	7.31	14.04	20.86	4.71	11.45	18.47

Table A3.3 GDGT data for CRP-2/2A used in Chapter 5.

BMC Number	Sample depth (mbsf)	Age (Ma)	TEX$_{86}$	RI	Calculated RI (Zhang et al. 2016b)	ΔRI	MI	%GDGT-0	BIT	GDGT 2 /GDGT-3	TEX$_{86}^{L}$ (°C)	Shevenell et al. 2011 (°C)	Kim et al., 2012 (°C)
123	108.99	21.29	0.59	2.72	2.30	-0.42	0.02	31.89	0.11	1.61			
131	110.96	21.29	0.38	1.28	1.78	0.50	0.05	68.20	0.13	1.40			
133	123.97	21.30	0.49	1.84	2.01	0.17	0.03	54.12	0.36	1.29			
128	127.98	21.30	0.46	1.60	1.93	0.33	0.04	60.23	0.12	2.68			
130	134.98	23.23	0.56	2.60	2.21	-0.39	0.02	34.88	0.37	1.07			
121	159.98	23.27	0.49	2.01	2.01	0.00	0.03	49.71	0.22	2.47	9.35	14.74	7.84
115	170.01	23.28	0.60	2.74	2.31	-0.43	0.02	31.34	0.40	1.03			
124	180.04	23.30	0.62	2.83	2.37	-0.46	0.02	28.95	0.14	1.87			
118	244.95	24.19	0.44	1.66	1.89	0.24	0.05	58.65	0.11	3.45	10.55	10.78	8.74
132	249.96	24.20	0.49	2.00	2.01	0.01	0.04	49.93	0.15	3.11	12.14	15.01	9.94
117	259.89	24.22	0.55	2.39	2.17	-0.22	0.03	40.13	0.60	1.56			
114	269.98	24.24	0.54	2.06	2.14	0.09	0.04	48.50	0.22	4.78	18.95	18.97	15.06
122	290	24.27	0.45	1.59	1.92	0.33	0.07	60.42	0.07	4.39			
125	299.94	24.29	0.45	1.32	1.92	0.60	0.06	67.37	0.32	1.25			

Table A3.4 BAYSPAR temperature data for CRP-2/2A. 5th, 50th and 95th refer to percentiles.

			BAYSPAR SST STD (°C)			BAYSPAR SubT STD (°C)			BAYSPAR SST Analogue (°C)			BAYSPAR SubT Analogue (°C)		
BMC Number	Sample depth (mbsf)	Age (Ma)	5th	50th	95th	5th	50th	95th	5th	50th	95th	5th	50th	95th

121	159.98	23.27	0.50	7.38	14.31	1.07	6.96	13.04	8.18	14.95	22.11	5.59	12.42	19.78
118	244.95	24.19	-2.76	4.08	10.96	-1.98	3.84	9.93	3.80	11.13	17.79	1.66	8.55	15.46
132	249.96	24.20	0.79	7.62	14.63	1.31	7.15	13.38	8.36	15.18	22.40	5.83	12.65	20.10
114	269.98	24.24	3.96	10.87	18.02	4.36	10.19	16.58	12.35	19.02	27.17	9.61	16.57	24.63

Table A3.5 GDGT data for AND-2A, from Levy et al. (2016).

Sample depth (mbsf)	Age (Ma)	TEX$_{86}$	RI	Calculated RI (Zhang et al. 2016b)	ΔRI	MI	%GDGT-0	BIT	GDGT-2 /GDGT-3	TEX$_{86}^{L}$ (°C)	Shevenell et al. 2011 (°C)	Kim et al., 2012 (°C)
142.9	11.51	0.44	2.00	1.89	-0.11	0.06	49.75	0.25	2.14	4.21	10.90	3.97
198.41	11.95	0.47	2.13	1.97	-0.16	0.04	46.62	0.08	1.78	4.57	13.44	4.25
225.42	14.45	0.43	1.92	1.88	-0.04	0.05	51.76	0.20	2.08	5.84	10.37	5.20
229.46	14.46	0.44	1.93	1.89	-0.04	0.06	51.63	0.10	1.96	5.69	10.60	5.09
235.11	14.49	0.43	1.90	1.88	-0.02	0.05	52.39	0.11	2.07	6.08	10.36	5.38
237.46	14.50	0.43	1.95	1.88	-0.07	0.06	51.08	0.15	2.02	5.79	10.38	5.16
240.47	14.51	0.45	1.88	1.91	0.04	0.06	53.03	0.15	2.27	7.61	11.53	6.53
274.92	15.91	0.43	1.94	1.87	-0.07	0.05	51.32	0.08	1.71	3.26	10.12	3.26
280.6	15.93	0.46	1.96	1.95	-0.01	0.05	50.93	0.11	1.93	6.95	12.79	6.03
284.37	15.94	0.47	1.93	1.95	0.02	0.05	51.60	0.08	1.88	7.17	12.97	6.20
285.35	15.94	0.45	1.95	1.91	-0.04	0.05	51.21	0.11	1.95	7.10	11.48	6.15
292.52	15.96	0.45	1.98	1.92	-0.06	0.05	50.36	0.09	1.79	6.72	11.95	5.86
295.25	15.97	0.44	1.96	1.89	-0.07	0.05	50.90	0.07	1.77	2.91	10.76	2.99
299.42	15.98	0.44	1.87	1.90	0.03	0.05	53.23	0.18	1.70	3.09	11.06	3.13
307.01	16.00	0.47	1.86	1.97	0.11	0.05	53.56	0.15	1.83	6.82	13.59	5.94

310.24	16.00	0.44	1.98	1.89		-0.10	0.06	50.23	0.07	2.23	7.64	10.57	6.55
311.07	16.01	0.44	1.96	1.88		-0.08	0.05	50.78	0.09	2.18	7.20	10.52	6.22
312.75	16.01	0.46	2.11	1.93		-0.18	0.05	47.08	0.03	1.57	2.64	12.11	2.79
316.57	16.02	0.46	1.86	1.93		0.07	0.06	53.42	0.19	1.68	2.19	12.32	2.45
336.13	16.07	0.42	1.83	1.85		0.02	0.05	54.18	0.32	1.95			
351.59	16.11	0.43	2.33	1.87		-0.46	0.03	41.40	0.03	1.63			
392.56	16.22	0.64	2.39	2.46		0.06	0.11	39.70	0.20	1.00	10.55	26.90	8.74
426.29	16.30	0.45	1.99	1.92		-0.07	0.05	50.16	0.17	2.07	6.50	11.74	5.70
431.63	16.34	0.45	1.99	1.91		-0.08	0.06	50.13	0.10	2.21	7.59	11.39	6.52
433.49	16.37	0.44	1.94	1.90		-0.04	0.05	51.25	0.14	2.37	8.21	11.29	6.98
437.2	16.44	0.42	1.71	1.84		0.14	0.06	57.37	0.25	1.97	2.29	8.91	2.53
445.07	16.52	0.44	1.86	1.89		0.04	0.05	53.54	0.23	1.87	3.42	10.92	3.38
455.27	16.58	0.44	1.83	1.90		0.07	0.06	54.11	0.29	2.07	5.74	11.29	5.12
463.26	16.62	0.45	1.85	1.91		0.06	0.06	53.80	0.33	2.41			
483.51	16.73	0.52	1.95	2.08		0.13	0.11	51.08	0.31	3.61			
490.26	16.76	0.38	1.91	1.77		-0.14	0.05	51.97	0.16	1.81	-1.39	5.98	-0.24
496.76	16.79	0.42	1.83	1.86		0.04	0.06	54.35	0.13	1.73	1.70	9.68	2.08
501.02	16.82	0.44	1.92	1.89		-0.03	0.05	51.88	0.25	1.60	1.18	10.80	1.69
513.31	16.88	0.46	1.96	1.95		-0.01	0.05	51.08	0.31	1.68			
526.28	16.95	0.46	1.88	1.94		0.06	0.06	52.87	0.12	2.07	6.58	12.59	5.76
530.6	16.97	0.41	2.06	1.84		-0.22	0.05	48.35	0.08	1.48	-0.58	8.84	0.36
532.41	16.98	0.41	2.03	1.83		-0.20	0.04	49.09	0.10	1.60	-0.63	8.53	0.33
538.56	17.01	0.44	2.03	1.90		-0.12	0.06	49.15	0.09	2.14	5.85	11.20	5.20
546.49	17.05	0.48	1.85	1.99		0.14	0.06	53.92	0.26	2.16	6.65	14.20	5.81
553.44	17.09	0.42	1.93	1.86		-0.07	0.05	51.68	0.08	1.56	0.62	9.63	1.27

557.54	17.11	0.38	1.87	1.78		-0.09	0.05	53.27	0.29	1.62	-2.99	6.08	-1.45
578.49	17.22	0.42	2.08	1.85		-0.23	0.04	47.76	0.04	1.59	-1.04	9.31	0.02
595.5	17.26	0.46	2.00	1.93		-0.07	0.05	49.91	0.07	1.73	4.99	12.25	4.56
618.56	17.31	0.46	2.20	1.94		-0.26	0.04	44.85	0.05	1.64	1.38	12.62	1.84
629.38	17.34	0.42	2.33	1.86		-0.47	0.03	41.34	0.03	1.76			
632.09	17.34	0.47	2.02	1.97		-0.05	0.05	49.44	0.02	1.72	3.58	13.55	3.50
663.69	17.41	0.43	2.01	1.87		-0.14	0.05	49.51	0.15	1.67	1.15	9.99	1.67
673.17	17.43	0.47	1.97	1.97		-0.01	0.06	50.56	0.18	2.13	6.30	13.47	5.55
692.24	17.47	0.48	1.96	1.99		0.03	0.05	51.04	0.09	1.80	4.39	14.14	4.11
700.49	17.49	0.46	2.06	1.93		-0.13	0.04	48.50	0.17	1.63	1.50	12.12	1.93
732.04	17.60	0.47	2.02	1.97		-0.04	0.05	49.54	0.16	1.81	4.78	13.67	4.40
739.35	17.65	0.45	2.04	1.92		-0.12	0.05	48.81	0.06	1.98	5.01	11.79	4.57
741.9	17.67	0.46	2.05	1.94		-0.11	0.05	48.59	0.06	1.84	4.43	12.47	4.14
745.99	17.69	0.48	2.00	1.99		-0.01	0.06	49.82	0.09	2.09	6.43	14.37	5.64
747.43	17.70	0.47	2.08	1.96		-0.11	0.05	47.92	0.06	1.67	3.64	13.36	3.54
753.75	17.73	0.45	2.01	1.92		-0.08	0.05	49.73	0.57	1.91			
761.85	17.75	0.46	2.00	1.95		-0.05	0.05	49.94	0.07	2.08	5.82	12.75	5.18
778.5	18.72	0.40	2.08	1.81		-0.26	0.05	47.86	0.14	1.58	-2.46	7.75	-1.05
786.52	18.76	0.40	1.95	1.81		-0.15	0.06	50.94	0.16	2.08	1.19	7.40	1.70
807.76	18.88	0.45	2.02	1.91		-0.10	0.05	49.52	0.07	1.73	1.57	11.50	1.99
820.6	18.95	0.43	2.09	1.87		-0.22	0.04	47.60	0.25	1.57	-0.73	9.88	0.25
827.51	18.99	0.45	2.06	1.92		-0.14	0.05	48.45	0.06	1.92	2.38	11.68	2.59
837.64	19.05	0.42	2.11	1.85		-0.26	0.04	47.04	0.08	1.72	-0.42	9.04	0.49
858.37	19.16	0.43	2.19	1.88		-0.31	0.04	45.09	0.05	1.28			
871.5	19.24	0.43	2.16	1.86		-0.30	0.04	45.81	0.05	1.59			

896.27	19.37	0.42	2.19	1.86		-0.33	0.05	44.93	0.06	1.75			
905.74	19.43	0.48	2.14	1.98		-0.16	0.05	46.28	0.10	1.71	4.44	13.80	4.15
939.35	19.61	0.47	2.11	1.96		-0.15	0.05	47.14	0.14	1.58	1.89	13.17	2.22
1009.07	20.07	0.52	2.11	2.09		-0.02	0.06	47.14	0.13	1.78	5.63	17.51	5.04
1022.36	20.08	0.49	1.98	2.01		0.03	0.06	50.38	0.07	1.93	5.67	14.91	5.07
1125.97	20.20	0.50	2.08	2.03		-0.06	0.06	47.87	0.10	1.61	2.41	15.39	2.61

Table A3.6 BAYSPAR temperature data for AND-2A. 5th, 50th and 95th refer to percentiles.

Sample depth (mbsf)	Age (Ma)	BAYSPAR SST STD (°C)			BAYSPAR SubT STD (°C)			BAYSPAR SST Analogue (°C)			BAYSPAR SubT Analogue (°C)		
		5th	50th	95th	5th	50th	95th	5th	50th	95th	5th	50th	95th
142.9	11.51	-2.67	4.24	11.08	-1.88	3.96	10.01	2.96	10.90	18.44	1.33	8.47	16.31
198.41	11.95	-0.49	6.32	13.33	0.09	5.89	12.02	5.92	13.56	21.44	3.93	11.06	19.28
225.42	14.45	-2.98	3.74	10.68	-2.36	3.50	9.54	2.42	10.38	17.83	0.78	7.92	15.74
229.46	14.46	-2.87	4.00	10.91	-2.15	3.74	9.80	2.69	10.61	18.08	0.99	8.16	15.92
235.11	14.49	-3.12	3.75	10.66	-2.24	3.55	9.54	2.39	10.38	17.84	0.79	7.86	15.62
237.46	14.50	-2.96	3.83	10.72	-2.37	3.58	9.60	2.45	10.41	17.82	0.79	7.90	15.70
240.47	14.51	-2.14	4.66	11.65	-1.39	4.43	10.45	3.67	11.57	19.25	1.98	9.09	17.04
274.92	15.91	-3.47	3.59	10.46	-2.52	3.30	9.31	2.04	10.12	17.50	0.51	7.65	15.35
280.6	15.93	-1.06	5.73	12.76	-0.43	5.44	11.52	5.24	12.90	20.69	3.23	10.40	18.57
284.37	15.94	-0.99	5.92	12.83	-0.24	5.55	11.69	5.39	13.04	20.97	3.55	10.57	18.80
285.35	15.94	-2.20	4.70	11.73	-1.51	4.37	10.42	3.68	11.55	19.09	1.94	9.03	16.97
292.52	15.96	-1.91	5.04	11.96	-1.02	4.75	10.75	4.21	11.98	19.71	2.45	9.53	17.47
295.25	15.97	-2.76	4.12	11.07	-1.96	3.81	9.95	2.94	10.80	18.39	1.18	8.29	16.11

299.42	15.98	-2.48	4.39	11.40	-1.79	4.08	10.17	3.17	11.10	18.63	1.50	8.61	16.57
307.01	16.00	-0.49	6.35	13.35	0.22	6.04	12.29	6.14	13.70	21.72	4.05	11.23	19.52
310.24	16.00	-2.79	3.91	10.85	-2.21	3.71	9.75	2.58	10.61	18.07	1.01	8.14	15.90
311.07	16.01	-2.95	3.87	10.81	-2.24	3.65	9.69	2.55	10.55	17.99	0.98	8.05	15.80
312.75	16.01	-1.55	5.24	12.07	-0.96	4.90	10.99	4.39	12.18	19.91	2.67	9.69	17.75
316.57	16.02	-1.53	5.30	12.33	-0.75	5.00	11.04	4.62	12.40	20.12	2.74	9.87	17.98
392.56	16.22	10.07	17.42	24.89	10.52	16.48	23.19	19.42	27.11	40.60	16.56	24.79	37.18
426.29	16.30	-1.99	4.89	11.80	-1.22	4.51	10.75	3.97	11.81	19.41	2.22	9.32	17.35
431.63	16.34	-2.22	4.59	11.49	-1.53	4.37	10.47	3.57	11.42	18.96	1.83	8.96	16.93
433.49	16.37	-2.27	4.52	11.49	-1.67	4.20	10.38	3.43	11.35	18.90	1.80	8.87	16.80
437.2	16.44	-4.34	2.55	9.44	-3.68	2.37	8.48	0.65	8.87	16.17	-0.75	6.41	14.08
445.07	16.52	-2.60	4.21	11.09	-1.79	3.95	9.94	3.01	10.94	18.44	1.40	8.48	16.30
455.27	16.58	-2.30	4.50	11.53	-1.58	4.22	10.36	3.45	11.35	18.89	1.77	8.86	16.72
490.26	16.76	-6.69	0.16	6.99	-5.86	0.13	6.11	-2.98	5.87	12.97	-4.02	3.36	10.74
496.76	16.79	-3.72	3.22	10.16	-2.88	2.97	9.00	1.58	9.67	16.99	0.10	7.22	14.91
501.02	16.82	-2.76	4.14	11.07	-1.97	3.88	9.92	2.88	10.83	18.29	1.23	8.36	16.22
526.28	16.95	-1.22	5.55	12.58	-0.62	5.23	11.39	4.90	12.66	20.51	3.06	10.17	18.25
530.6	16.97	-4.32	2.47	9.30	-3.67	2.36	8.33	0.56	8.82	16.01	-0.81	6.33	13.90
532.41	16.98	-4.57	2.28	9.21	-3.88	2.10	8.07	0.18	8.47	15.71	-1.13	6.02	13.58
538.56	17.01	-2.30	4.52	11.57	-1.71	4.18	10.23	3.29	11.22	18.79	1.66	8.79	16.72
546.49	17.05	0.06	6.94	13.93	0.64	6.50	12.73	6.75	14.30	22.42	4.74	11.87	20.33
553.44	17.09	-3.68	3.08	10.09	-2.88	2.96	9.02	1.43	9.62	16.95	0.05	7.14	14.87
557.54	17.11	-6.49	0.30	7.06	-5.79	0.19	6.15	-2.85	5.91	13.14	-3.89	3.50	10.88
578.49	17.22	-3.90	2.90	9.84	-3.20	2.65	8.68	1.14	9.28	16.62	-0.29	6.83	14.50
595.5	17.26	-1.49	5.30	12.22	-0.85	4.98	11.03	4.58	12.33	20.10	2.74	9.83	17.99

618.56	17.31	-1.29	5.60	12.60	-0.49	5.26	11.47	4.98	12.69	20.48	3.14	10.21	18.32
632.09	17.34	-0.48	6.42	13.39	0.25	6.04	12.30	5.98	13.61	21.59	4.06	11.20	19.49
663.69	17.41	-3.39	3.46	10.33	-2.61	3.24	9.18	1.91	10.00	17.29	0.32	7.48	15.22
673.17	17.43	-0.43	6.34	13.35	0.12	5.96	12.21	5.93	13.58	21.52	3.94	11.09	19.37
692.24	17.47	-0.02	6.89	13.91	0.61	6.45	12.77	6.65	14.24	22.40	4.65	11.78	20.33
700.49	17.49	-1.70	5.22	12.41	-1.06	4.85	10.89	4.44	12.19	19.81	2.60	9.71	17.79
732.04	17.60	-0.32	6.43	13.52	0.42	6.11	12.18	6.14	13.78	21.81	4.23	11.30	19.74
739.35	17.65	-1.94	4.93	11.93	-1.19	4.67	10.73	4.06	11.82	19.49	2.34	9.40	17.38
741.9	17.67	-1.43	5.51	12.41	-0.75	5.19	11.27	4.78	12.55	20.34	2.91	10.05	18.24
745.99	17.69	0.35	7.04	14.15	0.78	6.62	12.85	6.91	14.45	22.69	4.88	12.04	20.51
747.43	17.70	-0.59	6.25	13.22	0.05	5.89	11.99	5.81	13.47	21.45	3.82	11.00	19.19
761.85	17.75	-1.22	5.73	12.68	-0.44	5.41	11.58	5.16	12.84	20.71	3.25	10.36	18.55
778.5	18.72	-5.17	1.61	8.45	-4.51	1.52	7.40	-0.78	7.67	14.87	-2.04	5.22	12.70
786.52	18.76	-5.47	1.35	8.17	-4.63	1.23	7.25	-1.14	7.30	14.50	-2.41	4.83	12.32
807.76	18.88	-2.13	4.69	11.66	-1.42	4.37	10.49	3.66	11.52	19.19	1.97	9.06	17.01
820.6	18.95	-3.57	3.30	10.28	-2.58	3.20	9.21	1.75	9.88	17.25	0.28	7.38	15.07
827.51	18.99	-1.98	4.89	11.92	-1.28	4.56	10.71	3.87	11.76	19.27	2.15	9.25	17.17
837.64	19.05	-4.25	2.67	9.59	-3.35	2.51	8.48	0.77	9.00	16.25	-0.65	6.56	14.16
905.74	19.43	-0.33	6.58	13.53	0.35	6.17	12.35	6.31	13.91	22.00	4.29	11.39	19.78
939.35	19.61	-0.84	6.05	13.03	-0.03	5.70	11.82	5.65	13.24	21.22	3.63	10.76	19.04
1009.07	20.07	2.76	9.63	16.72	3.26	9.08	15.42	10.29	17.67	26.91	7.98	15.22	24.51
1022.36	20.08	0.71	7.47	14.53	1.35	7.10	13.34	7.62	15.04	23.36	5.42	12.56	21.23
1125.97	20.20	0.96	7.85	14.88	1.73	7.44	13.74	8.07	15.50	24.02	5.87	13.06	21.79

Table A3.7 GDGT data for DSDP 274 used in Chapter 5.

BMC Number	Sample depth (mbsf)	Age (Ma)	TEX$_{86}$	RI	Calculated RI (Zhang et al. 2016b)	ΔRI	MI	%GDGT-0	BIT	GDGT-2 /GDGT-3	TEX$_{86}^L$ (°C)	Shevenell et al. 2011 (°C)	Kim et al., 2012 (°C)
453	142.7	17.11	0.43	1.65	1.88	0.22	0.08	58.91	0.07	2.65	3.33	10.27	3.31
444	143.3	17.14	0.45	1.91	1.93	0.02	0.09	52.09	0.06	4.95	12.07	12.07	9.89
452	144.2	17.18	0.42	1.89	1.85	-0.04	0.07	52.73	0.03	2.67	2.96	9.21	3.03
457	144.8	17.21	0.39	1.43	1.80	0.37	0.11	64.75	0.05	2.98			
446	145.2	17.22	0.39	1.99	1.80	-0.19	0.07	50.04	0.04	2.90	3.96	7.14	3.78
459	146.7	17.29	0.46	1.64	1.94	0.30	0.06	59.19	0.05	1.94			
431	154.7	17.64	0.45	1.94	1.92	-0.03	0.06	51.35	0.08	2.70	6.12	11.75	5.41
436	155.8	17.69	0.42	1.85	1.86	0.02	0.06	53.85	0.06	2.14	2.25	9.67	2.50

Table A3.8 BAYSPAR temperature data for DSDP 274. 5th, 50th and 95th refer to percentiles.

			BAYSPAR SST STD (°C)			BAYSPAR SubT STD (°C)			BAYSPAR SST Analogue (°C)			BAYSPAR SubT Analogue (°C)		
BMC	Sample depth (mbsf)	Age (Ma)	5th	50th	95th	5th	50th	95th	5th	50th	95th	5th	50th	95th
453	142.7	17.11	-2.67	3.72	10.10	-2.41	3.40	9.20	1.98	10.05	17.99	0.35	7.68	15.98
444	143.3	17.14	-1.07	5.25	11.57	-1.06	4.86	10.65	4.08	11.99	20.26	2.30	9.63	18.33
452	144.2	17.18	-3.59	2.87	9.15	-3.10	2.49	8.28	0.67	8.93	16.64	-0.72	6.54	14.75
446	145.2	17.22	-5.33	1.09	7.34	-4.90	0.89	6.59	-1.81	6.77	14.25	-2.95	4.41	12.21
431	154.7	17.64	-1.41	4.99	11.36	-1.19	4.52	10.41	3.68	11.64	19.76	2.00	9.24	17.89
436	155.8	17.69	-3.18	3.27	9.57	-2.82	2.87	8.62	1.30	9.49	17.15	-0.25	7.04	15.23

Table A3.9 GDGT data for AND-1B Miocene used in Chapter 5.

BMC Number	Sample depth (mbsf)	Age (Ma)	TEX$_{86}$	RI	Calculated RI (Zhang et al. 2016b)	ΔRI	MI	%GDGT-0	BIT	GDGT-2 /GDGT-3
57	1030	9.57	0.45	2.31	1.92	-0.39	0.03	41.99	0.19	2.03

Table A3.10 GDGT data for AND-1B Plio-Pleistocene, from McKay et al. (2012).

Sample depth (mbsf)	Age (Ma)	TEX$_{86}$	RI	Calculated RI (Zhang et al. 2016b)	ΔRI	MI	%GDGT-0	BIT	GDGT-2 /GDGT-3	TEX$_{86}^{L}$ (°C)	Shevenell et al. 2011 (°C)	Kim et al., 2012 (°C)
86.75	1.03	0.37	1.62	1.76	0.14	0.06	59.57		1.66	-4.52	5.08	-2.60
88.29	1.03	0.35	1.60	1.72	0.12	0.08	59.95	0.02	1.85	-5.50	3.43	-3.34
89.09	1.04	0.34	1.55	1.71	0.16	0.07	61.27	0.03	1.87	-5.27	2.89	-3.16
89.68	1.04	0.35	1.59	1.72	0.13	0.06	60.22	0.02	2.06	-2.98	3.40	-1.44
90.21	1.05	0.39	1.69	1.80	0.10	0.11	57.75	0.06	2.29	1.89	6.95	2.23
91.67	1.06	0.39	1.72	1.79	0.07	0.06	56.98	0.05	2.06	-2.30	6.60	-0.93
93.21	1.07	0.46	2.02	1.94	-0.08	0.17	48.64	0.78	5.69			
154.05	2.12	0.44	2.04	1.89	-0.15	0.03	48.79	0.02	1.45	0.01	10.80	0.81
155.28	2.13	0.46	2.33	1.94	-0.39	0.03	41.59	0.04	1.49			
158.44	2.14	0.44	2.31	1.90	-0.41	0.03	42.02	0.10	1.60			
159.07	2.15	0.40	1.90	1.82	-0.08	0.04	52.35	0.02	1.51	-0.81	7.93	0.19
164.9	2.19	0.49	2.41	2.01	-0.40	0.03	39.43	0.06	1.47			
165.09	2.22	0.41	2.01	1.84	-0.17	0.04	49.58	0.02	1.69	0.82	8.74	1.42
167.94	2.22	0.39	1.95	1.79	-0.16	0.04	51.04	0.06	1.56	-0.43	6.73	0.48
170.02	2.22	0.47	2.09	1.97	-0.12	0.05	47.61	0.06	1.79	4.15	13.52	3.92
175.05	2.22	0.43	1.91	1.87	-0.05	0.04	52.13	0.03	1.61	1.20	9.86	1.71

176.11	2.23	0.46	2.34	1.93	-0.41	0.03	41.15	0.07	1.62			
180.04	2.23	0.42	1.82	1.85	0.02	0.04	54.37	0.02	1.69	1.35	9.16	1.82
184.15	2.24	0.45	2.13	1.91	-0.22	0.03	46.57	0.02	1.56	1.19	11.63	1.70
191.5	2.60	0.45	2.16	1.92	-0.24	0.03	45.92	0.02	1.54	2.82	11.78	2.93
191.76	2.60	0.43	1.98	1.88	-0.10	0.04	50.47	0.01	1.52	0.65	10.42	1.29
194	2.60	0.42	1.93	1.86	-0.07	0.04	51.61	0.02	1.59	0.95	9.55	1.52
197.05	2.61	0.43	1.88	1.88	-0.01	0.04	52.86	0.01	1.50	1.13	10.27	1.65
200.05	2.61	0.42	1.89	1.86	-0.03	0.04	52.81	0.04	1.59	0.66	9.58	1.30
200.6	2.61	0.44	2.15	1.88	-0.26	0.03	46.15	0.02	1.66	1.42	10.53	1.88
211.64	2.97	0.48	2.25	1.98	-0.26	0.03	43.69	0.02	1.29	2.63	14.08	2.78
212.04	2.97	0.45	1.99	1.91	-0.08	0.04	50.26	0.01	1.35	0.86	11.31	1.45
213.94	2.97	0.46	2.00	1.95	-0.06	0.04	49.81	0.01	1.29	1.99	12.75	2.30
217.5	2.97	0.44	1.93	1.89	-0.05	0.04	51.55	0.01	1.33	1.22	10.63	1.72
223.5	2.98	0.45	2.12	1.92	-0.20	0.03	46.82	0.01	1.34	0.58	11.89	1.24
252.09	3.08	0.47	2.36	1.96	-0.40	0.03	40.80	0.02	1.43			
254.48	3.08	0.41	2.04	1.84	-0.20	0.03	48.79	0.01	1.72	0.98	8.86	1.54
257.38	3.08	0.49	2.35	2.02	-0.33	0.03	41.14	0.01	1.86			
257.6	3.08	0.49	2.62	2.00	-0.62	0.02	34.19	0.02	1.91			
283.29	3.25	0.49	2.51	2.02	-0.49	0.03	36.93	0.31	1.72			
286.47	3.25	0.56	2.94	2.20	-0.73	0.02	26.21	0.02	1.41			
287.2	3.25	0.45	2.20	1.91	-0.29	0.03	44.82	0.01	1.55	1.68	11.55	2.07
289.18	3.25	0.45	2.30	1.92	-0.38	0.03	42.18	0.01	1.51			
291.21	3.25	0.48	2.56	1.99	-0.57	0.02	35.73	0.01	1.43			
291.86	3.25	0.51	2.34	2.07	-0.26	0.03	41.38	0.03	1.16	4.91	16.85	4.50
366.01	3.40	0.52	2.67	2.09	-0.58	0.03	32.91	0.09	1.62			

380.1	3.42	0.37	2.15	1.75	-0.40	0.04	45.88	0.01	1.86			
386.2	3.42	0.33	2.34	1.70	-0.64	0.02	41.31	0.02	1.93			
391.95	3.46	0.46	2.49	1.93	-0.56	0.03	37.48	0.04	1.73			
396	3.44	0.38	2.36	1.77	-0.59	0.05	40.45	0.01	1.85			
400.1	3.48	0.46	2.48	1.94	-0.54	0.03	37.69	0.04	1.88			
406	3.50	0.38	2.18	1.78	-0.39	0.04	45.27	0.01	1.67			
412.24	3.52	0.45	2.47	1.92	-0.56	0.03	37.90	0.02	1.60			
416.03	3.54	0.37	2.44	1.75	-0.69	0.06	38.20	0.01	1.80			
420.32	3.56	0.47	2.59	1.97	-0.62	0.03	34.91	0.01	1.66			
424.15	3.56	0.46	2.37	1.93	-0.45	0.03	40.34	0.02	1.73			
427.96	3.58	0.47	2.33	1.95	-0.38	0.03	41.46	0.02	1.82			
432.13	3.61	0.49	2.66	2.00	-0.65	0.03	33.25	0.01	1.80			
436.04	3.63	0.30	2.25	1.65	-0.60	0.00	43.73	0.00	2.29			
440.97	3.63	0.39	2.44	1.79	-0.64	0.03	38.66	0.01	1.70			
443.93	4.39	0.51	2.12	2.06	-0.06	0.05	46.90	0.03	1.37	5.32	16.57	4.81
446.02	4.40	0.40	2.21	1.81	-0.40	0.05	44.37	0.01	1.63			
452	4.41	0.39	2.51	1.80	-0.71	0.03	36.95	0.01	1.71			
458.65	4.61	0.47	2.03	1.95	-0.08	0.06	49.04	0.02	1.58	5.06	12.91	4.61
503.6	4.76	0.55	2.43	2.18	-0.24	0.04	38.97	0.01	3.53	16.60	20.01	13.30
510.18	4.76	0.58	2.57	2.27	-0.30	0.04	35.35	0.10	4.24			
551.39	4.82	0.52	2.64	2.09	-0.55	0.03	33.74	0.08	1.99			
553.58	4.82	0.53	2.52	2.11	-0.41	0.03	36.69	0.06	2.70			
566.02	4.83	0.53	2.60	2.12	-0.47	0.03	34.76	0.04	2.23			
580.28	4.87	0.61	2.15	2.35	0.20	0.07	45.88	0.18	6.86	26.47	24.38	20.73

Table A3.11 BAYSPAR temperature data for AND-1B Plio-Pleistocene. 5th, 50th and 95th refer to percentiles.

Sample depth (mbsf)	Age (Ma)	BAYSPAR SST STD (°C)			BAYSPAR SubT STD (°C)			BAYSPAR SST Analogue (°C)			BAYSPAR SubT Analogue (°C)		
		5th	50th	95th	5th	50th	95th	5th	50th	95th	5th	50th	95th
86.75	1.03	-7.28	-0.38	6.57	-6.36	-0.46	5.51	-3.90	5.02	12.50	-4.73	2.51	10.06
88.29	1.03	-8.58	-1.69	5.11	-7.70	-1.68	4.20	-5.98	3.32	10.89	-6.57	0.85	8.31
89.09	1.04	-9.10	-2.35	4.53	-8.27	-2.27	3.57	-7.19	2.49	10.03	-7.49	0.03	7.42
89.68	1.04	-8.63	-1.70	5.12	-7.64	-1.57	4.32	-6.04	3.31	10.90	-6.57	0.84	8.31
90.21	1.05	-5.92	0.89	7.86	-5.12	0.80	6.72	-1.90	6.67	14.26	-3.00	4.16	11.92
91.67	1.06	-5.85	0.91	7.74	-5.10	0.79	6.83	-1.84	6.71	14.27	-2.89	4.16	11.90
154.05	2.12	-2.69	4.20	11.04	-2.00	3.92	9.99	3.05	10.89	19.07	1.31	8.30	16.80
159.07	2.15	-5.31	1.56	8.46	-4.41	1.46	7.46	-0.88	7.55	15.16	-2.08	5.00	12.81
165.09	2.22	-4.51	2.19	9.05	-3.84	2.06	8.18	0.07	8.37	16.09	-1.23	5.79	13.78
167.94	2.22	-5.94	0.88	7.80	-5.07	0.81	6.78	-1.90	6.71	14.27	-2.94	4.14	11.89
170.02	2.22	-0.69	6.18	13.15	-0.03	5.81	12.00	5.72	13.41	22.32	3.77	10.75	19.78
175.05	2.22	-3.27	3.59	10.51	-2.48	3.31	9.36	2.01	10.06	18.10	0.43	7.46	15.69
180.04	2.23	-3.90	2.93	9.93	-3.17	2.74	8.67	1.01	9.23	17.13	-0.37	6.65	14.75
184.15	2.24	-2.07	4.87	11.77	-1.38	4.51	10.66	3.87	11.77	20.11	2.10	9.07	17.71
191.5	2.60	-1.95	4.85	11.84	-1.33	4.59	10.69	3.90	11.73	20.18	2.15	9.09	17.73
191.76	2.60	-3.26	3.54	10.48	-2.55	3.27	9.23	1.98	10.04	18.06	0.48	7.48	15.76
194	2.60	-4.04	2.93	9.71	-3.15	2.71	8.70	1.04	9.24	17.10	-0.38	6.62	14.76
197.05	2.61	-3.32	3.54	10.52	-2.56	3.33	9.35	2.00	10.06	18.14	0.48	7.48	15.73
200.05	2.61	-4.13	2.84	9.77	-3.16	2.66	8.70	1.08	9.24	17.12	-0.43	6.67	14.76
200.6	2.61	-2.71	4.15	11.16	-1.90	3.95	10.03	2.96	10.89	19.15	1.29	8.28	16.77
211.64	2.97	0.02	6.81	13.86	0.62	6.45	12.61	6.62	14.22	23.33	4.54	11.59	20.89

212.04	2.97	-1.82	4.89	11.78	-1.27	4.63	10.72	3.89	11.73	20.14	2.09	9.11	17.66
213.94	2.97	-1.36	5.48	12.54	-0.70	5.22	11.30	4.82	12.55	21.25	2.96	9.95	18.74
217.5	2.97	-2.65	4.19	11.02	-1.95	3.93	9.97	2.96	10.90	19.13	1.34	8.30	16.73
223.5	2.98	-1.90	4.94	11.83	-1.25	4.59	10.68	3.89	11.73	20.12	2.14	9.12	17.72
254.48	3.08	-4.53	2.23	9.08	-3.89	2.02	7.95	0.07	8.39	16.09	-1.20	5.80	13.85
287.2	3.25	-1.97	4.86	11.98	-1.29	4.59	10.64	3.89	11.72	20.12	2.14	9.13	17.71
291.86	3.25	1.81	8.80	15.79	2.53	8.33	14.57	9.19	16.69	26.94	6.85	14.06	23.98
443.93	4.39	1.86	8.78	15.94	2.48	8.29	14.53	9.17	16.71	26.84	6.82	14.05	24.02
458.65	4.61	-0.72	6.18	13.24	-0.05	5.75	11.89	5.68	13.41	22.22	3.74	10.77	19.75
503.6	4.76	4.51	11.45	18.58	5.03	10.84	17.26	12.43	19.94	31.79	9.87	17.31	28.41
580.28	4.87	8.21	15.38	22.73	8.69	14.54	21.18	16.99	24.87	39.43	14.19	22.19	35.24